Optimization & Performance Evaluation of Smart Antenna Techniques for Wireless Applications

A THESIS SUBMITTED IN PARTIAL FULFILLMENT FOR THE DEGREE OF

DOCTOR OF PHILOSOPHY

In Electronics and Telecommunication Engineering

GOA UNIVERSITY



By

Ms. Mohini Narendra Naik

Research Centre in Electronics and Telecommunication Engineering Department

Goa College of Engineering

October, 2024

Declaration

I, Mohini Narendra Naik hereby declare that this thesis represents work which has been carried out by me and that it has not been submitted, either in part or full, to any other University or Institution for the award of any research degree.

Ms. Mohini Narendra Naik

Place:
Date:

Certificate

I hereby certify that the above Declaration of the candidate, Mohini Narendra Naik is true and the work was carried out under my supervision

Dr.Hassanali Gulamali Virani
Professor & Head
Department of Electronics & Telecommunication Engineering
Goa college of Engineering, Goa

THESIS APPROVAL

This thesis entitled " Optimization & Performance Evaluation of Smart Antenna Techniques for Wireless Applications" submitted by Ms. Mohini Narendra Naik (P.R.No 1631103002) is approved for the award of degree of Doctor of Philosophy in Electronics & Telecommunication Engineering.

Examiners

1. .....

2. .....

3. .....

Research Guide

.....

Dr. Hassanali G. Virani

Principal

.....

Dr. Krupashankara M. S.

Date:

Place:

Acknowledgments

I would like to express my sincere gratitude and appreciation to all those who have contributed to the successful completion of this Thesis on Optimization & Performance Evaluation of Smart Antenna Techniques for Wireless Applications.

First and foremost, i would like to thank God Almighty for giving me the opportunity to undertake the research and complete it satisfactorily.

I would like to extend my sincere appreciation to my guide, Dr. Hassanali Gulamali Virani , Professor & Head of the ETC Department,Goa College of Engineering, for his expert guidance, constant encouragement, and valuable insights. His unwavering support and commitment to excellence have been instrumental in shaping this research. It is a great honour to work under his supervision.

I would also like to express my special thanks to my internal examiner Dr. Nitesh Guinde, Associate Professor, Goa college of Engineering and external examiner Dr. Mahabaleshwar S.K.,Professor, Basaveshwar Engineering College, Bagalkot for their constructive recommendations.

I would like to thank Dr. M.S.Krupashankara, Principal of Goa College of Engineering, Dr R.B.Lohani and Dr.V.N.Shet, former principals, for providing the necessary resources, facilities, and a conducive environment for conducting this research.

My special thanks to Dr. V.N.Shet, Dean of Engineering, Goa University & Professor, Electrical and Electronics Department, Goa College of Engineering, for providing me with countless valuable advices throughout my research journey.

My special thanks extended to Rev.Fr.Kinley D'Cruz, Director, Don Bosco College of Engineering, Dr.Neena Panandikar, Principal,Don Bosco College of Engineering, Staff of Don Bosco College of Engineering, Staff of Goa College of Engineering, Staff of Goa University for their constant support and encouragement.

I would like to express my deepest gratitude to my family for their constant support and encouragement throughout this journey. My parents, Shri Narendra Naik and Smt. Anandi Narendra Naik, always motivated me to pursue endeavors that inspire others and supported every decision I made. They have been instrumen-

tal and a source of inspiration throughout.I am also very grateful to my brother, Shri Pranay Naik, for his continued encouragement and belief in me. His support has been invaluable.I extend my gratitude to my mother-in-law, Smt. Vrushali Gadekar, for her understanding and moral support. My profound thanks go to my very supportive and caring husband, Shri Rajkiran Gadekar, who ensured that my focus on research was never distracted, taking charge of household responsibilities while I completed my work.A very special thanks to my son, Vardhaman Gadekar, and my daughter, Vaidehi Gadekar, for making this journey even more beautiful.

Finally, I would like to offer my gratitude to each and every person who directly or indirectly helped, encouraged and motivated me during my research Journey.Thank you all.

Abstract

Smart antennas are widely regarded being among the most important components in wireless communication. A smart antenna is primarily used to improve wireless performance. The antenna's efficiency in terms of bandwidth and gain is improved by modelling microstrip patch smart antenna for millimeter wave frequency application. The first objective of this research work, proposes and presents phased array based rectangular microstrip patch antenna at 28 GHz, 38 GHz and 60 GHz and a microstrip MIMO antenna with small envelope correction coefficient (ECC) and strong isolation at 28 GHz and 60 GHz. The electromagnetic design and verification tool IE3DTM was utilized to advance and simulate the antennas.

The second objective of this research, suggested method an eight-port Butler matrix is used to construct a microstrip hexagonal patch antenna with a Z-slot for mm-wave frequency application. The outcome port of the Butler matrix uses four antenna components. When utilized as a beam-forming network, the Butler matrix creates orthogonal beams that may be directed in a variety of ways. With a central frequency of 33 GHz, the overall structure has an operational frequency range of 28 GHz to 39 GHz. There are two butler matrices, one of which has two phase shifters that are rotated by 45 degrees. Two phase shifters at 45 degrees and one at 120 degrees are used in the construction of the other butler matrix.

The third objective of this research is to develop a smart antenna (SA) with a beam-steering method. The antenna was made from Roger substrate. The 5G network is designed with two frequency ranges: frequency range 2 (FR2- mm Wave) includes the region from 24.25 - 52.6 GHz, and frequency range 1 (FR1- sub-6 GHz range) includes the range from 450 MHz - 6 GHz. The FR2-mmWave frequency band, which spans 24.25 to 52.6 GHz, is used in our study. On the other hand, the DENLMS beam steering algorithm is introduced to improve the beam steering capabilities, directional gain, and side lobe level. To increase the pace of convergence, the LMS method is modified by normalizing, causing in delayed error normalized LMS (DENLMS).The DENLMS method, which uses a gradient-based approach, employs an iterative process to execute successive weight vector modifications in the direction of the gradient vector's negative, ultimately resulting

in the current time's lowest mean square error (MSE).

The fourth objective of this research defines the design and construction of a unique elliptical printed monopole antenna with deflected ground structure (DGS) for dual band 5G applications. Throughout the whole band, the antenna works between 2 and 3.7 GHz with a voltage standing wave ratio (VSWR) of less than 2. Ansoft HFSS modelling software is utilized to simulate it, and the antenna has been constructed and experimentally evaluated utilizing Vector Network Analyzer (VNA). When simulated and computed results are compared, they accord rather well.

List of Acronyms

MIMO-Multiple Input Multiple Output
ECC-Envelope correlation coefficient
DOA-Direction of arrival
DENLMS-Delayed error normalized LMS
DGS-Deflected ground structure
VSWR-Voltage standing wave ratio
VNA-Vector Network Analyzer
PCS-Personal Communications Services
WPAN-Wireless Personal Area Networks
WLAN-Wireless Local Area Networks
MSE-Mean Square Error
SIR-Signal-to-Interference Ratio
IoT-Internet of Things
AAS-Advanced Antenna System
SISO-Single Input Single Output
ME-Magneto-Electric
PIFA-Planar Inverted F Antenna
IFA-Inverted F Antenna
SAS-Smart Antenna Systems
SIMO-Single-Input Multiple Output
MISO-Multiple-Input Single Output

DOA-Direction of Arrival
SBS-Switched beam antennas
MSPAs-Microstrip patch antennas
TRMSA-Traditional rectangle microstrip antenna
MSSA-Microstrip slot antennas
MTWA-Microstrip traveling wave antennas
TE-Transverse Electric
TEM-Transverse Electric and Magnetic
FDTD-Finite Different Time Domain technique
TMSAs-Traditional microwave antennas
CRLB-Cramer-Rao lower bound
DOA-Matrix for direction of arrival
MUSIC-Multiple signal classification
WAIMS-Wide-angle impedance matching slab
FSS-Frequency-Selective Surface
CCM-Current Cancellation Method
RFICs-Radio Frequency Integrated Circuits
AR-Axial Ratio
T/R-Transmit and Receive
BFN-Beamforming networks
SATCOM-Satellite Communications
WAIM-Wide-angle scanning impedance matching
MMPTE-Method of Maximum Power Transmission Efficiency
ODEs-Optimal Distribution of Excitations MS-Meta-Surface
CP-MIMO Circularly Polarized MIMO
HFSS-High-Frequency Structure Simulator
ISS-MIMO-ANM-AAS-Interference Signal Superposition-aided Multiple-Input Multiple-Output with Antenna Number Modulation and Adaptive Antenna Selection
ISS-Interference Signal Superposed
BM-Butler Matrix
MPT-Microwave wireless Power Transmission

ADS-Advanced Design System
SLM-Selective Laser Melting
MSA-Microstrip Antenna
ESPAR-Electrically Steerable Parasitic Array Radiator
RSS-Received Signal Strength
MCP-Multiple Calibration Planes
PPCC-Power-Pattern Cross-Correlation
AQGA-Automatic quantum genetic algorithm
CPW-Coplanar Waveguide
ANN-Artificial neural network
VNA-Vector Network Analyzer
RMPA-Rectangular microstrip patch antenna
ECC-Envelope correction correlation
ESPRIT-Estimating Signal Parameters via Rotational Invariance Techniques
WSF-Weighted Subspace Fitting
OP-Orthogonal Propagator
CRLB-Cramer-Rao Lower Bound
MPA-Micro strip Patch Antenna
DLMS-Delayed LMS
LMS-Least Mean Square
SCD-Surface Current Distribution
AUT-Antenna Under Test
NLMS-Normalized Least Mean Square
VSSLMS-Variable Step-Size Least Mean Square
SELMS-Signum Error Least Mean Square
DENLMS-Delayed Error Normalized Least Mean Square

Contents

Declaration ii

THESIS APPROVAL iv

Acknowledgments vi

Abstract viii

List of Acronyms x

1 Introduction 1

1.1 Overview . . . 1
1.2 Wireless Communication . . . 3
1.3 5G and its Requirements . . . 3
1.4 Components of 5G Network . . . 4
1.4.1 5G Spectrum . . . 5
1.4.2 5G Antenna . . . 5
1.4.3 5G Macro Cells . . . 6
1.4.4 5G Small Cells . . . 6
1.4.5 5G Millimeter Wave . . . 7
1.5 Antenna used for 5G . . . 7
1.5.1 Classification Using Input and Output Ports . . . 7
1.5.2 Classification Using Different Types of Antennas . . . 8
1.6 Smart Antenna Systems (SAS) . . . 9
1.6.1 Switched Beam Antennas (SBS) . . . 10

1.6.2 Adaptive Beam Antennas System 11
1.7 Microstrip Antenna (MSA) 12
1.7.1 Types of MSAs 13
1.7.2 Radiation Mechanism of MSAs 15
1.7.3 Design considerations for MPA 17
1.7.4 Different types of Microstrip Patch Antennas (MPAs) and its Advantages 19
1.7.5 Designing Models 21
1.7.6 Advantages of MPAs 23
1.8 Research Gap and Motivation 23
1.9 Scope 25
1.10 Research Objectives 25
1.11 Research Methodology 25
1.12 Thesis Outline 26
1.13 Summary 27

2 Literature Survey **29**
2.1 Overview 29
2.2 Antenna for 5G Communication using Lower Band & High mm Band 30
2.3 Slotting techniques in Microstrip Patch Antenna 31
2.4 Techniques based on Phased Array Antenna for 5G Communication 32
2.5 Techniques based on MIMO Antenna 34
2.6 Techniques based on Smart Antenna with Butler Matrix 36
2.7 Techniques based on Smart Antenna using Algorithms 38
2.8 Techniques based on Elliptical Monopole Antenna 40
2.9 Summary 42

3 Microstrip Patch Antenna at Millimeter Wave Frequency **43**
3.1 Overview 43
3.2 Microstrip Patch Antenna based on Phased Array 44

3.2.1 Design of Rectangular microstrip patch antenna (RMPA) . . 44
3.2.2 Performance Metrics 47
3.2.3 Design of Rectangular Microstrip Patch Antenna for 28 GHz 50
3.2.4 Design of Rectangular Micro strip Patch Antenna for 38 GHz 58
3.2.5 Design of Rectangular Microstrip Patch Antenna (RMPA) for 60 GHz 66
3.2.6 Design of Slotted MPA Phased Array for 28 GHz 72
3.3 Microstrip Patch Antenna based on MIMO 80
3.3.1 Design of MIMO for 28 GHz 81
3.3.2 Design of MIMO for 60 GHz 88
3.3.3 Design of 4 Port MIMO 93
3.3.4 Design of a 4 Port Slotted RMPA MIMO 104
3.3.5 Summary 108

4 Switched Beam Antenna using Butler Matrix at Millimetre Wave Frequency 109
4.1 Overview 109
4.2 Proposed Micro Strip Patch Antenna with Beam Forming Network 111
4.2.1 Switched Beam Antenna Architecture 114
4.2.2 Butler Matrix (BM) 115
4.2.3 Direction of Arrival (DOA) Estimation using Cra -mer Rao Lower Bounds (CRLB) Computation 121
4.2.4 Optimization Procedure 124
4.3 Results and Discussion 125
4.3.1 Performance Evaluation for the Proposed Antenna 126
4.3.2 Performance Evaluation for the Proposed 90° Hy -brid Coupler and 0dB Crossover 128
4.3.3 Performance Evaluation for the Proposed 45° Phase Shifter 130

4.3.4 Performance Evaluation for the Proposed 4 × 4 Butler Matrix with 45° Phase Shifter . . . 131
4.3.5 Performance Evaluation for the Proposed 45° Phase Shifter Butler Matrix with Antenna . . . 132
4.3.6 Performance Evaluation for the Proposed 120° Phase Shifter 136
4.3.7 Performance Evaluation for the Proposed 4 × 4 Butler Matrix with 45° and 120° Phase Shifters . . . 137
4.3.8 Performance Evaluation for the Proposed 45° and 120° Phase Shifters Butler Matrix with Antenna . . . 138
4.3.9 Performance Evaluation for the Proposed DOA Estimation Algorithm . . . 142
4.4 Summary . . . 148

5 Design of Millimeter-Wave Frequency Micro Strip Smart Antenna with the DENLMS Beam Steering Algorithm 149
5.1 Overview . . . 149
5.2 Proposed Methodology . . . 150
5.2.1 Design of Antenna . . . 151
5.2.2 An Antenna Array . . . 156
5.2.3 Weight Valuation of Beam Steering Antenna based on DENLMS . . . 158
5.3 Result and Discussion . . . 159
5.3.1 Radiation Pattern for 36.75GHz for Different Angle Values . . . 159
5.3.2 Radiation Pattern for 39.75 GHz for Different Angle Values . . . 165
5.3.3 Radiation Pattern for 44.62 GHz for Different Angle Values . 169
5.3.4 Gain and Directivity Examination by Varying Theta (degree) 173
5.3.5 Comparison with Existing State-of-Art Techniques . . . 176
5.3.6 Discussion . . . 181
5.4 Summary . . . 182

6 Design and Fabrication of Elliptical Printed Monopole Antenna with DGS **183**
6.1 Overview . . . 183
6.2 Mathematical Modelling of Elliptical Antenna . . . 184
6.3 Results Analysis . . . 188
6.3.1 Return Loss . . . 188
6.3.2 VSWR . . . 188
6.3.3 2D Radiation Pattern . . . 189
6.3.4 Gain . . . 191
6.3.5 Directivity . . . 192
6.3.6 Radiation Efficiency . . . 192
6.3.7 SCD (Surface Current Distribution) . . . 193
6.4 Fabricated Analysis . . . 194
6.5 Summary . . . 196

7 Conclusion and Future Scope **199**
7.1 Conclusion . . . 199
7.1.1 General Conclusion . . . 199
7.1.2 Research Contribution . . . 201
7.2 Future Scope . . . 202

References **203**

List of Publications **217**

List of Figures

1.1 Requirements of 5G 4
1.2 Architecture of 5G Network 6
1.3 SAS Block Diagram 10
1.4 Block Diagram for SBS 11
1.5 Block Diagram for Adaptive Beam Antenna System 11
1.6 Basic MPA 12
1.7 Various Configuration of MPA 13
1.8 Various Configuration for MSSA 14
1.9 Various Configuration for MTWA 15
1.10 MSA's Radiation Mechanism, (a) Rectangle Patch, (b) Side View and (c) Top View 16
1.11 Microstrip Antenna and its Circuit Equivalent; (a) Microstrip Patch Antenna with a Microstrip Line Feed; (b) An Equivalent Circuit for a Microstrip Patch; and (c) An Equivalent Circuit for a Microstrip Line Feed 17

3.1 Design of Single Element Patch for 28 GHz 51
3.2 Rectangular Patch Antenna at 28 GHz (a) 1 x 2 Array (b) 1 x 4 Array (c) 1 x 8 Array (d) 4 x 8 Array 52
3.3 RL vs. Frequency of Single Element of RPA for 28 GHz 53
3.4 RL vs. Frequency Graph for 1 x 2 and 1 x 4 RPA for 28 GHz . . . 54
3.5 RL vs. Frequency Graph for 1 x 8 RPA for 28 GHz 54
3.6 RL vs. Frequency Graph for 4 x 8 RPA for 28 GHz 55

3.7 VSWR vs. Frequency Graph for Single element, 1 x 2 and 1 x 4 RMPA for 28 GHz 55
3.8 Gain & Directivity vs. Frequency Graph for (a) Single element (b) 1 x 2 Array (c) 1 x 4 Array (d) 1 x 8 Array and (e) 4 x 8 Array of RMPA for 28 GHz 56
3.9 Performance for RPA for 28 GHz (a) single element (b) 1 x 2 array (c) 1 x 4 array (d) 1 x 8 array antenna 57
3.10 Design of Single Element Patch for 38 GHz 59
3.11 RL vs. Frequency of Single Element of RMPA for 38 GHz 60
3.12 RL vs. Frequency graph for 1 x 2, 2 x 4 and 2 x 8 RMPA for 38 GHz 61
3.13 RL vs. Frequency Graph for 4 x 8 RMPA for 38 GHz 61
3.14 VSWR vs. Frequency Graph for Single Element, 1 x 2, 2 x 4 and 2 x 8 RMPA for 38 GHz 62
3.15 VSWR vs. Frequency Graph for 4 x 8 RMPA for 38 GHz 62
3.16 Gain & Directivity vs. Frequency Graph for (a) Single element (b) 1 x 2 Array (c) 2 x 4 Array (d) 2 x 8 Array and (e) 4 x 8 Array of RMPA for 38 GHz 63
3.17 Performance for RMPA for 38 GHz (a) single element (b) 1 x 2 array (c) 2 x 4 array (d) 2 x 8 array (e) 4 x 8 array 64
3.18 Design of Single Element Patch for 60 GHz 67
3.19 RL vs. Frequency of Single Element, 1 x 2, 1 x 4, 2 x 8 and 4 x 8 RPA for 60 GHz 68
3.20 VSWR vs. Frequency Graph for RMPA for 60 GHz 68
3.21 Gain & Directivity vs. Frequency Graph for (a) Single element (b) 1 x 2 Array (c) 1 x 4 Array of RMPA for 60 GHz 69
3.22 Performance for RPA for 60 GHz (a) single element (b) 1 x 2 array (c) 1 x 4 array (d) 2 x 8 array 70
3.23 Slotted MPA at 28 GHz for (a) Single, (b) 1 x 2, (c) 1 x 4, and (d) 1 x 8 73
3.24 RL v/s Frequency Graph for Single Element Slotted MPA 75
3.25 RL v/s Frequency Graph for 1 x 2 array of Slotted MPA 75

3.26 RL v/s Frequency Graph for 1 x 4 Array of Slotted MPA 76
3.27 RL v/s Frequency Graph for 1 x 8 Array of Slotted MPA 76
3.28 VSWR v/s Frequency Graph for Single element, 1 x 2 array, 1 x 4 array and 1 x 8 array Slotted MPA 77
3.29 Gain & Directivity vs. Frequency Graph for (a) Single element (b) 1 x 2 Array (c) 1 x 4 Array (d) 1 x 8 Array of Slotted RMPA for 28 GHz 78
3.30 Radiation patterns for slotted MPA (a) single element (b) 1 x 2 array (c) 1 x 4 array (d) 1 x 8 array 79
3.31 1 x 2 Array Antenna at 28 GHz with the Feed Line Network 81
3.32 MIMO Antennas for 28 GHz with (a) 2 Ports, (b) 8 Ports and (c) Proposed 16 Ports 82
3.33 Return loss for Proposed 2, 8 and 16 Port MIMO Microstrip Patch Antenna 84
3.34 Mutual Coupling for Proposed 16 Port MIMO Microstrip Patch Antenna 85
3.35 Gain & Directivity for Proposed (a) 2 Ports (b) 8 Ports (c) 16 Ports MIMO Microstrip Patch Antenna 86
3.36 VSWR for Proposed 16 Ports MIMO Microstrip Patch Antenna . . 86
3.37 Radiation Pattern for Proposed (a) 2 Ports (b) 8 Ports (c) 16 Ports MIMO Microstrip Patch Antenna 87
3.38 Single Element of RMPA at 60 GHz 89
3.39 RL S11 Simulation Results for Proposed 16 Port MIMO MPA . . . 90
3.40 Insertion Loss Simulation Results for a 16 Port MIMO MPA 90
3.41 Gain and Directivity Simulation Results for a Proposed 16-Port MIMO MPA 91
3.42 Single Port MPA with Dimensions 94
3.43 (a) 2 Port and (b) 4 Port MIMO Patch Antenna 94
3.44 |S11| of the Single Port MPA 95
3.45 S Parameter of the Two Port MPA 95
3.46 S Parameter of the Four Port MPA 96

3.47 Isolation Loss of Four Port MPA 96
3.48 Gain and Directivity of a Single Port MPA 97
3.49 Gain and Directivity of the Two Port MPA 97
3.50 Gain and Directivity of the Four Port MPA 97
3.51 VSWR for (a) Single Port, (b) 2-Port and (c) 4-Port MIMO Antenna 98
3.52 ECC Values from Patterns of Far-Field Radiation 101
3.53 ECC Values from S Parameters 101
3.54 Diversity Gain 102
3.55 MEG_1/MEG_2 and MEG_3/MEG_4 103
3.56 4 Port Slotted RMPA MIMO Design 104
3.57 RL vs. Frequency Graph for single port Slotted MIMO Antenna . . 105
3.58 S Parameter of the Four Port slotted MIMO MPA Antenna 106
3.59 Gain and Directivity of single port of Slotted RMPA 106
3.60 Gain and Directivity of 4 port of Slotted RMPA 107
3.61 VSWR vs. Frequency Graph for single and 4 port Slotted MIMO Antenna 107

4.1 (a)Proposed Micro Strip Patch Antenna Array with 45° Phase Shifter Butler Matrix, (b) Proposed Microstrip Patch Antenna Array with 120° and 45° Phase Shifters Butler Matrix 113
4.2 Micro-Strip Hexagon Patch Antenna with Z-Slot 116
4.3 Proposed 90° Hybrid Coupler 118
4.4 Proposed 0 dB Crossover 118
4.5 (a)45° Phase Shifter, (b)120° Phase Shifter 119
4.6 (a)Proposed 4×4 Butler Matrix with 45° Phase Shifter, (b)Proposed 4×4 Butler Matrix with 120° Phase Shifters 120
4.7 (a)Return Loss of Patch Antenna, (b)3D Radiation Pattern of Patch Antenna, (c)2D Gain Pattern of Patch Antenna, (d)VSWR of Antenna Array 127
4.8 Angle of 90° Hybrid Coupler 128
4.9 (a)Return Loss for 0db Crossover, (b)2D Radiation Pattern for 0 dB Crossover 129

4.10 (a)Angle of 45° Phase Shifter, (b)Return Loss for 45° Phase Shifter 130
4.11 (a)Return Loss 4 × 4 Butler Matrix with 45° Phase Shifter, (b)Transmission Coefficient 131
4.12 Return Loss for 45° Phase Shifter Butler Matrix with Antenna . . . 132
4.13 Bandwidth for 45° Phase Shifter Butler Matrix with Antenna . . . 133
4.14 VSWR for 45° Phase Shifter Butler Matrix with Antenna 133
4.15 3D Radiation Pattern for 45° Phase Shifter Butler Matrix with Antenna 134
4.16 2D Radiation Pattern for 45° Phase Shifter Butler Matrix with Antenna 135
4.17 Angle of 120° Phase Shifter 136
4.18 Return Loss for 120° Phase Shifter 137
4.19 Return Loss for 4×4 Butler Matrix with 45° and 120° Phase Shifters 138
4.20 Return Loss for 45° and 120° Phase Shifters Butler Matrix with Antenna 139
4.21 VSWR for 45° and 120° Phase Shifters Butler Matrix with Antenna 139
4.22 3D Radiation Pattern for 45° and 120° Phase Shifters Butler Matrix with Antenna 140
4.23 2D Radiation Pattern for 45° and 120° Phase Shifters Butler Matrix with Antenna 141
4.24 RMSE for the Proposed Algorithm 143
4.25 RMSE for DOA Estimation Algorithms 144
4.26 The Connection Between the Proposed Algorithm and the Array Element Spacing 145
4.27 The Connection Between the Proposed Algorithm and the Snapshots 146
4.28 DOA Estimation of CLRB, MUSIC, and MVDR 147
4.29 RMSE Graph 147

5.1 Framework of Proposed Methodology 151
5.2 Measurements of Antenna 153
5.3 Measurements of Antenna Array 153
5.4 Geometry of the Antenna 157

5.5 DENLMS Algorithm 159
5.6 Return Loss Measurement 160
5.7 3D Radiation Pattern 160
5.8 Gain Plot for 39.75GHz Frequency 165
5.9 Gain Plot for 44.62 GHz 169
5.10 Directivity of Antenna in 36.75 GHz 173
5.11 Gain of Antenna in 36.75 GHz 174
5.12 Directivity of the Antenna in 39.75 GHz 174
5.13 Gain of Antenna in 39.75GHz 175
5.14 Directivity of Antenna in 44.62 GHz 175
5.15 Gain of Antenna in 44.62GHz 176
5.16 Output Signal 179
5.17 Normalized Array Factor 180
5.18 Mean Square Error 180
5.19 VSWR of the Proposed Antenna 181

6.1 Geometry of the Antenna (a) Proposed Design, (b) Dimension of the Antenna (c) Dimension of the Slot, (d) DGS and (e)-(f) Closer View of the Design 185
6.2 Return Loss Analysis 189
6.3 VSWR Analysis 190
6.4 2D Radiation Pattern Analysis (a, b) E-Plane and H-Plane at 2.4 GHz, (c, d) E-Plane and H-Plane at 3.2 GHz 190
6.5 Gain Analysis (a) at 2.4 GHz and (b) at 3.2 GHz 191
6.6 Directivity Analysis (a) at 2.4 GHz and (b) at 3.2 GHz 192
6.7 Radiation Efficiency Analysis 193
6.8 SCD Analysis (a) at 2.4 GHz and (b) at 3.2 GHz 194
6.9 Fabricated Design (a) Top View (b) Bottom View 195
6.10 (a) Experimental Set-up (b) Anechoic Chamber 196

List of Tables

3.1 Performance parameters for RPA for 28 GHz 58
3.2 Performance parameters for RPA for 38 GHz 65
3.3 Performance parameters for RMPA for 60 GHz 71
3.4 Performance Parameters for Slotted MPA for 28 GHz 80
3.5 Comparison Table for Various Ports MIMO MPA for 28 GHz 88
3.6 Results Gained for Suggested 16 Port MIMO Antenna for 60 GHz . 91
3.7 Comparative Analysis for MIMO Antenna for 60 GHz 92
3.8 Comparative Analysis of Proposed MIMO Antennas 99
3.9 Performance Metrics for a Four-Port MIMO Antenna 103
3.10 Comparative Analysis of Proposed MIMO Antennas for 28 GHz . . 108

4.5 Comparison of RMSE Parameters with Varying SNR Values 144

5.1 Design Specification of the Antenna 154
5.2 Analysis of Antenna for 44.6 GHz 155
5.3 Analysis of Antenna for 36.75 GHz 155
5.4 Analysis of Antenna for 39.75 GHz 156
5.5 Radiation Pattern for 36.75 GHz for Different Angle Values 161
5.6 Radiation Pattern for 39.75 GHz for Different Angle Values 166
5.7 Radiation Pattern for 44.62 GHz for Different Angle Values 170
5.8 Comparison with State-of-the Art Techniques 178
5.9 Comparison with Beam Steering Algorithm 178

6.1 Dimensions of the Antenna 187
6.2 Comparison of Various Approaches based on Monopole Antenna . . 197

Chapter 1

Introduction

1.1 Overview

In the recent decades, wireless telecommunications technology has revolutionized daily life. Mobile portable gadgets provide people in homes, offices, and educational institutions more freedom so that they can communicate with one another wherever they are and whenever they choose [1]. Wireless Personal Area Networks (WPAN), Personal Communications Services (PCS), Wireless Local Area Networks (WLAN), and several more Telecommunication systems that offer stable wireless connections between computers, mobile devices, and consumer gadgets within a limited range, are just a few of the many applications of wireless communication that are currently used in almost every area of life [2].

The antennas used in communication systems are crucial to wireless technology, hence it is necessary to build antennas with higher functionality, improved performance, smaller size, and lower development costs [3]. A device used to effectively send and obtain electromagnetic (EM) waves is called an antenna. An antenna of some sort is required for any radio that can broadcast or receive. Energy from the transmitter is sent to the antenna, which emits it into space as an electromagnetic or radio wave. A comparable antenna takes energy from electromagnetic wave flowing through the receiving end of the circuit and transforms it into an alternating electric current or signal that the receiver can detect. The depend-

ability and quality of communications are directly impacted by how well antennas transmit and receive electromagnetic waves. Whether an antenna is transmitting or receiving determines its function [4-6].

In order to monitor the uncontrollable expansion of wireless technologies, many academics are currently interested in emerging technologies like the Internet of Things and the 5th generation. Although the coverage area has risen, conventional antennas are unable to meet the demands created by this exponential growth in capacity, radio frequencies, excessive demand for signal processing, and space limits. Additionally, the usage of passive antennas wastes a substantial amount of energy, which is a significant co-channel interference component, prompting researchers to look for other solutions to these issues [7-9].

The greatest solution to these issues is thought to be smart antenna technology. It can create a network that is extremely effective, boosting capacity while enhancing quality and coverage [10]. It was also used to describe adaptive array antennas, which have a tendency to produce an adaptive beam by using a focused beam to block out interference signals while directing the intended signal [11]. These antennas are employed in a various applications, containing millimeter waves (mm-wave), RFID, MIMO, and more. These adaptive antennas can be utilized to boost data rates by multiplexing spatially or diversity, or a combination of the two, in communication systems to increase dependability. The algorithm that controls the smart antenna layout is based on the signal processing techniques use specific criteria to fully control the antenna radiation pattern [12]. These adaptive algorithms, to mention a few, reduce the MSE, steer towards a signal of interest, cancel out the signals that caused interfering, or tracing a varying emitter to progress the signal-to-interference ratio (SIR) [13]. A continuous adaptation to an electromagnetic environment that is constantly changing is then made possible by adaptive algorithms.

1.2 Wireless Communication

Wireless communication refers to the transmission of information among two or more unconnected sites. Its application in cellular networks, wireless broadband networks, and the internet was further established when the term "wireless" entered common usage to describe a radio receiver or transmitter [14]. Long distance communication is made possible via wireless communication, which is not possible with the usage of wires or cables. Recent years have seen a surge in mobile connection. As a result, antennas on portable devices are becoming more common. Additionally, connections are required for persons who travel long distances by rail, automobile, or air. Many different antenna designs have been created over time and installed on mobile devices. Another problem for the scientific community is to retain connectivity at high speeds in the face of ambient scatters without the signal becoming garbled [15]. There has been a tonne of study in this area as well. The compactness and throughput of factors like continuous communication have evolved greatly in antenna technology over time.As a result of advancements in antenna technology, wireless communication is now in its fifth generation. Microstrip patch antennas are one of the pioneers in this field, which are needed for planar antenna systems in miniature portable devices for simplicity of fabrication [16]. The current study is an attempt to propose a low cost and effective planar antenna system to sustain connection throughout India while taking dispersion from common objects in the environment into consideration.

1.3 5G and its Requirements

The next significant advancement in wireless communication, known as 5G, is being driven by emerging applications and specialized requirements. Therefore, 5G systems overcome the shortcomings of 4G systems, includes high spectrum efficiency, high data rate, and low latency as seen from figure 1.1.

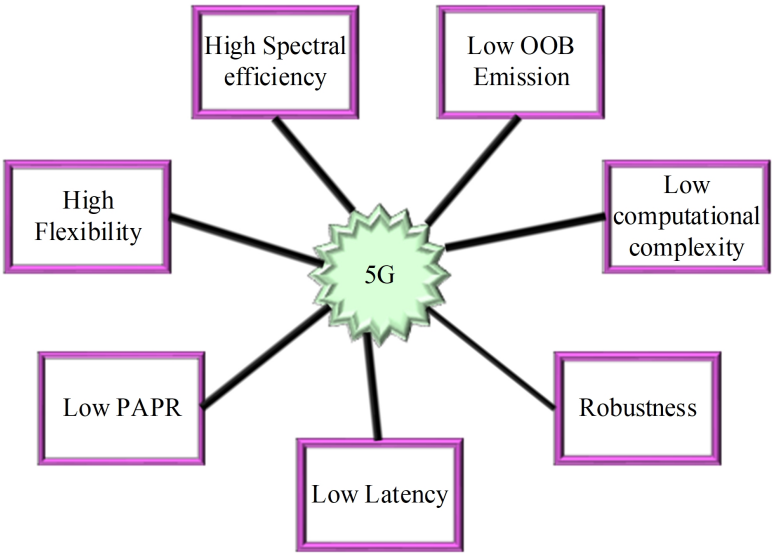


Figure 1.1: Requirements of 5G

The following eight crucial 5G requirements are listed [17]:

- High bandwidth per unit area.
- A roundtrip latency of 1 ms.
- Data rates of 1 to 10 Gbps for actual networks.
- Massive number of connected devices.
- Long battery life
- A decrease in energy consumption.
- A perceived 99.99% uptime.

1.4 Components of 5G Network

The basic components of 5G network such as 5G spectrum, 5G antenna, 5G macro cells, 5G small cells and 5G mm waves are described in the following sub sections.

1.4.1 5G Spectrum

Defragmenting and clearing prime bands should be given priority since 5G calls for a sizable quantity of fresh, harmonized mobile spectrum. To accommodate all use cases and provide network coverage across a larger geographic region, 5G spectrum includes low, mid, and high frequencies [18].

- In order to offer Internet of Things (IoT) services, low-band spectrum (such as Sub-1 GHz) boosts coverage for suburban, urban, and rural regions broadly.
- Mid-bands often provide a nice balance of capacity and coverage advantages. The bulk of marketable 5G networks are said to use spectrum between 3.3 and 3.8 GHz. Other bands that might be allocated to or reformed by operators for 5G contain 2.3 GHz, 1800 MHz, and 2.6 GHz.
- High-band 5G spectrum is being utilized to deliver high throughput services and localised installations at ultra-high broadband rates intended for new-age wireless networks. For instance, offering interior coverage so that industrial IoT can run smoothly. Internationally, the 5G frequencies of 26 GHz, 28 GHz, and 40 GHz are now used extensively.

1.4.2 5G Antenna

Because various applications being developed with 5G technology are based on multiple frequency bands, 5G mobile communication requires a 5G antenna [19]. As a result, several 5G antennas are needed to support various frequency bands. The Advanced Antenna System (AAS), which combines AAS radio and a number of AAS features, will be used by 5G. AAS incorporates beamforming and MIMO, two multi-antenna methods (multiple-input and multiple-output). While the network is being developed, antenna equipment are required to handle all 5G frequencies.

1.4.3 5G Macro Cells

Base stations for small and large (macro) cells with edge computing abilities are used to build 5G networks. These cells may cover a large area and work by utilising the MIMO method that was previously discussed [20]. Use MIMO antennas, which have several components, points, or connections, to broadcast and receive more data concurrently. It will help users connect to the network while maintaining high throughput concurrently. Operators may proactively monitor cell performance for crucial VIP or high ARPU customer's cell tower network locations using their mobile network latency, Cell tower signals, speed, call setup success rate, and other QoE KPIs. The network architecture of 5G shown in Figure 1.2.

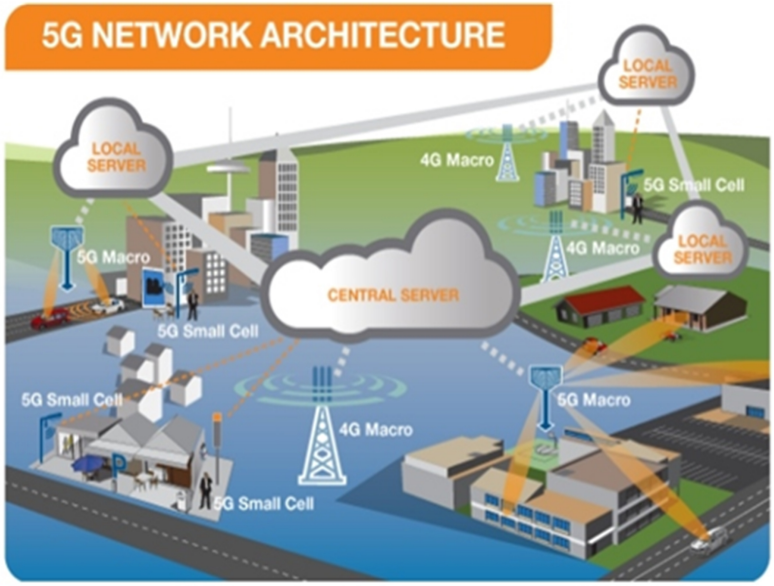


Figure 1.2: Architecture of 5G Network

1.4.4 5G Small Cells

Small cells are being regarded as the cornerstone for next-generation wireless networks since they improve network coverage, capacity, and density, particularly when present inside. For 5G networks, it provides higher capacity without requiring substantial investments in pricey macro sites.

1.4.5 5G Millimeter Wave

5G mm wave is a high-frequency, short-range wave that has the ability to provide large amounts of bandwidth in 5G networks. The European Union's first band for cutting-edge wireless networks, or 5G, is designated as "3.25 GHz" of spectrum in 26 GHz (24.25 - 27.5 GHz) band by UK regulator, OFCOM.

1.5 Antenna used for 5G

There are several type of antennas used in 5G communication. This section categorizes the antenna designs according to the antenna types and input/output ports [21].

1.5.1 Classification Using Input and Output Ports

The antenna can be generically categorized depend on the usage of input and output ports as follows:

1.5.1.1 Single Input Single Output (SISO)

For 5G applications, numerous researchers have created antenna of SISO, which can be a single or multi-component antenna. Designing and implementing the SISO-antenna is modest [22]. Additionally, it is simple to integrate into equipment of 5G communication. A single component antenna's size is greater to attain a high gain. The quality of service suffers and signal propagation losses are larger in the frequency bands over 6 GHz. Therefore, a multi- component antenna must be utilized in place of a single component antenna to get a uniform and good performance. The fundamental purpose of a multi- component antenna is to maximize gain at the expenditure of larger bulk and design complexity.

1.5.1.2 Multiple Input Multiple Output (MIMO)

Radiation losses, fading multipath, and interference are risks to communication without wire. Additionally, at higher frequencies, it gets worse. The use of MIMO

antennas is vital to resolving these problems since it extends the broadcast range deprived of sacrificing signal strength [23]. In order to attain maximum throughput, minimal latency, and high performance, design of MIMO can be employed in 5G. With MIMO, additional signals may be launched intelligently by employing several antennas, significantly expanding the channel's capacity. MIMO is complex, but it has been employed in mobile technology for a long time. MIMO algorithms control where energy is focused in space and how data is transmitted through antennas. MIMO requires precise coordination between the mobile devices and the infrastructure to perform.

1.5.2 Classification Using Different Types of Antennas

Depending on types of antenna, is another significant classification technique. The following are some antenna types that are appropriate for 5G applications, according to the literature:

1.5.2.1 Monopole Antenna

It is composed of a straight, single microstrip line of length $\lambda/4$, where the wavelength of an antenna's resonant working frequency. A monopole antenna's effectiveness is largely influenced by the type of material that makes up the antenna's second half. A condition precedent could be something as simple as an insulated copper fill on the circuitry or a metal enclosure. Because the RF stage is related to the circuit ground, this plane, or the enclosure, is also referred to as being linked to ground. The VSWR and gain of antenna will be strongly influenced by positioning and size of ground plane counterpoise.

1.5.2.2 Dipole Antenna

It includes of dual straight microstrip lines, every measuring $\lambda/4$ in length, with nourishing given in the space among the lines. Consequently, the dipole antenna's overall length is $\lambda/2$.

1.5.2.3 Magneto-Electric (ME) Dipole Antenna [24]

It is made up of a vertically shorted planar magnetic dipole and a planar electric dipole. The lowest side of substrate is used to supply the magnetic dipole.

1.5.2.4 Planar Inverted F Antenna (PIFA)

It is created using ground plane and patch antenna, which is combined using a pin for shorting. While lowest side of substrate helps in feeding. So it utilize a smaller amount of area since it vibrates at a quarter wavelength.

1.5.2.5 Fractal Antenna

It entails of numerous iterations of same structure. An iterative mathematical rule is used in its design. Different shapes, including circle, rectangle, triangle, star, and leaf, are possible for the fractal antenna.

1.5.2.6 Inverted F Antenna (IFA)

It involves a straight portion of microstrip line receives feeding, and a microstrip line having single bend. The feed point is close to bent section, giving the antenna its overall inverted F type appearance.

1.6 Smart Antenna Systems (SAS)

A smart antenna [25] is a communication connection that contains several antenna components on both the transmitter and reception sides. Depending on the function of processing at the transmitter, receiver, or together sides of communication connection, it is split into 3 categories: multiple-input single output (MISO), multiple-input multiple output (MIMO), and single-input multiple output (SIMO). By integrating intervention and the spread of diverse data streams from various antennas, the smart antenna can improve link quality and increase capacity. Utilizing smart antennas in real-time applications has a number of advantages, including increased coverage, reduced power requirements, cheap costs,

improved reliability, and improved spectral efficiency. The direction of arrival estimation (DOA) and beam forming provided by adaptive algorithms are the two core components of SASs. The conventional SAS model is depicted in Figure 1.3.

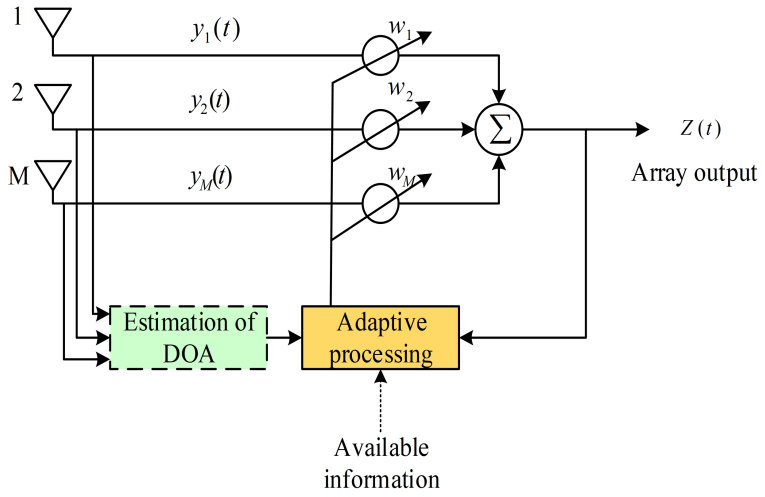


Figure 1.3: SAS Block Diagram

One of the most difficult difficulties for identifying and following multiple moving sources in many contexts, such as radar, sonar, and mobile communications, is the DOA. By determining the DOA of signals from terminal sources, sources can be located using distributed sensor arrays. SAS are classified into two types: switched beam antennas system and adaptive beam antennas system.

1.6.1 Switched Beam Antennas (SBS)

According to the directive antenna with the best received power performance, SBS (Figure 1.4) switches between them. Here, the signal received by each element of the array is given complex weights for determining the number of beams. The strongest beam is then chosen at that point. SBS have been found to either boost radio coverage or capacity by increasing the carrier to interference ratio.

These antenna systems track signal strength, elect one of many fixed, predefined beams, and then switch between them as the user goes around the sector. SBSs unite the outcomes of many antennas in order to create finely sectorized (directed)

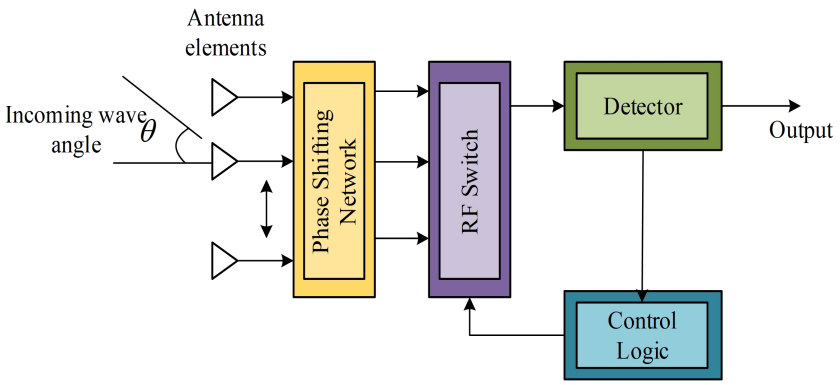


Figure 1.4: Block Diagram for SBS

beams with greater selectivity in spatial than is possible with traditional, single-component methods. This is done without modifying the metallic features and physical design of directional antenna pattern (like a sectorized antenna).

1.6.2 Adaptive Beam Antennas System

The current intelligent antenna strategy is represented by smart/adaptive beam antenna systems (Figure 1.5). The smart adaptive beam antenna system makes use of its capacity to efficiently pinpoint and follow numerous kinds of signals to energetically limit interference and increase targeted signal response using a number of powerful DSP algorithms.

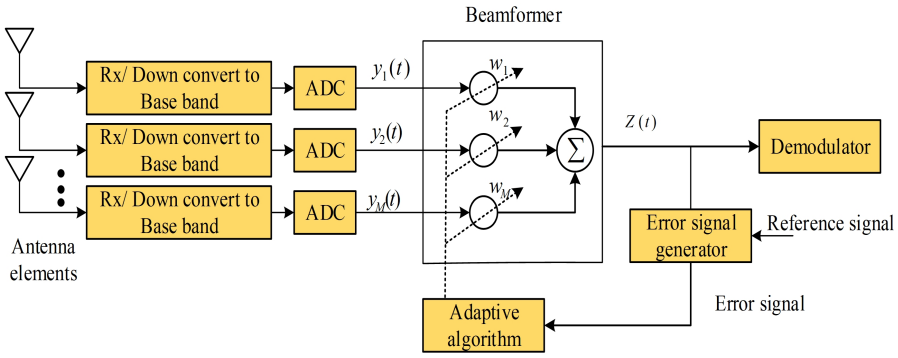


Figure 1.5: Block Diagram for Adaptive Beam Antenna System

1.7 Microstrip Antenna (MSA)

A thin sheet of low-loss insulating material is used as the dielectric substrate to create microstrip structures [26]. The ground plane is the side that is entirely covered in metal, while the printed antenna patterns are on the side that is just partially metallized. The lines for feeding and patch for radiating are typically photo etched onto the dielectric substrate. Microstrip patch antennas (MSPAs) are lightweight, straightforward, low profile, inexpensive, and simple to make. Due to its exceptional qualities, it is one of the most studied and used components in a variety of fields, including mobile radio, radar engineering, military systems, wireless communication, and space communication. The elementary design of a MSPA is presented in Figure 1.6.

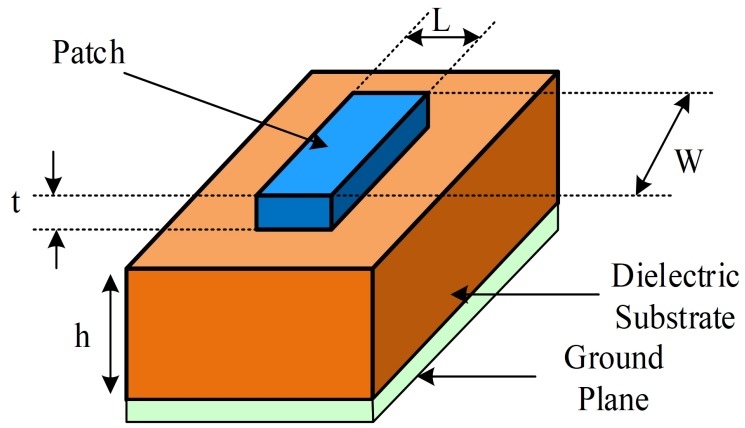


Figure 1.6: Basic MPA

The dielectric substrate serves as the microstrip antenna's mechanical framework. It has a radiating "patch" of metallization that is positioned above the grounded substrate and supplied with energy by a suitable feeding mechanism. Through the concentration of electromagnetic fields, the substrate also performs an electrical function.

1.7.1 Types of MSAs

There are three kinds of MSAs dependent on structure are MSPA, microstrip slot antennas and microstrip travelling antennas.

MSPAs: The ground plane of a MSPA is covered with a rectangle, copper or square patch on a thin dielectric layer known as the substrate. Figure 1.6 depicts the shape of a traditional rectangle microstrip antenna (TRMSA). The several arrangements of microstrip patch antennas are shown in Figure 1.7.

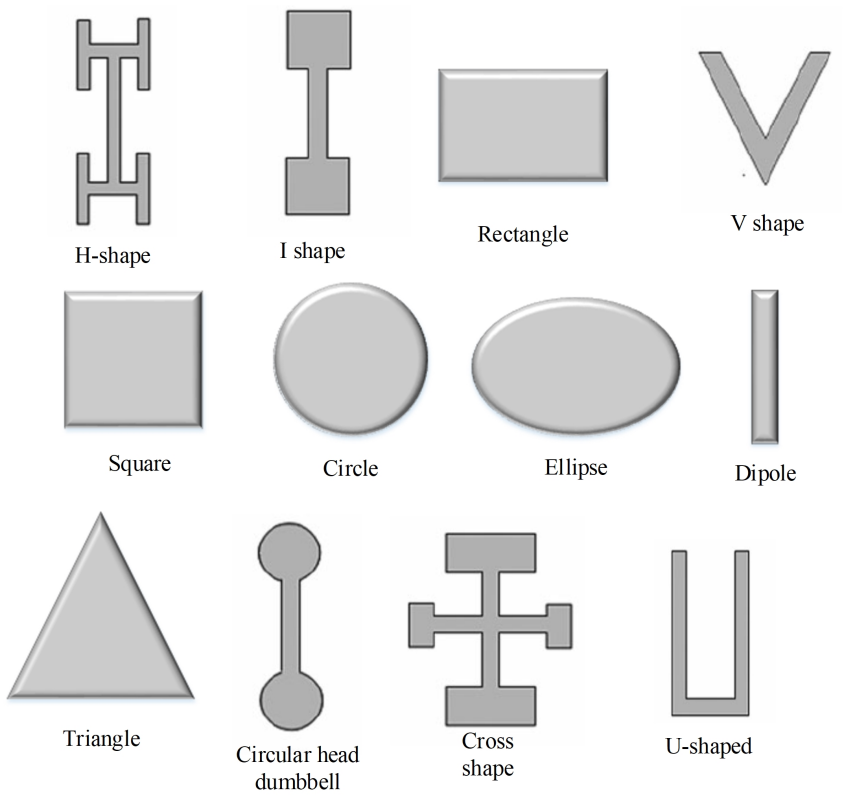


Figure 1.7: Various Configuration of MPA

Microstrip Slot Antennas (MSSA): It has a microstripline-fed slot in the radiating patch. According to Figure 1.8, the slot might be a rectangle, a circle, or an annular ring. Microstrip slot antennas have the benefit of producing both unidirectional and bidirectional radiation patterns. The patch and slot combinations used in MSA design provide an extra level of flexibility. This is so that the

MSAs' slots, which have an important influence on antenna's radiation properties and can radiate independently or in phase with the patch, can do both.

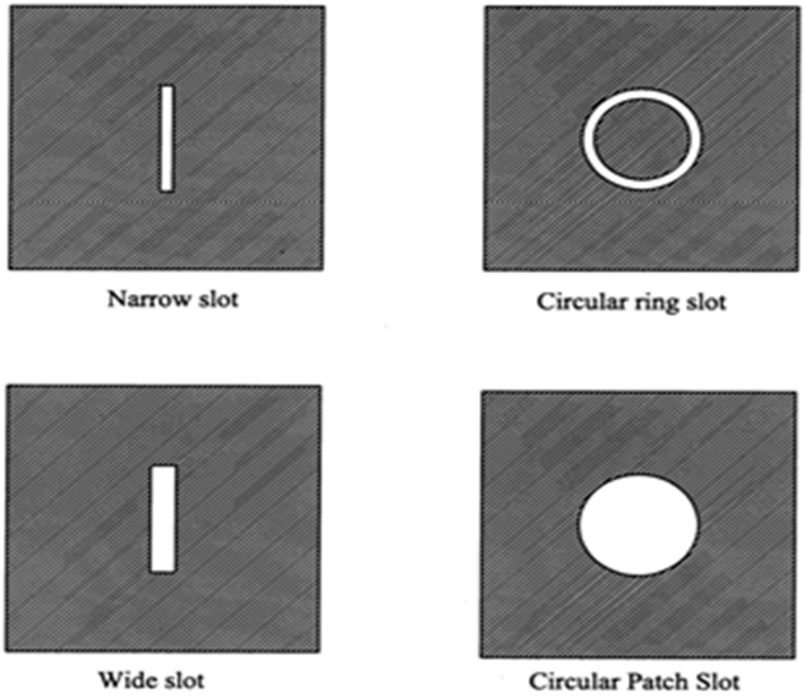


Figure 1.8: Various Configuration for MSSA

Microstrip Traveling Wave Antennas (MTWA): A chain-shaped periodic conductor is one of the antenna's components. It can sustain a TE (transverse electric) mode on a substrate that is supported by a ground plane in addition to being a typical long transverse electric and magnetic (TEM) line. The construction of the antennas may be configured to allow the primary beam to point in any direction, from broadside to endfire, and they also enable travelling waves. The several arrangements of microstrip travelling wave antennas are presented in Figure 1.9.

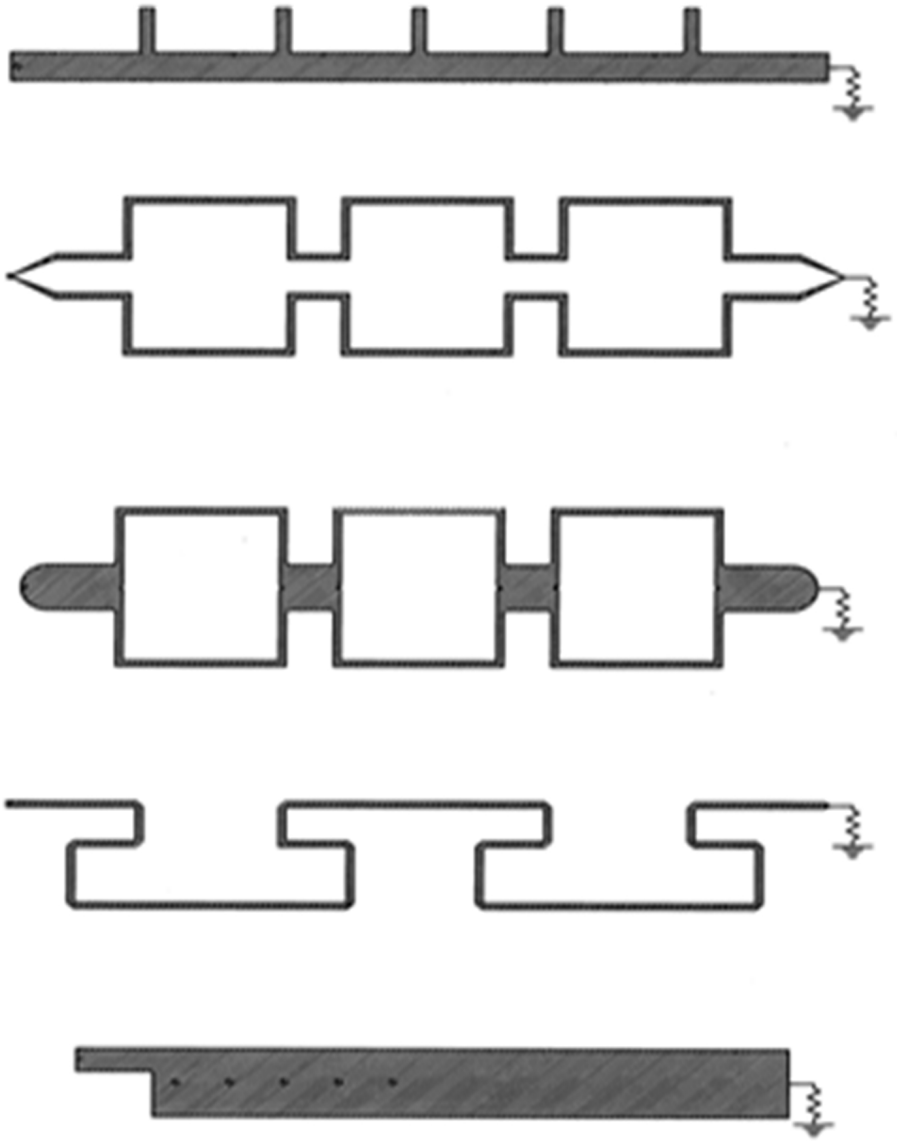


Figure 1.9: Various Configuration for MTWA

1.7.2 Radiation Mechanism of MSAs

The MSA radiation is generated by the fringing fields at the ground plane's and conducting element's margins. Lewin initially checks for microstrip defects in the radiation and current flow in the conductors. Consider the straightforward situation of a rectangular MSPA spaced a tiny portion of a wavelength directly

above a ground plane, as illustrated in Figure 1.10a. This will help to understand the radiation from microstrip antennas.

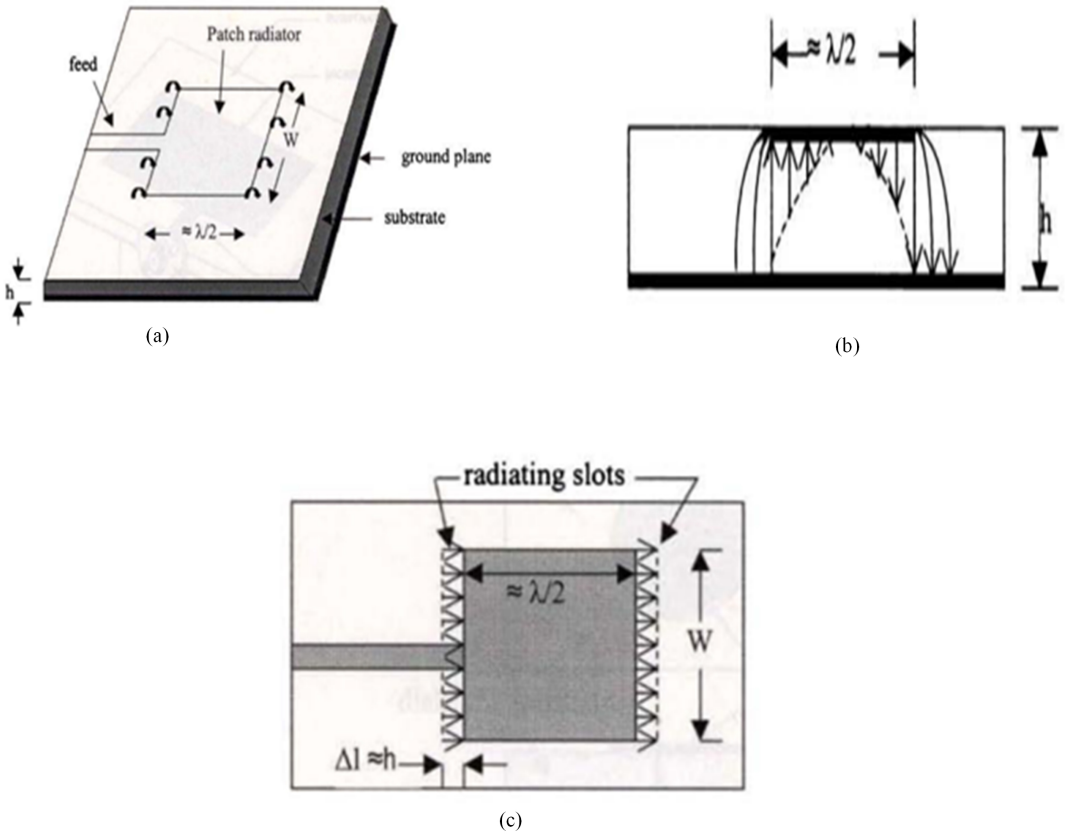


Figure 1.10: MSA's Radiation Mechanism, (a) Rectangle Patch, (b) Side View and (c) Top View

The electric field configuration of the radiator may be described as illustrated in Figure 1.10b, assuming that there are no fluctuations in the electric field throughout the thickness and width of microstrip configuration. The patch length, which is around half a wavelength, varies the fields ($\lambda/2$).

In regard to ground plane, the fringing fields at end may be separated into tangential and normal constituents. The ($\lambda/2$) length of the patch line causes the normal components to be out of phase, which causes the far field they create to cancel in the broadside direction. The resultant fields unite to produce an extreme

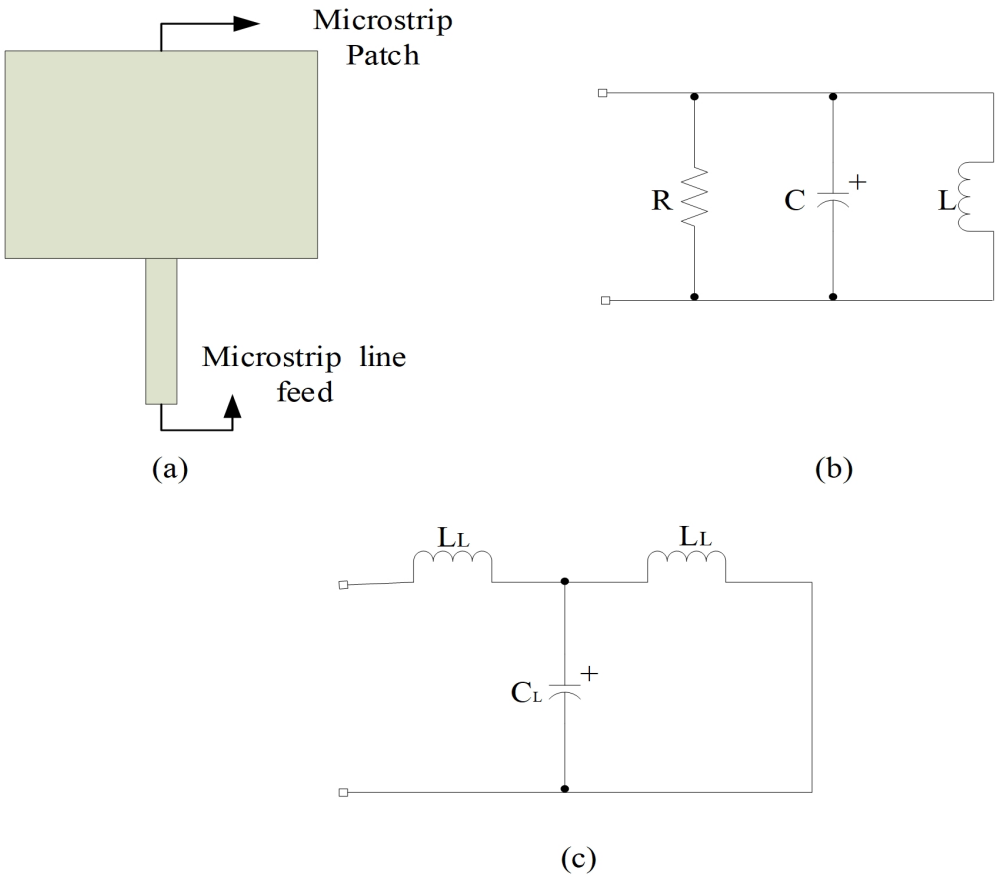


Figure 1.11: Microstrip Antenna and its Circuit Equivalent; (a) Microstrip Patch Antenna with a Microstrip Line Feed; (b) An Equivalent Circuit for a Microstrip Patch; and (c) An Equivalent Circuit for a Microstrip Line Feed

radiated field normal to surface of the structure because the tangential components are in phase.

As shown in Figure 1.10 c, the patch might thus be signified by 2 slots spaced ($\lambda/2$) apart, active in phase, and radiating in the half space directly above ground plane. The equivalent circuit of the MPA is shown in figure 1.11

1.7.3 Design considerations for MPA

To guarantee performance and efficiency, a microstrip patch antenna's design must take into account a number of crucial factors. The following are some important

design factors for a microstrip patch antenna:

- **Substrate:** The MPA's performance depends greatly on its substrate material. Low loss tangent, a low dielectric constant, and excellent thermal stability should all be present in the substrate. The substrate materials that are most frequently utilised are FR-4, Rogers, and Duroid.

- **Patch size and form:** The patch's size and shape influence the antenna's resonance bandwidth, frequency, and radiation properties. Dependent on the requirements of application, the patch may have a square, rectangular, circular, or elliptical form. To obtain the specified performance criteria, the patch's size needs to be optimised.

- **Feed mechanism:** The MPA's feed mechanism need to effectively link the transmission line and the patch. Coaxial probe, microstrip line, and aperture-coupled are typical feed methods.

- **Size and geometry of the ground plane:** These factors have an impact on the antenna's emission pattern, impedance matching, and polarisation. In order to reduce edge effects and create a low-loss, high-quality RF ground, the ground plane should be developed.

- **Bandwidth and frequency:** The MPA can be created for a particular frequency range, such as 5.8 GHz for satellite communication or 2.4 GHz for Wi-Fi. To obtain a broad working range and effective impedance matching, the antenna's bandwidth should be tuned.

- **Radiation effectiveness:** The MPA's radiation effectiveness is crucial for minimizing power loss and enhancing communication range. To attain a high efficiency, the design should take the antenna's radiation efficiency into account and optimize the size and feed mechanism.

- **Antenna array:** To maximise the gain, directivity, and coverage area of antenna, the MPA can be set up in an array configuration. To obtain the

intended performance, the array design should take the components' spacing, phase, and amplitude into account.

1.7.4 Different types of Microstrip Patch Antennas (MPAs) and its Advantages

In this research used different type of microstrip patch antenna for various objectives of research. The following are patch antennas used in this:

1.7.4.1 Rectangular MPA (RMPA)

The most typical kind of MPA is this one. It comprises of a ground plane-top placement of a rectangular patch produced on a dielectric substrate. The size of patch and substrate affect the antenna's resonance frequency. It comprises of a rectangular conducting material patch produced on a dielectric substrate that is commonly constructed of copper or aluminium. A coaxial cable or microstrip transmission line attached to a feeding point on the patch feeds the patch. It has a basic design, is cheap, and is simple to integrate with other electrical components. The advantages of RMPA are: simple to manufacture and incorporate with other electronic parts, simple and inexpensive design and narrow beamwidth and high gain.

1.7.4.2 Slotted Rectangular Patch Antenna

For improving performance, slots are carved into the patch in the RMPA variation recognized as the slotted RMPA (S-RMPA). On the patch, the slots are typically arranged in the shapes of a cross, T, or L. With the help of the slots, the antenna's bandwidth, surface wave losses, and polarization purity may all be improved. In contrast to the standard rectangular microstrip patch antenna, it can operate across a larger bandwidth. This is brought on by the slots' improved radiation resistance and decreased surface wave losses.

1.7.4.3 Hexagonal Patch Antenna

The hexagonal MPA is a hexagonal version of the RMPA. It has comparable benefits to the RMPA, such as a straightforward design, low price, and straightforward integration with other electrical parts. Yet, it has several further benefits over the RMPA, such as a larger bandwidth and a smaller dimension.

1.7.4.4 Circular Microstrip Patch Antenna

This kind of antenna has a dielectric substrate with a circular patch printed on it. In situations when circular polarisation is required, it is employed. It is made out of a circular conducting patch, usually made of copper that has been etched into a dielectric substrate like fibreglass or polyimide. A coaxial cable or microstrip transmission line linked to a feed point in the patch's centre typically feeds the patch.

An electromagnetic field emanates from the antenna from the circular patch, which serves as a resonator. The frequency at which the antenna resonates is calculated by the size of patch and its position in relation to the ground plane. The patch's circular form offers a wide bandwidth and favourable radiation properties, making it a desirable option for many wireless applications. The advantages of circular MPA are:

- Provides circular polarisation for radiation with omnidirectional patterns.
- Simple to manufacture and incorporate with other electronic parts.
- Low profile and compact dimensions.

1.7.4.5 Elliptical Microstrip Patch Antenna

An elliptical patch is printed on a dielectric substrate to create this kind of antenna. When circular polarisation is required, it is employed in certain applications. Compared to circular patch antennas, it has a more compact size because to its elliptical design.An etched conducting patch on a dielectric substrate, such

fibreglass or polyimide, makes up the antenna. A coaxial cable or microstrip transmission line linked to a feed point in the patch's centre typically feeds the patch.

The patch's elliptical form has a few benefits over its circular version. For instance, compared to a circular patch of the same size, it can offer a larger bandwidth and greater gain. A polarised radiation pattern that is more directed than the pattern created by a circular patch may also be created using an ellipse shape. Elliptical microstrip patch antennas provide the following benefits over certain other popular types:

- **Larger Bandwidth:** In comparison to rectangular and slotted RMPAs, which have a narrower bandwidth, elliptical MPAs can offer a greater bandwidth.
- **Greater Gain:** In comparison to circular microstrip patch antennas, which have a lesser gain, elliptical microstrip patch antennas can offer a higher gain.
- Elliptical microstrip patch antennas feature a more focused radiation pattern compared to circular MPAs, which emit radiation in all directions.
- **Small Size:** In contrast to hexagonal microstrip patch antennas, which need a bigger space, elliptical MPAs can provide a compact size.

1.7.5 Designing Models

The many MPA design models can be roughly categorized into the following:

- **Transmission Line Model:** It is the utmost basic theoretical method of analysing a MPA. Munson has released the original transmission line model [4]. In this model, the space among the patch borders and ground plane at each end of line is treated as two parallel radiating slots with dimensions of L, W, and h.The design employed the following calculating process[112].
  -The antenna's width (W) is estimated as follows:

$$W = \frac{c}{2f\sqrt{\frac{\varepsilon_\gamma + 1}{2}}} \tag{1.1}$$

- The effective dielectric constant ε_{ref} calculation:

$$\varepsilon_{\text{ref}} = \frac{\varepsilon_\gamma + 1}{2} + \frac{\varepsilon_\gamma - 1}{2}\left(1 + 12\frac{h}{W}\right)^{-1/2} \tag{1.2}$$

- Measurement of the patch's effective length (L_e):

$$L_e = \frac{c}{2f\sqrt{\varepsilon_{ref}}} \tag{1.3}$$

- Calculating the length extension (ΔL):

$$\Delta L = 0.412h\left[\frac{(\varepsilon_{\text{ref}} + 0.3)\left(\frac{W}{h} + 0.26\right)}{(\varepsilon_{\text{ref}} - 0.258)\left(\frac{W}{h} + 0.8\right)}\right] \tag{1.4}$$

- Measurement of patch's real length:

$$L = L_e - 2\Delta L \tag{1.5}$$

Where, ε_r is dielectric constant of substrate, light velocity is c, f is operating frequency, and h is patch's height.

- **Finite Different Time Domain Technique (FDTD):** In this model, suggested a three-dimensional difference approximation for the Maxwell's curl equation that accounts for both space and time.

- **Cavity Model:** The cavity model proposes that MPA is a cavity with two electric walls and four perfect magnetic walls around it. It is permitted for the magnetic currents at the cavity's boundaries to radiate into space since it is presumed that they are uniformly distributed.

The transmission line model is the most popular and straightforward to use of these models since it offers strong physical understanding.

1.7.6 Advantages of MPAs

In comparison to traditional microwave antennas (TMSAs), the MPAs are more advantageous and have applications across a wide frequency range [27]. The following are some profits of MPAs versus TMSAs.

- Light weight, low profile, and minimal volume in a planar arrangement.
- The price of fabrication is cheap.
- It can be organized in a big array with half-wavelength spacing.
- The antenna is simple to attach to satellites, rockets, and missiles.
- Its scattering cross sections are smaller.
- Both circular and linear polarisations are acceptable.
- The antennas can operate on two, three, or more frequencies.
- It is not necessary to use cavity backing.
- Simple to feed (coaxial cable, microstripline, etc)

1.8 Research Gap and Motivation

For many wireless applications, researchers have recently been focused on constructing an efficient antenna. With the elimination of mm-wave frequency, there are significant obstacles in constructing the 5G wireless antenna. When doing antenna design, it's crucial to consider the quality of the antenna, the dependability of the bandwidth, and the reduction of multipath fading. In addition to the standard sub-6-GHz range, mmWave spectrum over 24 GHz is required for the 5G system since it offers significantly more signal capacity than the existing cellular bands. For 5G applications, an antenna array using beam steering capabilities in pattern of radiation is necessary. In order to create microstrip antennas that work with Wi-Fi and WiMAX applications, researchers must overcome many

challenges. However, it has a number of good limitations that make it difficult to satisfy demands and use antenna skills. Since the MPA with beam steering has such great results in wireless communication for 5G spectrum applications, many researchers are interested in constructing one. In building a MPA dependent on a beam steering technique, only auxiliary tests were conducted. Designing a better antenna is urgently needed for the next generation's effective communication. Despite the introduction of peripheral techniques, significant limitations including high radiation emission and bandwidth needs also exist. These flaws motivate us to create a clever design of antenna for communication systems.

Research has mainly concentrated on improving spatial reuse, link quality, coverage, and capacity of air interface, as well as decreasing the interference between channels instigated by fading of multipath in wireless communication systems, as the usage of smart antenna technology has motivated significant attention to performance and efficiency. The two kinds of antenna are switching beam and adaptive array. The switched-beam array antenna can be simulated more easily and simply than an adaptive array antenna, and it offers simpler network administration, cheaper costs, less complexity, and higher mobility, boosting capacity and coverage. Switched-beam array antennas are utilized in systems for communication because of their many benefits, including increased signal-to-noise ratio and strong spatial directivity. A radio frequency (RF) phase shifter is employed to dynamically alter the phase of antenna components in order to direct the narrow pattern of beam of a phased array antenna in path of the desired signal. The drawbacks of these methods include high crossover levels, limited bandwidth, low efficiency, complicated manufacturing, a sizable power distribution network dimension, and a complex feeding structure as the number of necessary beams rises. Butler matrix problem was solved using a small-circuit design with wideband performance. Despite being relatively small, the suggested phased array antenna system cannot be used with a 2-D phased array antenna system due to its very complex design.

1.9 Scope

The main scope of this thesis study is to create several smart antenna techniques for mm Wave frequencies for 5G, which can send and receive signals. In this, microstrip smart antennas for 5G, switched beam antenna using butler matrix while MPA with beam steering algorithm are designed for increasing the gain.

1.10 Research Objectives

- To Design and simulate Phased array and MIMO structure of Rectangular microstrip patch antenna at millimeter frequency application to advance the antenna performance like gain and bandwidth.
- To Design a switched beam antenna for switched beam applications utilizing a butler matrix at millimetre wave frequencies where butler matrix use for beam forming network.
- To Develop DENLMS beam steering procedure to calculate weight evaluation for beam steering based on various angles for Interferer and intended user.
- To Design and fabricate elliptical printed monopole antenna with a defected ground structure (DGS) for 5G.

1.11 Research Methodology

Modelling and Simulation

- Antenna design and its simulation is done by using IE3D and HFSS
- Algorithms developed in the objectives is done by using MATLAB.
- Measurement of the antenna results is done using Vector network analyzer.

1.12 Thesis Outline

Chapter 1: Introduction

This chapter provided the information of antenna for wireless communication, 5G requirements and the brief description for various types of antennas along with detailed description about microstrip antenna and its types along with design shapes.

Chapter 2: Literature Survey

This chapter gives reviews of various recent research papers based on antennas for 5G, phased array antenna, butler matrix, and algorithms. Also, this chapter described about the advantages as well as disadvantages shown by reviewed papers.

Chapter 3: Microstrip Antenna at mm Wave for 5G

This chapter discussed about the designing of microstrip antenna at mm wave for 5G based on various configurations of Phased array and MIMO antenna. Result analysis also included in this chapter.

Chapter 4: Switched Beam Antenna using Butler Matrix at mm-Wave Frequency

In this chapter discussed about the switched beam antenna using butler matrix and estimation of the DOA at mm-wave frequency . Additionally results and comparative analysis also included in this chapter.

Chapter 5: Design of Millimeter-Wave Frequency Micro Strip Smart Antenna with the DENLMS Beam Steering Algorithm

This chapter discussed about the design of a millimeter-wave frequency microstrip smart antenna utilizing the DENLMS beam steering procedure. The evaluation analysis are also provided in this chapter.

Chapter 6: Design and Fabrication of Elliptical Printed Monopole Antenna with DGS

This chapter discussed about the design and fabrication of elliptical printed monopole antenna with DGS for 5G. Also included the comparative analysis of simulated and measured parameters.

Chapter 7: Conclusion and Future Scope of Research

This chapter discussed about the conclusion of the thesis work based on four objectives presented and the major research contributions of the thesis. Also future scope for this research topic also provided.

1.13 Summary

This chapter discussed about the role of antenna in wireless communication, 5G and its requirements, components of 5G network, type of antennas used in 5G, and detailed information about microstrip antenna. Additionally, research gap and motivation, scope, objectives, highlights, contributions and thesis organization for this research work are provided. Finally the chapter concluded with summary.

Chapter 2

Literature Survey

2.1 Overview

Nowadays, communication with the people of this generation can be accomplished by the way of telecommunication. Radio communication, which makes use of radio frequency as a means of communication, is one of the fundamental models of telecommunication. With regard to its hardware architecture and functional capabilities, this method of communication experienced substantial change [28]. In many fields, including transportation, business, and education, mobile communication and wireless communication systems are important [29]. Future wireless communication systems are expected to be built with greater bandwidth and transmitting rates, and they will only be able to operate in millimeter-wave frequency bands. Smart antennas with increased efficiency, optimal size, and other effective qualities should be developed based on the overuse of wireless communication systems [30].The beam antenna system includes an essential component called the beam-forming network. The major purpose of the beamforming network is to distribute phases and provide varying power levels in order to adjust beam directivity [31].This chapter covered the numerous techniques based on 5G communication using lower band & high mm band, phased array antenna for 5G communication, MIMO antenna, smart antenna with butler matrix and smart antenna using algorithms are examined.

2.2 Antenna for 5G Communication using Lower Band & High mm Band

Ata et al. [32], had designed a rectangular patch antenna of double U-slot will enable applications in ultiband. With the use of the [A] matrix formulation, the corresponding circuit of a U-slot patch was shown, and return loss was mathematically determined. The microstrip antenna with a transmission line feed was designed using CST Microwave Studio software, which was also used to analyze return loss and radiation patterns. An internal printed board CNC machine was used to construct the antenna, and a portable network analyzer was used to measure and compare the return loss. A lab antenna measurement device was used to measure the radiation patterns. The constructed antenna was mounted on a network access point and tested in terms of average power against range of distance.

Yang & Zhang, [33], had demonstrates a shared-aperture dual polarization antenna scheme in high-efficiency with a broad frequency range for use in 5G wireless communication systems. This method can achieve beam scanning in with a small gain decrease at Sub-6 GHz from 3.2 to 3.45 GHz and decrease the lens outline with great gain to steer in from 25.5 to 29.5 GHz. The antenna's gain can reach 9.0 dBi in the Sub-6G range and 19.31 dBi in the mm-wave band. The suggested antenna system's measurements and simulations were shown as examples of the properties of the antenna system. WAIMS for a Sub-6 GHz antenna array can be employed with the suggested flat lens because it was a pure dielectric structure. A dual-polarization, small dual-band, shared-aperture multiple antenna framework can therefore achieve beam steering ability in the Sub-6 GHz band and mm-wave with high aperture reuse efficiency and aperture efficiency (77.5% at 28 GHz).

Ullah et al. [34], had suggested antenna system spans the entire spectrum of possible frequencies for 5G communications, spanning a wide range of frequencies from 20 GHz to 65 GHz. Even though single element type-F had positive qualities including low weight, wide bandwidth, ease of fabrication, and consistent radiation patterns, it was not favored for 5G applications since it exhibits lower gain values

at the desired frequencies of 60 GHz, 38 GHz, and 28 GHz, respectively. The single element that was suggested were divided into two, four, and eight elements in an effort to obtain the needed gain values for 5G applications. While gain outcomes were enhanced at the targeted frequencies with the eight-element antenna design, better values were attained by adding a FSS. At 60 GHz, 38 GHz, and 28 GHz, respectively, the suggested eight-element antenna with FSS had good measured gain values of 11 dB, 12 dB, and 15dB. The suggested design was constructed, and measurements showed promising results.

2.3 Slotting techniques in Microstrip Patch Antenna

Srivastava et al. [107], had suggested the system utilizes a cutting-edge method that increases gain and bandwidth to a significant level concurrently. By including slots in the suggested RMPA, often denoted as the slotted array approach, they had attempted to get around these restrictions. The planned antenna was intended to operate at a frequency of 9 GHz, which was in the electromagnetic system's X-band. HFSS software was used to model it over the RT Roger/duroid 5880 material, which had a 2.2 dielectric constant. The RMPA had 425.2 MHz bandwidth, whereas slotted RMPA had a 920 MHz bandwidth, resulting in a 494.8 MHz increase in bandwidth.

Goshu et al. [108], had proposed microstrip patch antenna array for 5G broadband applications (8x8, 4x4, and 2x2) with semi-elliptical form etched ground structure and slotted patch was presented. The Rogers 5880 substrate, with a dielectric constant of 2.2 and a thickness of 0.3449 mm, was used to design the antenna's radiator element. It was intended to function in the LMDS spectrum at 28 GHz. The CST-MW simulator was used to evaluate the proposed structure's performance. According to the simulation results, the bandwidth, gain, and overall effectiveness of the investigated 2x2, 4x4, and 8x8 MPA arrays are 13.24 dBi, 16.54 dBi, and 21.45 dBi; 1.33 GHz, 1.461 GHz, and 1.561 GHz; respectively, and they are 97.03%, 81.72%, and 69%. Similarly, the system return losses are 22.678

dB, 40.665 dB, and 43.321 dB, respectively. Overall, compared to previous efforts, all of the suggested planar semi-elliptical slotted rectangular MPA arrays perform better and satisfy the antenna criteria for 5G systems.

Hussain et al. [109], had proposed a work to analyses dual band and one band communication at higher frequencies using a microstrip patch antenna as a communication instrument (mm-waves). Because of its straightforward design, compactness, low cost, and compatibility with circuit components, microstrip patch antenna is chosen. In this study, a dual band U-shaped slotted Microstrip patch antenna having operating bands at 28GHz and 38GHz is given. The Rogers RT 5880 substrate, which had a dielectric constant of 2.2, was utilised to design the antenna, which had a total area of 8.5x8x0.254 mm3. At 28GHz and 38GHz, respectively, the antenna produced return losses of -32dB and -40dB. The proposed dual band's simulated gain is 6.7 dB at 28 GHz and 7.92 dB at 38 GHz.

Nahas, [110], had suggested microstrip patch antenna was made to function at 26 and 28GHz, the first and most popular 5G frequency bands. In this work, a single rectangular patch, which is frequently used in other 5G antennas, is combined with a variety of different slot shapes in order to improve the gain and other radiation properties of the antenna. The findings demonstrate that a very high gain can be obtained by putting a square slot and two symmetric L-slots in the middle. The CST Studio Suite simulator was used to simulate and optimize the slot size. The suggested antenna has directivity and higher gain, extremely good VSWR and efficiency, and a relatively big enough bandwidth at the two resonance frequencies taken into consideration, according to a comparative research that was also carried performed.

2.4 Techniques based on Phased Array Antenna for 5G Communication

Yang & Zhang, [35], had suggested wide-angle scanning capabilities with dual-polarized phased array antenna were given. A current cancellation method (CCM) was suggested to increase the mutual coupling in the array by altering the existing

distribution on the stimulated unit to bring a group of the cancelled currents on the neighboring unit. This technique can also reduce the inter-unit distance for wide-angle scanning and optimise the array unit size. To test the suggested approach, a low-profile dual-polarization antenna that operates in the 4.4 to 5.0 GHz frequency range was created as both a planar array and a linear array. Whether the array was linear or planar, the mutual coupling was lower than -19 dB, which was superior to that of conventional arrays. The array antenna unit can emit a pattern of wide-beam in a meanwhile. For both polarizations, two arrays can scan over around 60 degrees. Realized gain reduction throughout the scanning range was less than 3 dB, and side-lobe level was less than -7.5 dB. Two array antenna prototypes were constructed and tested due to authorize the performance. The results of the experiment and the simulation match perfectly.

Chieh et al. [36], had described the design and creation of two Ku- and Ka-band radio frequency integrated circuits (RFICs) using 5G Silicon radio frequency arrays (PAAs). First, a scanning X-/Ku-band wideband dual circular polarised Transmit (Tx)/Receive (Rx) phased array antenna was introduced. Within the X/Ku-Bands, the operating frequency was centred at 12.5 GHz (3dB Axial Ratio (AR) bandwidth at broadside = 32 %). The 16-element array was laid out in a 4 by 4 lattice. The axial ratio (AR) bandwidth was improved by this array's use of a stacked sequential rotation architecture. The second topic discussed wasa dual slant linear polarisation Tx/Rx phased array antenna that functions in the Ka-Spectrum and gives the millimeter-wave 5G band (27.5-28.35 GHz). The beam scanning range in both polarizations was up to . The active beamforming networks (BFN) using 5G silicon Tx/Rx beamformer RFIC chips had been combined with the array apertures. Results from simulations and measurements of performance generally agree. In order to provide a greater gain for applications like 5G communications and SATCOM (Satellite Communications), these arrays can be scaled up to bigger sizes.

Zhang et al. [37], had proposed a dual-polarized scanning phased array antenna with leaky-wave improved lenses operating at 28 GHz. An antenna of this type can be utilized for point-to-point 5G communications that demand wide band-

width, high gain, and constrained steering ranges. The causing grating lobes were suppressed by directed and steerable array element patterns, and the suggested array had a periodicity of two wavelengths. Leaky-wave antenna were considered in plastic and printed circuit board were used for the lenses to attain a low-profile and low-cost outcome. To increase the array element aperture efficiency, the lenses in the nearest region of the feeds were optimized.

Yang et al. [38], had suggested a wide-angle scanning capabilities for mobile communication systems with wide-band phased array antenna. Each array element's substrate had an air cavity suitably inserted underneath it. By enhancing WAIM and taking into account the beam-width of array elements, this approach was incredibly straightforward and can effectively improve wide-angle scanning performance. With the suggested strategy, the operating bandwidth was also increased. Both the planar array and the linear array antennas (on large ground planes in detail) were used to analyse and verify the wide-angle scanning capacity. It was shown that one planar array and two linear arrays can accomplish beam scanning of about with realized gain reductions of 3.5 dB throughout a wide working bandwidth of 37.4 %.

2.5 Techniques based on MIMO Antenna

Wei & Geyi, [39], had proposed an eight-element MIMO smart antenna system with two distinct array modules for handheld devices. In order to support 5G, the initial module was six-element array that operates in the N78 (3.3–3.8 GHz) band and supports MIMO functionalities for receiving and beam scanning for sending. In the LTE/WWAN/N78 (0.7-0.91 GHz, 1.63-2.61 GHz, and 3.3-3.8 GHz) bands, the next module was a two-element antenna array. The first module's six elements and the second module's two elements are merged to create an array of 8-element in the intersecting N78 band, which maximizes the use of the mobile device's available antenna resources. When using the receiving mode, L-shaped slots for the combined module are loaded to produce good isolations and envelope correlation coefficients. It was necessary to identify the ideal ODEs for the configuration of

fixed antenna array in order to attain the highest gain in a preferred way in order to implement the beamforming function in the transferring mode according to current MIMO antenna array considered in the receiving mode. The MMPTE will be used in the sections that follow to calculate the ODE.

Baghel et al. [40], had provided a fundamental understanding of various MIMO antenna systems for 5G communication in the future. First, the performance characteristics of single element and multiple element antenna systems had been contrasted. The research clearly shows that adding more radiating parts improves the system's performance. On the basis of physical design, performance analysis, and various methodologies for system performance improvement, the design methodology for the MIMO antenna system had been discussed. Comparative analysis of the architecture and channel capacity of SISO and MIMO antenna systems had been published. Methods for beamforming antenna arrays are highly helpful for increasing system throughput while minimising mutual interaction.

Hussain et al. [41], had presented a CP MIMO antennas with wideband operation and a fifth-generation (5G) communication system MIMO configuration. A 2 x 2 periodic square of metallic plates and a truncated corner patch make up the antenna's meta-surface (MS). The unique aspect of this scheme was radiating components (MS and radiator) are printed on a dielectric substrate single layer, ensuring the antenna's low-profile and affordable properties while preserving high gain and wideband capabilities. Surface waves along the MS are used to realise wideband CP radiations, and the radiation mechanism was detailed in detail.

Khan et al. [42], hadexamined the performance of MIMO antennas requires a considerable deal of consideration of the isolation between microstrip patches. The patch antennas are mounted on top of a substrate made of Rogers RO3003 that was 1.46 mm thick, 60 mm long, 50 mm wide, and had a relative permittivity of 3. Two coaxial probes that had been extended from the bottom ground layer are used to excite the resonators, which are separated by 0.06. To achieve high isolation, the H-shape slot flawed ground structure was introduced on the bottom ground layer (mutual coupling reduction). The suggested MIMO antenna functions at a frequency of 5.3 GHz, which was suitable for WiMAX, Wi-Fi, and upcoming

5G services worldwide.A high-frequency structure simulator (HFSS) that uses the finite element approach had been used to model the outcomes of the intended structure.

Kirik & Hamamreh, [43], had presented a data transmission technique called ISS-MIMO-ANM-AAS to protect transmission schemes against eavesdropping attacks or share confidential data among two communication parties in circumstances where perfect secrecy and absolute confidentiality are essential to be attained. The recommended scheme aims to mix the data that the eavesdropper receives by an ISS with the original signal in order to prevent any potential wiretapping activities. Data was transmitted to the authorized receiver by utilising the features of MIMO-ANM by transmitting other data bits with the amount of active antennas in addition to those bits sent by using conventional M-PSK/QAM modulation. The suggested ISS-MIMOANM-AAS method's effectiveness was demonstrated by the conducted theoretical analysis and the produced numerical simulations, where MIMO-ANM broadcast was shown to be completely safeguarded by the ISS method.

2.6 Techniques based on Smart Antenna with Butler Matrix

Suryana & Munir, [44], had created a switched beam antenna with a 4×4 Butler matrix. Here, the butler matrix had formed on a FR4 epoxy dielectric substrate with a thickness of 0.8mm and a physical dimension of 136.4. In a wireless communication system, the interferences brought on by the high fluctuations limited the capacity of mobile networks. Multibeam antennas were used as a solution to this issue. A vector network analyzer was utilised to simulate this antenna. The highest frequency that could be obtained in this experimental setup was between 2.15GHz and 2.54GHz. However, this approach held up thanks to the 4×4 Butler matrix's reconfigurable properties.

Wen et al. [45], had developed the array design for a switched-beam wideband antenna. Four end-fire antenna elements and a single layer 4×4 butler matrix

were employed in this hybrid approach. The compact coupler approach achieved a bandwidth of more than 58% according to the theoretical study. The wideband switched beam antenna controls the beam in the bandwidth regions of 1.98GHz to 3.14GHz for beam changing. Using the HFSS tool, this antenna's simulation was carried out. The maximum gain realised in this experiment was around 5.5dB. The broader bandwidth for continuous beam scanning, however, hurt the technology.

Roy et al. [46], had proposed the switching beam antenna's detailed design. The model was validated using the 4×4 Butler matrix and planar microstrip technology. The beam-forming network was built using the 4×4 matrix through a single-layer substrate. The commercial usage of the WLAN network was the main focus of the suggested model. The HFFS platform, which functions at 5.5 GHz in the c-band, was extensively employed for the simulation of the antenna. Due to its low loss performance, the FR-4 substrate was frequently utilised for the beam steering of the 4×4 butler matrix. However, the approach suffered as a result of the challenging manufacture and measurement processes.

Bharath et al. [47], had performed a hybrid rectangular loop dipole antenna and quasi-Yagi-Uda model was created using a 4×4 Butler matrix as the foundation. In millimetre wavelengths, a four-stage switched beam antenna array was used to demonstrate the approach. The wideband switched beam antenna selected a frequency between 34.5 GHz and 35.5 GHz for beam shifting in order to achieve the 10 dB maximum return loss. The HFSS tool was extensively employed in the simulation to get the peak gain of 8.5 dB. The 4×4 Butler matrix was set up to scan in the direction of angle $15^\circ \pm 2^\circ, -45^\circ \pm 4^\circ, 38^\circ \pm 2^\circ and -15^\circ \pm 1^\circ$ for the beam forming network. However, the physical structural change required to scan the beam for a tilted beam made this method less effective.

Almorabeti et al. [48], had suggested the optimum design and construction of a switched beam smart antenna fed by a 4×4 BM in microstrip technology for a MPT system at 5.8 GHz. The proposed smart antenna comprises of a 4×4 Butler matrix beamforming network and an array of four linear microstrip patch antennas. It was able to create and direct four orthogonal beams in the directions of ($\pm$ 39° and $\pm$ 15°). Additionally, it demonstrated good simulated and observed

return losses as well as a high gain of 17.98 dB. Utilizing an advanced design system (ADS), the smart antenna component design, optimization, and simulation were carried out.

Almeshehe et al. [49], had suggested a low loss 4×4 Butler matrix for a millimeter-wave beamforming network that uses the iris coupling technique and rectangular waveguide cavity resonators. The advantage of this technique was that it may be used to adjust the electrical fields and the coupling factor inside of a complicated medium, like waveguide cavity resonators. The iris coupling k-value between the waveguide cavity resonators was tuned to produce a coupling factor of 6 dB for a 4×4 Butler matrix. In the upper millimeterwave frequencies, larger phase difference losses and component losses are thereby avoided. In order to attain a 6 dB coupling factor, simulations using the CST software are run under a variety of iris coupling k-values. Following that, the suggested 4×4 BM was 3D metal manufactured using the SLM technology.

2.7 Techniques based on Smart Antenna using Algorithms

Anas et al. [50], had developed an inverted T-shape ultra-wideband phased array for use in 5G applications utilising DGS with beam steering. To achieve ultra-wideband operation, the received T-shape slotted stub was utilized in this technique. For resonating the antenna, a DGS with a rounded bracket slot was sandwiched in the ground. 1×4 Phased array was utilized to guide the beam and aid in achieving high gain. At its working frequencies of 26, 28, and 43 GHz, the phased array may steer $\pm 30°$. The CST device was extensively used to simulate this antenna. The greatest gain achieved for the proposed antenna was around 16.5 dB.

Ozpinar et al. [51], had proposed the cutting-edge small, broad-band, millimeter-wave antenna with outstanding gain for 5G beam guiding scenarios. To achieve high gain or wideband operation, this technique utilised a phased array of clover antennas with steering capability of $\pm 45°$. At operating frequencies between 24

and 28 GHz, Clover's phased array antenna can direct the beam. The CST tool, which had an approximate 9 dB gain, was commonly used to simulate the antenna. This method also investigates the difference in peak gain and power density based on different scanning angles.

Das et al. [52], had investigated the beam steering of a MSA using phase shifting surface of single layer FSS. This technique improved micro strip antenna by adding a low loss passive frequency selective surface based on the PSS. Eight split-ring resonators with similar geometrical and wavelength parameters were used to build the PSS. The HFSS tool was frequently utilised for the antenna modelling. With a resonant frequency of 4.5GHz, a micro strip antenna with beam directing ability of $\pm 20^{\circ}$ was employed. To show the beam-steering functionality, a directional MSA running at 5.5 GHz was also constructed and coupled with this PSS. Beam-steering in the elevation plane was possible by rotating or shifting the PSS across the MSA, with a maximum gain of 8.9 dBi, without diminishing the properties of the beam's reflection coefficient. When the PSS was positioned vertically above the MSA, the antenna performs optimally in terms of gain and beam tilt. With a front-to-back ratio of 55.5, the MSA combined with the non-uniform metasurface exhibits 75 % radiation efficiency (17.4 dB). Fabrication and measurement of a prototype serve as proof of concept. The evaluated outcomes agree with the outcomes of the full-wave simulation.

Rzymowski et al. [53], had developed a two-row electrically steerable parasitic array radiator antenna for estimating DOA (ESPAR). Twelve passive antenna components make up the antenna. The simplest microcontroller, known as received signal strength (RSS) readings, was used to switch the elevation and azimuth of the beam. With many multiple calibration planes (MCP) and various radiation pattern sets, a method called power-pattern cross-correlation (PPCC) was developed. The effectiveness of the suggested method was assessed using simulation parameters like SNR and radiation pattern.

Alibakhshikenari et al. [54], had presented an automatic adaptive antenna impedance tuning approach that was based on a quantum-inspired genetic optimization method. The best configuration for a T-impedance matching LC-network

with low-pass passive placed among an RF transceiver and its antenna was determined using the suggested automatic quantum genetic algorithm (AQGA).For applications ranging from 1.4 to 5GHz, the AQGA tuning method's results are shown (radar systems, LTE networks, satellite services, and WiFi bands). The suggested approach converges substantially more quickly to offer a solution when compared to current genetic algorithm-based tuning strategies. The proposed AQGA was typically 75%, 49.2%, 64.9%, 54.7%, and 52.5% faster than traditional genetic algorithms at 1.4, 2.3, 3.4, 4.0, and 5.0GHz bands, respectively. The outcomes show that the suggested AQGA was practical for use in real-time RF-front-end systems.

Loshakov et al. [55], had proposed adaptive space-time signal processing in base station antennas, the potential for enhancing electromagnetic compatibility in mobile communication systems of the next generation was examined. Recurrent adaptation methods developed on the basis of the least mean square error criterion are studied for features of handling the interference suppression problem in adaptive antenna arrays. The outcomes of signal processing modelling adaption and its analysis are provided. Polarization-time processing of signals employing the best possible stochastic control was a promising approach to interference suppression.

2.8 Techniques based on Elliptical Monopole Antenna

Benkhadda et al. [56], had developed a CPW Fed monopole antenna for Wi-Fi, WLAN, and Wi-max applications. Here, the FR-4 substrate was used, and the dimensions were roughly 20 mm x 35 mm. An ellipse form slot was added to the radiator and circles and rectangles were added to the ground plane in order to attain the dual bands. The achieved radiation efficiency and gain were 98 % and 3.38 dB, respectively. Due to its many benefits of ample bandwidth, simple structure, omnidirectional radiation pattern, low profile, good radiation efficiency, and high gain, the designed dual-band antenna was ideal for Wi-Fi, WLAN, and WiMAX applications.

Sediq et al. [57], had constructed an eye-shaped monopole antenna for wide-

band and 5G applications. The antenna was created on a FR-4 substrate and had the following dimensions: 26 mm x 20 mm x 1.6 mm. The design had improved radiation patterns, and the first band's bandwidth and peak gain were 49.7 and 3.15 respectively (2.64 GHz-4.51 GHz).Due to its small size, the suggested antenna provides a broad working bandwidth at two resonance frequencies, good gain characteristics, high radiation efficiency, and appropriate radiation patterns.The dual-band antenna's simulation results and experimental results were in good agreement. The potential of the monopole antenna to be used in many wireless communication systems was confirmed by this agreement.

Islam et al. [58], had developed a low profile monopole antenna functioning in the 7 to 14 GHz frequency range for use in biomedical applications. The polyimide substrate was fed through the elliptical slot with CPW. Peak gains of 4.4 dB and 65 % radiation efficiency were attained. The suggested antenna operates with a constant bandwidth on three different flexible substrates. Moreover, the antenna performs consistently even when bent in four distinct directions. The proposed antenna had been developed as an improved prototype using a low-cost manufacturing method.

Sugumaran et al. [59], had presented ANN (artificial neural network) based ground plane with reconfigurable monopole antenna which operates at 4.8 GHz-5 GHz. Initially, the ground plane was designed by the dimension of 180 mm x 180 mm and it had copper layer. At frequency 4.8, the bandwidth achieved was 900 MHZ with the radiation pattern control. By increasing electrical resonance length, the suggested antenna attains suitable impedance matching with inductance loading, and a relationship calculation was formed between the radiator's size and the centre frequency. With a lower SAR level and less volatility owing to bending, the antenna's flexibility makes it ideal for wireless body area network applications.

The technology based on including phased array antennas, MIMO antennas, smart antennas with butler matrices, and smart antenna employing algorithms had a variety of shortcomings that limit its functionality. The current method had some drawbacks, such as computational complex, very low side lobe, difficulty in manufacturing, routing problem, data rate, network capacity, and communication

distance, configuration errors, power outages, rates of false positives and false negatives. Due to these consideration, there is a need of improvement in the antenna design which satisfy the sub 6-5G requirements. Hence this work presents a compact size elliptical slotted antenna with DGS for sub 6-5G applications.

2.9 Summary

Mobile communication and wireless communication systems are significant in a number of industries, such as transportation, business, and education. It is estimated that future wireless communication systems will only be able to function in millimeter-wave frequency ranges and will be constructed with increased bandwidth and sending rates. Due to the misuse of wireless communication systems, smart antennas with improved efficiency, ideal size, and other useful attributes should be created. The beam-forming network is a crucial element of the beam antenna system. Beam directivity can be adjusted by using the beamforming network to disperse phases and offer different power levels. This chapter investigated a number of 5G communication approaches, including phased array antennas, MIMO antennas, smart antennas with butler matrices, and smart antenna employing algorithms.

Chapter 3

Microstrip Patch Antenna at Millimeter Wave Frequency

3.1 Overview

In this era, wireless communication devices are everywhere, and usage is rapidly increasing. A few examples of these gadgets include cellular mobile phones, AM/FM radios, laptops, tablets, GPS devices, satellite phones, and radio-frequency identification (RFID) systems [60]. As the antenna is an necessary component of these devices, it has a significant impact on how well they work. Thus, careful consideration should be given to the design of an antenna for every wireless device to ensure optimum system-level performance. The need for wireless technologies has been rapidly increasing in recent years. One can see that the sub 3GHz spectrum is getting congested as demand for high bandwidth and connection increases. Nonetheless, a significant portion of spectrum in the band of 30-300 GHz is still unexploited. The 30-300 GHz spectrum, which has wavelengths between 1 and 100 mm, is referred known as the millimetre wave band [61, 62].

One can use this millimetre wave spectrum of frequencies to obtain the high capacity of channel and data rate needed for diverse applications. In mm wave range of frequencies, factors such atmospheric absorptions, fading of signal, and attenuation are extremely leading because the wavelength is equivalent to dimension of

components [63]. All of these issues have potential to lower system performance, thus they must be addressed. These considerations could be more important if the system just has one antenna. For millimetre wave communication, a MIMO antenna is therefore required. So in this chapter discussed about two objectives for antenna design that is, one is based phased array while other is based on MIMO MPA.

3.2 Microstrip Patch Antenna based on Phased Array

This work considered about the Rectangular microstrip patch antenna (RMPA) for the design of phased array based antenna. In this section discusses about the fundamental designing model of RMPA, 1 x 2, 1 x 4, 1 x 8 and 4 x 8 array RMPA for 28 GHz, 38 GHz, and 60 GHz. Additionally discussed about slotted microstrip patch antenna phased array for 28 GHz.

3.2.1 Design of Rectangular microstrip patch antenna (RMPA)

The selection of the substrate material is a key first step in design of MPAs. For certain substrates, the tangent of loss (tan) and relative dielectric constant (ε_r) are main electrical attributes taken into account. Because to the tiny patch created by the high dielectric constant, impedance bandwidth is decreased, and the manufacturing tolerances are also reduced. Due to the high loss tangent, which also raises feed losses and antenna efficiency, the antenna's efficiency is lowered. The design of a typical RMPA[112] is as trails with recognized values of r, h, resonant frequency (f) GHz, and λ_0.

Step 1: Elemental width (W) design

The formula for the elemental breadth of RMPA is,

$$W = \frac{c}{2f\sqrt{\frac{\varepsilon_\gamma+1}{2}}} \tag{3.1}$$

Step 2: Extension length (Δl) design.

In order to keep the real length of the patch constant constant, the extension length l is often subtracted from the RMPA's computed length L. The bordering fields practically cause the extension length, which is provide by,

$$\Delta L = 0.412h \left[\frac{(\varepsilon_{\text{ref}} + 0.3)\left(\frac{W}{h} + 0.26\right)}{(\varepsilon_{\text{ref}} - 0.258)\left(\frac{W}{h} + 0.8\right)} \right] \tag{3.2}$$

where ε_{ref} is the effective dielectric constant.

$$\varepsilon_{\text{ref}} = \frac{1+\varepsilon_r}{2} + \frac{\varepsilon_r - 1}{2}\left(1 + \frac{12h}{W}\right)^{-0.5} \tag{3.3}$$

Step 3: Elemental length (L) design

Equations (3.2) and (3.3) above are used to calculate the extension length (l) and effectual dielectric constant (ε_{ref}), respectively. Equation (3.4) finds the elemental length of RMSPA.

$$L = \frac{c}{2f\sqrt{\varepsilon_{ref}}} - 2\Delta L \tag{3.4}$$

Step 4: Microstripline feed design

By computing the $\frac{W}{h}$ ratio for the recognized values of characteristic impedance Z_0 and ε_r, the 50 Ω micro-stripline feed is created. The formulations are:

$$\frac{W_{\text{feed}}}{h} = \left(\frac{8e^B}{e^{2B} - 2}\right) \quad \text{for } \frac{W_f}{h} < 2 \tag{3.5}$$

$$\frac{W_f}{h} = \frac{2}{\pi}\left[A - 1 - \ln(2A-1) + \frac{\varepsilon_r - 1}{2\cdot\varepsilon_r}\left\{\ln(A-1) + 0.39 - \left(\frac{0.61}{\varepsilon_r}\right)\right\}\right] \quad \text{for } \frac{W_f}{h} > 2 \tag{3.6}$$

$$\text{Where, } B = \frac{Z_0}{60}\sqrt{\frac{1+\varepsilon_r}{2}} + \frac{\varepsilon_r - 1}{\varepsilon_r + 1}\left(0.23 + \frac{0.11}{\varepsilon_r}\right) \tag{3.7}$$

$$\text{and } A = \frac{377\pi}{2Z_0\sqrt{\varepsilon_r}} \tag{3.8}$$

The width of the microstrip line feed W_{feed} is estimated utilizing the aforementioned equations (3.5) to (3.8), depending on the $\frac{W_{\text{feed}}}{h}$ condition, by multiplying

the value of h by the value got from equation (3.5) or (3.6). The microstrip line feed length, L_{feed}, is determined by the effective guide wavelength, λ_{guide} . For a single element RMPA, the length L_{feed} is often considered to be $\frac{\lambda_{\text{guide}}}{4}$ for maintaining the lowermost possible loss in the microstrip line feed. L_{feed} is expanded to include any value that serves as a connection between the patch and the source. It is provided by,

$$L_{\text{feed}} = \frac{\lambda_{\text{guide}}}{4} \tag{3.9}$$

$$\lambda_{\text{guide}} = \frac{\lambda_0}{\sqrt{\varepsilon_{\text{effective}}}} \tag{3.10}$$

$$\text{Where, } \varepsilon_{\text{effective}} = \varepsilon_r - \frac{\varepsilon_r - \varepsilon_{\text{ref}}}{1 + G\left(\frac{f}{fp}\right)^2} \tag{3.11}$$

According to the aforementioned technique, the 50Ω microstripline feed is designed and it is linked at the centre point C_{point} along the width W of rectangle radiating patch. It's possible that the patch at C_{point} 's impedance is less than 50Ω. Given the impedance mismatch, the microstripline feed shouldn't be linked to this location. For improved impedance matching, the matching transformer is utilised between C_{point} and the 50Ω microstripline.

Step 5: Design of quarter wave transformer (QWT)

The quarter wave transformer (QWT), is a crucial circuit component in microstrip systems. The QWT's length is equivalent to 1/4 of guiding wavelength (λ_{guide}). The QWT is in charge of changing the impedance between two different parts. The QWT's impedance is provided by,

$$Z_{\text{tran}} = \sqrt{Z_1 * Z_3} \tag{3.12}$$

The difference between the two impedances as well as any potential impedance mismatch is transformed using this transformer. The impedance R_{in} at C_{point} throughout the width of RMPA is calculated using the formulae below.

$$R_{\text{in}} \cong \frac{(120\lambda_0)^2 + \left(\frac{377h}{\sqrt{\varepsilon_r}\cdot L}\right)^2 \tan^2 \alpha l}{240 * L * \lambda_0 \left(1 + \tan^2 \alpha l\right)} \tag{3.13}$$

$$\alpha = \frac{2\pi\sqrt{\varepsilon_r}}{\lambda_0} \tag{3.14}$$

$$l = \theta\pi/180\alpha = W/2 \tag{3.15}$$

$Z_{\text{tran}} = \sqrt{R_{\text{in}} * Z_0}$ represents the QWT's impedance. W_{tran} is the QWT's width as determined by equations (3.5) to (3.8). L_{tran} is the length of QWT as determined by use of equations (3.9) to (3.11) and the substitution of Z_0 by Z_{tran} .

Step 6: Design of ground plane (GP)

Magnitudes of the GP should be

$$L_{\text{ground}} = 6h + L \tag{3.16}$$

$$W_{\text{ground}} = 6h + W \tag{3.17}$$

3.2.2 Performance Metrics

There are many antenna parameters are considered for the proposed phased and MIMO microstrip patch antennas. The parameters and metrics used in this work are return loss, bandwidth, gain, resonant frequency, radiation efficiency, directivity, and antenna efficiency.

3.2.2.1 Return Loss (RL)

The RL is a metric that specifies how much power is 'lost' to load and doesn't return to the source as a reflection. This value also shows how effectively the transmitter and receiving antennas have been matched. At a certain location on the waveguide slotted section, R_{loss} is ratio of incident power (P_{in}) to reflected power (P_{re}), and it is represented in decibels (dB), as shown by

$$R_{\text{loss}} = 10\log\left(\frac{P_{\text{in}}}{P_{\text{re}}}\right) = 10\log\left(\frac{1}{|\Gamma|^2}\right) \tag{3.18}$$

where Γ stands for the power reflection coefficient. For understanding the relationship amongst the coefficient of reflection and VSWR.

$$|\Gamma| = (VSWR - 1)/(VSWR + 1) \tag{3.19}$$

The voltage standing wave ratio (VSWR), which results from the incident and reflected signals from load, is the ratio of minimum and maximum voltages. If the transmitter and antenna were perfectly matched, that is, if $\Gamma = 0$ and $R_{\text{loss}} = \infty$, no power would be reflected back. With $\Gamma = 1$ and $R_{\text{loss}} = 0$ dB implies that, all incoming power is reflected. VSWR of 2 is suitable for real applications since it equates to RL of -9.54 dB.

3.2.2.2 Bandwidth

The range of frequencies across which antenna resonates is mentioned to as the antenna bandwidth (BW). Impedance and gain are the parameters that restrict an antenna's bandwidth. The principal factor limiting the usable bandwidth of tiny antennas is typically the input impedance. With a tiny antenna's input impedance, the frequency fluctuates quickly. This restricts the antenna's frequency range. It is compatible with its feed line. The RL or VSWR is described in the bandwidth of impedance. The matching criterion is VSWR 2 or RL -10 dB. Calculating impedance bandwidth involves,

$$BW = (VSWR - 1)/Q\sqrt{VSWR} \tag{3.20}$$

$$BW(\%) = \left[\frac{F_h - F_l}{F_c}\right] * 100 \tag{3.21}$$

Where, F_l is lower frequency F_h is higher upper frequency, and F_c is centre frequency.

3.2.2.3 Radiation Efficiency

Efficiency of radiation is the proportion of total amount of power radiated by an antenna to net power obtained by that antenna from associated transmitter. It can be represented as,

$$E_{\text{rad}} = \frac{R_{\text{rad}}}{R_{\text{rad}} + R_{\text{loss}}} \tag{3.22}$$

Where R_{loss} is loss resistance while R_{rad} is radiation resistance.

3.2.2.4 Directivity

The directivity is calculated by dividing the subject antenna's highest radiation intensity by the maximum radiation strength of a reference or isotropic antenna that is outputting similar amount of power. The radiated power depends on the radial distance from the circuit as well as the angular location. As a result, it is stated by taking into account both terms and.

$$\text{Directivity} = \frac{\phi(\theta,\phi)_{\max}(\text{from subject antenna})}{\phi_0(\text{from isotropic antenna})} \tag{3.23}$$

The subject antenna's maximum radiation intensity is indicated by $\phi(\theta,\phi)_{\max}$. The radiation output of an isotropic antenna is ϕ_0 (antenna with zero losses).

3.2.2.5 Antenna Efficiency

Antenna efficiency is stated as the difference amongst input and output powers of an antenna. An antenna's function is to radiate energy from its input with least losses possible, to put it simply. How successfully an antenna transmits its output with the fewest losses in the transmission line is referred to as its effectiveness.

$$\text{Ant.efficiency} = \frac{P_{\text{radiation}}}{P_{\text{in}}} \tag{3.24}$$

Where, $P_{\text{radiation}}$ is radiated power and P_{in} is input power of antenna.

3.2.2.6 Gain

The difference among the strength of the radiation in single direction and intensity which would be attained if antenna were to emit the power it is used isotropically is known as an antenna's gain. It is expressed as,

$$G = \text{ Ant. efficiency * Directivity} \tag{3.25}$$

3.2.3 Design of Rectangular Microstrip Patch Antenna for 28 GHz

Initially, a single element antenna and phased array structure are built for wireless communication applications at a frequency of 28 GHz, and different factors including gain, RL, directivity, VSWR, and pattern for radiation of the antenna are investigated. A segment of rectangular Microstrip transmission line about half a wavelength long serves as the rectangular patch antenna.

The length of a RMPA is roughly half of a free-space wavelength when air is used as the substrate for antenna. When the substrate's relative dielectric constant rises, the length of antenna gets shorter. The expanded electric "fringing fields" enhance the electrical length of antenna just enough to shorten its resonant length marginally. Microstrip patch antenna has been simulated and modelled using IE3D software. It is a complete full-wave EM modelling and optimization programme for the study and design of digital circuits, high-speed printed circuit boards (PCB), antennas, MMIC, RFIC, and planar and three-dimensional microwave circuits. Analysis of RL plots, radiation patterns, current distributions, smith charts, VSWR, etc. are all done using it. The design of a single component patch with dimensions is given in Figure 3.1.

The patch has the following measurements for 28 GHz frequency: Length (L) = 2.33 mm, and Width (W) = 3.260 mm. Here, microstrip line is utilized for feeding. A QWT is employed to match patch's impedance to 50 ohm line. In IE3D, length and width are determined utilizing line gauge. For improved gain and directivity, a phased array structure with 1 x 2, 1 x 4, 1 x 8, and 4 x 8 elements is also created

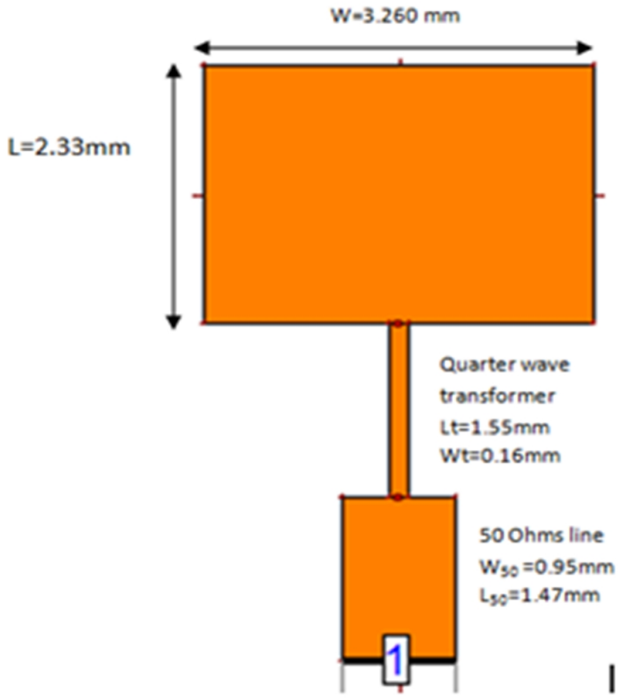


Figure 3.1: Design of Single Element Patch for 28 GHz

which is shown in Figure 3.2. Transformers, power dividers, bent-like components of 50 Ω, 100 Ωs, 70 Ω, etc. were employed to build the aforementioned array topologies. Feed line components such as 50 ohms line has (length = 1.47 mm and width = 0.95 mm), 70 ohms line has (length = 1.55 mm and width = 0.16 mm) and 100 ohms line has (length = 1.55 mm and width = 0.082 mm). 1 x 2 array has dimensions of Length = 6.3 mm and width = 15.05 mm. 1 x 4 array has lenth 8.72 mm and width = 37.77 mm. 1 x 8 array has lengt h= 12.10 mm and width =85.10mm. 4 x 8 structure has dimenions of lenth = 38 mm and width = 88 mm.

3.2.3.1 Results of Design of Rectangular Microstrip Patch Antenna (RMPA) for 28 GHz

The S11 characteristics (RL) for suggested single patch antenna resonate at 27.18 GHz with a value of -21.87 dB are shown in Figure 3.3. The frequencies's range

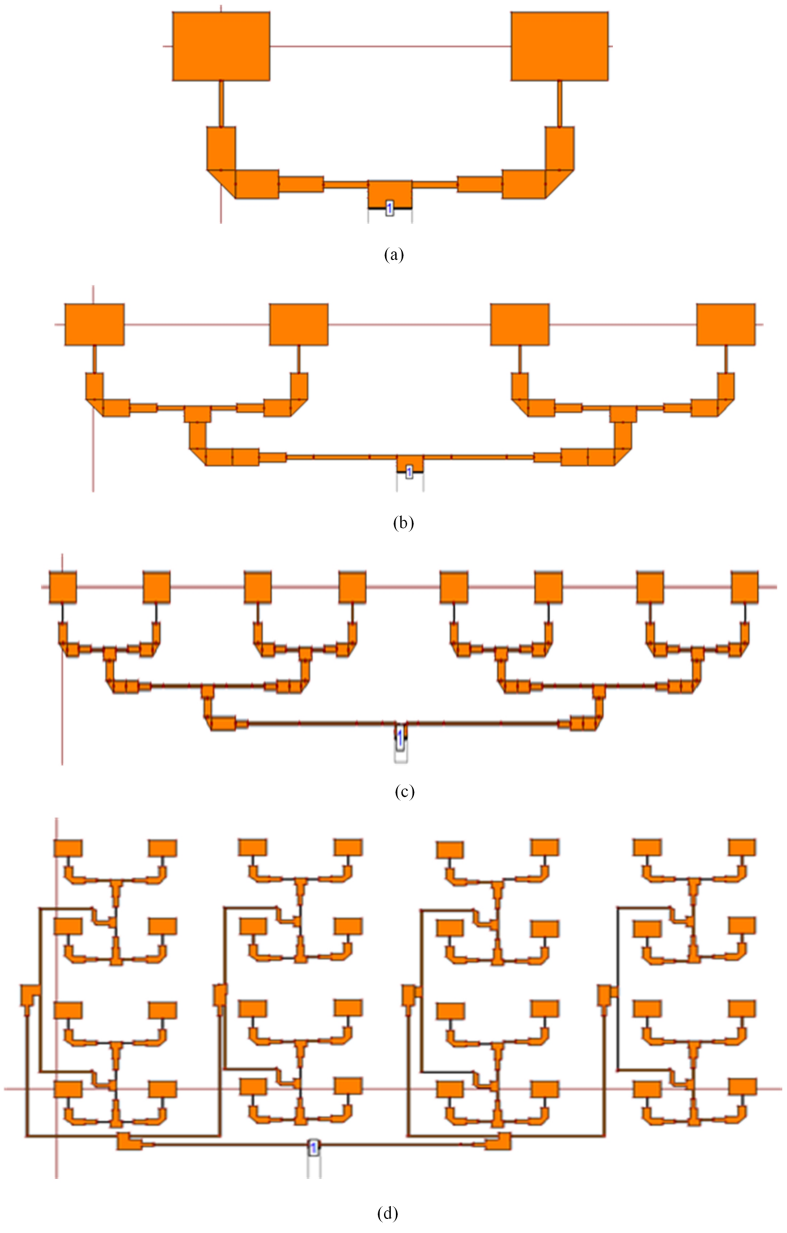


Figure 3.2: Rectangular Patch Antenna at 28 GHz (a) 1 x 2 Array (b) 1 x 4 Array (c) 1 x 8 Array (d) 4 x 8 Array

across which the RL > -10 dB (relates to a VSWR of 2) can be considered the antenna's bandwidth.This means that the RL vs frequency strategy may be used to determine the antenna's bandwidth. The recommended patch antenna has a

BW of 1.24 GHz and a range of 26.6–27.84 GHz. The return loss vs frequency plot for 1 x 2 patch array is presented in Figure 3.4.

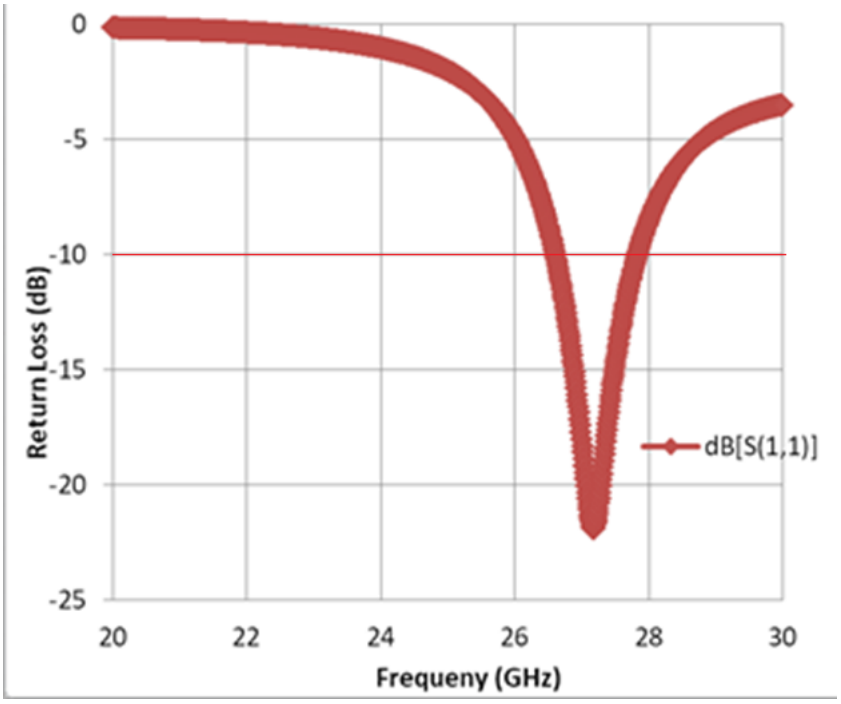


Figure 3.3: RL vs. Frequency of Single Element of RPA for 28 GHz

The Resonant frequency for a 1 x 2 patch array is 29.2 GHz with an RL of -15.90 dB. The suggested patch antenna has a BW of 0.8 GHz and a frequency range of 29-29.8 GHz.

Dual band antenna with RL of -17.24 dB and -18.95 dB is obtained using a 1 x 4 array of patch, resonating at frequencies of 20.98 GHz and 26.64 GHz, respectively displayed in Figure 3.4. The first band's bandwidth is 0.18 GHz, spanning the range of 20.86 to 21.04 GHz. The range of the second with 1.38 GHz's bandwidth is 25.82-27.2 GHz.

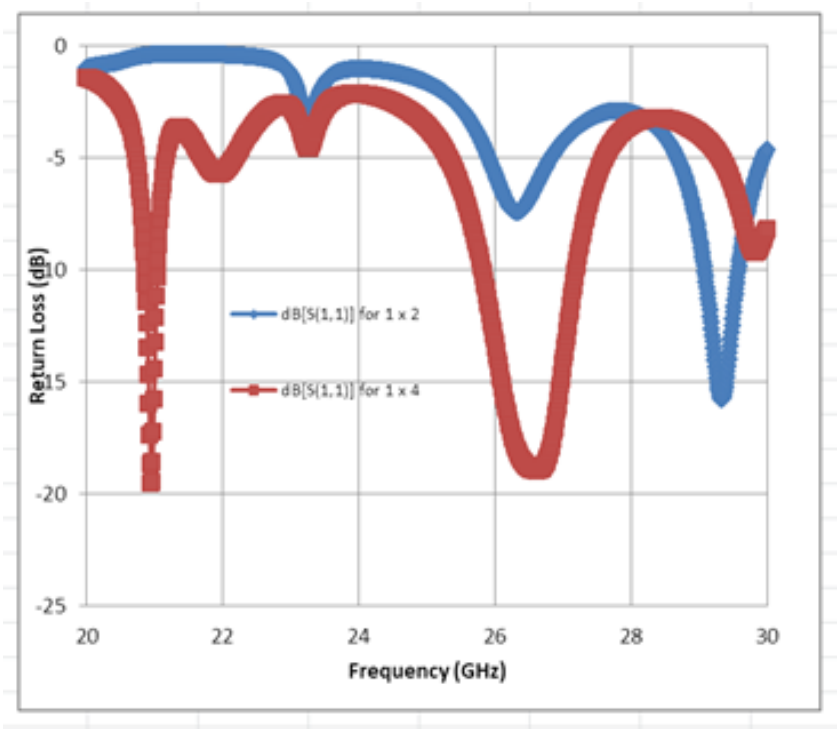


Figure 3.4: RL vs. Frequency Graph for 1 x 2 and 1 x 4 RPA for 28 GHz

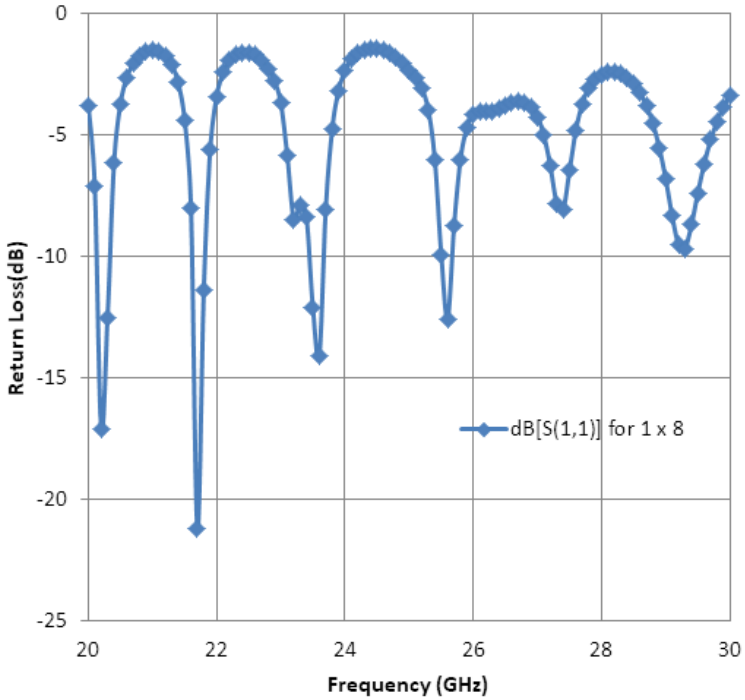


Figure 3.5: RL vs. Frequency Graph for 1 x 8 RPA for 28 GHz

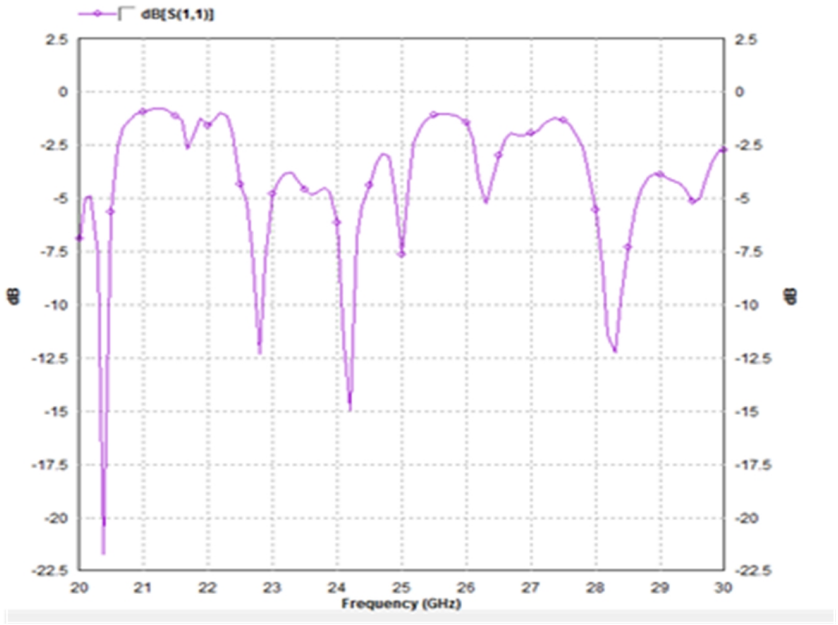


Figure 3.6: RL vs. Frequency Graph for 4 x 8 RPA for 28 GHz

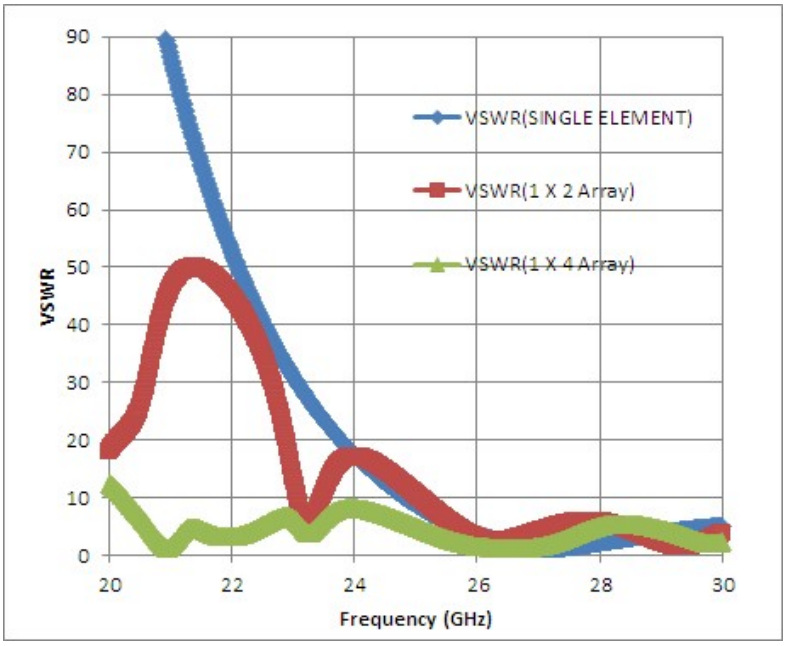


Figure 3.7: VSWR vs. Frequency Graph for Single element, 1 x 2 and 1 x 4 RMPA for 28 GHz

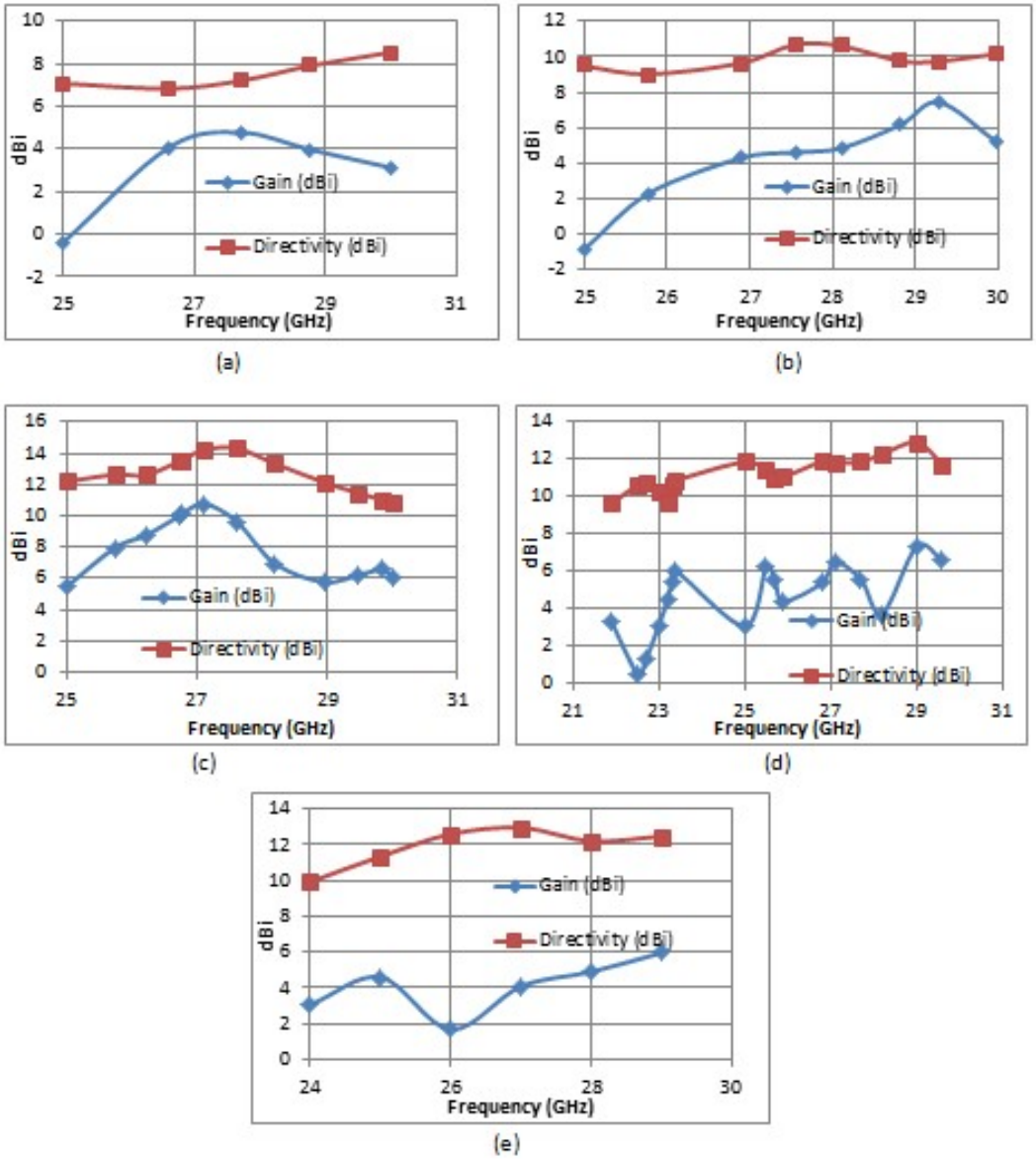


Figure 3.8: Gain & Directivity vs. Frequency Graph for (a) Single element (b) 1 x 2 Array (c) 1 x 4 Array (d) 1 x 8 Array and (e) 4 x 8 Array of RMPA for 28 GHz

A Quad band antenna is obtained for 1 x 8 array which resonantes at 20.2, 21.7, 23.62, and 25.6 GHz with RL -17, -21, -12, and -12 dB while giving 0.3, 0.2, 0.2, and 0.3 GHz of bandwidth, respectively. The return loss against frequency for 1 x 8 array RPA is displayed in Figure 3.5.

A Quad band antenna resonating at 20.4 GHz, 22.8 GHz, 24.18 GHz, and 28.3 GHz with respective RL values of -21.7,-12.33,-14.34, and -12.25 dB is obtained using a 4 x 8 array of patch antenna. A bandwidth of 0.2 GHz, 0.16 GHz, 0.1 GHz, and 0.22 GHz is provided as shown in figure 3.6. The VSWR plots for single, 1 x 2 array and 1 x 4 array is shown in figure 3.7, it can be seen that the VSWR is below 2 at the respective resonant frequencies.

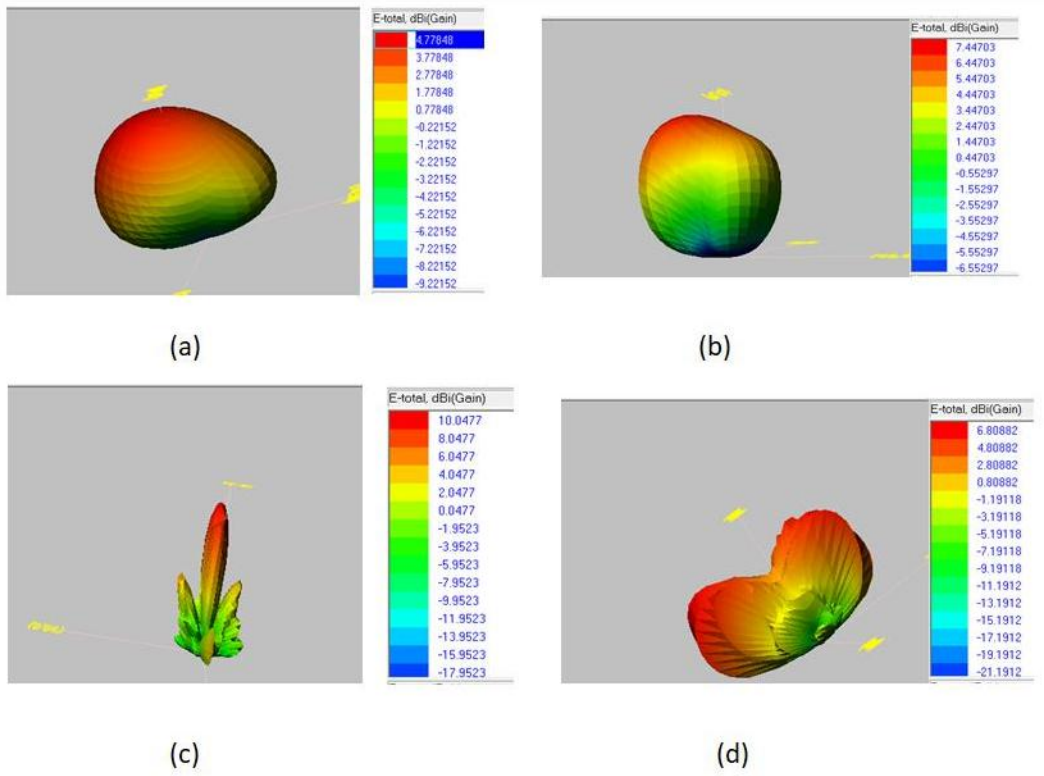


Figure 3.9: Performance for RPA for 28 GHz (a) single element (b) 1 x 2 array (c) 1 x 4 array (d) 1 x 8 array antenna

The Gain and directivity plots for all the array configuration is shown in figure 3.8. It can be seen that the gain and directivity for single element is 4.77 dBi and 7.2 dBi respectively. For 1 x 2 array the gain is 7.44 dBi and directivity is 9.7 dBi. For 1 x 4 array the gain is 10.34 dBi and directivity is 13.54 dBi. For 1 x 8 array the gain is 6.24 dBi and directivity is 11.42 dBi.For 4 x 8 array the gain is 6.9 dBi

Table 3.1: Performance parameters for RPA for 28 GHz

Parameters	**Single**	**1 x 2**	**1 x 4**	**1 x 8**	**4 x 8**
Frequency (GHz)	27.18	29.2	20.98/26.64	20.2/21.7/ 23.62/25.6	20.4/22.8/ 24.18/28.3
Return loss (dB)	-21.87	-15.90	-17.24/18.95	-17/-21/ -12/-12	-21/-12/ -14/-12
Bandwidth (GHz)	1.24	0.8	0.18/1.38	0.3	0.2
Gain (dBi)	4.77	7.44	10.34	6.24	6.9
Directivity (dBi)	7.2	9.7	13.54	11.42	12.89
Rad. Eff (%)	61.69	60.61	45.35	33.7	27.46
Ant. Eff (%)	56.89	58.81	44.73	30.2	25.48

and directivity is 12.89 dBi.

The performance of RPA for 28 GHz is provided in Table 3.1 and Figure 3.9(a -d) shows the radiation patterns of single element, 1 x 2 array, 1 x 4 array and 1 x 8 array antenna respectively.

3.2.4 Design of Rectangular Micro strip Patch Antenna for 38 GHz

For the design of Rectangular Microstrip Patch Antenna(RMPA) for 38 GHz following are measurements of single patch: 1.81 mm is length (L) and 2.40 mm is width (W). As similar to the design of RMPA for 28 GHz, here also microstrip line is used for feeding while QWT is employed to match the patch's impedance to the 50Ω line. Feed line components such as 50 ohms line has (length = 1.08 mm and width = 0.37 mm), 70 ohms line has (length = 1.11 mm and width =

0.20 mm) and 100 ohms line has (length = 1.14 mm and width = 0.082 mm). 1 x 2 array has dimensions of Length = 4.34 mm and width = 12.66 mm. 2 x 4 array has lenth 14.54 mm and width = 32.32 mm. 2 x 8 array has length = 18.4 mm and width = 71.64 mm. 4 x 8 structure has dimenions of lenth = 33 mm and width = 72.64 mm. Design of single RMPA is presented in Figure 3.10.

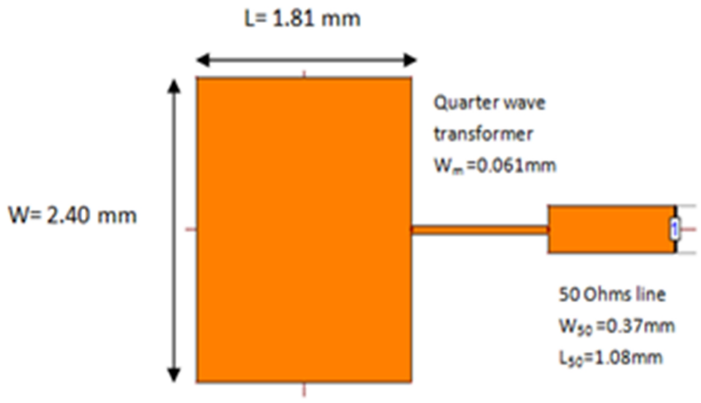


Figure 3.10: Design of Single Element Patch for 38 GHz

For improved gain and directivity, a phased array structure with 1 x 2, 2 x 4, 2 x 8, and 4 x 8 elements is also created similar to the structures done for 28 GHz.

3.2.4.1 Results of design of Rectangular Microstrip Patch Antenna (RMPA) for 38 GHz

Figure 3.11 depicts the S11 characteristics (RL) for the recommended single patch antenna, which resonate at 37 GHz with a value of -22 dB. Although designed at 38 GHz but the resonance is at 37 GHz, this could be due to factors such as the dielectric constant of the substrate, the thickness of the substrate, or the precision of the antenna's dimensions. The antenna's bandwidth is the variety of frequencies where the RL is superior than -10 dB (corresponding to a VSWR of 2).The recommended patch antenna has a 37 GHz range and a bandwidth of 1.2 GHz.

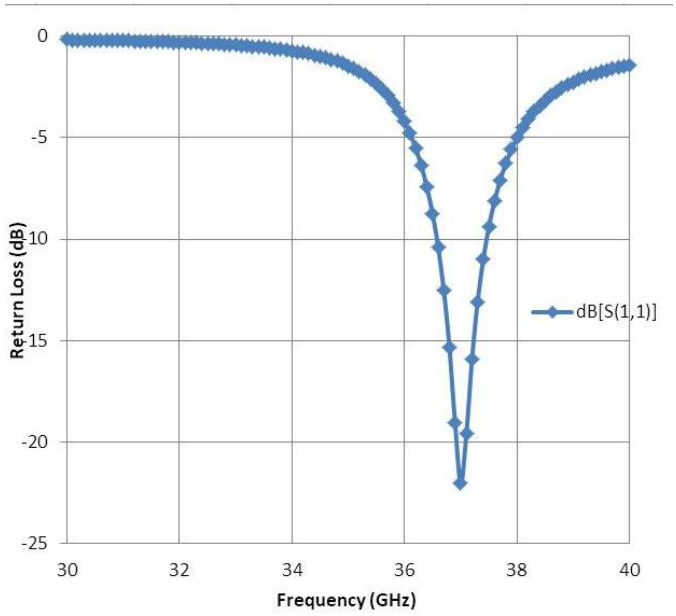


Figure 3.11: RL vs. Frequency of Single Element of RMPA for 38 GHz

Figure 3.12 depicts the RL vs. frequency curve for a 1 x 2 , 2 x 4 and 2 x 8 patch array. A 1 x 2 patch array's resonance frequency is 38.1 GHz, and its RL is -13 dB. The patch antenna that is recommended has a 38-38.8 GHz range of frequency and a BW of 0.8 GHz. 2 x 4 array structure gives triple band antenna with RL of -20.3 dB, -19 dB, and -21 dB that resounds at frequencies of 33.8 GHz, 35.9 GHz, and 39.2 GHz, respectively.The bandwidth is 0.3 GHz, covers frequencies between 33 GHz and 40 GHz.

A Quad band is achieved in 2 x 8 array RMPA while providing 0.4 of bandwidth at frequencies of 31.8, 36.4, 39, and 39.8 GHz with RL -21.8, -21, -12, and -17 db respectively.

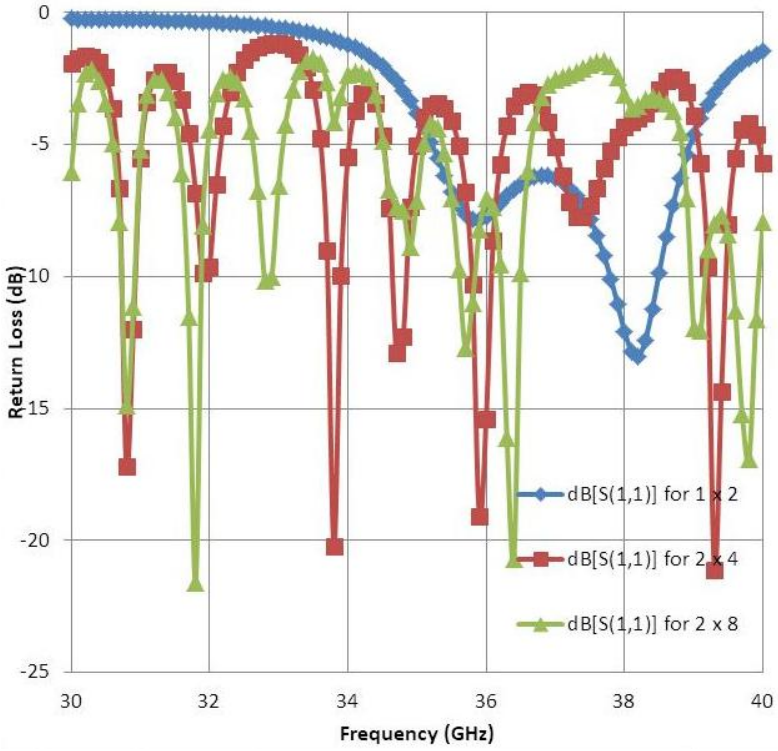


Figure 3.12: RL vs. Frequency graph for 1 x 2, 2 x 4 and 2 x 8 RMPA for 38 GHz

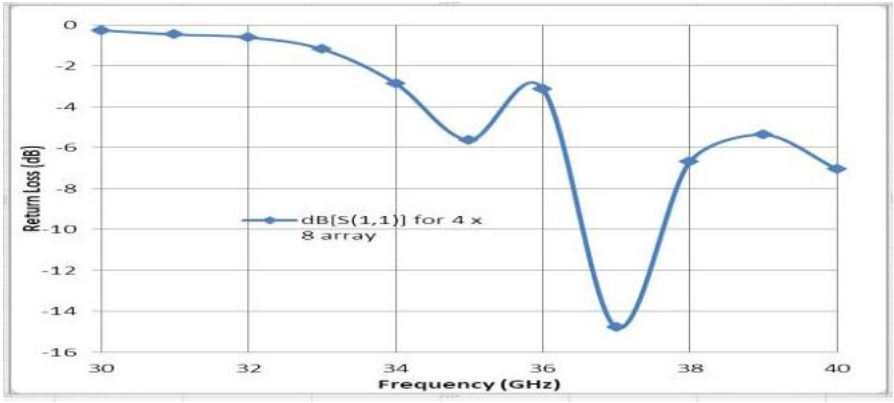


Figure 3.13: RL vs. Frequency Graph for 4 x 8 RMPA for 38 GHz

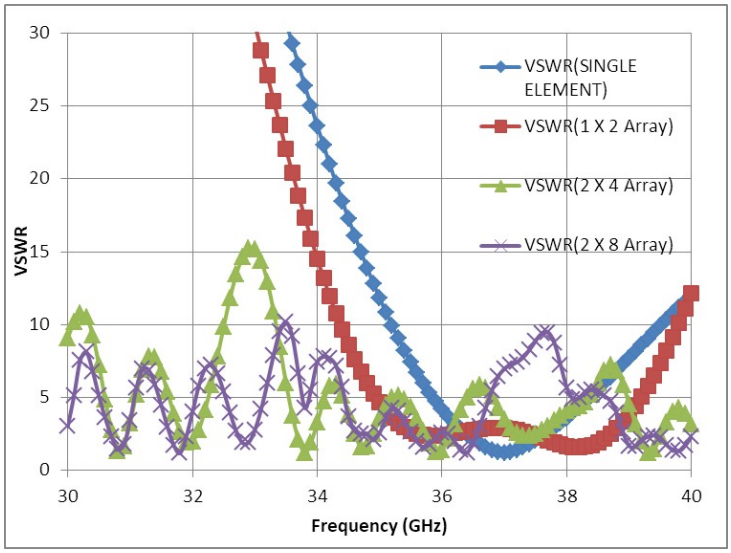


Figure 3.14: VSWR vs. Frequency Graph for Single Element, 1 x 2, 2 x 4 and 2 x 8 RMPA for 38 GHz

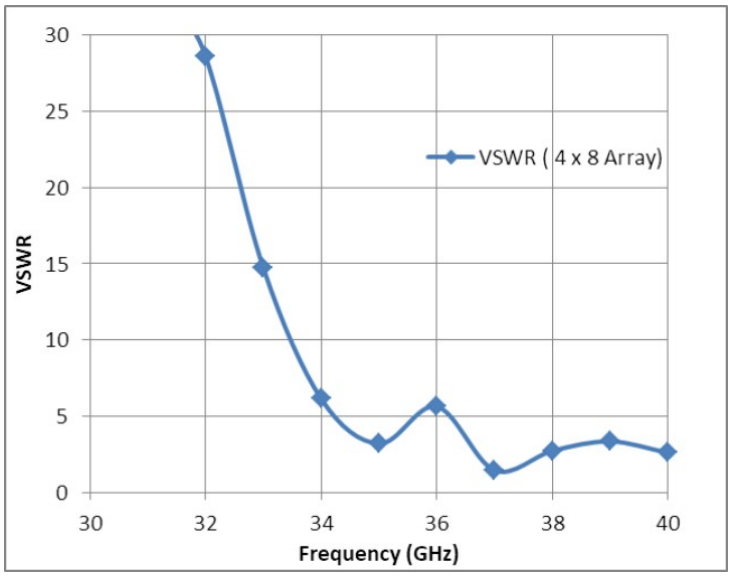


Figure 3.15: VSWR vs. Frequency Graph for 4 x 8 RMPA for 38 GHz

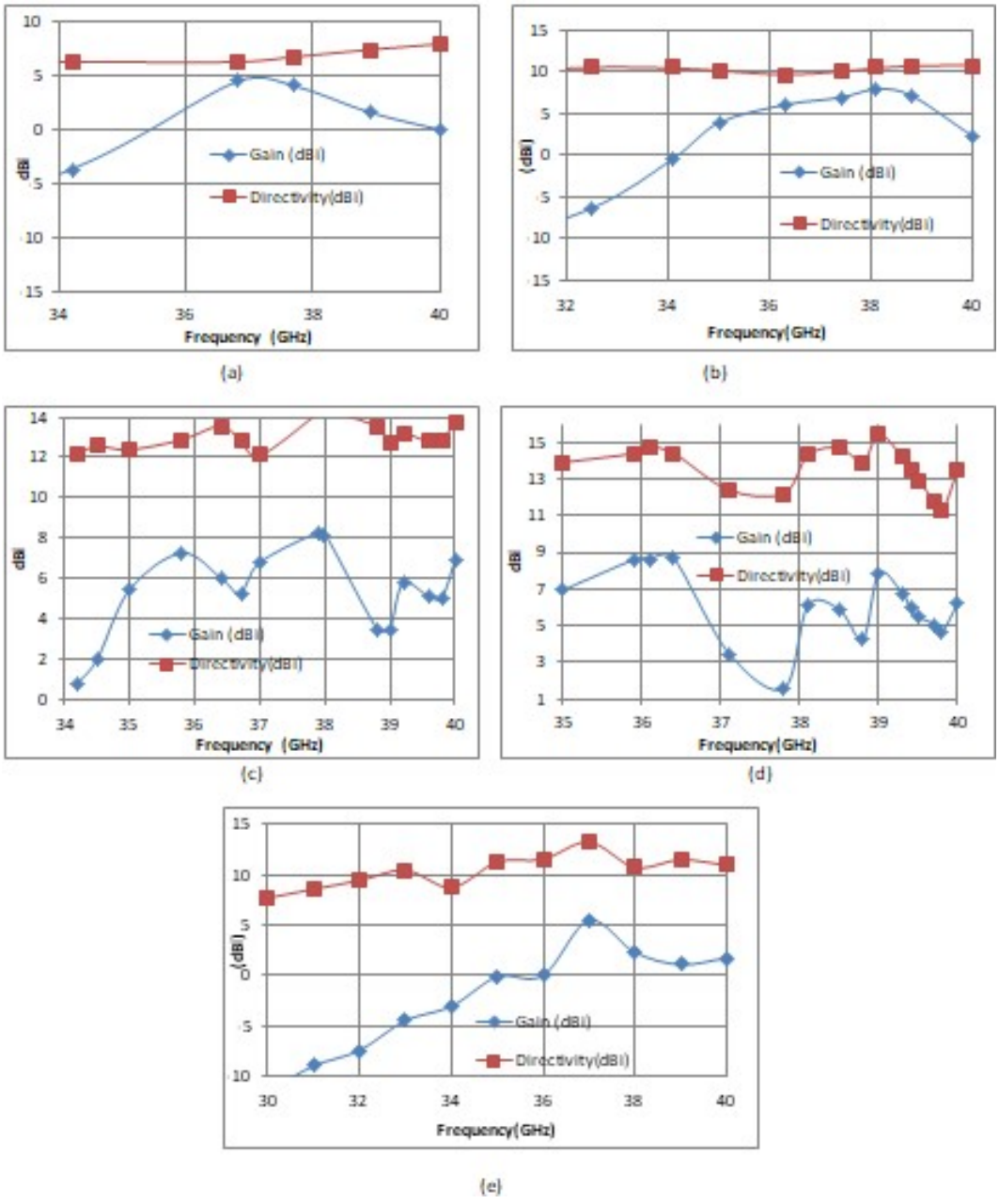


Figure 3.16: Gain & Directivity vs. Frequency Graph for (a) Single element (b) 1 x 2 Array (c) 2 x 4 Array (d) 2 x 8 Array and (e) 4 x 8 Array of RMPA for 38 GHz

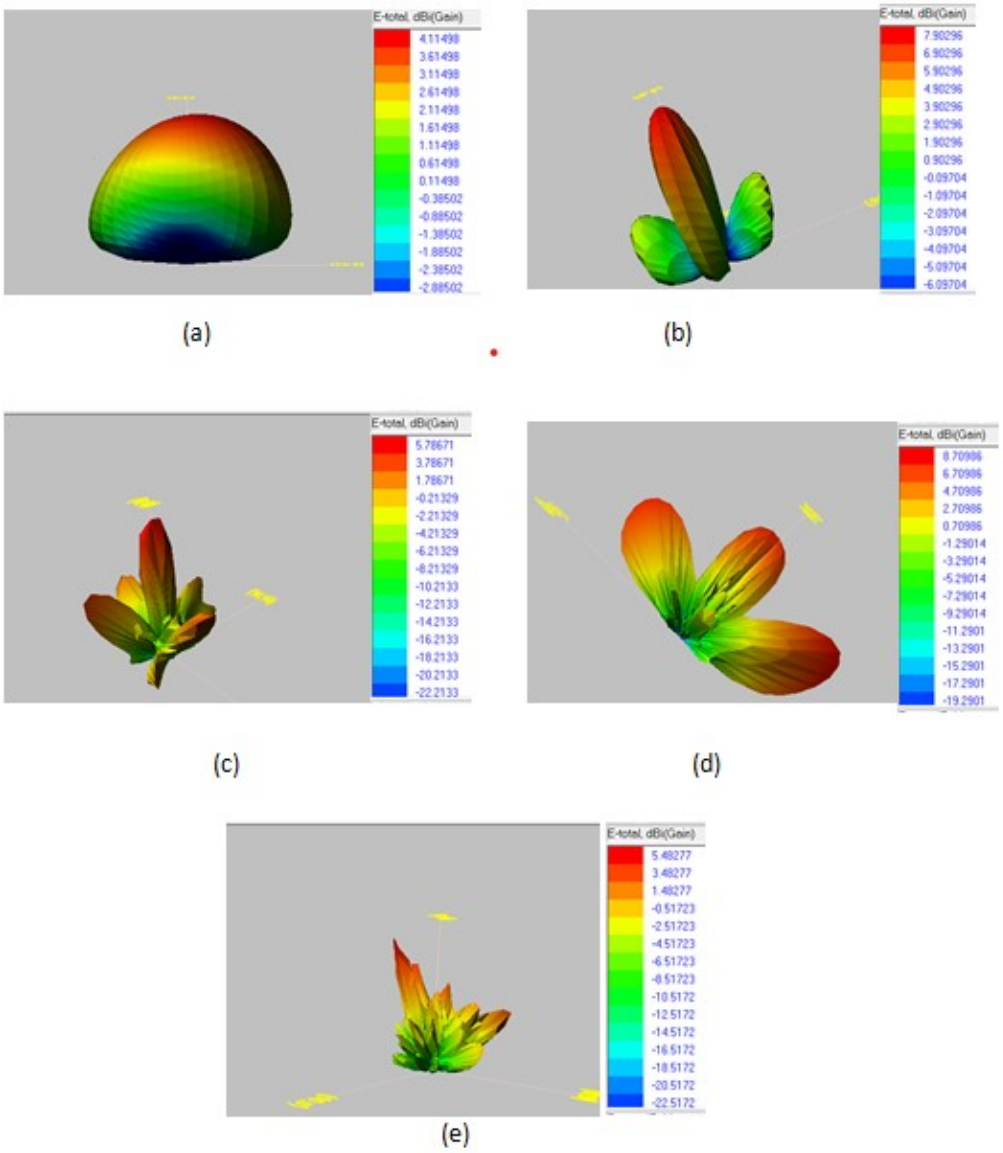


Figure 3.17: Performance for RMPA for 38 GHz (a) single element (b) 1 x 2 array (c) 2 x 4 array (d) 2 x 8 array (e) 4 x 8 array

Figure 3.13 displays the RL vs frequency for the 4 x 8 array RMPA. A 4 × 8 array of patch antennas is used to create a antenna that resonates at 37 GHz with respective RL values of -14.9 dB. The bandwidth is at range of 1.1 GHz.

Table 3.2: Performance parameters for RPA for 38 GHz

Parameters	**Single Element**	**1 x 2 array**	**2 x 4 array**	**2 x 8 array**	**4 x 8 array**
Resonant Frequency (GHz)	37	38.1	33.8, 35.9, 39.2 (TRIPLE BAND)	31.8, 36.4, 39, 39.8 (QUAD BAND)	37
Return Loss (dBi)	-22	-13	-20.3, -19, -21	-21.8, -21, -12, -17	-14.9
Bandwidth (GHz)	1.2	0.8	0.3	0.4	1.1
Gain (dBi)	4.56	7.9	5.7	8.7	5.48
Directivity (dBi)	6.34	10.38	13.20	14.4	13.26
Radiation Efficiency (%)	68.36	59.50	20.34	27.03	17.22
Antenna Efficiency (%)	66.37	56.41	18.11	26.80	16.65

As can be seen from the figure 3.14 and 3.15 the Voltage standing wave ratio of the single element, 1 x 2 array, 2 x 4 array , 2x 8 array and 4 x 8 array is below 2 at the respective resonant frequencies.

The Gain and directivity plots for all the array configuration is shown in figure 3.16. It can be seen that the gain and directivity for single element is 4.56 dBi and 6.34 dBi respectively. For 1 x 2 array the gain is 7.9 dBi and directivity is 10.38 dBi. For 2 x 4 array the gain is 5.7 dBi and directivity is 13.20 dBi. For 2 x 8 array the gain is 8.7 dBi and directivity is 14.4 dBi.For 4 x 8 array the gain is 5.48 dBi and directivity is 13.26 dBi.

The result of parameters for various designed RMPA is shown in Table 3.2 and Figure 3.17 (a -e) shows the radiation patterns of single element, 1 x 2 array, 2 x 4 array, 2 x 8 array and 4 x 8 array antenna respectively.

3.2.5 Design of Rectangular Microstrip Patch Antenna (RMPA) for 60 GHz

For designing RMPA for frequency of 60 GHz, length of patch is 1.11 mm while width of patch is 1.52. A quad wave transformer having width and length of 0.061 mm and 0.730 mm respectively is used for transitioning patch's impedance to the 50 Ω line. The 50 Ω line having dimensions of 0.68 mm length and 0.37 mm width with 50 Ω line. The single element design is shown in figure 3.18.

For array feeding line, 70 ohms line dimensions are width and length of 0.705 mm and 0.20 mm. The 50 line having dimensions of 0.68 mm length and 0.37 mm width. The 100 ohms line having dimensions of width of 0.083 mm and length of 0.725 mm. 1 x 2 array has dimensions of Length= 3.3 mm and width = 7.36 mm. 1 x 4 array has lenth 4.35 mm and width= 19.75 mm. 2 x 8 array has length = 9.76 mm and width = 44.64 mm. 4 x 8 structure has dimenions of lenth = 23.52 mm and width= 44.64 mm.For improved gain and directivity, a phased array structure with 1 x 2, 1 x 4, 1 x 8, 2 x 8 and 4 x 8 elements is also created similar to the 28 GHz.

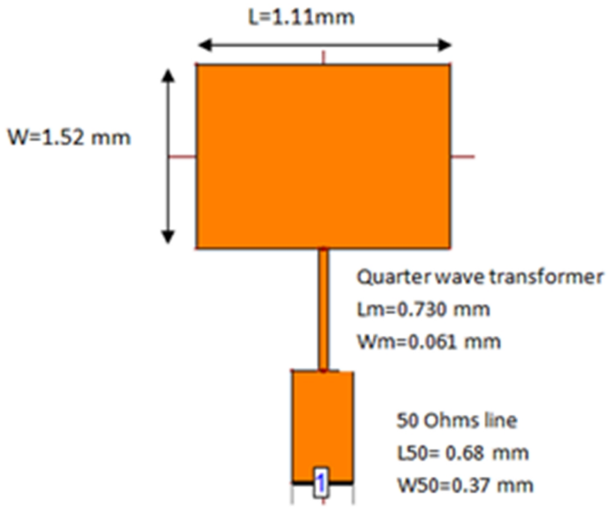


Figure 3.18: Design of Single Element Patch for 60 GHz

3.2.5.1 Results of design of Rectangular Microstrip Patch Antenna (RMPA) for 60 GHz

The RL against frequency for all the array configuration for 60 GHz is shown in Figure 3.19. According to graph, the RL for single element is -19.50 dB for a frequency range 58.2 GHz.While the bandwidth of suggested antenna is 2.2 GHz for the 58-59 GHz range frequency. For 1 x 2 array , RL at resonant frequency 60 GHz is -22 dB while the bandwidth of the suggested 1 x 2 array antenna at range of 60 GHz is 1.6 GHz.

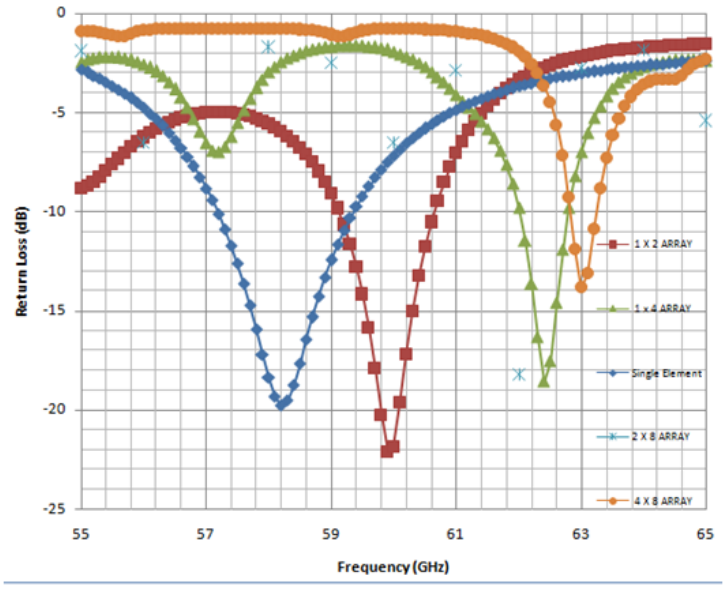


Figure 3.19: RL vs. Frequency of Single Element, 1 x 2, 1 x 4, 2 x 8 and 4 x 8 RPA for 60 GHz

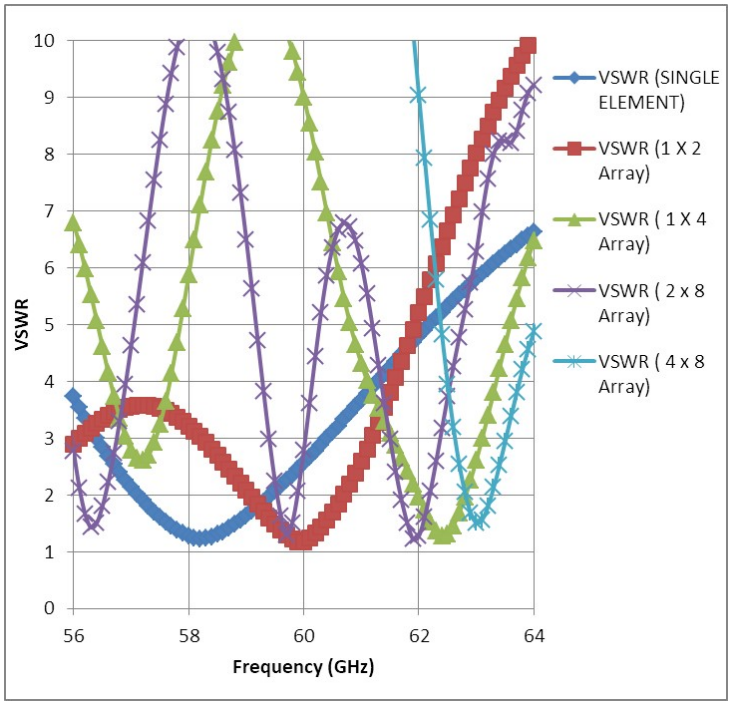


Figure 3.20: VSWR vs. Frequency Graph for RMPA for 60 GHz

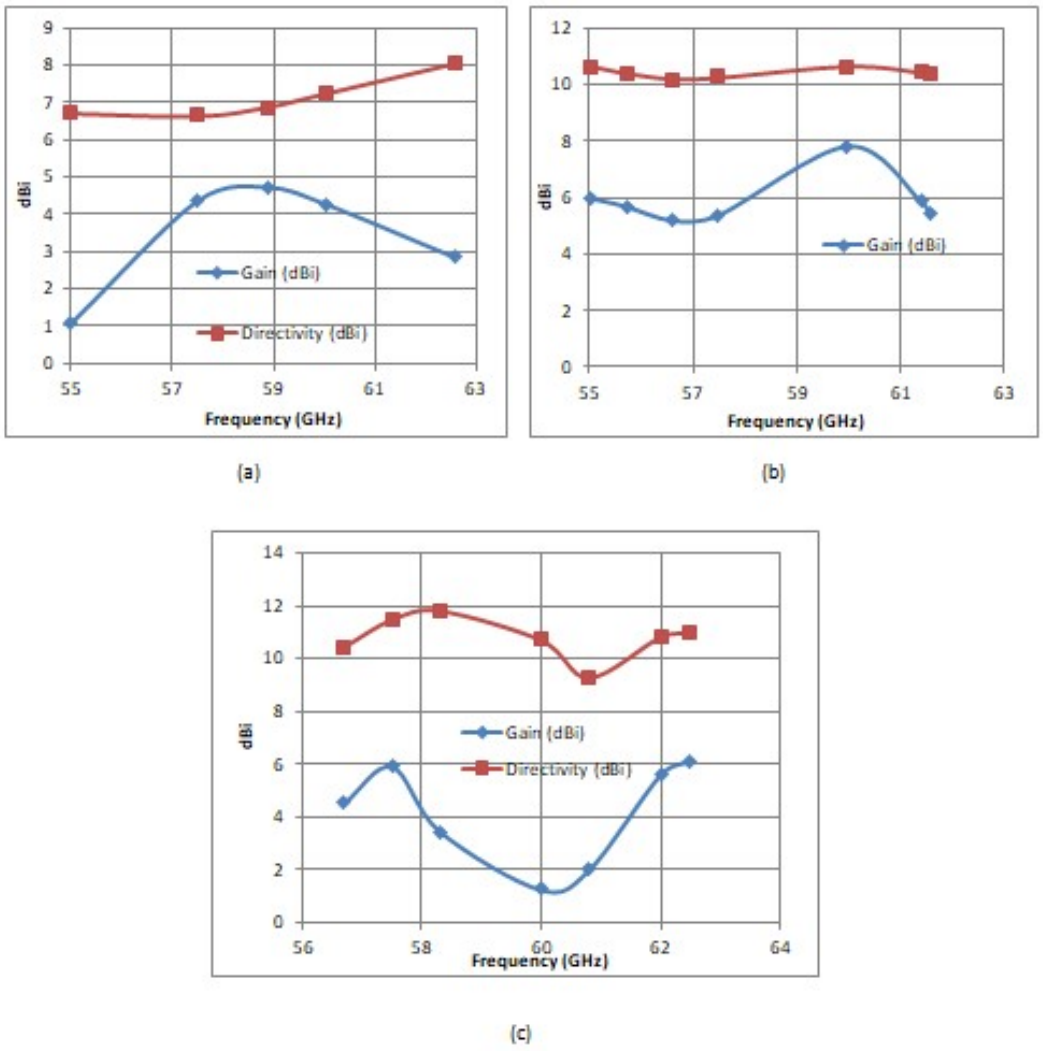


Figure 3.21: Gain & Directivity vs. Frequency Graph for (a) Single element (b) 1 x 2 Array (c) 1 x 4 Array of RMPA for 60 GHz

For 1 x 4 array, the resonant frequency is 62.3 GHz for RL of -15.5 dB is at range of 62-62.5 GHz while the bandwidth is 0.9 GHz.

For 2 x 8 array RMPA, return loss is -18.1 dB for resonant frequency 62 GHz while bandwidth of proposed antenna is 1.1 GHz.

Using a 4 x 8 array of patch antennas, a quad band antenna is produced with RL values of -14.1 dB that resonates at 63 GHz. The bandwidth is in the 0.4 GHz range.

As can be seen from the figure 3.20 the Voltage standing wave ratio of the single element, and all array configuration is below 2 at the respective resonant frequencies.

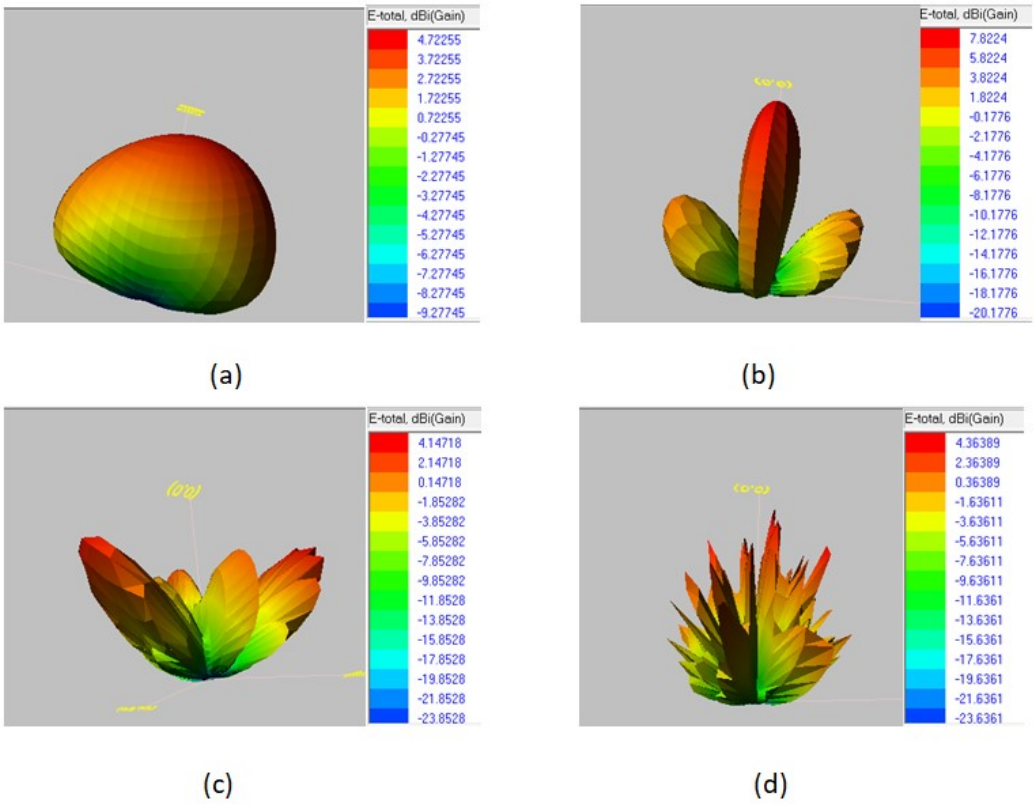


Figure 3.22: Performance for RPA for 60 GHz (a) single element (b) 1 x 2 array (c) 1 x 4 array (d) 2 x 8 array

The Gain and directivity plots for all the array configuration is shown in figure 3.21. It can be seen that the gain and directivity for single element is 4.7 dBi and 6.8 dBi respectively. For 1 x 2 array the gain is 7.8 dBi and directivity is 10.64 dBi. For 1 x 4 array the gain is 6.11 dBi and directivity is 10.96 dBi. For 2 x 8 array the gain is 4.81 dBi and directivity is 11.19 dBi. For 4 x 8 array the gain is 7.6 dBi and directivity is 9.01 dBi.

Table 3.3 displays the parameters results for various constructed RMPA.Figure 3.22 (a -d) shows the radiation patterns of single element, 1 x 2 array, 1 x 4 array

and 2 x 8 array antenna respectively.

Table 3.3: Performance parameters for RMPA for 60 GHz

Parameters	**Single Element**	**1 x 2 array**	**1 x 4 array**	**2 x 8 array**	**4 x 8 array**
Resonant Frequency (GHz)	58.2	60	62.3	62	63
Return Loss (dBi)	-19.50	-22	-15..5	-18.1	-14.1
Bandwidth (GHz)	2.2	1.6	0.9	1.1	0.4
Gain (dBi)	4.7	7.8	6.11	4.81	7.6
Directivity (dBi)	6.8	10.64	10.96	11.19	9.01
Radiation Efficiency (%)	63.61	52.52	33.29	23.60	14.5
Antenna Efficiency (%)	60.71	52.17	32.71	23.02	12.83

By analyzing the proposed RMPA for 28 GHz, 38 GHz and 60 GHz, it is possible to conclude that when antenna's length is inversely proportional to frequency and directly proportional to wavelength. The antenna may be made shorter by reducing wavelength and increasing the frequency. The directivity and gain of a RMPA decline and bandwidth increases as the thickness of the dielectric substrate rises. So in this analysis, single element antennas have high bandwidth (2.2 GHz) for 60 GHz, low return loss for 60 GHz, high gain for 28 GHz, high radiation efficiency for 38 GHz, high directivity for 28 GHz, and greater antenna efficiency for 38 GHz. For a 1 x 2 array MPA, the following characteristics are true: the

bandwidth is high for 60 GHz, the return loss is lower for 38 GHz, the gain is high for 38 GHz, the radiation effiency is high for 28 GHz, the directivity is high for 60 GHz, and the antenna efficacy is greater for 28 GHz.The bandwidth for the 4 x 8 array MPA is high for 38 GHz, the return loss is reduced for 28 GHz, the gain is high for 60 GHz, the radiation efficiency is high for 28 GHz, the directivity is high for 38 GHz, and the antenna effectiveness is greater for 28 GHz.

3.2.6 Design of Slotted MPA Phased Array for 28 GHz

Microstrip patch antennas that have one or more slots introduced on the patch are known as slotted microstrip patch antennas. Compared to a standard microstrip patch antenna, these slots offer the following benefits:

- Increased Bandwidth: By introducing extra resonance modes, slots can broaden the antenna's bandwidth. This can be very helpful for apps that need a lot of bandwidth.
- Polarization diversity may be provided by using slots, which can enhance the accomplishment of the antenna in multipath situations.
- Cross-Polarization May Be Reduced: Slots can help the antenna's radiation pattern have less cross-polarization. This can be helpful for applications that just need a little cross-polarization.

The analogous circuit of the MPA is altered by the adding of slots. The slots increase the antenna's capacitance and inductance, which might change its resonance frequency and alter its radiation pattern. A slotted MPA's equivalent circuit may be described by combining transmission lines with lumped components like capacitors, inductors, and resistors. For maximizing the performance of a slotted MPA for a given application, it is necessary to modify the size and placement of the slots as well as the feed point location.

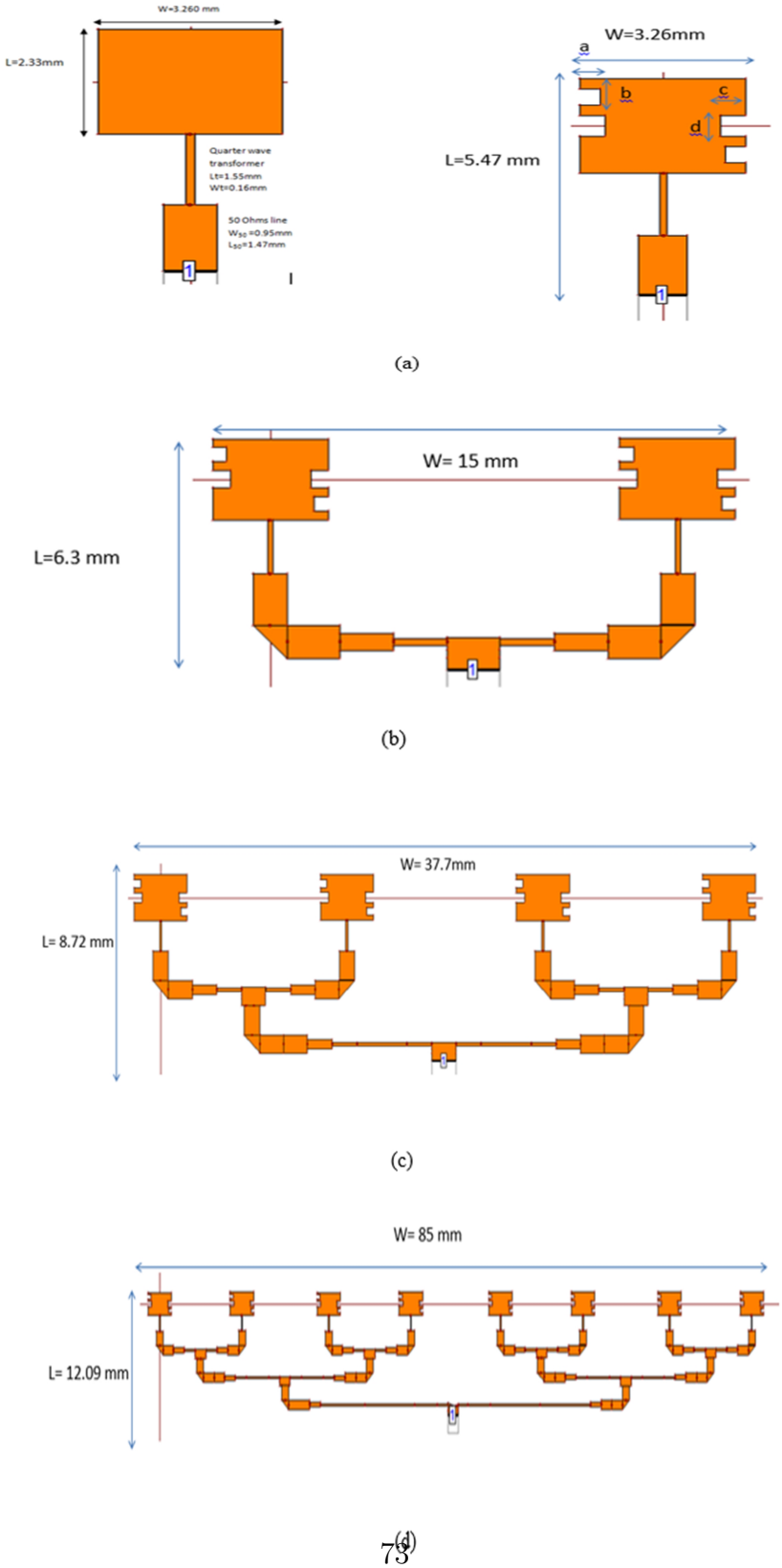


Figure 3.23: Slotted MPA at 28 GHz for (a) Single, (b) 1 x 2, (c) 1 x 4, and (d) 1 x 8

A RMPA becomes a slotted RMPA when slots are added to it. In comparison to a simple RMPA, the addition of slots alters the antenna's properties and can provide a number of benefits. Increasing the antenna's bandwidth is one of the main benefits of increasing slots. The slots add more resonant modes, which may enable the antenna to function successfully across a larger frequency range. The pattern for radiation of the antenna may also be changed by the addition of slots. A more directed radiation pattern or less cross-polarization can be attained by carefully planning the slot shape and positioning. This may come in handy for uses requiring a certain radiation pattern, such as radar or satellite communication systems. The addition of slots alters the antenna's equivalent circuit, adding more capacitance and inductance. As a result, both the input impedance and the antenna's resonant frequency may fluctuate. This may have an impact on how well the antenna and the transmission line that feeds it are matched.

Rectangular slotted MPA phased array for 28 GHz is designed using equations (3.1) to (3.17). The slot dimensions are calculated as the intended frequency wavelength in free space (λ_0). The parametric study was done while incorporating the slots on the sides of RMPA. Slot dimensions a, b, c and d are 0.4 mm, 0.4 mm, 0.5 mm and 0.5mm, respectively. The slotted patch antenna is planned on FR-4 substrate with dielectric constant 4.4 having height of 2.2 mm. The aforementioned slotted antennas were created for various phased array antennas shown in Figure 3.23.

3.2.6.1 Results of Design of Slotted MPA for 28 GHz

The single element of slotted antenna resonates at 24.65GHz giving a RL OF -13.45 dB as can be seen from figure 3.24.The bandwidth provided by single element is 2.68 GHz.

For 1 x 2 phased array, RL is -12.95 GHz while bandwidth is 0.42 dB for 29.14 GHz as shown in figure 3.25.

For 1 x 4 phased array as seen from figure 3.26,RL values of -11.56 dB at resonant frequency of 29.32 GHz is achieved giving a bandwidth of 0.22 GHz.

1 x 8 phased array,gives a quad band antenna having RL of -26.95 dB, -25.8

dB ,-22.61 dB and -11.74 dB for 21.77 GHz , 23.53 GHz ,25.76 GHz , 27.24 GHz respectively as shown in figure 3.27.The bandwidth achieved here is 0.16 GHz,0.24 GHz, 0.18 GHz and 0.13 GHz respectively at each band.

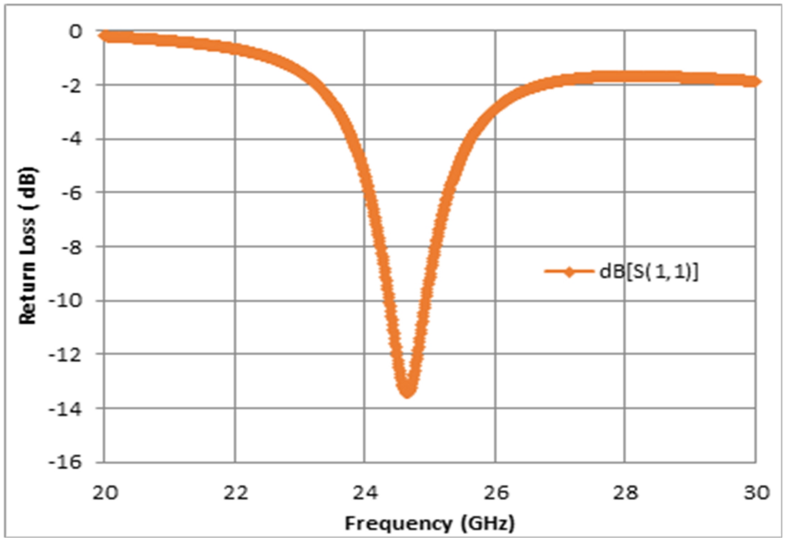


Figure 3.24: RL v/s Frequency Graph for Single Element Slotted MPA

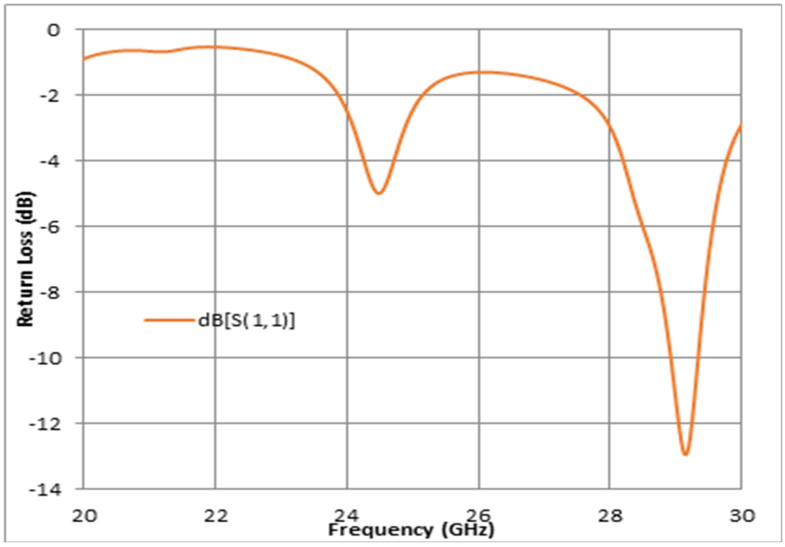


Figure 3.25: RL v/s Frequency Graph for 1 x 2 array of Slotted MPA

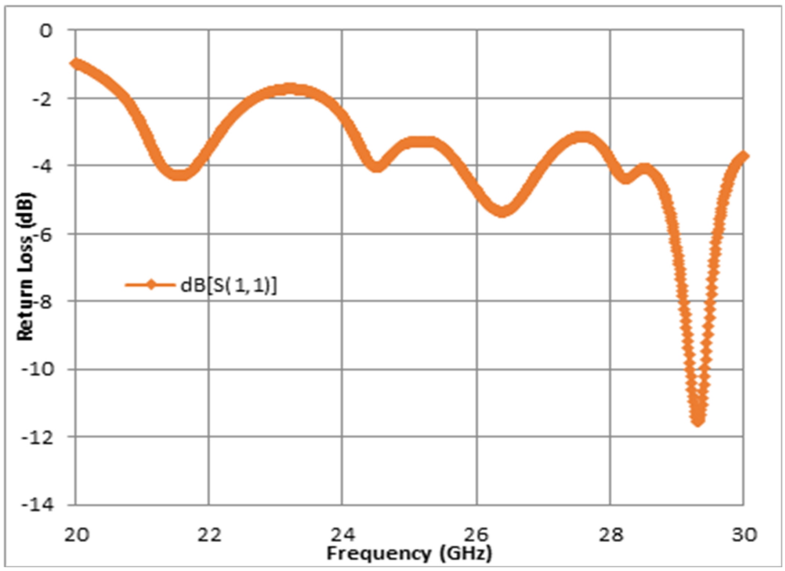


Figure 3.26: RL v/s Frequency Graph for 1 x 4 Array of Slotted MPA

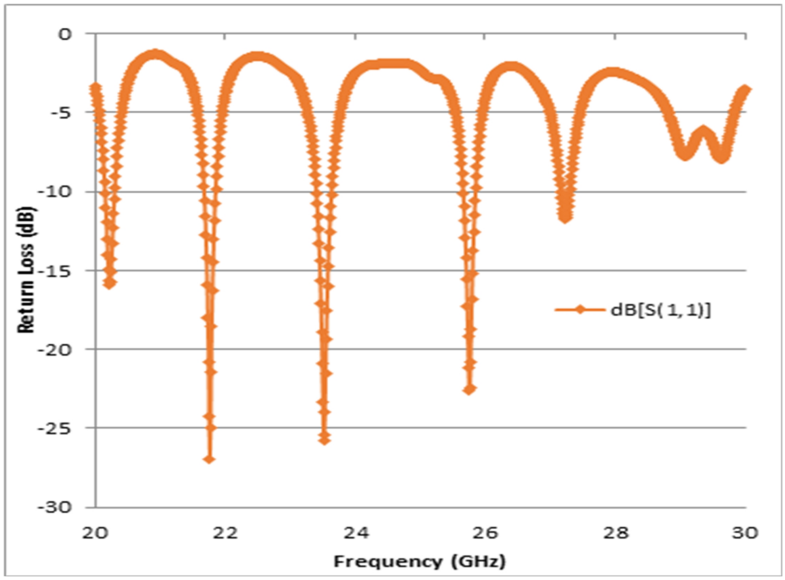


Figure 3.27: RL v/s Frequency Graph for 1 x 8 Array of Slotted MPA

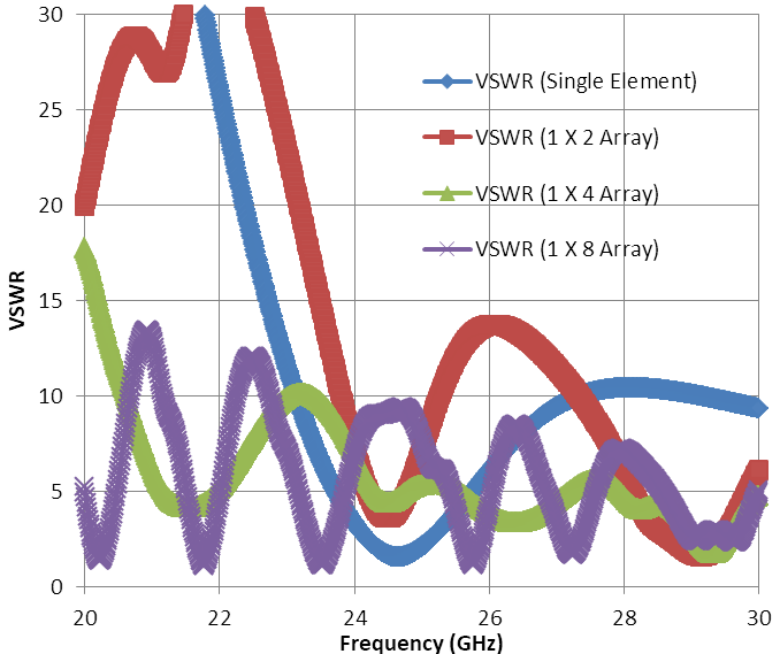


Figure 3.28: VSWR v/s Frequency Graph for Single element, 1 x 2 array, 1 x 4 array and 1 x 8 array Slotted MPA

Figure 3.28 shows the Voltage standing wave ratio of the single element, and all array configuration is below 2 at the respective resonant frequencies.The Gain and directivity plots for all the array configuration is shown in figure 3.29. It can be seen that the gain and directivity for single element is 2.68 dBi and 6.38 dBi respectively. For 1 x 2 array the gain is 5.32 dBi and directivity is 9.13 dBi. For 1 x 4 array the gain is 8.97 dBi and directivity is 13.13 dBi. For 1 x 8 array the gain is 9 dBi and directivity is 14.80 dBi. Figure 3.30 (a -d) shows the radiation patterns of single element, 1 x 2 array, 1 x 4 array, and 1 x 8 array of slotted antenna respectively. Table 3.4 shows the peformance parameters of the slotted MPA.

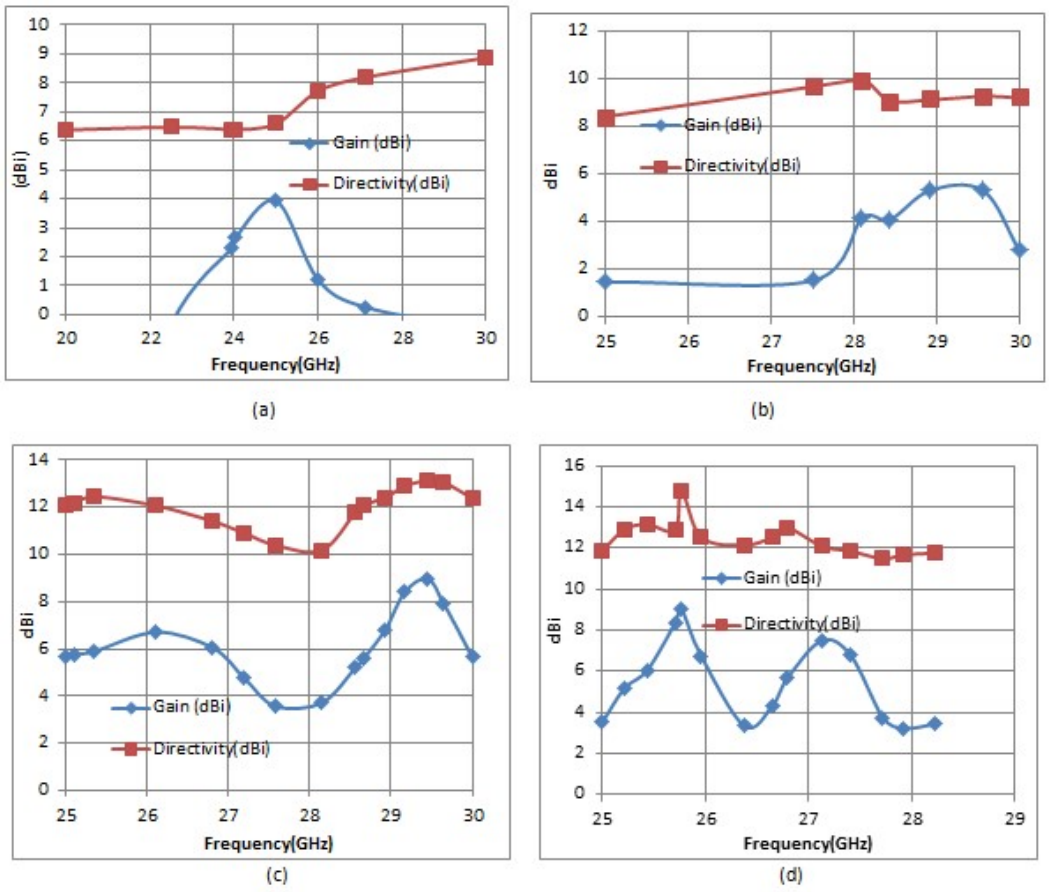


Figure 3.29: Gain & Directivity vs. Frequency Graph for (a) Single element (b) 1 x 2 Array (c) 1 x 4 Array (d) 1 x 8 Array of Slotted RMPA for 28 GHz

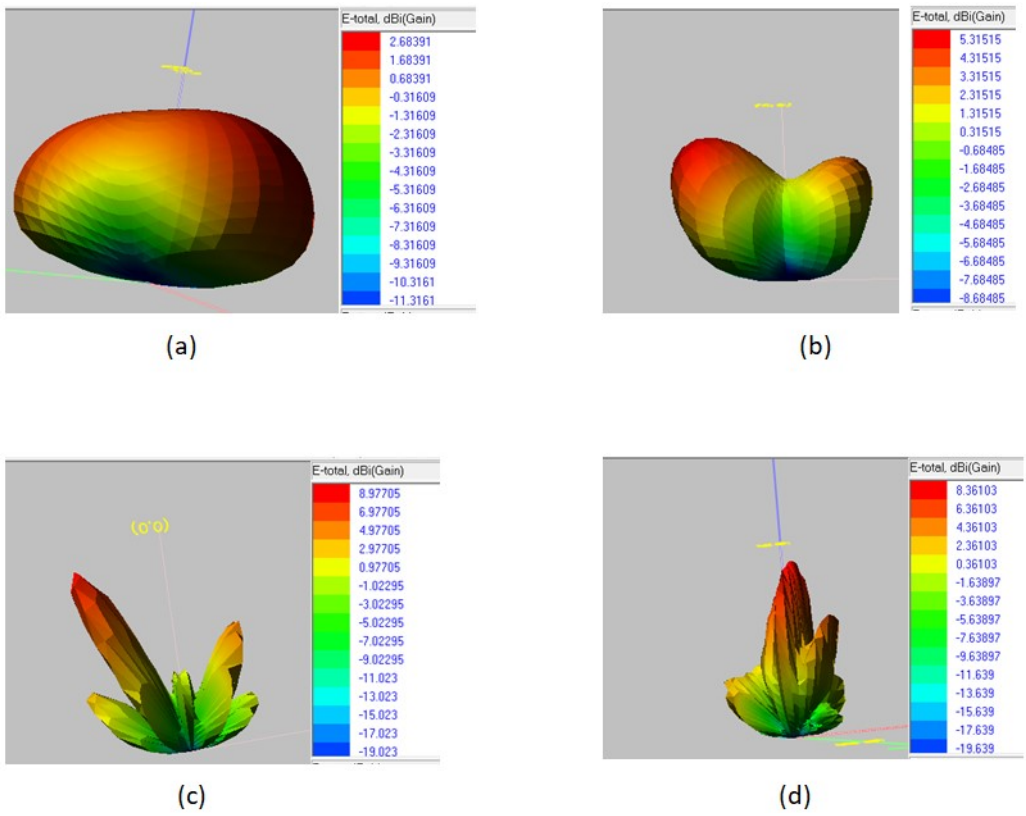


Figure 3.30: Radiation patterns for slotted MPA (a) single element (b) 1 x 2 array (c) 1 x 4 array (d) 1 x 8 array

Table 3.4: Performance Parameters for Slotted MPA for 28 GHz

Parameters	**Single Element**	**1 x 2 Array**	**1 x 4 Array**	**1 x 8 Array**
Resonant Frequency (GHz)	24.65	29.14	29.32	21.77/23.53 /25.76/27.24
Return Loss (dBi)	-13.45	-12.95	-11.56	-26.95/-25.8/ -22.61/-11.74
Bandwidth (GHz)	0.56	0.42	0.22	0.16/0.24/ 0.18/0.13
Gain (dBi)	2.68	5.32	8.97	9.00
Directivity (dBi)	6.38	9.13	13.13	14.80
Radiation Efficiency (%)	58.29	48.19	43.24	40.85
Antenna Efficiency (%)	42.62	41.63	38.36	39.79

3.3 Microstrip Patch Antenna based on MIMO

Signal transmission using multiple antennas at receiver and transmitter sides is known as MIMO antenna. A fading coefficient is used in the parallel signal transmission from transmitter to receiver. At both the transmitter and receiver, there are several antennas. The signal should fluctuate separately and uncorrelated at the receiver and transmitter. So, for MIMO systems to work, the following two requirements must be met:

- The antenna system should receive several copies of the signal, or there should be multipath of signal at the connection.
- The signal sent to the receiver should be created in a way that preserves the diversity among them.

Several connections between the transmitter and receiver are diversity. It serves as protection against the antenna system's fading. There is another connection available for communication between the transmitter and receiver in the event that one link is destroyed or attenuated. A diversity-enhanced antenna system will have little 3D cross correlation.

In this section discussed about the MIMO antenna based on the RMPA for 2 ports, 4 ports and 16 ports for 28 GHz and 60 GHz.

3.3.1 Design of MIMO for 28 GHz

A rectangular patch antenna with two, eight, and sixteen MIMO ports, built for 28 GHz, makes up the proposed antenna system. The design procedure is initially utilized to make a single RPA element. The antenna's width (w) and length (l) are estimated as 3.47 mm and 4.23 mm respectively. The feed line network is used to further develop the phased array of the 1 x 2 array. Figure 3.31 depicts the construction of the 1 x 2 array with a single port.

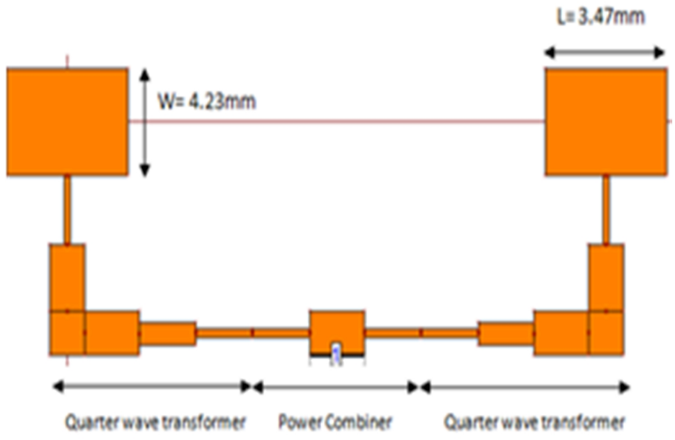


Figure 3.31: 1 x 2 Array Antenna at 28 GHz with the Feed Line Network

As demonstrated in Figure 3.31, the feed line network for every 1 x 2 array is created utilizing 50 Ω lines, a QWT, and a power combiner. Line gauge is used in the IE3D programme to determine the dimensions of the feed network's component parts. The impedances of a quarter wave transformer are 50, 70, and 100 Ωs. The impedances for a power combiner are 100, 50, and 100 Ωs. Using line gauge, the computed dimensions for 50 Ω lines are 0.76 mm and 1.95 mm in width and length. The dimensions for 70 Ω lines are 0.44 mm and 1.98 mm in width and length. The 100 Ω line is 0.21 mm wide and 2.02 mm long.

The 16 ports in the MIMO of 2 x 16 antennas are each composed of a 1 x 2 array of RPAs. The suggested antenna system's geometry for 2 ports, 8 ports, and 16 ports is depicted in figures 3.32 respectively.

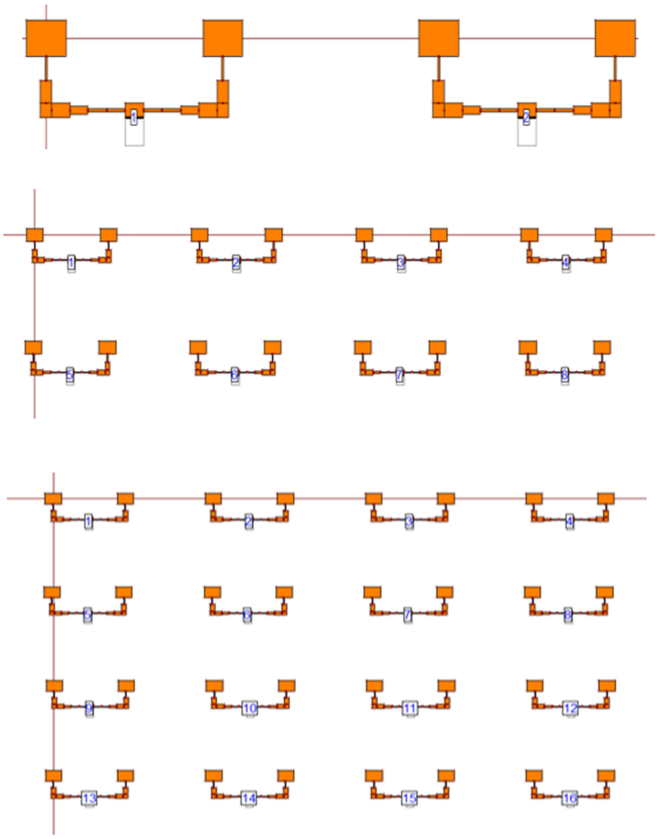


Figure 3.32: MIMO Antennas for 28 GHz with (a) 2 Ports, (b) 8 Ports and (c) Proposed 16 Ports

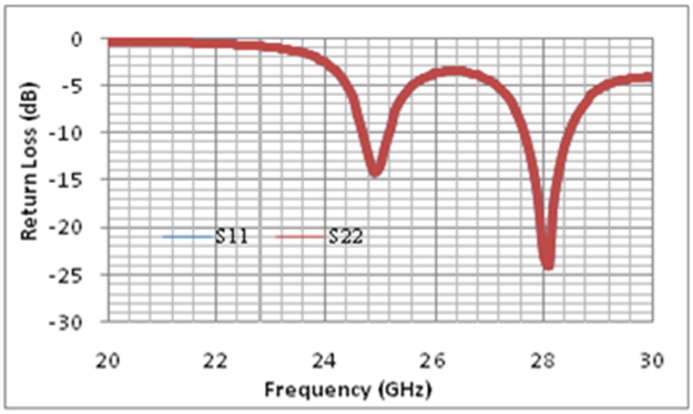
3.3.1.1 Result for MIMO Antenna for 28 GHz

Proposed antennas are modelled and simulated utilizing IE3D simulation software. The modelled S parameters (RL) results for all the 2 ports, 8 ports, and 16 ports are shown in figure 3.33. The RL for 2 ports, 8 ports and 16 ports is around -23 dB. 2 ports MIMO antenna can attain a BW of 0.80 GHz for VSWR < 2 ($|S11| < -10$ dB) from 27.65-28.45 GHz which is as per the standard for 5G communication use. 8 ports and 16 ports MIMO antenna can attain a BW of 0.90 GHz for VSWR < 2, from 27.65-28.45 GHz.

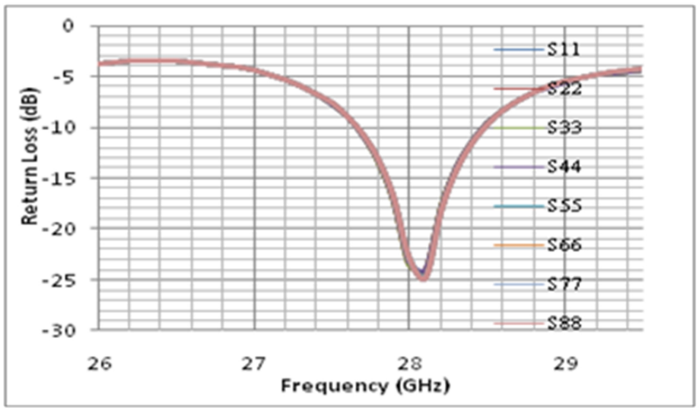
It can be noticed from the figure 3.25 that isolation among the port 16 and additional neighboring ports of antenna in complete band is in range of -22.31 dB to -72.48 dB. Insertion loss (s parameters) defines the matching between the ports. It's always higher the better. Hence it is noticed that the mutual coupling among the ports has been lessened.

The directivity and gain of 2 ports MIMO antenna are obtained as 13.37 dBi & 9.8 dBi respectively as can be comprehended from figure 3.35(a). Suggested antenna with 2 ports shows the radiation efficiency of 48.48 % and antenna efficiency of 44.94 % with VSWR of 1.15(< 2) for both the ports.

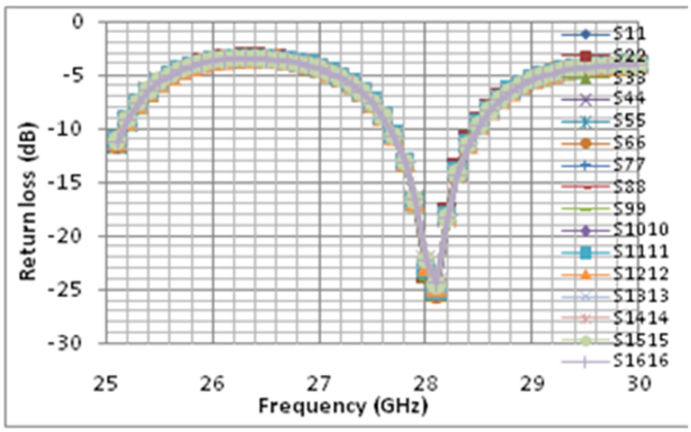
The simulated directivity and Gain for the 8 ports MIMO antenna are obtained as 16.49 dBi & 19.07 dBi respectively as noticed from figure 3.35 (b). Radiation efficiency is obtained of around 55.56 % and Antenna efficiency is 55.29 %, with VSWR of 1.15 for all 8 ports



(a)



(b)



(c)

Figure 3.33: Return loss for Proposed 2, 8 and 16 Port MIMO Microstrip Patch Antenna

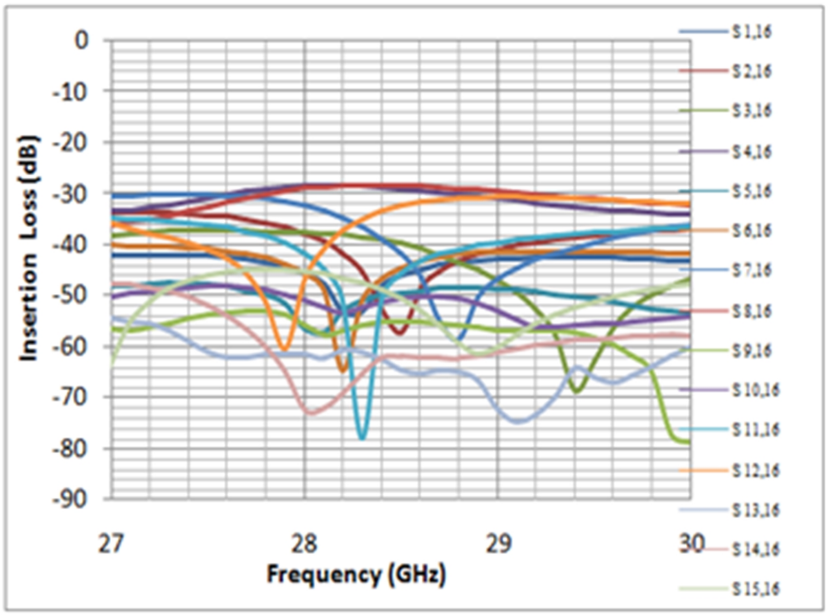


Figure 3.34: Mutual Coupling for Proposed 16 Port MIMO Microstrip Patch Antenna

The directivity and gain of 16 ports MIMO antenna are obtained as 22.38 dBi & 18.90 dBi respectively as can be comprehended from figure 3.35(c). Proposed antenna displays the radiation efficiency of 45.16 % and antenna efficiency 44.78 %, and VSWR of 1.15 for all 16 ports as presented in figure 3.36. The patterns of radiation for suggested antennas are computed and presented in figure 3.37.In this performance of various antenna parameters for MIMO MPA for 28 GHz is provided in Table 3.5. According to table when number of ports increases, the bandwidth, gain, radiation efficiency and directivity increases. Directivity and gain are assessed by enlarging the antenna elements and ports. The suggested MIMO antenna performs well throughout the frequency range 28 GHz, with a BW of 0.90 GHz, and an observed RL of all 16 ports |S11| of fewer than -10 dB.

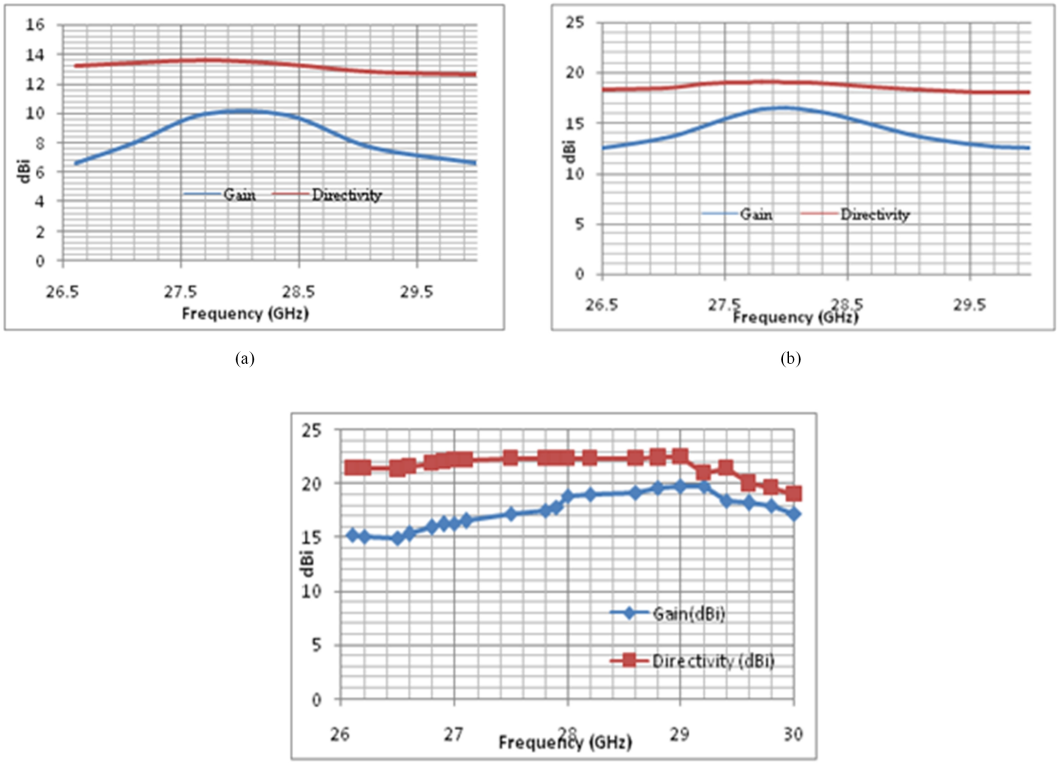


Figure 3.35: Gain & Directivity for Proposed (a) 2 Ports (b) 8 Ports (c) 16 Ports MIMO Microstrip Patch Antenna

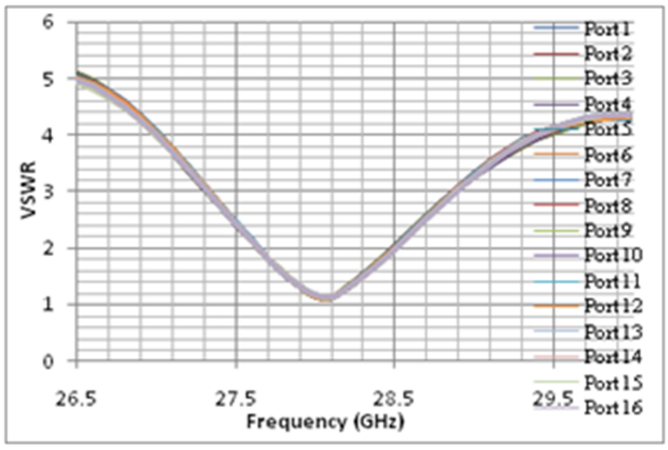


Figure 3.36: VSWR for Proposed 16 Ports MIMO Microstrip Patch Antenna

Gain at peak of 18.90 dBi and directivity of 22.38 dBi are attained at 28 GHz. The efficiency of the antenna and the simulated radiation are 44.78 % and 45.16 %, respectively. It is clear from the comparison table that massive MIMO technology enables the development of antennas with high gain and excellent directivity.

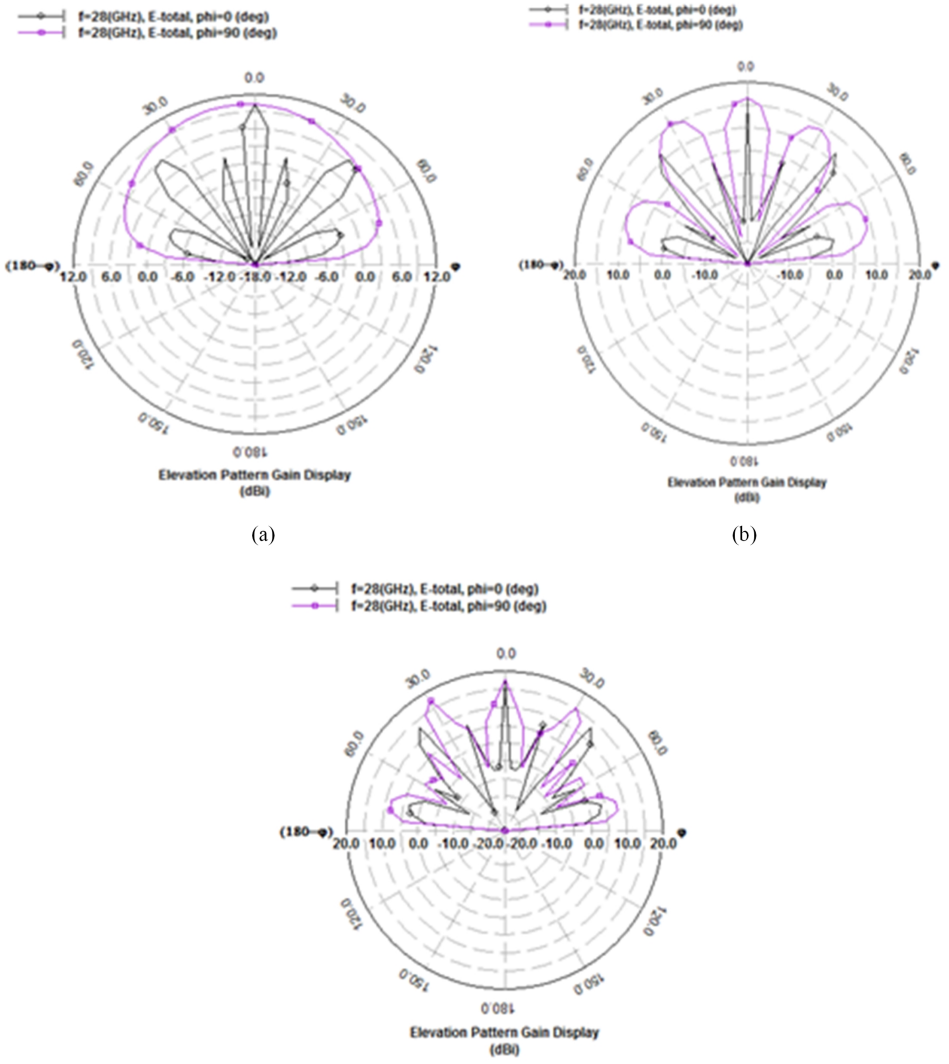


Figure 3.37: Radiation Pattern for Proposed (a) 2 Ports (b) 8 Ports (c) 16 Ports MIMO Microstrip Patch Antenna

Table 3.5: Comparison Table for Various Ports MIMO MPA for 28 GHz

Parameters	**2 Ports**	**4 Ports**	**8 Ports**	**12 Ports**	**16 Ports**
Frequency (GHZ)	28	28	28	28	28
RL (DB)	-22.98	-22.98	-23	-23	-23
Bandwidth (GHZ)	0.80	0.80	0.90	0.90	0.90
Gain (DBI)	9.8	12.90	16.49	17.83	18.90
Directivity (DBI)	13.37	15.9	19.07	20.88	22.38
Radiation Efficiency (%)	48.48	53.36	55.56	49.94	45.16
Antenna Effeciency (%)	44.94	49.43	55.29	49.52	44.78

3.3.2 Design of MIMO for 60 GHz

Figure 3.38 depicts the single port RMPA at 60 GHz. A 32 element MIMO RPA with 16 ports is the suggested antenna designed similar to 28 GHz.

Using the traditional design method, a single rectangular patch antenna is created, with dimensions of w and l are 1.11 mm and 1.52 mm respectively.

A 2 x 16 antenna array is made up of 16 ports, each housing a 1 x 2 array of RPAs as seen for 28 GHz in similar manner. The feed line network for every 1 x 2 array is created utilizing a 50 Ω lines, QWT, and a power combiner. The IE3D software's Line gauge is used to specify the length and breadth of the aforementioned components. Impedances for the quarter-wave transformer are 50 Ω, 70 Ω, and 100 Ω; for the power combiner, they are 100 Ω, 50 Ω, and 100 Ω. The length

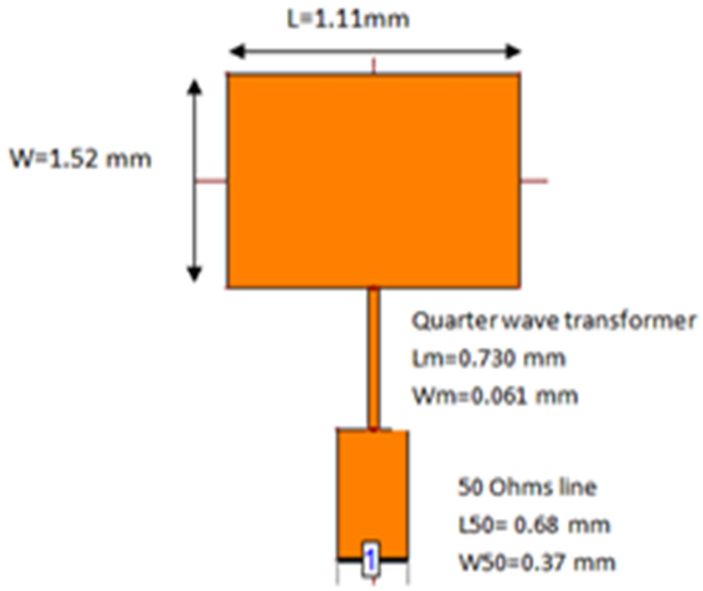


Figure 3.38: Single Element of RMPA at 60 GHz

and width are 0.68 mm and 0.37 mm respectively, for 50 Ω lines. The size of 70 Ω lines is 0.200 mm in width and 0.705 mm in length. The 100 Ω line is 0.725mm long and 0.082mm wide. The suggested antenna measures 48.56 mm and 21.82 mm overall.

3.3.2.1 Result for MIMO Antenna for 60 GHz

IE3D simulation software is utilized to design and model suggested antenna. The simulated S parameter results for each of the 16 ports are displayed in Figure 3.39. All of the ports have a return loss of about -22 dB. The 16 port MIMO antenna can operate between 59.15 and 60.65 GHz with a VSWR 2 (|S11|) -10 dB and a 1.5 GHz bandwidth.

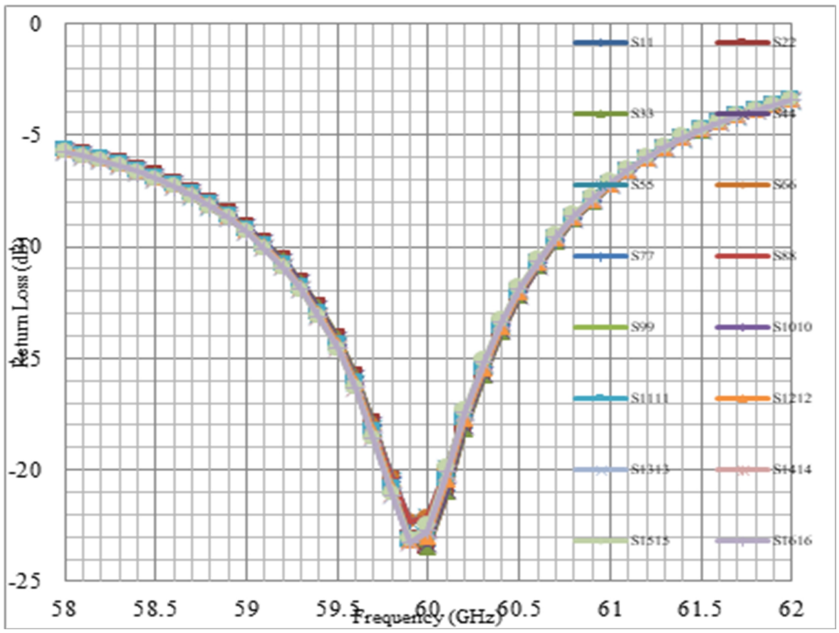


Figure 3.39: RL S11 Simulation Results for Proposed 16 Port MIMO MPA

As demonstrated in Figure 3.40, the isolation among the antenna's final port 16 and other nearby ports in entire band ranges from -27 dB to -65.5 dB.

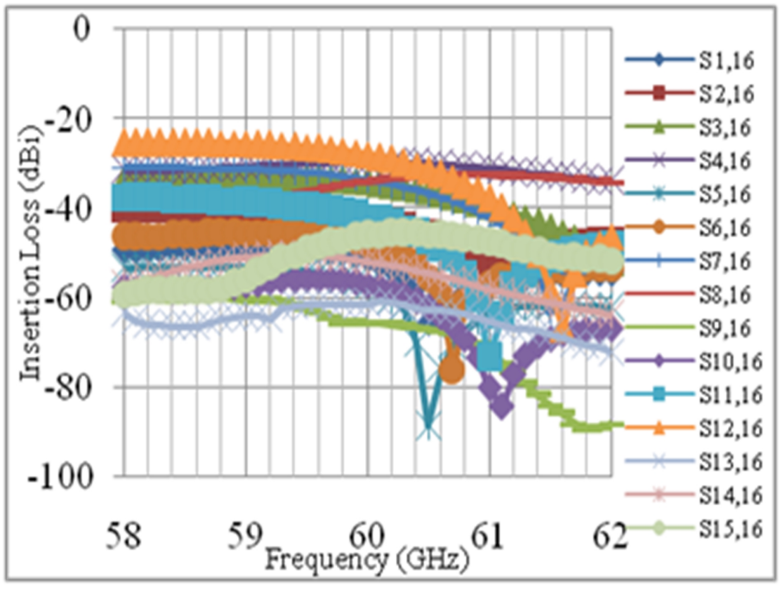


Figure 3.40: Insertion Loss Simulation Results for a 16 Port MIMO MPA

Figure 3.41 demonstrate the simulated directivity and gain of suggested antenna. The suggested 32-element antenna's computed directivity and gain at 60 GHz are 19.89 dBi and 21.59 dBi, respectively. The suggested antenna's obtained directivity and gain are suitable for 5G communication.

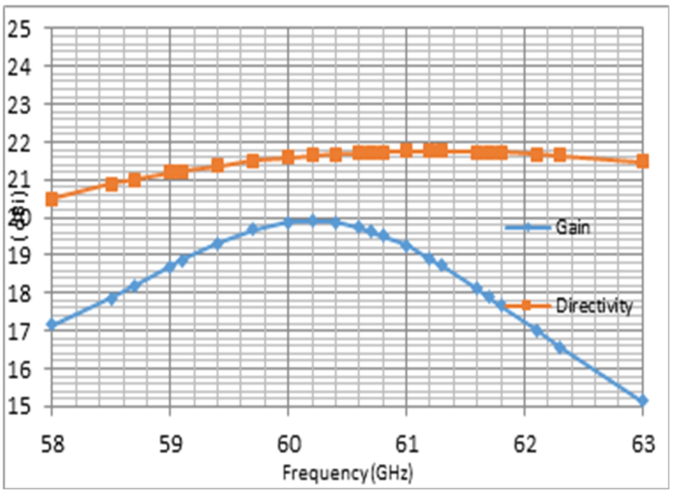


Figure 3.41: Gain and Directivity Simulation Results for a Proposed 16-Port MIMO MPA

The suggested antenna's efficiency and radiation efficiency are 67.51 % and 68.05 %, respectively. The comprehensive outcomes for the suggested antenna are showed in Table 3.6.

Table 3.6: Results Gained for Suggested 16 Port MIMO Antenna for 60 GHz

Parameters	**Proposed Antenna**
Frequency (GHz)	60 GHz
Return Loss (dB)	∼- 22 dB
Bandwidth (GHz)	1.5 GHz
Gain (dBi)	19.89 dBi
Directivity (dBi)	21.59 dBi
Radiation Efficiency (%)	68.05 %
Antenna Efficiency (%)	67.57%
VSWR	∼<2

Table 3.7 displays the comparison study performed by adding each port for antenna one at a time. It is obvious that an antenna with more ports would have higher gain and higher directivity. Our findings pave the road for huge MIMO configurations that will improve antenna performance at millimetre waves.

Table 3.7: Comparative Analysis for MIMO Antenna for 60 GHz

Parameters	2 Ports	4 Ports	6 Ports	8 Ports	12 Ports	16 Ports
Frequency (GHz)	59.9	59.9	60	60	60	60
Antenna Effeciency (%)	52.16	58.77	52.36	58.81	61.51	67.57
Bandwidth (GHz)	1.4	1.4	1.52	1.49	1.49	1.5
Directivity (dBi)	13.62	16.12	18.09	18.85	20.59	21.59
Gain (dBi)	10.80	13.78	15.2	16.54	18.48	19.89
Radiation Efficiency (%)	52.51	58.36	52.87	59.39	62.02	68.05
Return Loss (dB)	-22.15	-22.15	-22.05	-22.06	-22.16	-22.15

By expanding the ports and antenna components, both gain and directivity are evaluated. The suggested MIMO antenna performs well throughout the frequency band 59.15-60.65 GHz, having a BW of 1.5 GHz, and an observed loss in return of all 16 ports |S11| of less than -10 dB. Gain at peak is 19.89 dBi and 21.59 dBi directivity are attained at 60 GHz. The efficacy of the antenna and the simulated radiation are 68.05 % and 67.57 %, respectively. In the E- and H-planes, the 3 dB width of the beam at 60 GHz is approximately $\pm$ 5° and $\pm$ 11°, respectively.

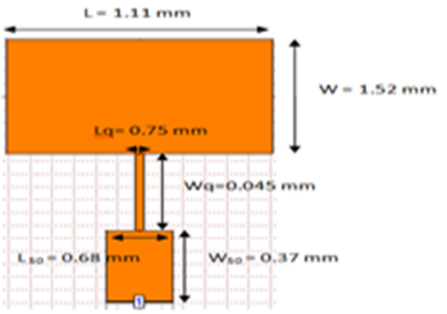
It is clear from the comparison table that massive MIMO technology enables the development of antennas with significant gain and excellent directivity. A 60-GHz wireless system that complies with the IEEE 802.11ad wireless networking standard is the perfect application for the newly built 16 ports MIMO antenna.

3.3.3 Design of 4 Port MIMO

At a millimetre wave frequency of 60 GHz, a single patch of a MPA has been advanced on a low-cost, FR-4 substrate with a height of 0.2 mm and a dielectric constant of 4.4. Use of 50 transmission line was utilized to feed this straightforward patch antenna. A QWT has been created to match 50Ω transmission line and the impedance of patch antenna. Equations (3.1) – (3.4) were utilized to determine the single patch antenna's sizes, which are W = 1.52 mm and L = 1.11 mm. The patch antenna is powered by a feed line of 50 that has been developed for 60 GHz. The 50 ohm line has the following measurements: length L50=0.68 mm and width W50 = 0.37 mm. The magnitudes of the suggested antenna is presented in Figure 3.42.

Two designs of MIMO antenna with 2 and 4 ports are shown to study the optimal MIMO antenna design that delivers the greatest outcomes for millimetre wave applications. The 2 port antenna is created by combining the existing single patch antenna with another. To reduce influence of mutual coupling, the distance among both patch antennas is kept at more than or equal to 1/2. The 2 port antenna is 3.22 x 1.93 mm^2 in size which is shown in Figure 3.43.

Figure 3.43 (a) displays an antenna setup with two ports. Four patch antennas have been spaced apart by a distance more than or equal to 1/2 in a four port antenna system. The 4 port antenna's dimensions are 3.22 x 4.86 mm^2. In Figure 3.43(b), the 4 port antenna system is displayed.

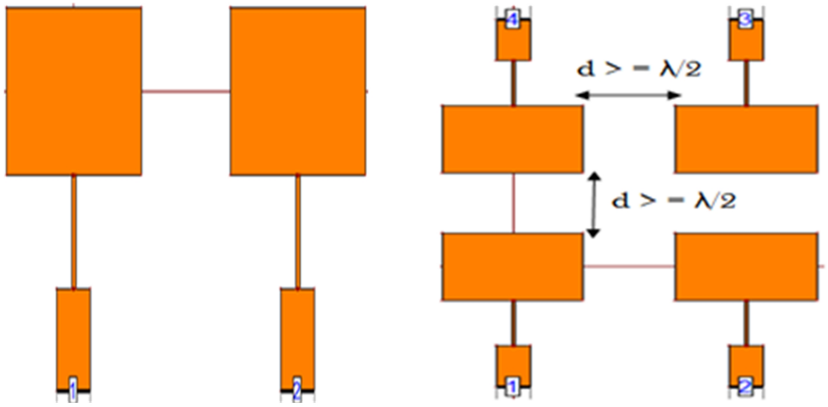


(a)

Parameter	Width (mm)	Length (mm)
50 Ω line	W_{50} = 0.37	L_{50} = 0.68
QWT	Wq=0.045	Lq= 0.75
RPA	W=1.52	L= 1.11

(b)

Figure 3.42: Single Port MPA with Dimensions



(a) (b)

Figure 3.43: (a) 2 Port and (b) 4 Port MIMO Patch Antenna

3.3.3.1 MIMO Antenna Performance Results

This part uses the IE3D^{TM} simulator, which is based on moments of techniques, to analyse and simulate the MPAs that were shown in the preceding sections.

The single port MPA is found to resonate at 58.1 GHz, giving a 2.4 GHz bandwidth while casing a band of frequencies between 57.1 and 59.2 GHz. Figure 3.44 shows the S11 for single port antenna at -19.84 dB.

The 2 ports MIMO antenna has a 2.3 GHz bandwidth and resonates at 58.1 GHz, casing the range of 57 to 59.3 GHz. Figure 3.45 shows S- parameter graph of 2 port MPA.The reflection coefficient was determined to be -18.41 dB.

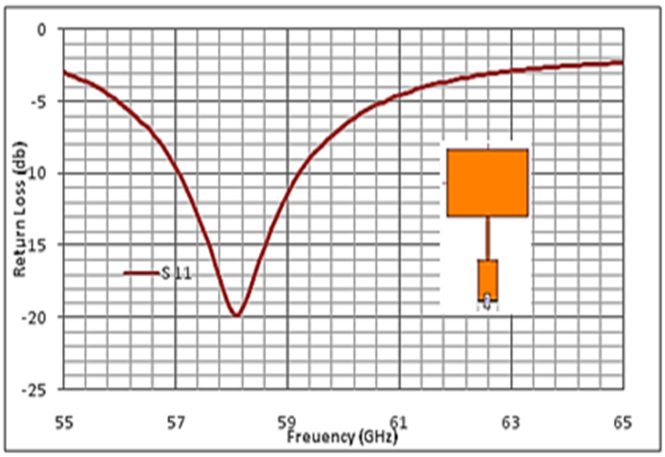


Figure 3.44: |S11| of the Single Port MPA

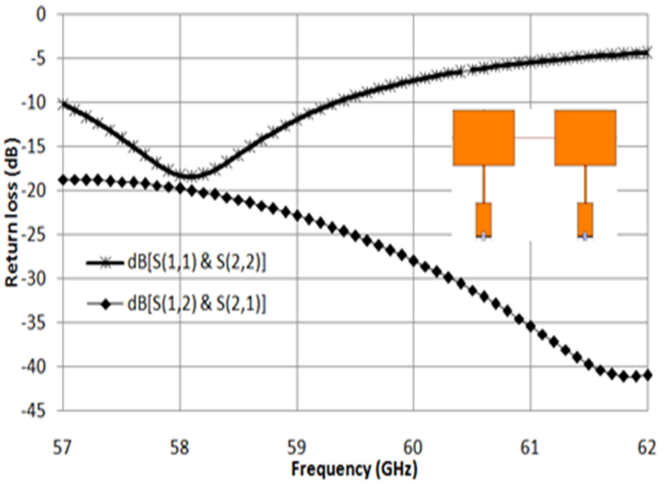


Figure 3.45: S Parameter of the Two Port MPA

The 4 port MIMO antenna resonates at 58 GHz and offers a BW of 2.3 GHz spanning the 56.9-59.2 GHz range frequency with an given reflection coefficient of -18.09 dB which is shown in Figure 3.46. The more ports there are, the more mutual coupling there will be among the ports, which will harm the antenna system. Figure 3.47 shows isolation loss of proposed four port MPA.

Figure 3.47 shows that it offers strong isolation of -19 dB to -30 dB. The technology is useful for millimetre wave communication due to the 4 port MIMO antenna's excellent isolation among all four ports.

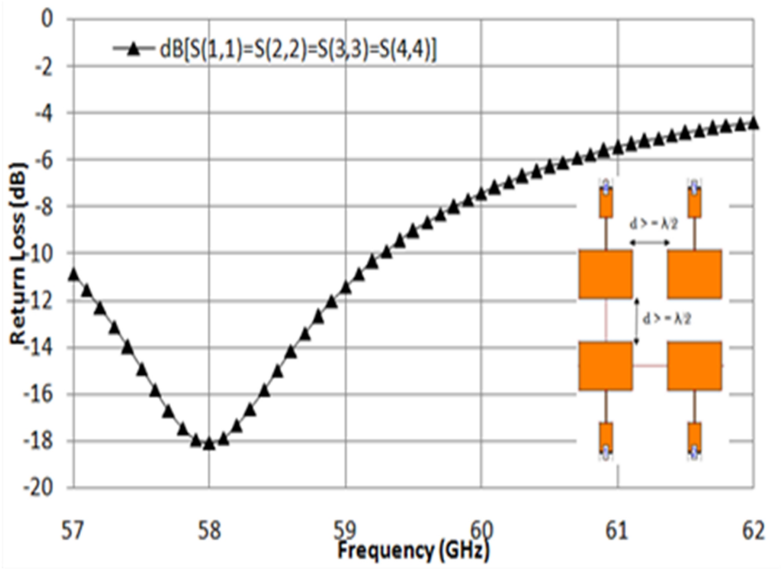


Figure 3.46: S Parameter of the Four Port MPA

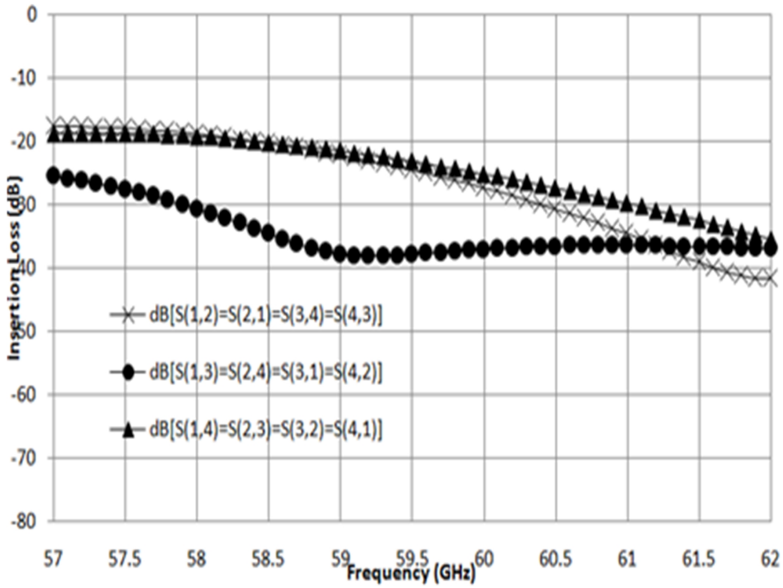


Figure 3.47: Isolation Loss of Four Port MPA

Figures 3.48 to Figure 3.50 shows the single port, 2 port, and 4 port MIMO antenna's peak gain and directivity plots.

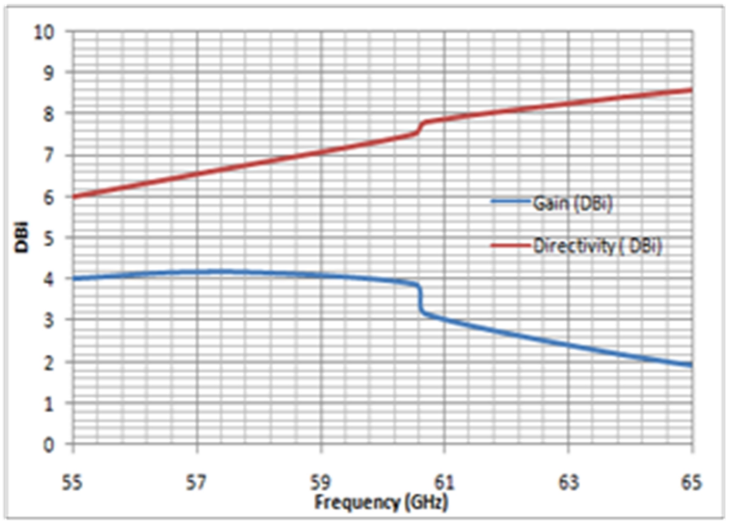


Figure 3.48: Gain and Directivity of a Single Port MPA

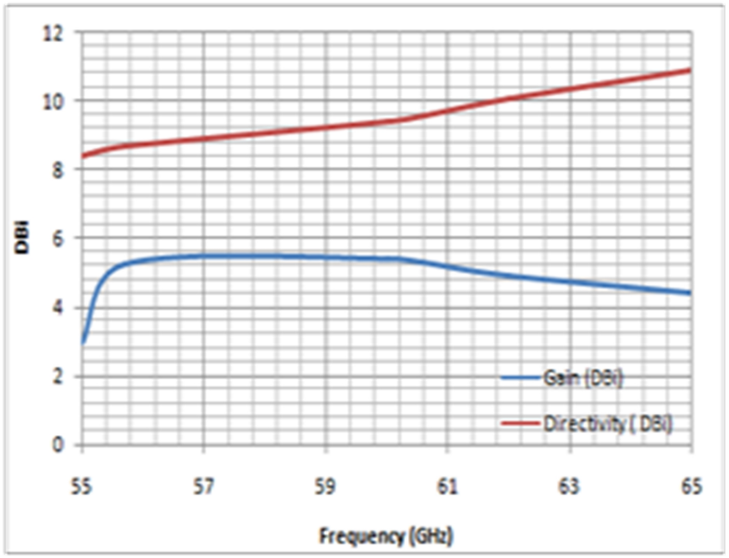


Figure 3.49: Gain and Directivity of the Two Port MPA

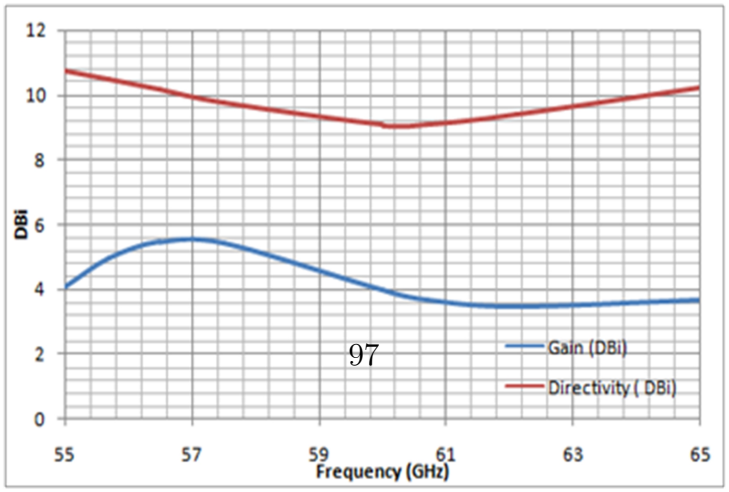
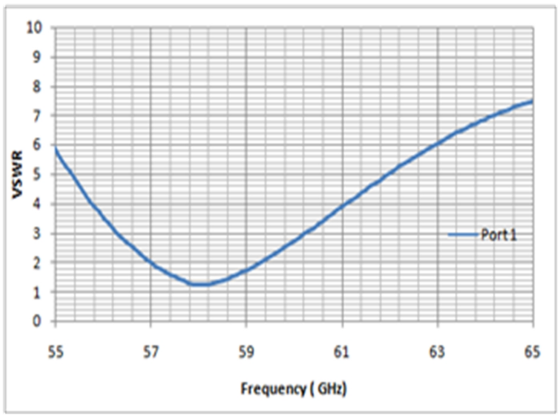
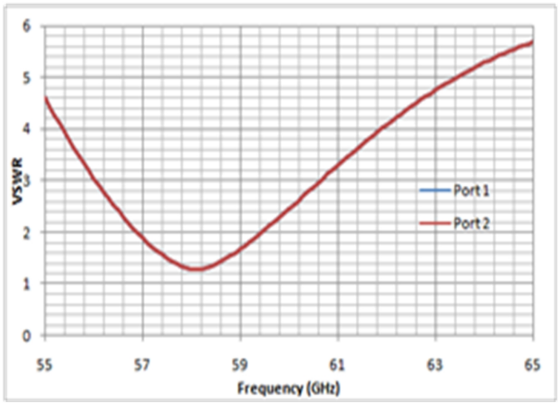


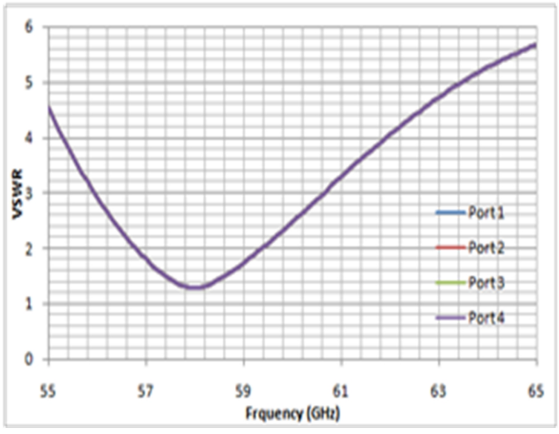
Figure 3.50: Gain and Directivity of the Four Port MPA



(a)



(b)



(c)

Figure 3.51: VSWR for (a) Single Port, (b) 2-Port and (c) 4-Port MIMO Antenna

It has been shown that the gain and directivity for single port antenna are 3.10 dBi and 6.99 dBi, respectively. The directivity and gain for the 2-port MIMO antenna are observed to be 8.67 dBi and 5.2 dBi, respectively. It provides a gain of 5.44 dBi and a directivity of 9.75 dBi for the four port MIMO antenna. As seen in Figures 3.51, the VSWR for each of the 3 designs is < 2.

The comparison of the three antennas' performance is shown in Table 3.8, and it is determined that the 4 ports MIMO antenna does superior in terms of directivity and gain, which are necessary for millimetre wave applications.

Table 3.8: Comparative Analysis of Proposed MIMO Antennas

Parameters	**Single Port**	**2 Ports**	**4 Ports**
Resonant Frequency (GHz)	58.1	58.1	58
Antenna Efficiency (%)	40.90%	45.71%	37.10%
Bandwidth (GHz)	2.4	2.3	2.3
Directivity (dBi)	6.99	8.67	9.75
Gain (dBi)	3.10	5.2	5.44
Input reflection coefficient (dB)	-19.84	-18.41	-18.09
Radiation Efficiency (%)	42.44%	47.76%	37.47%

The important performance characteristics like ECC, DG, and MEG were es-

timated to analyse the efficacy of the 4 ports MIMO antenna.

3.3.3.2 Envelope Correction Correlation (ECC)

One among the important performance factors for MIMO antenna is ECC. It is a measurement of how well the antenna components of a MIMO configuration correlate with one another. It is assessed using equation (3.26) and the far field radiation characteristics [64, 65] as well as the S-parameters [66, 67] equation (3.27). Only antennas with better antenna efficiency can benefit from the second technique [68].

$$\text{ECC } = \frac{\left|\iint \left[F_1(\theta,\phi)^* F_2(\theta,\phi) d\Omega\right]\right|^2}{\iint \left|F_1(\theta,\phi)\right|^2 d\Omega \iint \left|F_2(\theta,\phi)\right|^2 d\Omega} \tag{3.26}$$

Where * designates the Hermitian product and F_i represents the antenna system's far field radiation pattern when port i is energised.

$$\rho_{ij} = \frac{\left|S_{ii} * S_{ij} + S_{ji} * S_{ij}\right|^2}{\left(1 - \left|S_{ii}\right|^2 - S_{ij}^2\right)\left(1 - \left|S_{ji}\right|^2 - S_{jj}^2\right)} \tag{3.27}$$

where there are i and j ports. There are four ports in this scenario, and i and j can range from one to four. IE3D ™ simulation programme simulates the ECC values in relation to frequency. The simulated ECC values for 4 port MIMO antenna from both techniques are shown in Figures 3.52 and 3.53.

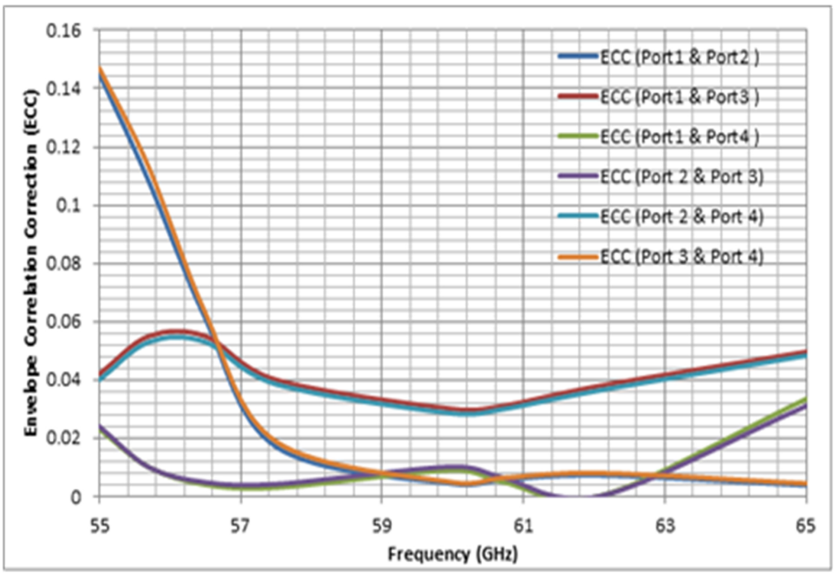


Figure 3.52: ECC Values from Patterns of Far-Field Radiation

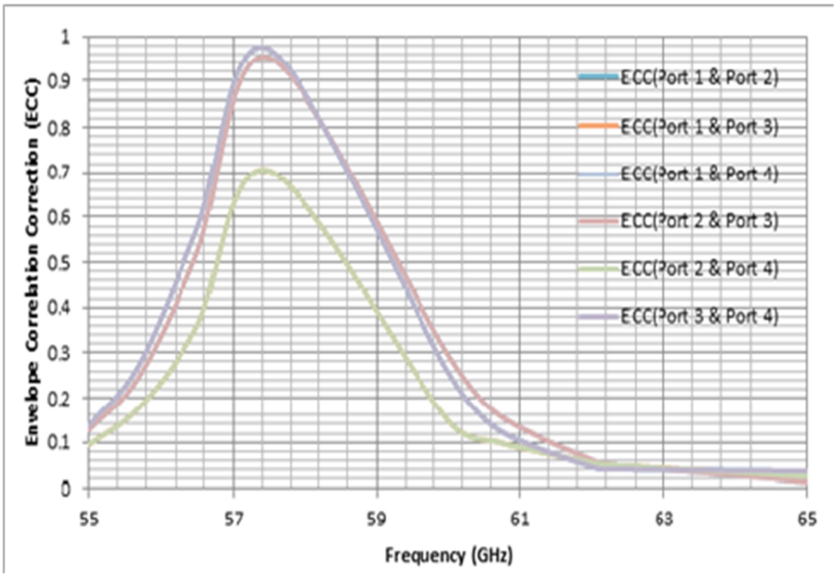


Figure 3.53: ECC Values from S Parameters

ECC must be zero in the ideal scenario, while less than 0.5 is acceptable in a realistic setting [69]–[71]. The ECC value for whole antenna is under the necessary threshold, ensuring the MIMO antenna's successful functioning.

3.3.3.3 Diversity Gain

For a good, dependable system, the DG of MIMO antenna essential to be high [72], and it is esttimated utilizing equation (3.28). Figure 3.54 displays that across the operational range, DG is over 9.8 dB, guaranteeing the MIMO antenna's successful operation.

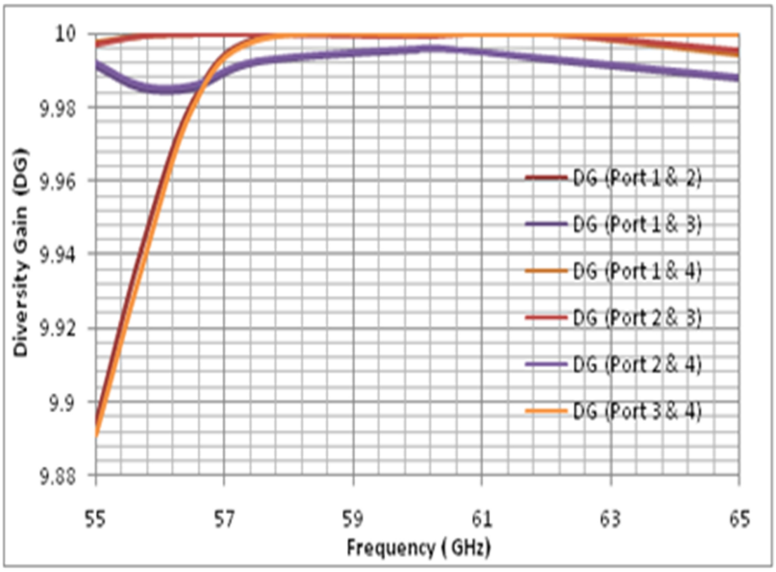


Figure 3.54: Diversity Gain

$$D_{\text{gain}} = 10\sqrt{1 - |\rho_{ij}|^2} \tag{3.28}$$

Where ρ_{ij} is the antenna's envelope correlation.

3.3.3.4 Mean Effective Gain

MEG is a metric utilized to compare the power achieved by a diversity antenna in a fading setting to power obtained by an antenna, which is isotropic. It is determined using equation (3.29), and Figure 3.55 displays a graph of the same.

$$MEG_i = 0.5\left\{1 - \sum_{j=1}^{k} |S_{ij}|^2\right\} \tag{3.29}$$

Where i is the antenna under examination and k is the total quantity of antennas. For 4 port antenna in this instance, $k = 4$.

Hence, here have,

$$\begin{aligned} \text{MEG}_1 &= 0.5 * \left\{1 - |S_{11}|^2 - |S_{12}|^2 - |S_{13}|^2 - |S_{14}|^2\right\} \\ MEG_2 &= 0.5 * \left\{1 - |S_{21}|^2 - |S_{22}|^2 - |S_{23}|^2 - |S_{24}|^2\right\} \\ MEG_3 &= 0.5 * \left\{1 - |S_{31}|^2 - |S_{32}|^2 - |S_{33}|^2 - |S_{34}|^2\right\} \\ \text{MEG}_4 &= 0.5 * \left\{1 - |S_{41}|^2 - |S_{42}|^2 - |S_{43}|^2 - |S_{44}|^2\right\} \end{aligned} \tag{3.30}$$

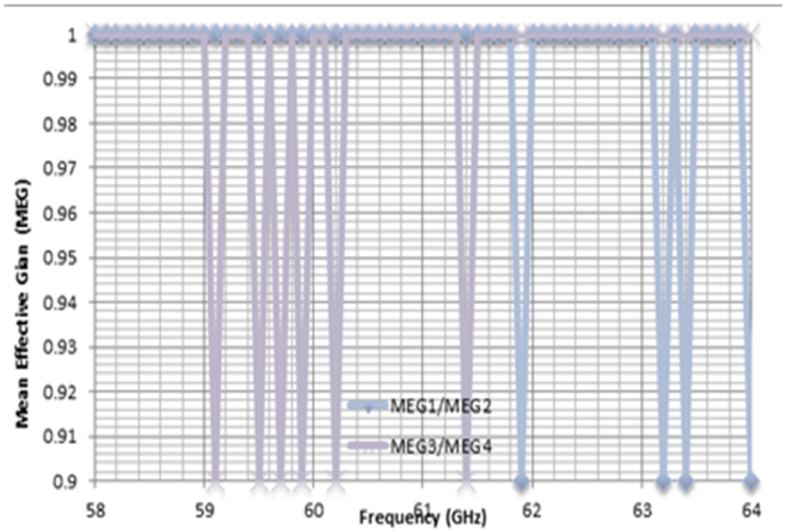


Figure 3.55: MEG_1/MEG_2 and MEG_3/MEG_4

Table 3.9: Performance Metrics for a Four-Port MIMO Antenna

Parameters	**Results**
DG	>9.8 dB
ECC	<0.9 (Utilizing S parameter technique)
	<0.06 (utilizing far field radiation technique)
MEG	<1 dB
Resonant Frequency	58 GHz

According to the MEG study, the proportion of MEG_1/MEG_2 and MEG_3/MEG_4 for proposed four port element antenna should be less than 3 dB [73, 74]. Since MEG values are fewer than 1 dB, Figure 3.55 serves as validation. The suggested four port antenna's MIMO performance mesures are shown in Table 3.9, which demonstrates that the antenna has high diversity properties and is well right for millimetre wave applications.

3.3.4 Design of a 4 Port Slotted RMPA MIMO

The four ports MIMO antenna has been modeled and simulated for slotted MPA at 28 GHz. The structure of the proposed antenna is shown in figure 3.56. The slotted patch antenna is designed on FR-4 substrate with dielectric constant 4.4 having height of 2.2 mm.

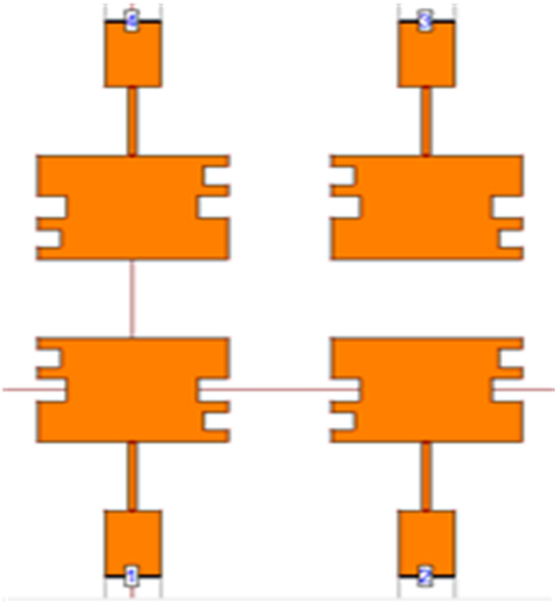


Figure 3.56: 4 Port Slotted RMPA MIMO Design

3.3.4.1 Result of the Slotted Rectangular RMPA MIMO Antenna

The single port slotted antenna resonates at 24.65 GHz, giving a bandwidth of 0.55 GHz as can be seen from figure 3.57. It provides a gain of 3.9 dBi and directivity

of 6.59 dBi as shown in figure 3.59.

As there is a requirement of higher gain and directivity the four ports MIMO antenna has been designed which provides a bandwidth of 0.36 GHz having resonating frequency of 24.67 GHz as noticed from figure 3.58. The four port antenna gives a gain of 5.7 dBi and directivity of 10 dBi as noticed from figure 3.60.

The VSWR of the single port and 4 port antenna is shown in figure 3.61 and can be shown that its below 2 at the respective resonant frequencies.

Table 3.10 shows the comparative analysis of both the designs.

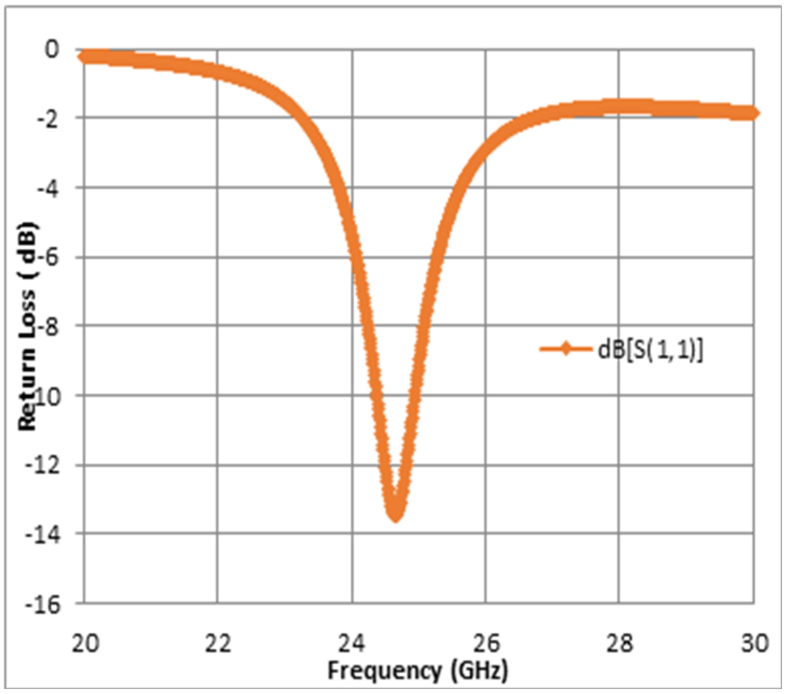


Figure 3.57: RL vs. Frequency Graph for single port Slotted MIMO Antenna

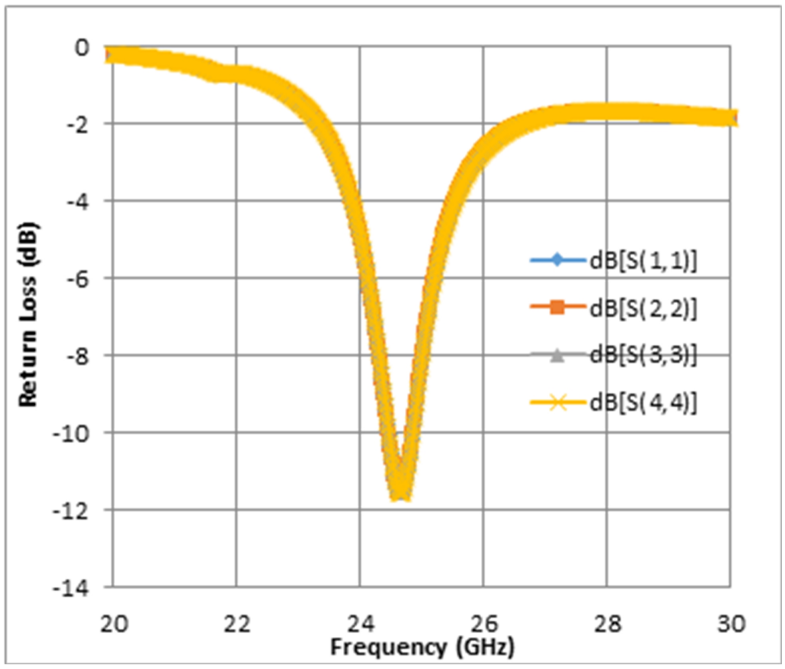


Figure 3.58: S Parameter of the Four Port slotted MIMO MPA Antenna

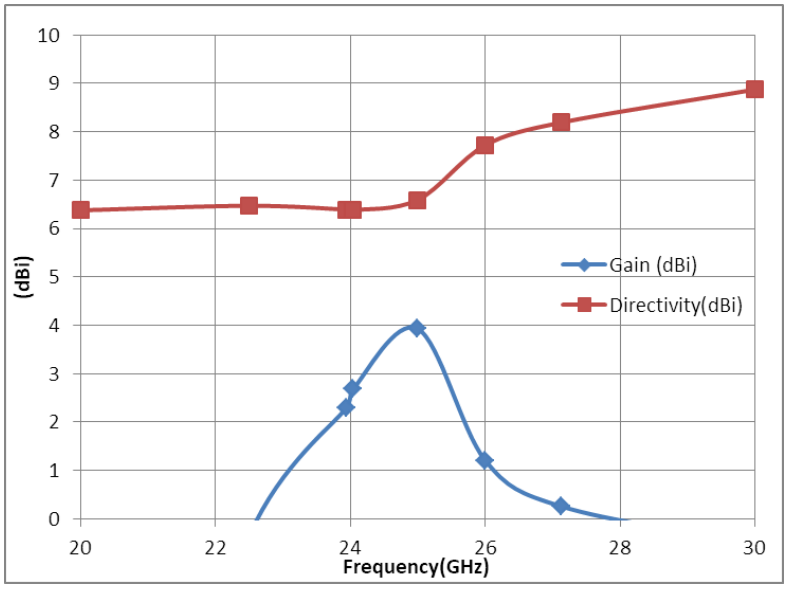


Figure 3.59: Gain and Directivity of single port of Slotted RMPA

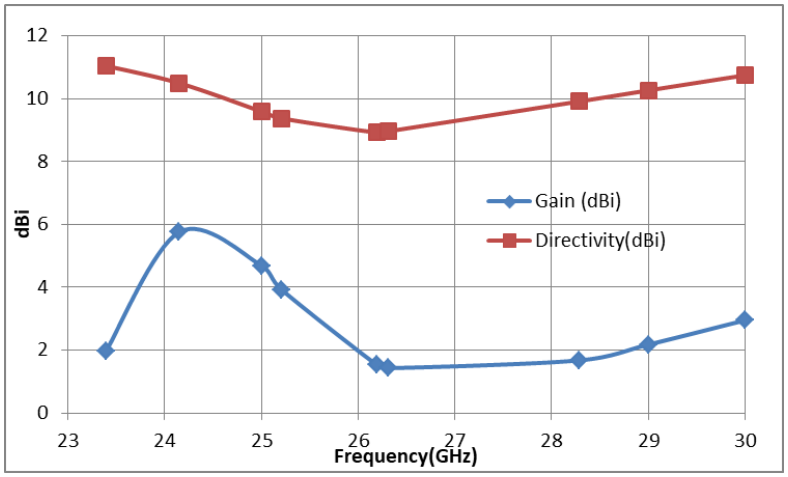


Figure 3.60: Gain and Directivity of 4 port of Slotted RMPA

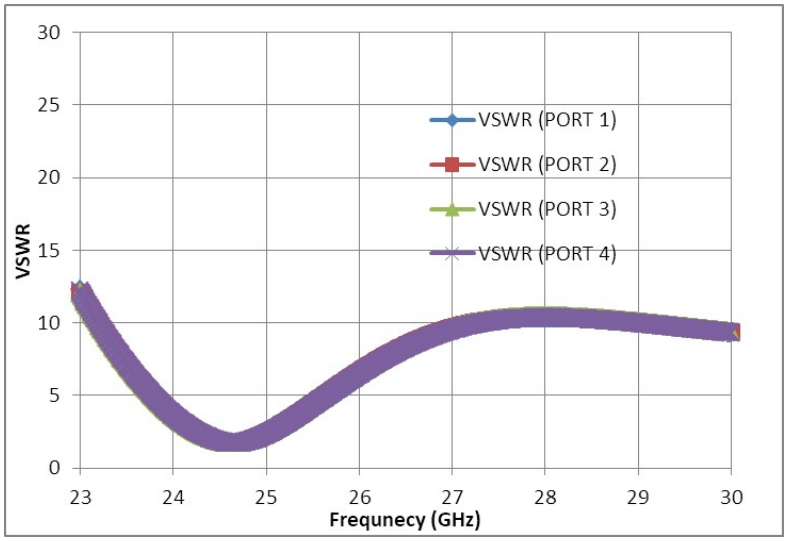


Figure 3.61: VSWR vs. Frequency Graph for single and 4 port Slotted MIMO Antenna

Table 3.10: Comparative Analysis of Proposed MIMO Antennas for 28 GHz

Parameters	**Single Port**	**4 Ports**
Resonant Frequency (GHz)	24.65	24.67
Bandwidth (GHz)	0.55	0.36
Input reflection coefficient (dB)	-13.45	-11.57
Gain(dBi)	3.9	5.7
Directivity(dBi)	6.59	10
Antenna Efficiency (%)	54.18%	48.10%
Radiation Efficiency (%)	61.74%	33.47%

3.3.5 Summary

This chapter discussed about the designs of phased array and MIMO rectangular MPA for various frequencies such as 28 GHz, 38GHz, and 60 GHz. The parametric study was done in all designs in order to optimize the results. The result of the designs from IE3D software for each antenna for various antenna parameters and MIMO antenna parameters are provided with graphical and tabular representation. The design diagram for single element and various array for RMPA along with 2 port, 4 port, 16 port MIMO MPA also provided.

Chapter 4

Switched Beam Antenna using Butler Matrix at Millimetre Wave Frequency

4.1 Overview

A means of reaching this generation is through telecommunication. Radio communication is one of the important types of telecommunication, using radio frequency as the means of communication. The hardware design and functionality of this form of communication significantly altered it [75]. However, there are numerous problems with this communication method, which has problems with interference, system quality, and data rate. Currently, mobile communication and wireless communication systems are very significant in many sectors, including transportation, business, and education [76]. Future wireless communication systems are anticipated to have larger bandwidths, greater transmit rates and a limited operating range of millimetre-wave frequency bands [77]. Wireless communication systems are being used excessively, so it is necessary to develop smart antennas with increased effectiveness, optimised size, and other useful qualities [78]. A smart antenna is made up of a few different individual antennas that combine to form an array system with some digital signal processing that can transmit and receive data

sensitively. Future wireless communication will mostly depend on smart antennas with great gain and switching beam capabilities operating at mm-wave frequency. The benefits of creating these intelligent antennas will be greater capacity, fewer high-frequency loss, and reduced co-channel interference.

The smart antenna system with the two common qualities of an adaptive array and a switched beam is known as a switched beam smart antenna system (SBSAS), and the adaptive array SAS is known as an AASAS. To switch the beam property to the required type of antenna, a switch beam antenna requires an optimal algorithm and an easy processing system [79]. The adaptive array antenna, on the other hand, necessitates a clever algorithm and a simple processing system. The beam property can be used in both electrical and mechanical applications [80]. Using the electronic beam technique necessitates the use of RF MEMS and certain diodes, specifically varactor and pin-diodes, as well as an extra biasing circuit, causing in a sophisticated feed system [81]. The mechanical beam method necessitates the use of a mechanical framework that rises the weight and size of system. Several beams are produced by the switched beam system, and a correct beam with a high signal level is chosen to follow the surroundings using a mobile [82]. The beam is changed by the system as the mobile moves. Beam forming technologies can also be utilized to progress performance of the switch beam antenna system. Beam forming methods that can be used include brass, Rotman lenses, butler matrices, reflector lenses, and the Nolen matrix [83]. The radiation element in the switching beam antenna is critical in creating a well-organized system at mm-wave frequencies. The beam-forming network is a key constituent of the switch beam antenna system. The fundamental role of the beam forming network is to provide varying levels of power and phase distribution to achieve control over the beam's directivity. The butler matrix (BM) is a sort of beam forming priority mechanism that is important in the 5G sector of mobile communication systems. Because of wireless data traffic, the future mobile system for communication will utilize mm-wave frequencies to gain a broad frequency range and fast transmission rates.

The valuation of the DOA, one of the fundamental technologies of radar and wireless communications, has been researched for a long time. MUSIC (Multi-

ple signal classification) and assessing signal parameters thru rotational invariance techniques (ESPRIT) algorithms, as well as several optimized algorithms like maximum likelihood (ML), weighted subspace fitting (WSF), and orthogonal propagator (OP) algorithms, have all been proposed as ways to increase the resolution of DOA estimation. The fundamental idea underlying all of these techniques is that the DOA estimates are based on phase-array antennas. Array antennas, however, typically come with expensive and complicated technology. Modern methods of DOA estimation rely on signal phase variations (assumed to be narrowband signals) between antenna array members. Using an antenna array necessitates a sophisticated receiver structure even though DOA estimate techniques are well understood. It is necessary to have a separate receiver channel for each element of the array, and both the receiver channels and the system calibration must be accurate. Another option is to estimate DOA using measurements of signal power, or received signal strength indicator (RSSI), for low-cost applications. Understanding the antenna design is necessary for this, as is the ability to predict or cancel out the signal's unknown route loss. Frequently, the Cramer-Rao Lower Bound (CRLB) is used to describe how well antenna arrays perform DOA estimation. The use of the CRLB to improve performance has been studied from a number of angles, including array geometries. Recently, a number of closed-form CRLB equations for isotropic antennae and multidimensional array shapes were obtained.

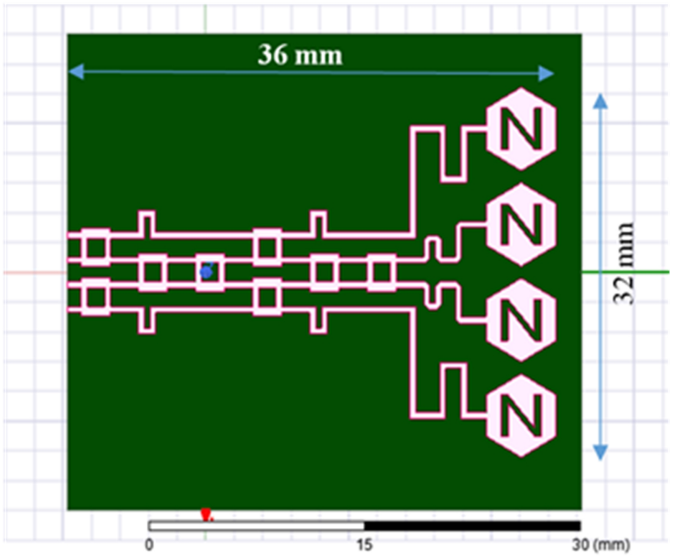
4.2 Proposed Micro Strip Patch Antenna with Beam Forming Network

A conducting patch with a ground plane on opposite side of a dielectric substrate makes up a MSPA, which can have any non-planar or planar design. For narrow-band microwave wireless communications that demand a semi-hemispheric average, this printed resonant antenna is a common choice. The MSPA has been widely investigated and is regularly employed as a constituent of an array because of its configuration (planar) and easiness of integration with micro strip technology. MSPAs have been investigated widely up to this point. There is a complete list of

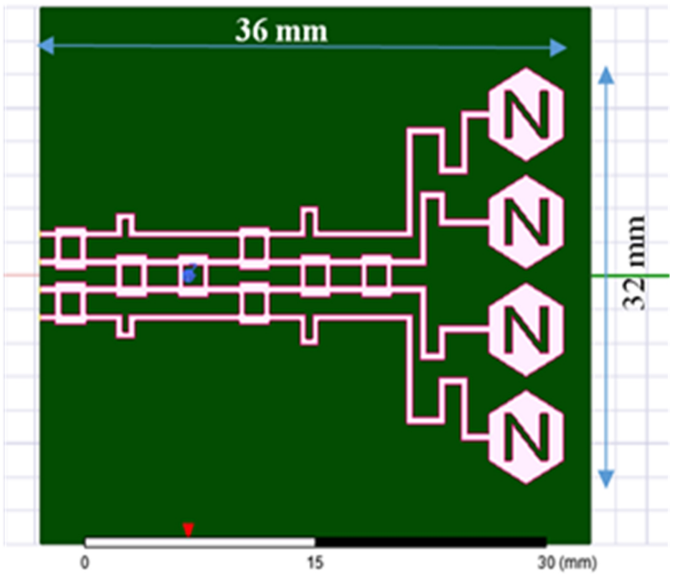
the geometries, along with a description of their key characteristics. The fundamental and most popular types of microstrip antennas are circular and rectangular patches. A hexagonal patch antenna is combined with a Z-slot microstrip patch antenna to form the proposed switching beam antenna. The fact that hexagonal patch antennas have a variety of benefits over other forms makes them a popular choice for antenna design. They offer a more uniform radiation pattern, which might enhance the effectiveness of antenna, which is one of its key advantages. The antenna's bandwidth may be increased by the bigger surface area made possible by the hexagonal form.

As a result, it enhanced radiation properties and decreased cross-polariza tion levels. While the Z-slot provides a means for introducing a switchable phase delay, which allows for the establishment of multiple beams with different directions. The use of the Z-slot also helps to decrease the cross-polarization levels and improves the polarization purity of antenna. BM is also utilized as a beam-forming network with a patch antenna. Two BMs are created with four antenna elements at the BM's output ports. The BM is designed using two separate phase shifters, 45° and 120°. One of the butler matrices has two 45° phase shifters, while the other has two 45° phase shifters and two 120° phase shifters. DOA estimation is also performed for the proposed antenna design using a novel CRL technique for DOA estimation.

The benefit of utilising the CRLB for DOA estimating is that, independent of the specific technique utilised, it offers a theoretical lower constraint on the possible estimate accuracy. This enables us to assess the algorithm's performance and contrast it with the theoretical limit. Other DOA estimate procedures, like ESPRIT (estimate of Signal Parameters through Rotational Invariance Techniques), Capon beamforming, and MUSIC (Multiple Signal Classification), are also often employed in antenna design. But these methods have drawbacks, such as noise sensitivity, computational complexity, or the need for previous knowledge of the number of sources. But the proposed CRLB technique is devoid of these drawbacks. The width and length of proposed antenna with butler matrix are 32 mm and 36 mm, respectively. Figure 4.1(a) portrays a MSPA array with a 45° phase



(a)



(b)

Figure 4.1: (a)Proposed Micro Strip Patch Antenna Array with 45° Phase Shifter Butler Matrix, (b) Proposed Microstrip Patch Antenna Array with 120° and 45° Phase Shifters Butler Matrix

shifter butler matrix. Figure 4.1(b) depicts a MSPA array with 120° and 45° phase shifters butler matrix.

The innovative antenna design is printed on a Rogers RT/duroid 5880(tm) substrate with a thickness of 0.127 mm and a dielectric loss tangent of 0.0009 mm. The complete structure is developed with the HFSS tool, and the DOA estimation algorithm is simulated in MATLAB. The proposed design's efficiency is tested using several performance criteria, revealing that it is well-suited for mm-wave frequency applications.

4.2.1 Switched Beam Antenna Architecture

Switched Beam Antennas (SBA) can replace complicated, mechanically-pointed antennas and pricey phased-array antennas by offering quick steering, high gain, and decreased size, weight, and power for line-of-sight communications. A switched beam antenna's construction includes a microstrip hexagonal patch antenna with Z-slot and a butler matrix. A unique switching beam architecture can be created by integrating both components.

4.2.1.1 Proposed Micro-Strip Hexagonal Patch Antenna Array

The proposed switching beam architecture is made up of a linear array with four antenna elements denoted as $F = 4$ and the spacing among the antenna elements denoted as $C_{\text{is}} = \lambda/2$. Because of its resilience, low charge, and easy implementation, a micro-strip antenna with a hexagon patch and Z slot is commonly employed. The antenna is created using the HFSS tool and printed on Rogers RT/duroid 5880(tm) with a thickness of 0.127 mm and a dielectric loss tangent of 0.0009 mm. The micro strip patch antenna utilized measures 8×8 mm. Figure 4.2 depicts a micro strip hexagon patch antenna with Z-slot. The width of MSPA[112] is estimated utilizing Equation 4.1, which can be written as;

$$U_j = \frac{c}{2 \times f_r} \times \sqrt{\frac{2}{\varepsilon_r + 1}} \tag{4.1}$$

Where dielectric loss tangent of substrate is denoted as ε_r of 0.0009 mm, and the speed of light is denoted as 3×10^8 m/s, frequency f_{r} is stated as 33GHz.

The antenna length can be estimated using the effective dielectric constant ED_r and the thickness T_S of substrate. As a result, the mathematical expression for calculating the effective length of the MSPA from ED_r is as follows;

$$ED_r = \frac{\varepsilon_r + 1}{2} + \frac{\varepsilon_r - 1}{2}\left(1 + 12 \times \frac{T_s}{U_j}\right)^{\frac{1}{2}} \tag{4.2}$$

$$L_h = \frac{c}{2 \times f_r \times \sqrt{ED_r}} \tag{4.3}$$

The length extension can be expressed numerically as;

$$\Delta l_{\mathrm{engtth}} = 0.412 \times T_s \times \frac{(ED_r + 0.3)}{(ED_r - 0.258)} \times \frac{\left(\frac{U_j}{T_s} + 0.264\right)}{\left(\frac{U_j}{T_s} + 0.8\right)} \tag{4.4}$$

Eventually, the actual length of patch antenna is produced by combining length extension and effective length, which is represented as;

$$length = L_e - 2 \times \Delta length \tag{4.5}$$

4.2.2 Butler Matrix (BM)

It is a microwave network that is utilized to generate beams in a particular patch of antenna arrays. The usual version of the butler matrix is $A \times A$, which a network is made up of crossovers, phase shifters, and hybrid couplers. The first A in $A \times A$ represents the quantity of input and output ports, while second A represents the number of distinct beams created. It is made up of several junctions that connect the input to output port through transmission lines. BM is made of phase shifters and couplers. The most frequently utilised component is the 90° coupler, which is a 2×2 circuit with a 90° phase transition across the two outputs. It is possible to use 180° couplers in place of 90° couplers. It is conceivable to first add filtering functions to the couplers before using these couplers to build the filtering Butler

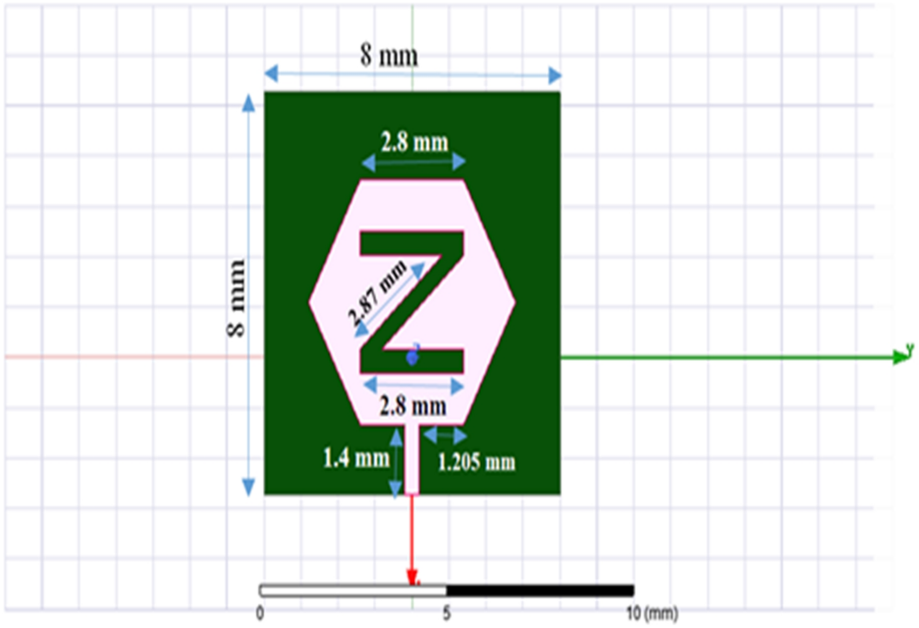


Figure 4.2: Micro-Strip Hexagon Patch Antenna with Z-Slot

matrix since the couplers are the most crucial part of the BM. In order to produce power at different phases and amplitudes at the 4×4 matrix's output, the 0 dB coupler, 3 dB coupler, and phase shifters were employed in the design. Secondly, two 3 dB couplers have been created to act as the Butler matrix's input ports.BM consists of $(A/2)\log_2(A)$ hybrid couplers, phase shifters of $(A/2)\log_2(A-1)$, and crossovers of $\sum_{i=1}^{\log_2(A)} \left[\frac{A}{2}\left(2^{i-1}-1\right)\right]$ respectively. A standard BM is represented as $A \times A$, where $A = 2^n$. As a result, the couplers are placed in n ranges of $B_m/2$ inside each range. The phase shifters are positioned in a $n-1$ range. The phase shifter's position and count may differ depending on the type of couplers utilised. As a result, the phase shifter is dependent on the hybrid couplers. The directed beams are measured using the BM dimension. A butler matrix with $B \times B$ the network in which the value of A is assigned to be 4 then it is said to be 4×4 a butler matrix, and the beams created are $2\mathrm{L}, 1\mathrm{L}, 1\mathrm{R}$, and 2R, respectively.

4.2.2.1 Components of Proposed 4 × 4 Butler Matrix

A basic BM has hybrid couplers, a phase shifter, and a crossover. The proposed BM includes two 0 dB crossovers, two 45° phase shifters, and four 90° hybrid couplers.

- $> 90°$ ***hybrid couplers***

Initially, 90° hybrid couplers were also called as quadrature hybrid couplers. These are four-port directional couplers with an identical -3 dB power split. The optimal symmetric answer for a matched, lossless, reciprocal 4-port device is contained in its scattering matrix[113]:

$$S = \begin{bmatrix} 0 & \frac{-j}{\sqrt{2}} & \frac{-1}{\sqrt{2}} & 0 \\ \frac{-j}{\sqrt{2}} & 0 & 0 & \frac{-1}{\sqrt{2}} \\ \frac{-1}{\sqrt{2}} & 0 & 0 & \frac{-j}{\sqrt{2}} \\ 0 & \frac{-1}{\sqrt{2}} & \frac{-j}{\sqrt{2}} & 0 \end{bmatrix}. \tag{4.6}$$

The proposed hybrid couplers are examined. In the suggested butler matrix, only one input is powered. As a result, the coupler is used as a divider. The power invaded in port 1 in figure 4.3 is uniformly distributed to ports 3 and 2 with a 90° phase difference, and power is not linked to port 4. The two 90° hybrid couplers are printed on Rogers RT/duroid 5880(tm) substrate and simulated using the HFSS tool.

- 0 dB ***Crossover***

A crossover is defined as a 0 dB coupler used to connect two transmission lines that have idealized no coupling. Only by combining two branch-line couplers and modifying line lengths can it be accomplished. The design is produced on Rogers RT/duroid 5880(tm) substrate and then simulated with the HFSS tool. Figure 4.4 depicts the intended 0 dB crossover. When power enters port 1, 100 percent of that power will be transported to port 3 that is on other side of P1 but it must first pass another transmission line from port 4 - 2. Crossover is a symmetrical and reciprocal device with the same characteristics as a hybrid coupler.

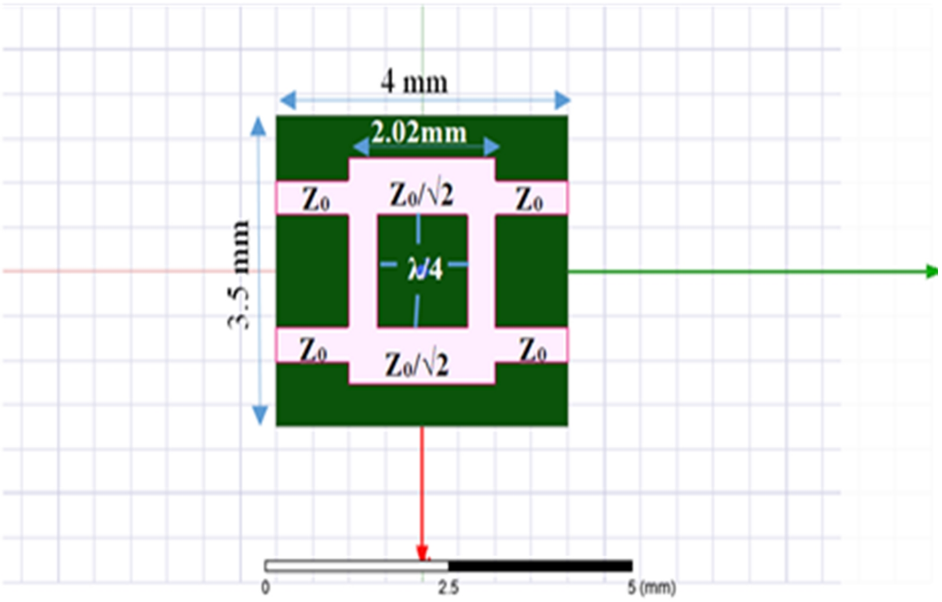


Figure 4.3: Proposed 90° Hybrid Coupler

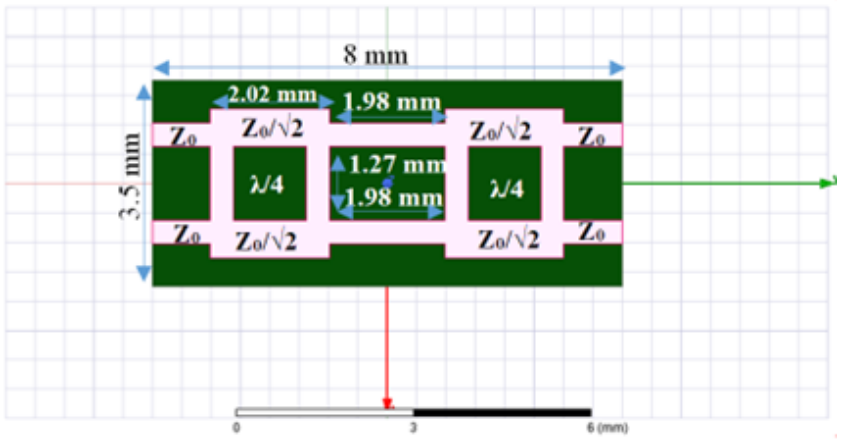


Figure 4.4: Proposed 0 dB Crossover

- ***45° and 120° Phase Shifters***

A 4×4 BM requires 2 phase shifters, which are easily built using microstrip transmission lines. The necessary phase shift can be produced by fluctuating

length of the transmission line. Two-phase shifters are employed to build one of the 4×4 butler matrices for this purpose. A 45° phase shifter can be constructed using a quarter-wave transmission line. The electrical length of a quarter-wave line is given by:

$$L = (\lambda/4) = (\nu/(4 * f)) \tag{4.7}$$

where λ is the wavelength of signal, ν is the transmission line's propagation speed, and f is the signal frequency.

A 120° phase shifter can be constructed using a transmission line with a length of two-thirds of a wavelength. The electrical length of a two-thirds wavelength line is given by:

$$L = (2\lambda/4) = (2\nu/(3f)) \tag{4.8}$$

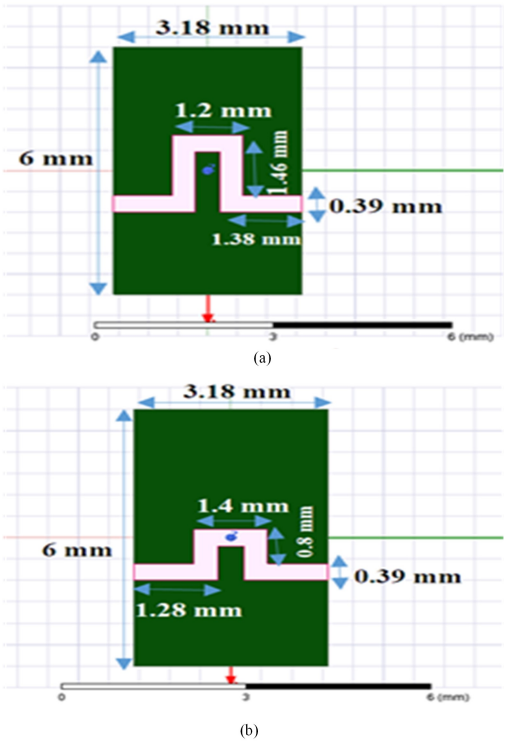
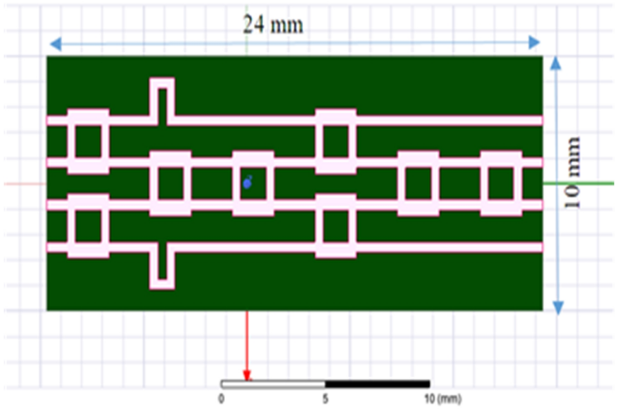


Figure 4.5: (a)45° Phase Shifter, (b)120° Phase Shifter

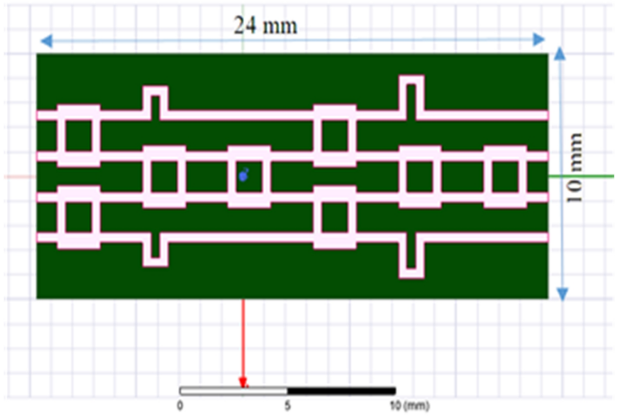
Two 45° and two 120° phase shifters are used in another butler matrix. 120° phase shifters offer the 120° phase shift required to produce a beam in the preferred direction. Figure 4.5(a) depicts the proposed 45° phase shifter, while Figure 4.5(b) depicts the proposed 120° phase shifter.

- ***Proposed*** 4×4 ***Butler matrix***

The suggested architecture of the 4×4 BM with two 45° phase shifters is shown in Figure 4.6(a).



(a)



(b)

Figure 4.6: (a)Proposed 4×4 Butler Matrix with 45° Phase Shifter, (b)Proposed 4×4 Butler Matrix with 120° Phase Shifters

While in Figure 4.6(b) portrays a 4×4 BM with two 45° phase shifters and two 120° phase shifters. The two 4×4 BMs are suggested using the proposed components. These matrices are built on a Rogers RT/duroid 5880(tm) substrate with a loss tangent of 0.127 mm and a thickness of 0.0009 mm. The planned butler matrices have lengths of 24 mm and widths of 10 mm. In the proposed matrix, there are eight ports, with ports $1 - 4$ serving as input ports. Ports 5 through 8 are used as output ports. Four 90° hybrid couplers, 45° phase shifters, two 0 dB crossovers, and 120° phase shifters are used to create the 4×4BM. There are two 4×4 BMs proposed, one of which comprises of four 90° hybrid couplers, two 0 dB crossovers, and two 45° phase shifters. The remaining 4×4 suggested butler matrices are made up of four two 45° phase shifters, 90° hybrid couplers, two 0 dB crossovers, and two 120° phase shifters. The suggested matrix was created with HFSS tool.

4.2.3 Direction of Arrival (DOA) Estimation using Cra -mer Rao Lower Bounds (CRLB) Computation

The CRLB estimates the variance of an unbiased estimator more conservatively. Estimators located near the CLRB are more impartial (and thus preferable to utilize) than estimators located further away. The CRLB is theoretical; it is possible that a perfectly unbiased estimator (i.e. one that encounters the CRLB) does not exist in some cases. Therefore, unless the circumstance is relatively basic, calculating the CRLB is challenging. There are simpler, more general alternatives for choosing the best estimator.

The DOA Estimation initially calculated the linear spectrum using the Fourier transform approach. It mostly used the perio-dogram approach. Because of the Rayleigh limit, it was unable to attain a high-resolution performance or withstand the noise, resulting in an unsatisfactory result. The direction from which a wave typically propagates until it reaches a place where typically a collection of sensors are located is referred to as the direction of arrival (DOA) in signal processing. These sensors collectively form a sensor array. Signal assessment from a certain direction is typically combined with beam shaping. The radio wave's array an-

tenna's DOA stands for direction of arrival. It can interpret the front of the radio wave as a plane if the radio wave achieved satisfies the requirement of a far-field narrowband. The angle formed by the array normal and the plane wave's vector for direction is known as the DOA. When the same signal arrives various array elements, it causes a wave-way discrepancy, which is common for far and wide transmissions. A phase discrepancy between the arrival array elements results from this wave-way difference. The fundamental idea behind DOA estimation is that the signal azimuth may be calculated from the phase difference between the signal's array elements.

4.2.3.1 Data Model

An antenna array's performance may be assessed utilising the CRLB for single route scenario. Any estimate of the variance will produce a lower bound when using the CRLB. The work's suggested improvement of the antenna array technique is solely dependent on the waves that are impinging on the antenna array. The following is a representation of the data model[111] for the impinging wave on the antenna array M:

$$C_n = H(\vartheta, \varphi)Ka + P \tag{4.9}$$

The feature derived from the antenna array's output is represented by the vector $C_n \in S^{M\times 1}$. The polarimetric array's steering vectors make up the columns of matrix $A(\vartheta, \varphi) \in S^{M\times 2}$. A is influenced by the angle of arrival. The antenna array is being impinged upon by the signal $b \in S$. The Jones vector $K \in S^{2\times 1}$ is used to perform the polarization b. These vectors are joined by a new vector with the name zero-mean complex Gaussian noise vector of $N \in S^{M\times 1}$ and a convergence matrix of T_{mm}. The CRLB is shown as; for a single deterministic single snap-shot and path case.

$$\sum_{crlb}(\vartheta, \varphi) = 0.5P^{-1}\left\{G^{C}(\vartheta, \varphi)T_{mm}^{-1}G(\vartheta, \varphi)\right\} \tag{4.10}$$

The matrix G composed of azimuth and elevation parameters of the received

vector which is given by;

$$G(\vartheta,\varphi)=\left[\frac{\partial z}{\partial \vartheta}\frac{\partial z}{\partial \varphi}\frac{\partial z}{\partial P\left\{K^{t}b\right\}}\frac{\partial z}{\partial Y\left\{K^{t}b\right\}}\right] \tag{4.11}$$

Where the expansion of the matrix G is given by;

$$\frac{\partial z}{\partial \vartheta}=\frac{\partial A(\vartheta,\varphi)}{\partial \vartheta}Kb,\frac{\partial z}{\partial \varphi}=\frac{\partial A(\vartheta,\varphi)}{\partial \varphi}Kb \tag{4.12}$$

$$\frac{\partial z}{\partial P\left\{K^{t}b\right\}}=A(\vartheta,\varphi),\frac{\partial z}{\partial Y\left\{K^{t}b\right\}}=SA(\vartheta,\varphi) \tag{4.13}$$

The CRLBs are present in the diagonal elements of $\sum_{crb}(\vartheta,\varphi)$. The information extracted from the matrix $\sum_{\text{crlb}}$ are as follows;

$$\sigma^{2}_{crlb,\vartheta}(\vartheta,\varphi)=\left|\sum_{crlb}(\vartheta,\varphi)_{11}\right| \tag{4.14}$$

$$\sigma^{2}_{crlb,\varphi}(\vartheta,\varphi)=\left|\sum_{crlb}(\vartheta,\varphi)\right|_{22} \tag{4.15}$$

For ϑ and φ parameters there is no unbiased estimator because they possess a lower variance around the true value than $\sigma^{2}_{crlb,\vartheta}(\vartheta,\varphi)$ and $\sigma^{2}_{crb,\varphi}(\vartheta,\varphi)$.

4.2.3.2 The Effective Aperture Distribution Function

The CRLB is merely a fundamental framework for assessing how well an antenna array can determine direction. Azimuth and elevation, which contain both derivatives and polarimetric steering vectors, are needed to satisfy the matrix in equation 4.11, though. Moreover, there isn't a closed-form solution for the arrays found in conventional antenna arrays. Hence, they should be standardized in an anechoic chamber. If the intended directions have no representation in the calibration grid, an interpolation process is required to generate the polarimetric steering vectors. Also, each point must be approximated for the arrays' derivatives. A 2D discrete Fourier transform of an augmented beam pattern is how EADF is typically defined in analyses. Interpolation will be simple and quick, and approximation derivatives will be simple in a certain frequency domain. The optimization procedure involves

choosing several antenna array geometries with various butler matrix configurations. The Ansoft HFSS tool simulates each configuration's separate beam pattern for the array antenna. To do additional operations like interpolation and derivative approximation, this data will then be transferred to the EADF. To calculate the CRLBs of equations 4.14 and 4.15, the EADF process's results are employed.

4.2.4 Optimization Procedure

4.2.4.1 Performance Evaluation of DOA

Just the application of CRLB serves as a benchmark for DOA estimate performance. Equations 4.14 and 4.15 two measurements $\sigma_{crlb,\vartheta}(\vartheta,\varphi)$ and $\sigma_{crlb,\vartheta}(\vartheta,\varphi)$ provide a succinct summary of the DOA estimation of an antenna array's performance. The study paper only uses one single figure of merit to support the antenna array improvement that is suggested. Hence, $\sigma_{\text{crlb}}(\vartheta,\varphi)$ adds a new single parameter. The area that $\sigma_{crlb,\vartheta}(\vartheta,\varphi)$ and $\sigma_{crlb,\varphi}(\vartheta,\varphi)$ Bridge on the unit area, normalized to the sphere of the entire unit area, is what is meant by the new parameter [111]and is denoted by;

$$\sigma_{crlb}(\vartheta,\varphi) = \frac{1}{4\pi}\int_{\vartheta-\sigma_{crlb,\vartheta}}^{\vartheta+\sigma_{crlb,\vartheta}} \cos\left(\sigma''\right)\cdot 2\sigma_{crlb,\varphi}d\vartheta" \tag{4.16}$$

$$= \frac{1}{\pi}\cos(\vartheta)\sin\left(\sigma_{crlb,\vartheta}\right)\sigma_{crlb,\varphi} \tag{4.17}$$

The basic goal of optimization is to determine an expected value for array geometry parameters. The expected value is calculated by minimising all elevation-angle pairings and is provided by;

$$\sigma_{crlb}^{n} = F\left\{\sigma_{crlb}(\vartheta,\varphi)\right\} \tag{4.18}$$

Because $\sigma_{\text{crlb}}(\vartheta,\varphi)$ has no closed solution, an approximation solution for equation 4.18 must be determined. The evaluation of CRLB is performed on a finite grid in direction 1 elevation and azimuth direction $\Delta'\varphi$ with $\Delta'\vartheta$ spacing for this purpose. It is discovered that the grid is denser at the poles than at the equator,

thus a simple interpolation depend on the area encompassed by pixels is introduced and expressed as;

$$A(\vartheta) = \int_{\vartheta - \frac{\Delta'\vartheta}{2}}^{\vartheta + \frac{\Delta'\vartheta}{2}} \Delta'\varphi \cos\left(\vartheta''\right) d\vartheta'' = \beta \cos(\vartheta) \tag{4.19}$$

The constant parameter β is expressed as $\beta = 2\Delta\varphi'' \sin\left(\frac{\Delta\vartheta''}{2}\right)$. The expression $A(\vartheta)$ does not depends on the azimuth angle. The total area covered by a regular grid is represented as;

$$A_{\text{total}} = \sum_{n\varphi=1}^{N\varphi} \sum_{n\vartheta=1}^{N\vartheta} A(\vartheta, \varphi) = \beta N_{\varphi} \sum_{n\vartheta=1}^{N\vartheta} \cos\left(\vartheta_{m\vartheta}\right) \tag{4.20}$$

Using equation 4.21, a weight factor is derived for CRLB $U_f(\vartheta)$ is given by;

$$U_f(\vartheta) = \frac{A(\vartheta)}{A_{\text{total}}} = \frac{\cos(\vartheta)}{N_{\varphi} \sum_{n\vartheta=1}^{N\vartheta} \cos\left(\vartheta_{n\vartheta}\right)} \tag{4.21}$$

Finally, mean CRLB is obtained as;

$$\sigma'''_{crlb} \approx \sum_{n\varphi=1n}^{N\varphi} \sum_{n\vartheta=1}^{M\vartheta} U_f\left(\vartheta_{n\vartheta}\right) \sigma_{crlb}\left(\vartheta_{n\vartheta}, \varphi_{n\varphi}\right) \tag{4.22}$$

The array geometry is determined by the computed scalar value σ''_{crlb}, which should be as small as possible. As a result, the optimization process is provided to reduce the acquired value by adjusting the geometry of the antenna array.

4.3 Results and Discussion

This section contains results for suggested switching beam antenna and DOA estimation technique. The suggested antenna with butler matrix is constructed and simulated in the HFSS tool, and the DOA estimation algorithm is simulated in the MATLAB tool. The butler matrix and antenna are printed on a Rogers RT/duroid 5880(tm) substrate with a thickness of 0.127 mm and a dielectric loss tangent of 0.0009 mm. The entire physical size of the suggested antenna with butler matrices is 36×32 mm. The efficiency of the switching beam antenna is measured using

multiple performance metrics such as return loss, transmission coefficient, 2D and 3D radiation patterns, and VSWR. The suggested DOA estimating technique is compared to other existing algorithms such as MUSIC and MVDR.

4.3.1 Performance Evaluation for the Proposed Antenna

Figure 4.7(a) depicts the RL plot in dB for the suggested antenna. The RL of a single patch antenna is -24.23dB. When port 1 is energized, the observed RL is less than -10dB from 34.50 GHz to 36.58 GHz. The fact that the suggested antenna's RL is less than -10dB indicates that the antenna utilized for beam steering is more efficient. Antenna radiation patterns depict the radiation properties of an antenna. Radiations from an antenna are depicted as a function of radial distance and angular position from antenna. There are two kinds of radiation patterns: 2D and 3D. The distinction between these two patterns is that the antenna's 3D radiation pattern will have a lower resolution than the 2D radiation pattern. The subtleties of the pattern are not missing in the 3D radiation pattern, but the pattern outside the measuring planes is. Radiation efficiency may be computed accurately in 3D rather than 2D. Figure 4.7(b) shows the suggested antenna's 3D radiation pattern, while Figure 4.7(c) depicts the suggested antenna's 2D radiation pattern. Figure 4.7 (d) depicts the simulated VSWR value for the suggested antenna. Because the VSWR values achieved are 1-2, the suggested antenna is particularly suitable for low VSWR antenna applications.

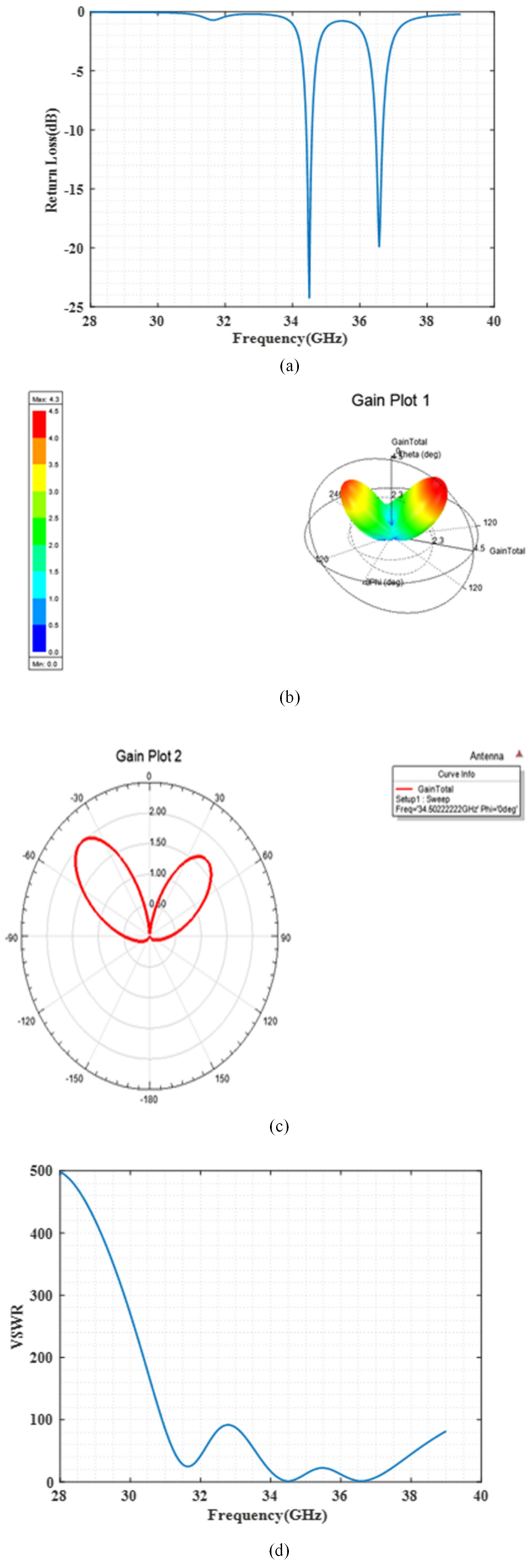


Figure 4.7: (a)Return Loss of Patch Antenna, (b)3D Radiation Pattern of Patch Antenna, (c)2D Gain Pattern of Patch Antenna, (d)VSWR of Antenna Array

4.3.2 Performance Evaluation for the Proposed 90° Hy -brid Coupler and 0dB Crossover

Figure 4.8 depicts the angle of the 90° hybrid coupler. Figure 4.9 (a) displays the RL for the suggested 0 dB crossover. The measured RL for a 0 dB crossover is less than -10 dB at 34 GHz, indicating that the crossover is well suited for designing a butler matrix. Figure 4.9(b) depicts the 2D radiation pattern for the anticipated 0 dB crossover.

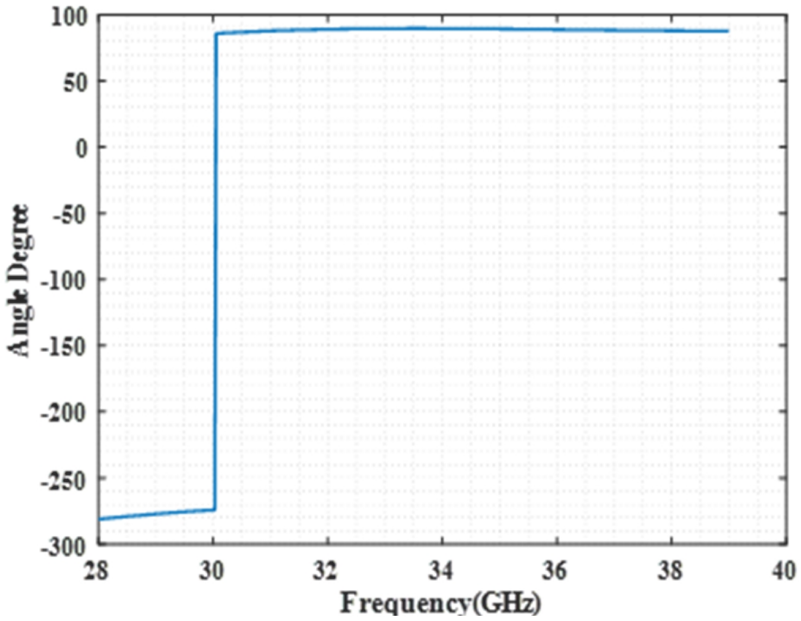
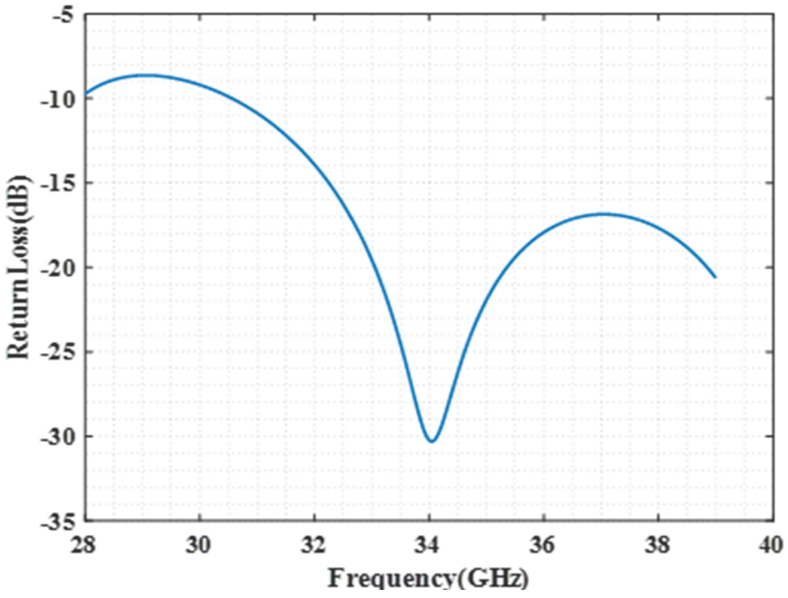
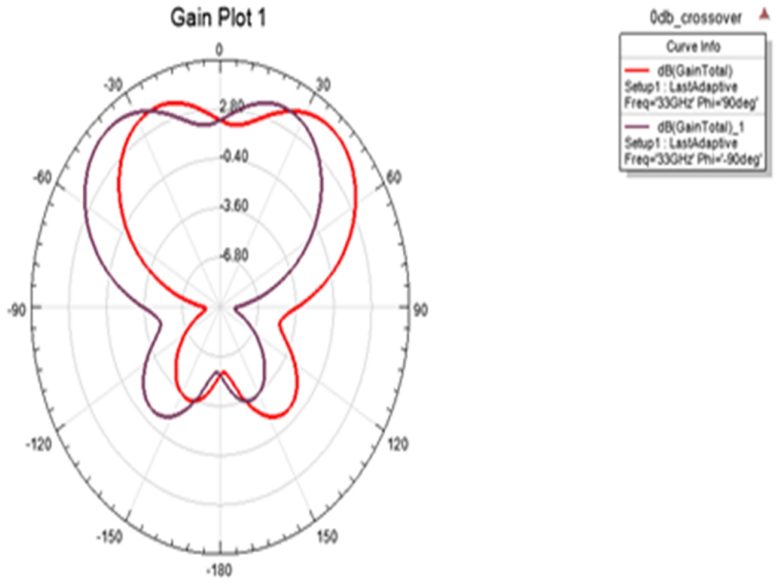


Figure 4.8: Angle of 90° Hybrid Coupler



(a)

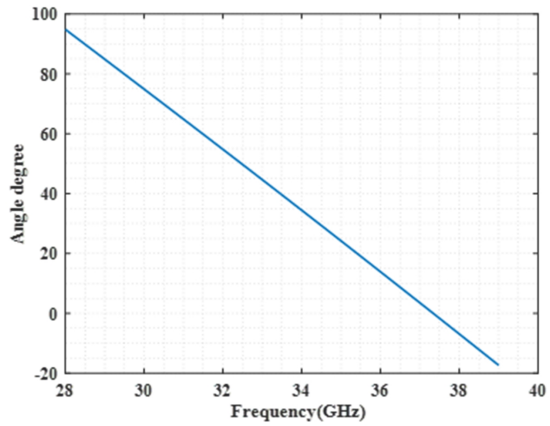


(b)

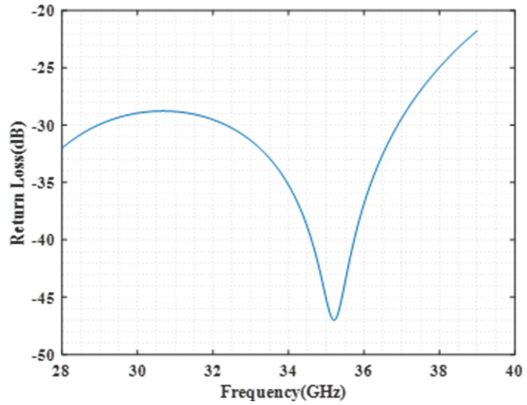
Figure 4.9: (a)Return Loss for 0db Crossover, (b)2D Radiation Pattern for 0 dB Crossover

4.3.3 Performance Evaluation for the Proposed 45° Phase Shifter

Figures 4.10(a) and 4.10(b) depict the angle and return loss of a 45° phase shifter. The phase shifter provides the necessary phase shifts for beam creation in the appropriate direction. The angle of the 45° phase shifter is simulated to shift the angle to 45°. At 33.01 GHz, the phase shifter achieves -10 dB of return loss and the angle moves 45°.



(a)

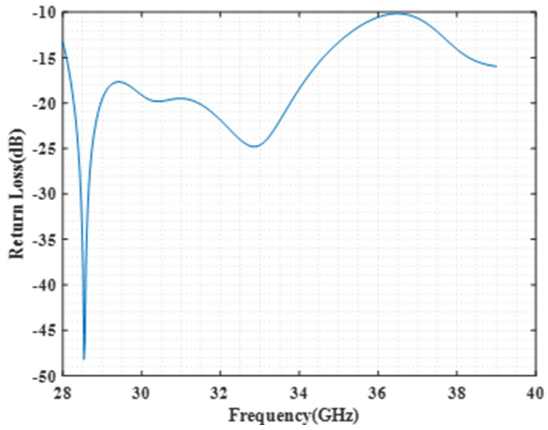


(b)

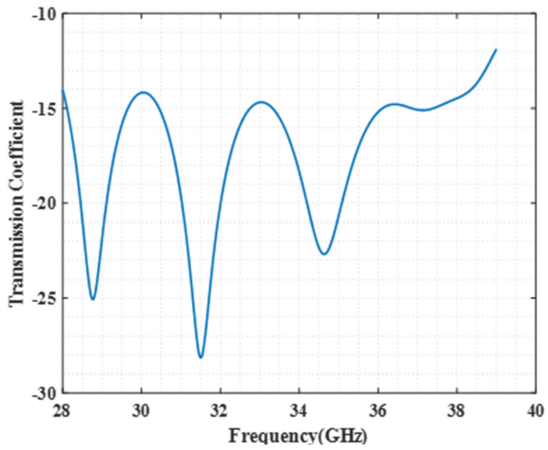
Figure 4.10: (a)Angle of 45° Phase Shifter, (b)Return Loss for 45° Phase Shifter

4.3.4 Performance Evaluation for the Proposed 4 × 4 Butler Matrix with 45° Phase Shifter

Figure 4.11 (a) depicts the simulated RL for the suggested 4 x 4 BM with a 45° phase shifter. At 28.53 GHz, the return loss for the suggested 4x4 BM with a 45° phase shifter is less than -10db. Figure 4.11(b) depicts the transmission coefficients of the suggested 45° phase shifter BM as modelled by HFSS tools.



(a)



(b)

Figure 4.11: (a)Return Loss 4 × 4 Butler Matrix with 45° Phase Shifter, (b)Transmission Coefficient

4.3.5 Performance Evaluation for the Proposed 45° Phase Shifter Butler Matrix with Antenna

Figure 4.12 depicts the simulated return loss for proposed 45° phase shifter butler matrix and antenna. At 33.62 GHz frequency, the measured return loss is less than -10dB. Figure 4.13 depicts the simulated bandwidth of the proposed 45° phase shifter butler matrix with antenna. Figure 4.14 depicts the simulated VSWR for the proposed 45° phase shifter butler matrix and antenna. Antenna characterization, analysis, planning, design, and applications all rely on 3D radiation patterns. The two-dimensional design can be created by dividing the three-dimensional pattern into vertical and horizontal planes. Figure 4.15 depicts the 3D radiation pattern for the proposed 45° phase shifter butler matrix with antenna, while figure 4.16 depicts the 2D radiation pattern for the proposed 45° phase shifter butler matrix with antenna.

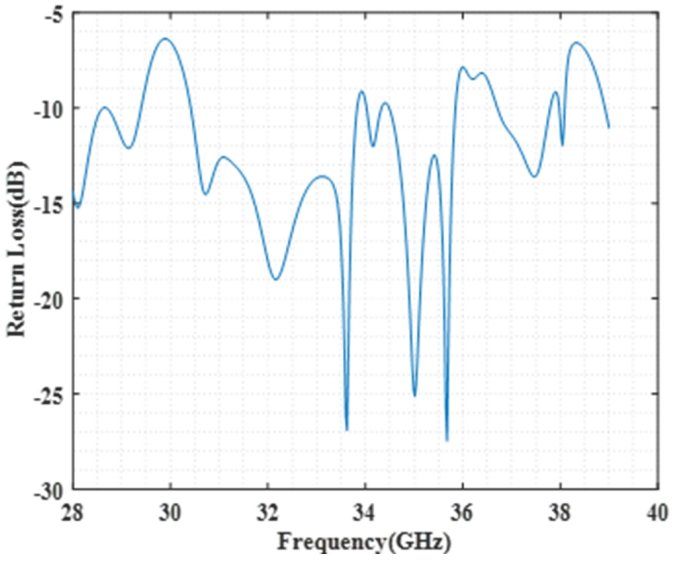


Figure 4.12: Return Loss for 45° Phase Shifter Butler Matrix with Antenna

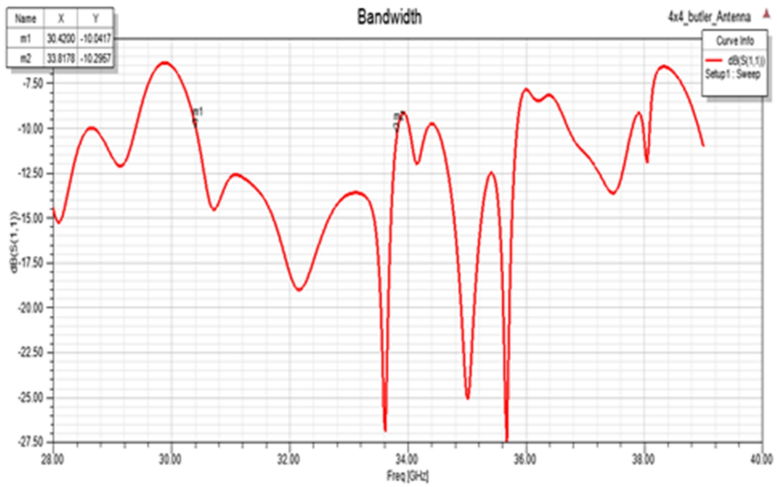


Figure 4.13: Bandwidth for 45° Phase Shifter Butler Matrix with Antenna

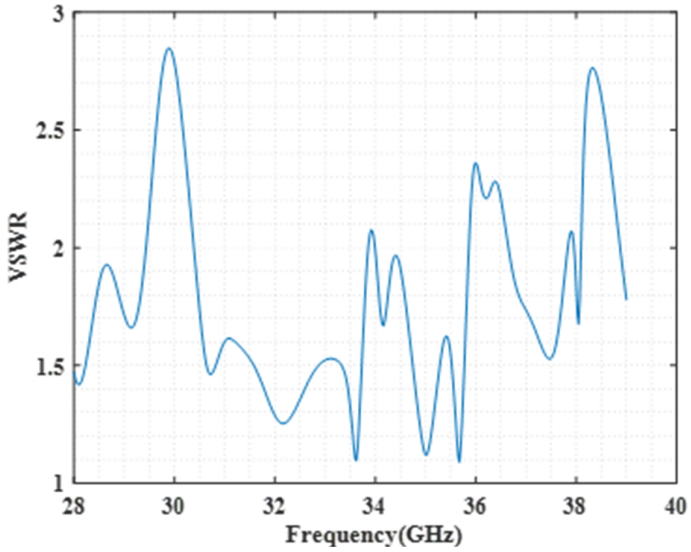


Figure 4.14: VSWR for 45° Phase Shifter Butler Matrix with Antenna

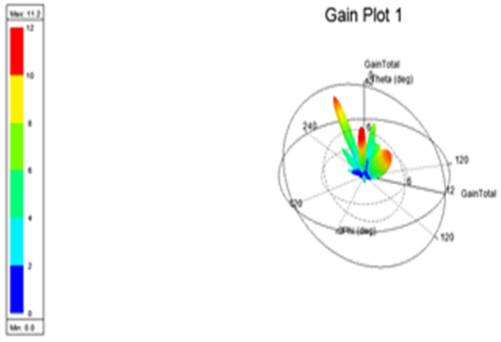
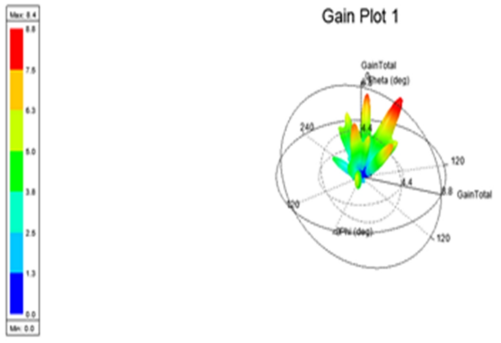
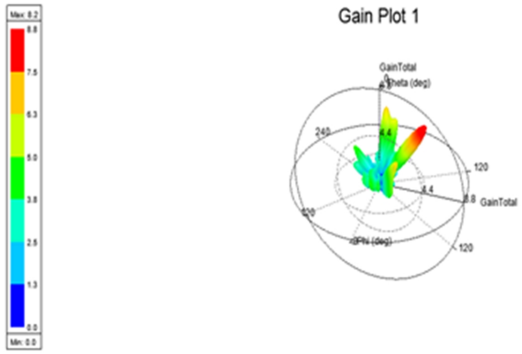
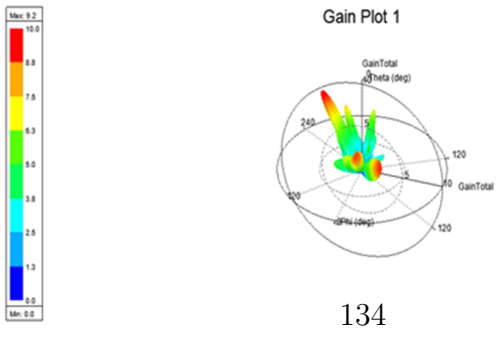
Port	Radiation Plot	Angle of Beam Shift	Maximum Gain
Port 1		-45º	11.2 dB
Port 2		+45º	8.4 dB
Port 3		+45º	8.2 dB
Port 4	 134	-45º	9.2 dB

Figure 4.15: 3D Radiation Pattern for 45° Phase Shifter Butler Matrix with Antenna

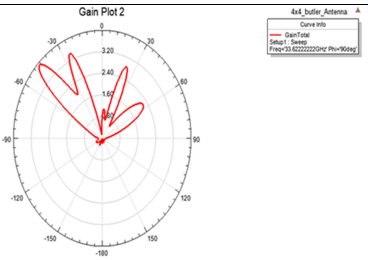
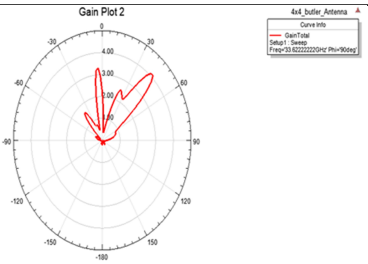
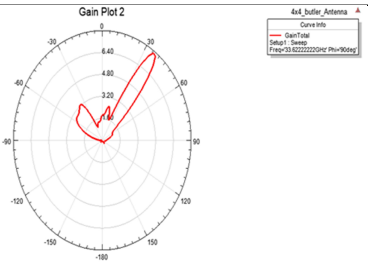
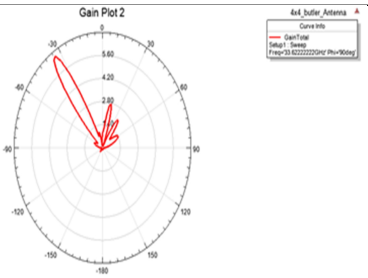
Ports	Radiation Pattern
Port 1	
Port 2	
Port 3	
Port 4	

Figure 4.16: 2D Radiation Pattern for 45° Phase Shifter Butler Matrix with Antenna

4.3.6 Performance Evaluation for the Proposed 120° Phase Shifter

The 120° phase shifter provides the essential phase shift for beam creation in the anticipated direction.The angle of the 120° phase shifter is simulated to shift the angle to 120° and generate a beam in the desired direction.Figure 4.17 depicts the simulated angle of the 120° phase shifter, whereas Figure 4.18 depicts the return loss for the suggested 120° phase shifter. At 33GHz, the phase shifter achieves a -10 dB gain. As a result, the component is extremely beneficial when creating a butler matrix. Return loss is the loss of signal strength caused by signal reflection or transmission line. A higher return loss is preferable since it results in less insertion loss. At 32.42 GHz, the return loss was less than -10 dB.

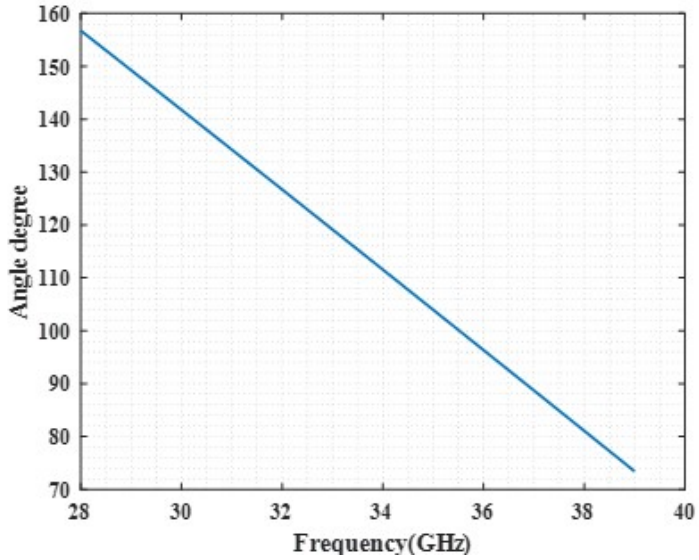


Figure 4.17: Angle of 120° Phase Shifter

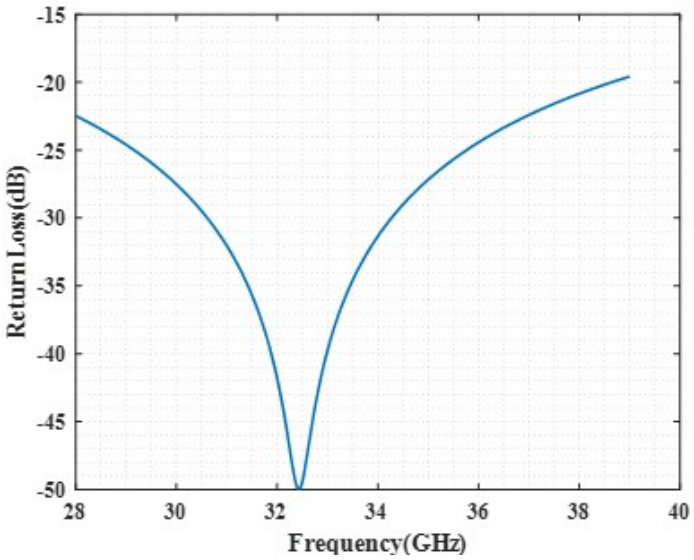


Figure 4.18: Return Loss for 120° Phase Shifter

4.3.7 Performance Evaluation for the Proposed 4 × 4 Butler Matrix with 45° and 120° Phase Shifters

Figure 4.19 depicts the predicted return loss for the planned 4 x 4 butler matrix with 45° and 120° phase shifters. At 29.17 GHz, the return loss for the suggested BM with 45° and 120° phase shifters is less than -10db. As a result, the butler matrix with several phase shifters is regarded as the optimum beam-forming network for patch antennas.

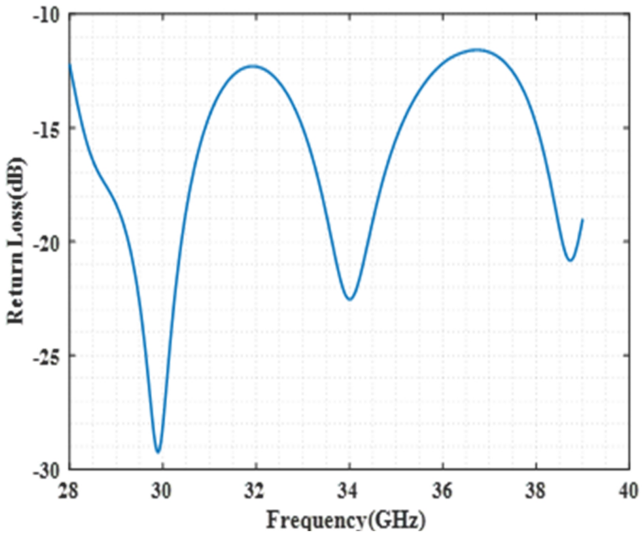


Figure 4.19: Return Loss for 4×4 Butler Matrix with 45° and 120° Phase Shifters

4.3.8 Performance Evaluation for the Proposed 45° and 120° Phase Shifters Butler Matrix with Antenna

Figure 4.20 depicts the simulated return loss for proposed 45° and 120° phase shifters butler matrix with antenna. The suggested antenna with 45° and 120° phase changers butler achieves -10 dB at three frequencies: 29.54 GHz, 33.98 GHz, and 35.99 GHz. The VSWR shows how much mismatch exists among the antenna and the feed line that connects to it. A VSWR of less than 2 is generally acceptable for most antenna applications. The suggested antenna with a BM meets the bandwidth requirement specified by VSWR. Figure 4.21 depicts the VSWR for the planned 45° and 120° phase shifters butler matrix with antenna. The proposed design achieves VWSR in the 1-2 range, indicating that the suggested BM is well suited for beam formation in the antenna.

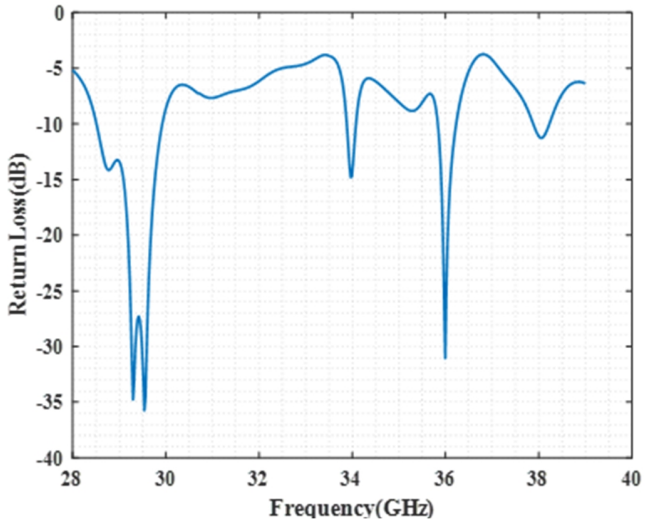


Figure 4.20: Return Loss for 45° and 120° Phase Shifters Butler Matrix with Antenna

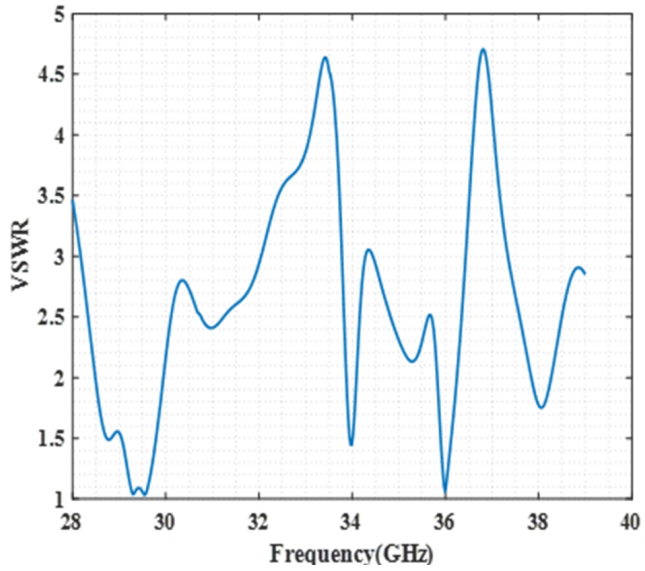


Figure 4.21: VSWR for 45° and 120° Phase Shifters Butler Matrix with Antenna

Figure 4.22 depicts the 3D Radition pattern and figure 4.23 depicts the 2D Radition pattern for the proposed 45° and 120° phase shifters BM with antenna

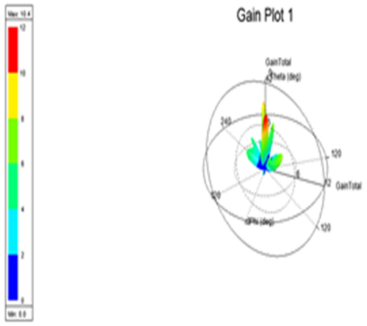
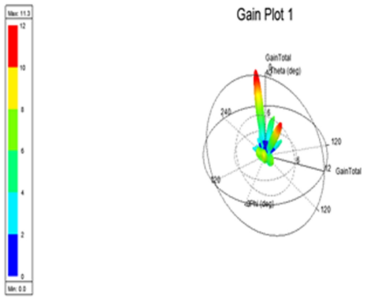
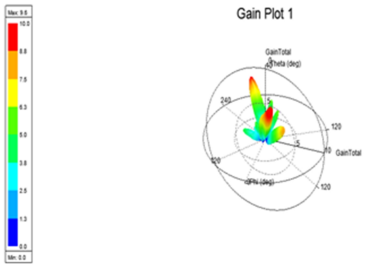
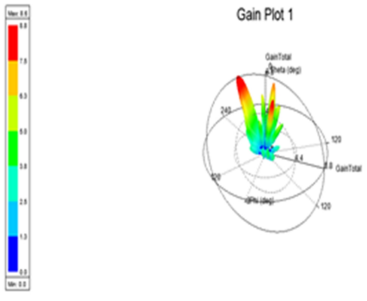
Port	Radiation Plot	Angle of Beam Shift	Maximum Gain
Port 1		-45º	10.4 dB
Port 2		+120º	11.3 dB
Port 3		-120º	9.6 dB
Port 4		+45º	8.6 dB

Figure 4.22: 3D Radiation Pattern for 45° and 120° Phase Shifters Butler Matrix with Antenna

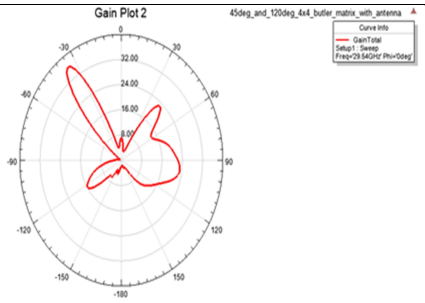
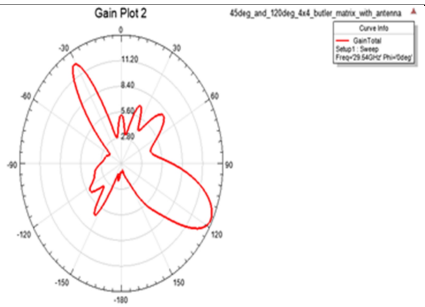
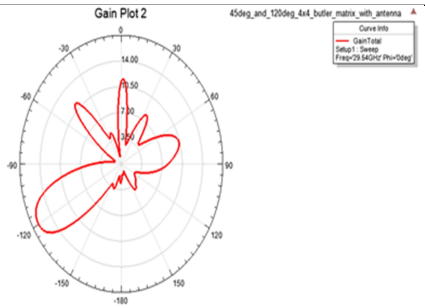
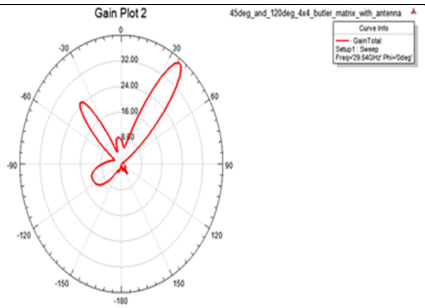
Ports	Radiation Pattern
Port 1	
Port 2	
Port 3	
Port 4	

Figure 4.23: 2D Radiation Pattern for 45° and 120° Phase Shifters Butler Matrix with Antenna

respectively.

4.3.9 Performance Evaluation for the Proposed DOA Estimation Algorithm

The RMSE (Root mean square error) is calculated as the number of simulations performed. As a first step, the DOA estimator returns a value for the angular estimate from which the error associated with each of the estimations is evaluated. In the second stage, the errors are squared and the average of the squared errors is calculated. The third step is to calculate the square root of the amount obtained. As a result, some values are acquired for a particular SNR, and new RMSE values are obtained by modifying the SNR values. RMSE is estimated as the square root of the averaged squared angular errors over repeated DOA estimation trials, as shown in equation 4.20. The RMSE for the suggested approach with input SNR is shown in Figure 4.24. The proposed DOA estimating algorithm obtained an improved gain of 3 dB at 0.4RMSE.

$$R_{MSE} = \sqrt{\frac{1}{E}\sum_{E=1}^{E}\frac{1}{M}\sum_{n=1}^{M}\left(\theta_n - \hat{\theta}_n\right)^2} \tag{4.23}$$

Where E is the number of DOA estimate trials used to average the error, M denotes the number of impinging waves on the antenna array, θ_n denotes the curve for up to four beams from the switching beam antenna, and $\hat{\theta}_n$ denotes the angle of separation between neighboring signals.

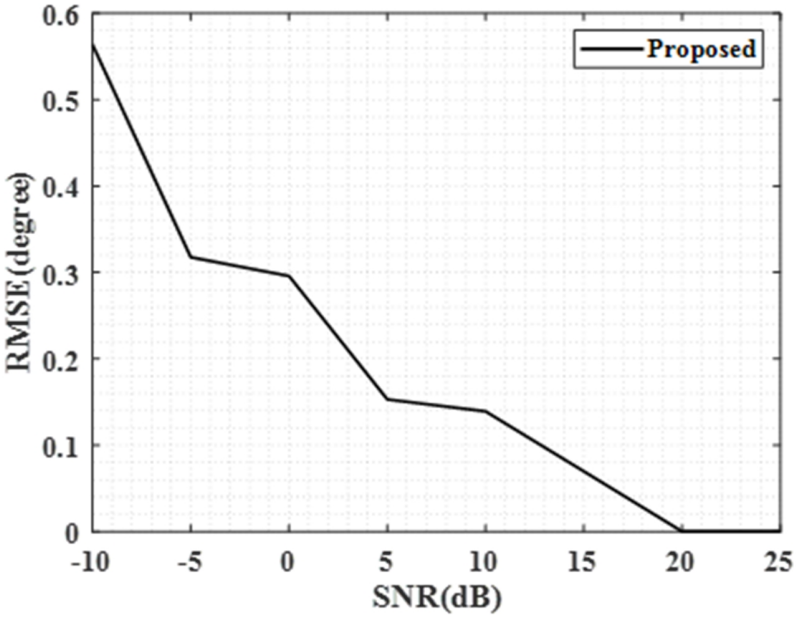


Figure 4.24: RMSE for the Proposed Algorithm

By altering SNR values, the suggested work is compared with MUSIC and MVDR for the RMSE performance study, as shown in figure 4.24. As compared to previous DOA estimating algorithms, the suggested DOA estimation has a lower RMSE. The proposed approach outperformed the MUSIC and MVDR algorithms by 5 dB with an RMSE of 0.14. As a result, when compared to other current DOA estimate techniques, the suggested algorithm has lower error values. Table 4.1 compares the RMSE for known and new DOA estimate techniques with varied SNR values.

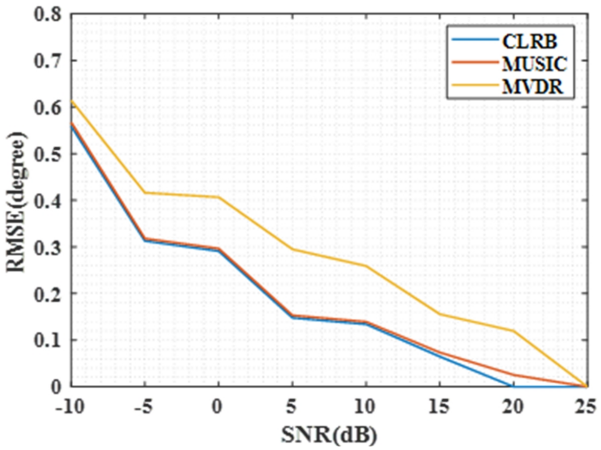


Figure 4.25: RMSE for DOA Estimation Algorithms

Table 4.5: Comparison of RMSE Parameters with Varying SNR Values

SNR Values	**CRLB**	**MUSIC**	**MVDR**
-10	0.559	0.5672	0.6144
-5	0.3127	0.3177	0.4159
0	0.2909	0.2962	0.4065
5	0.148	0.1531	0.2948
10	0.1341	0.1392	0.2588
15	0.0647	0.0734	0.1556
20	0	0.0252	0.1195
25	0	0	0

After analyzing all of the butler matrices and their components' results, the proposed butler matrix functions as an efficient beam-forming network for the proposed hexagonal patch antenna. In addition, the DOA estimation technique is more efficient than other DOA estimate algorithms already in use. In figure 4.26, provided stimulation result of DOA estimation of the proposed against array elemental spacing.

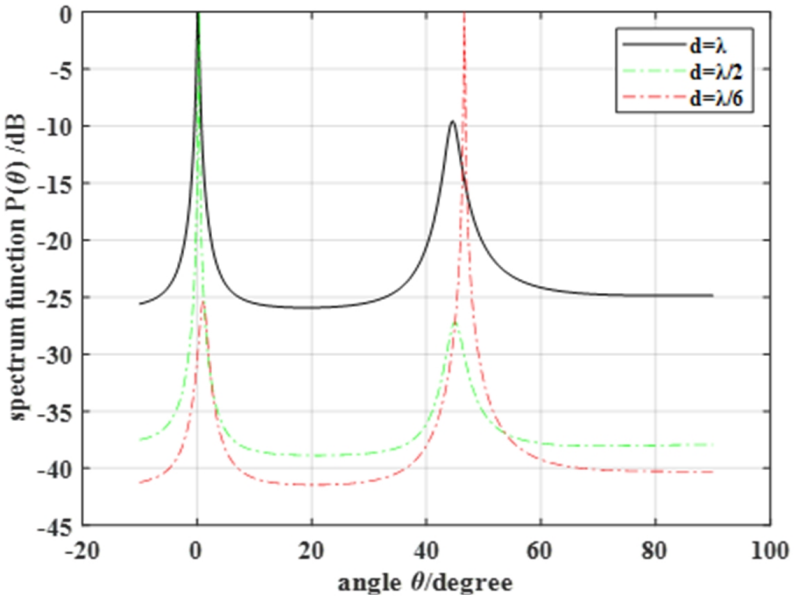


Figure 4.26: The Connection Between the Proposed Algorithm and the Array Element Spacing

According to Figure 4.26, the dashed-dotted line in red colour indicates that the array elements' spacing is $\lambda/6$, the solid line indicates that it is λ, and the dashed-dotted line in green colour indicates that it is $\lambda/2$. When all other aspects remain constant, the width of beam for the DOA estimate spectrum narrows as the array element spacing increases, and the array elements' orientation improves; that is, the suggested algorithm's resolution increases as the array element spacing increases, however the estimated spec falls when the array element spacing is more than half of wavelength. The element spacing of the array can be enlarged, but it must not go over half the wavelength, which is a critical factor. However, in practical applications, the spacing of the components of the array should be given more thought. The ideal element spacing is half the wavelength.

According to Figure 4.27, the dashed-dotted line in red colour indicates that the number of snapshots is N = 100, the solid line indicates that it is N = 10, and the dashed-dotted line in green colour indicates that it is N = 50. With the other conditions being the same and the number of photos growing, the beam breadth

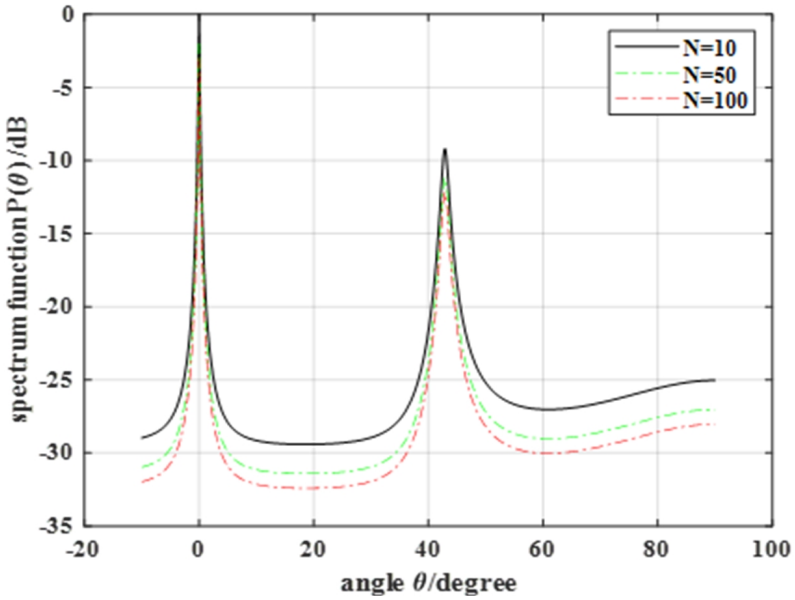


Figure 4.27: The Connection Between the Proposed Algorithm and the Snapshots

of the DOA estimate spectrum becomes narrow, the array element's orientation becomes excellent, and the precision of the suggested method is also enhanced. Figure 4.28 displays the stimulation results of DOA estimation of various algorithms.

As can be seen in Figure 4.28, the dashed-dotted line in red colour indicates that the DOA estimation of MVDR algorithm, the solid line indicates that of CLRB, and the dashed-dotted line in green colour indicates that of MUSIC algorithm.

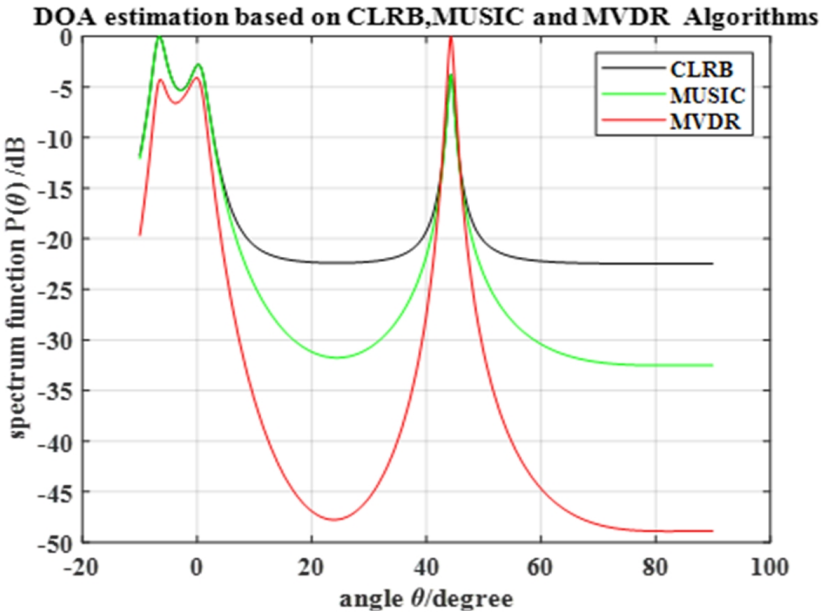


Figure 4.28: DOA Estimation of CLRB, MUSIC, and MVDR

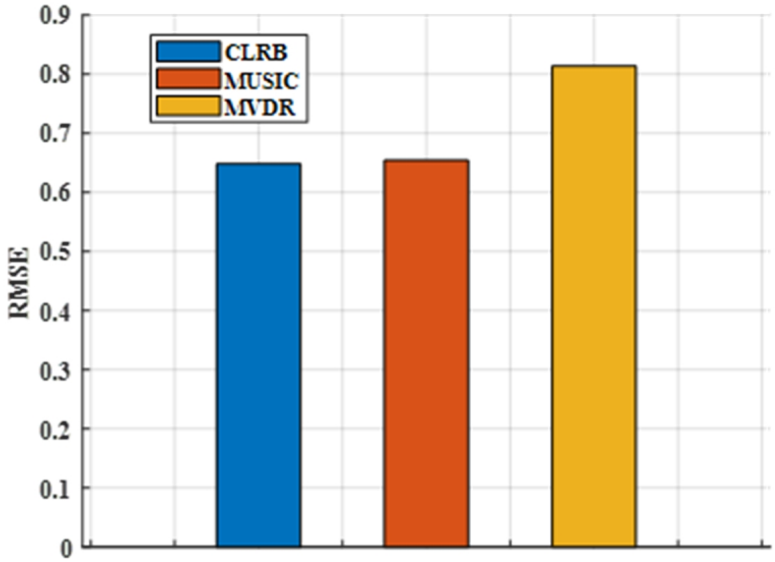


Figure 4.29: RMSE Graph

Figure 4.29 displays the comparison graph of RMSE for various algorithms.In

this graph, RMSE value for the proposed CLRB has the lowest value while MVDR has highest RMSE values. So from the stimulation results and values of RMSE provided, possible to conclude that the suggested algorithm achieves better than others.

4.4 Summary

In this study, a unique SBA with a novel BM is built for switched beam applications at mm-wave frequencies ranging from 28 to 39 GHz. The suggested approach's three key contributions are well satisfied by developing a switching beam antenna, butler matrix, and DOA estimation. The beam-forming network is the research work's standout innovation. On a micro-strip hexagonal patch antenna with a Z-slot, the beam-forming property is used. The beam-forming network known as the 4x4 butler matrix is built in two ways, each with a different degree of the phase shifter. The phase changes are 45° and 120°. One of the butler matrices is created by combining two 45° phase shifters. The other BM is built with two 45° and two 120° phase shifters.

Chapter 5

Design of Millimeter-Wave Frequency Micro Strip Smart Antenna with the DENLMS Beam Steering Algorithm

5.1 Overview

The improvement of contemporary wireless methodology has increased the demand for high data rates and high speed. Using 5G technologies, these requirements can be met. The sluggish data rates and resulting data traffic make the 4G communication technology insufficient for ongoing operation. A 4G data connection system can't take the lead in emerging wireless applications since they need a lot of bandwidth. The millimeter wave bands, which have a maximum performance of 20 gigabits per second, are the core technologies used in 5G. These bands include 60, 28, 26, and 38 GHz. Antennas are being thought about for 5G applications are somewhat different from standard antennas of low-frequency. The antenna should be very small for use in 5G applications and have good directivity and gain. The antenna should be the phased array antenna, where the beam location changes depending on the relative phase change among the inputs applied to var-

ious ports. Additionally, using the methods of wireless smart antenna networks will have several benefits, including cost savings and service quality improvement.

For effective data transfer and reduce data traffic with the network, a 5G network is strongly advised. The millimeter wave (mm) frequency range is compatible with the 5G framework. Antennas are crucial for wireless communications in a wide range of uses, including radio communications, wireless communications in the medical field, satellite applications, etc. The demand-driven manufacturing process for the current antenna makes its design for every wireless application debatable. The receiver sides and transmitter sides of the communication link each contain several antenna elements that make up the smart antenna. It is divided into three categories according to the processing function at the receiver, transmitter, or both ends of the communication link like SIMO, MISO, and MIMO. The transmission and interference of numerous information streams from separate antennas are combined by the smart antenna to improve link quality and maximum capacity. Smart antennas have several advantages in real-time applications, including increased coverage, reduced power requirements, low costs, improved reliability, and improved spectral efficiency. Smart antennas come in two varieties: switching beam antennas and adaptive beam antennas.

5.2 Proposed Methodology

The system in this study employs HFSS to deliver a six-item smart array. Performance metrics for directivity gain and return loss are investigated for single, dual, quad, and eight elements. To evaluate the adaptive array beam steering capabilities, more complex weights made in MATLAB using the DENLMS method are transmitted back into HFSS. By assuming the interferer and user commands, this collection is tested in a few scenarios. Figure 5.1 shows framework of proposed model.

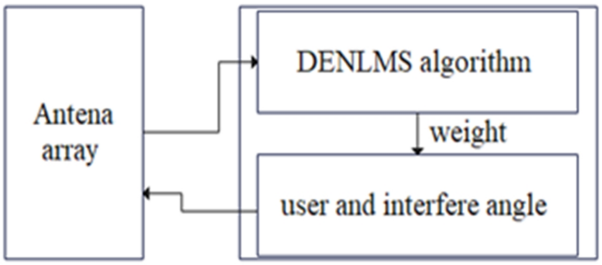


Figure 5.1: Framework of Proposed Methodology

5.2.1 Design of Antenna

Six microstrip patch antennas in the beam-steering array had their reflection properties and emission patterns studied. All the objectives of the work are achieved by this design, which also produces the appropriate reflection qualities and radiation patterns. Another common type of microstrip patch antenna is this, which follows rectangular patch antenna. Compared to a patch antenna, it is smaller. It measures how much of an antenna's entire power is radiated and how much is absorbed as full input power. The input power is efficiently released to space when the radiation antenna efficiency is high.

The majority of the input power is wasted due to intrinsic loss, which includes magnetic losses, metal conduction, dielectric losses, and other losses. For millimeter wave frequency applications, the microstrip patch smart antenna is created to enhance the performance, gain, and bandwidth of the antenna. In particular, with modern antenna propagation, beam-steerable antennas have become extremely widespread. Because the microstrip antenna's bandwidth and gain are increased, energy is conserved, and noise is reduced. Antennas that can produce directional beams with minimal side lobes are known as beam steering antennas. This study's primary goal is develop a smart antenna which employs a beam-steering technique with use of circular patch antenna. The ability of circular patch antennas to achieve directional radiation patterns, combined with their compact size, low cost, low profile, and low cross-polarization, make them an ideal choice for use in smart antennas that employ beam-steering techniques.

The patch radius is characterized as,

$$r = \frac{F}{\sqrt{1 + \frac{2h}{\pi \in F\left[\ln\left(\frac{F\pi}{2h}\right)+1.7726\right]}}} \tag{5.1}$$

$$F = \frac{8.791 \times 10\text{^}9}{f\sqrt{\in}} \tag{5.2}$$

h is the height of the substrate, the dielectric constant of the substrate is represented as $\in$, and the frequency of f. Frequencies like 39.75 GHz, 44.62 GHz, and 36.75 GHz increase capacity and speed of network by allowing more procedures to function in the high-frequency spectrum. The feed line width is given as,

$$\frac{w}{h} = \begin{cases} \frac{8e^{-4}}{e^2 2A-2} & \text{for } \frac{w}{h} < 2 \\ \frac{2}{\pi}\left[B - 1 - (2B-1) + \frac{n-1}{2n}\left\{\ln(B-1) + 0.39 - \frac{0.61}{n}\right\}\right] & \text{for } \frac{w}{h} > 2 \end{cases} \tag{5.3}$$

Where,

$$A = \frac{z_0}{60}\sqrt{\frac{\in +1}{2}} + \frac{\in -1}{\in +1}\left(0.23 + \frac{0.11}{\in}\right) \tag{5.4}$$

$$B = \frac{377\pi}{2Z_0\sqrt{\in}} \tag{5.5}$$

The slots are added to achieve additional control over the beam direction, increase antenna gain, and reduce interference. However, this comes at the cost of a more complex design, narrower bandwidth, and reduced efficiency. Roger substrate is create the antenna, which is 20 mm in length, 20 mm in width, and 0.5 mm in height. The 5G network is divided into two frequency bands. Frequency band 1 (FR1-sub-6 GHz range) spans from 450MHz to 6GHz, whereas Frequency range 2 spans from 24.25GHz to 52.6GHz. In this study, it selected a frequency range of 24.25 GHz to 52.6 GHz. Figure 3.2 depicts the antenna structure with its dimensions, whereas Figure 3.3 depicts the array of antenna design with its dimensions. Table 5.1 lists the design of antenna specifications. Table 5.2 represents the suggested antenna's study for 44.6GHz. Table 3.3 represents the analysis of

antenna for 36.75GHz. The outcomes of the antenna 39.75GHz examination shows in Table 5.4.

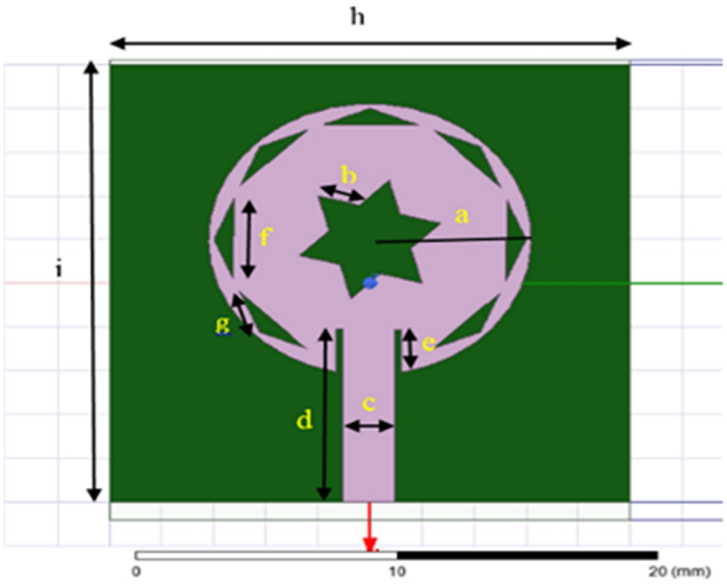


Figure 5.2: Measurements of Antenna

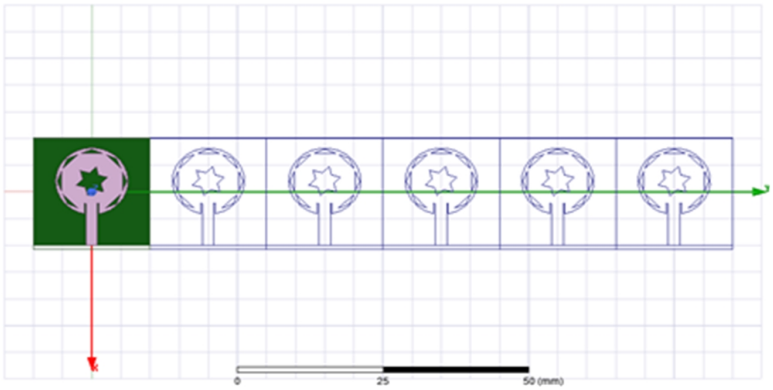


Figure 5.3: Measurements of Antenna Array

Table 5.1: Design Specification of the Antenna

SR. No	Value (mm)	Parameter
Single Antenna Measurements		
1	4.7	Length of the star slot
2	4.7	Width of the star slot
3	6.2	a(Radius of the patch)
4	1.6	b
10	7.8	c (Length of the feed line)
5	2	d (Width of the feed line)
6	12.4	Diameter of the Patch
7	1.9	e
8	3.65	f
9	1.93	g
11	20	h (Length of the substrate)
12	20	I (Width of the substrate)
Antenna Array Measurements		
13	120	A
14	20	B
15	7.7	C

The table 5.1 provides various parameters and their corresponding values for both single antenna and antenna array measurements. The values are given in millimeters (mm).

The given table 5.2 lists different quantities and their corresponding values for a system operating at a frequency of 44.6 GHz. The peak directivity and gain of the system are 14.9 and 15.21 dB, respectively, and the peak realized gain and system gain are slightly lower at 15.154 and 15.14 dB, respectively. The system has a radiated power of 3.0312, accepted power of 2.9884 W, and incident power of 3 W, with a radiation efficiency of 1.143 W. Overall, these values give an indication of the performance and characteristics of the system at the given frequency.

Table 5.2: Analysis of Antenna for 44.6 GHz

S. No	Value	Quantity
1	15.14 dB	Peak system gain
2	14.9	Peak directivity
3	44.6 GHz	Frequency
4	15.154 dB	Peak realized gain
5	15.21 dB	Peak gain
6	2.9884 W	Accepted power
7	1.143 W	Radiation efficiency
8	3 W	Incident power
9	3.0312	Radiated power
10	3 W	System power

Table 5.3: Analysis of Antenna for 36.75 GHz

S. No	Value	Quantity
1	15.22 dB	Peak system gain
2	15.932	Peak directivity
3	36.75 GHz	Frequency
4	15.22 dB	Peak realized gain
5	15.80 dB	Peak gain
6	2.88 W	Accepted power
7	0.991 W	Radiation efficiency
8	3 W	Incident power
9	2.86	Radiated power
10	3 W	System power

The given table 5.3 describe the performance of an antenna system operating at a frequency of 36.75 GHz. The system has a peak directivity of 15.932 and a peak gain of 15.80 dB.

The peak realized gain and peak system gain are both 15.22 dB. The system radiates a power of 2.86 W and accepts a power of 2.88 W, with an incident power

of 3 W and a system power of 3 W. The radiation efficiency is 0.991 W. Overall, these values provide an indication of the effectiveness of the antenna system at the given frequency and power levels. The statistics shown in table 5.4 depict a system that runs at 39.75 GHz. Peak directivity, or the highest gain in a certain direction, for the system is 18.3.

Table 5.4: Analysis of Antenna for 39.75 GHz

S. No	**Value**	**Quantity**
1	17.8 dB	Peak system gain
2	18.3	Peak directivity
3	39.75 GHz	Frequency
4	17.8 dB	Peak realized gain
5	18.1 dB	Peak gain
6	2.94 W	Accepted power
7	0.98 W	Radiation efficiency
8	2.91	Radiated power
9	3 W	Incident power
10	3 W	System power

The highest gain of the system is 18.1 dB, which is the most signal amplification it is capable of. Peak realised gain and peak system gain, which measure the system's greatest gain after accounting for system losses, are both 17.8 dB. The system accepts a power of 2.94 watts while radiating electricity at a level of 2.91 watts. The system power is 3 watts, and incident power is known as the power provided to the system-is also 3 watts. The system is very effective in converting input power into radiated power because its radiation efficiency, which is the ratio of radiated power to incident power, is 0.98.

5.2.2 An Antenna Array

The antenna array is a scheme that allows us to design radiation properties without significantly influencing the antenna's impedance. A radiation pattern of the single

element is relatively broad, causing in poor directional gain as compared to the array in every cases. The actual communicators gain are necessary for many areas. Increasing the electrical size of antenna, i.e. the count of array elements, for practical determinations is performed. The maximum radiation is determined by the intensity dispersion and phase of the excitation source sent to the linear beam-steering array elements. The direction of maxima is determined by the phase shift allocated to each element, but the shape of the radiation pattern is estimated by the amplitude. When array components are organized on the x-axis, a diffraction pattern in the xz-plane can be realized as a combination of spatial dispersal vector and a totally changeable weighting factor vectors supplied in the equation (5.6).

$$P(\theta) = P_e(\theta)P_a(\theta) = P_e(\theta) \begin{bmatrix} A_1 e^{j\varphi 1} \\ A_2 e^{j\varphi 2} \\ : \\ A_n e^{j\varphi n} \end{bmatrix} \begin{bmatrix} e^{j2\pi \frac{d1}{\lambda} \sin\theta} \\ e^{j2\pi \frac{d2}{\lambda} \sin\theta} \\ e^{j2\pi \frac{dn}{\lambda} \sin\theta} \end{bmatrix} \tag{5.6}$$

$P_a(\theta)$ and $P_e(\theta)$ are the antenna's array pattern elements. The complex weight factor is represented by $A_n e^{j\varphi n}$, while the distance from the centroid is represented by d. Figure 5.4 depicts a three-dimensional image of the planned antenna.

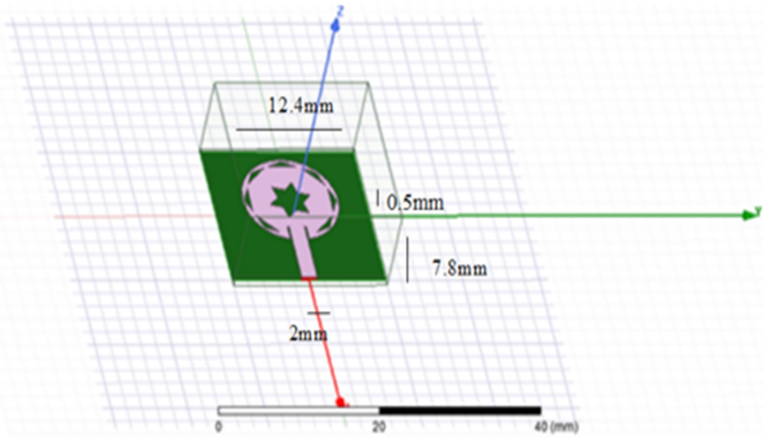


Figure 5.4: Geometry of the Antenna

5.2.3 Weight Valuation of Beam Steering Antenna based on DENLMS

The weights assigned to the elements of individual excitation signals determine the adaptive array's ideal directional gain. The DENLMS algorithm offers faster convergence and improved performance compared to the standard LMS, Recursive Least Squares (RLS), and Normalized LMS (NLMS) algorithms in some scenarios. LMS approach is a gradient-based technique that involves an iterative process that executes sequential weight vector adjustments in the vector of gradient -ve path, resulting in the least mean square error at this moment. Pipeline topologies having delay components frequently reduce the critical path in VLSI implementation, providing the essential sample time to be attained. In this work, a DENLMS is created for a low-latency, high-speed framework with minimum cost of computing. Three main stages of the DLMS approach are given in Equations. (5.7), (5.8), and (5.9).

$$W(n+1) = W(n) + \mu e(n-kD)x(n-kD) \tag{5.7}$$

The updated weight is represented by $W(n+1)$, the prior weight is represented by $W(n)$, and the step size is represented by $\mu.e(n-kD)$ Can be calculated as follows:

$$e(n-kD) = d(n-kD) - y(n-kD) \tag{5.8}$$

$$y(n-kD) = w^T(n-kD)x(n-kD) \tag{5.9}$$

kD the number of delay elements, w^T denotes the weight's transposition and $x(n-kD)$ the input. The work flow of the DENLMS approach is demonstrated in figure 5.5.

Figure 5.5 displays more elements of the proposed DENLMS approach. The parameter step size determines the steady-state performance and filter convergence speed of the DENLMS. The weight update equation, based on the NLMS approach principles, is as follows.

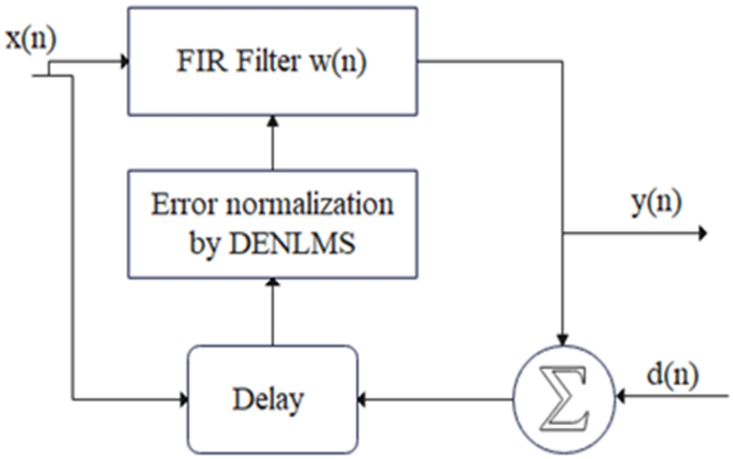


Figure 5.5: DENLMS Algorithm

$$W(n+1) = W(n) + \mu e(n)x(n) \tag{5.10}$$

5.3 Result and Discussion

The planned parameter of antenna is calculated in this experiment based on gain and return loss at 39.75 GHz, , and 36.75 GHz 44.62 GHz. Firstly, the complex weight of antenna is computed, followed by the determination of the angle of interferer and direction about the DENLMS approach.

Figure 5.6 depicts the antenna's return loss, which is indicated as -33dB for the frequency of 44.62 GHz.

5.3.1 Radiation Pattern for 36.75GHz for Different Angle Values

Figure 5.7 depicts the antenna's 3D radiation pattern at 36.75 GHz. Table 5.5 displays the radiation pattern for 36.75GHz at various angles of 0, 30, -30, 45, -45, 60, -60, 90, and -90 degrees. The maximum gain of 16 dB is achieved by the radiation pattern with 0 degrees. The direction angle is set at -50 degrees, and

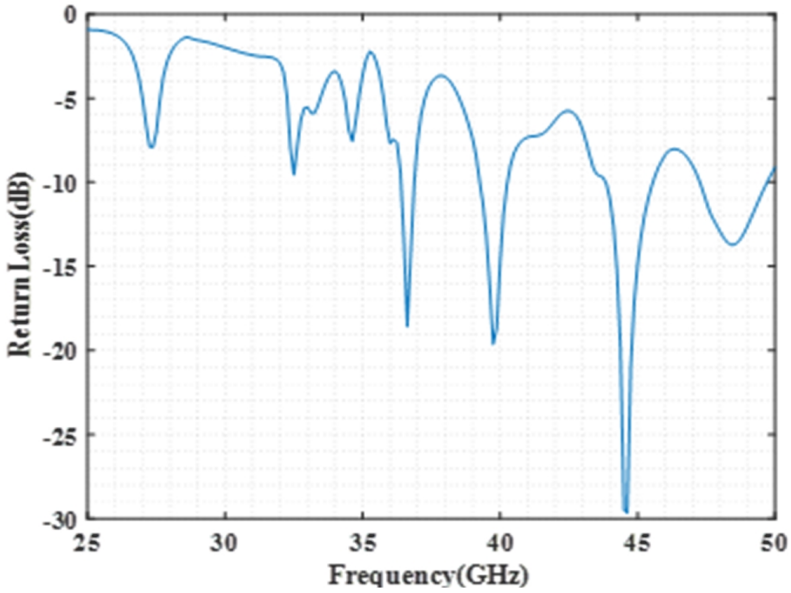


Figure 5.6: Return Loss Measurement

provided -25 degrees of the interferer angle. Rest of all are given a gain of less than 0 degrees.

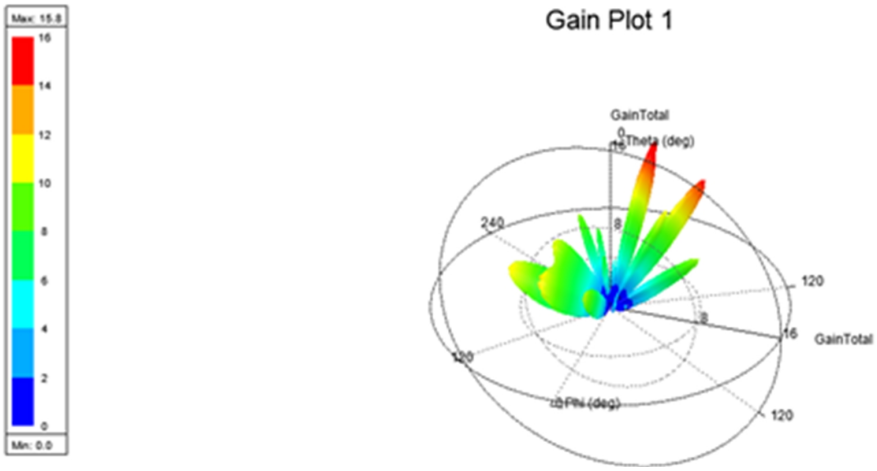
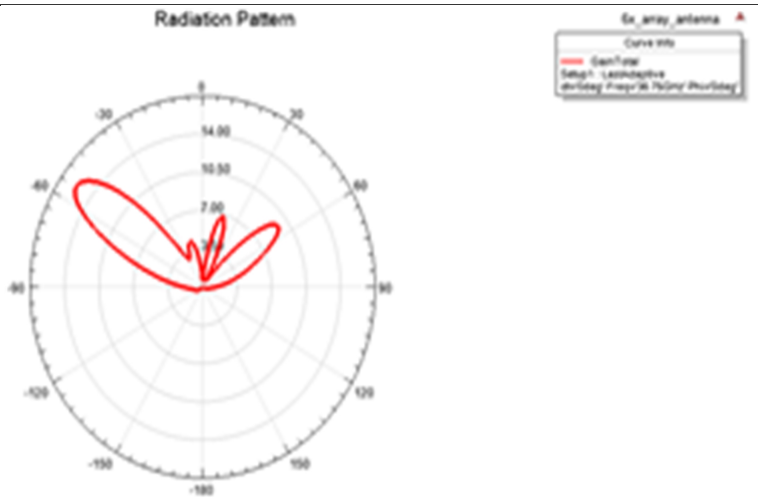
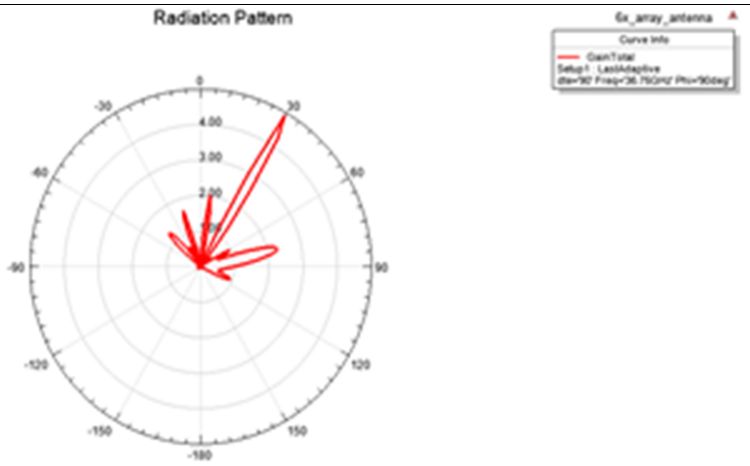
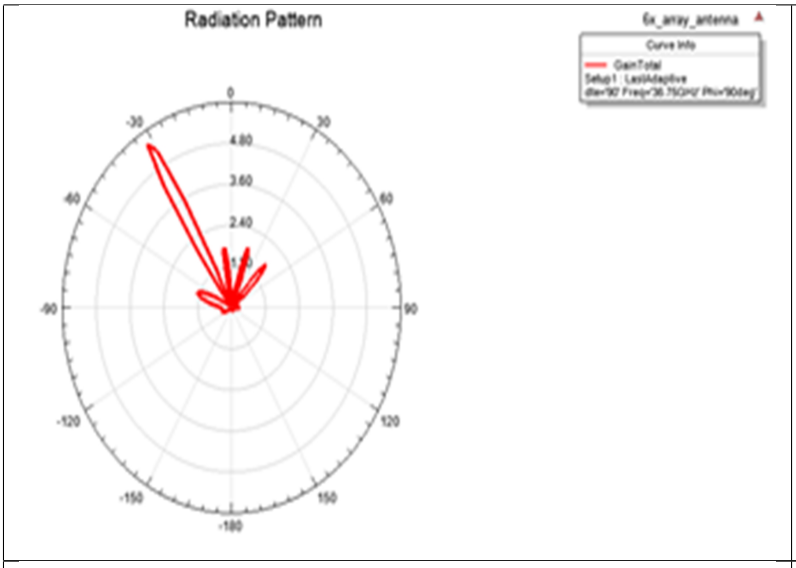
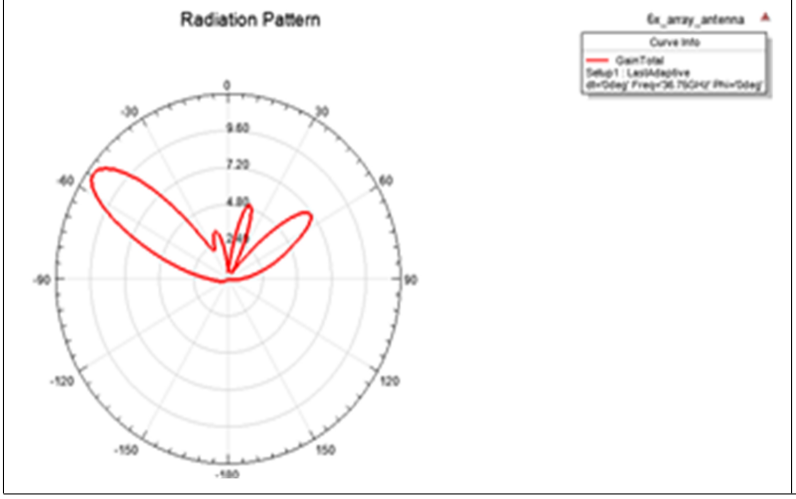
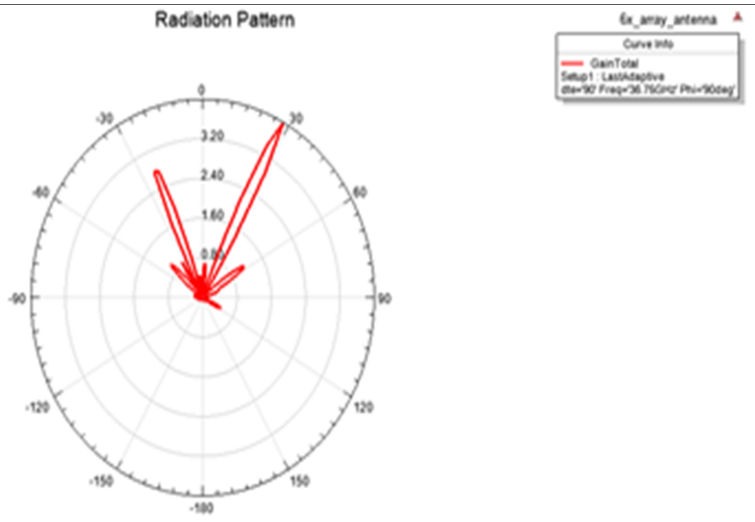
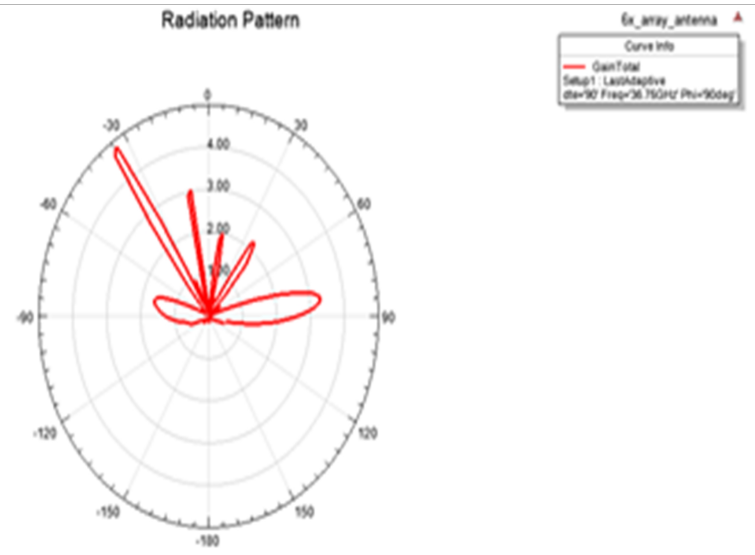


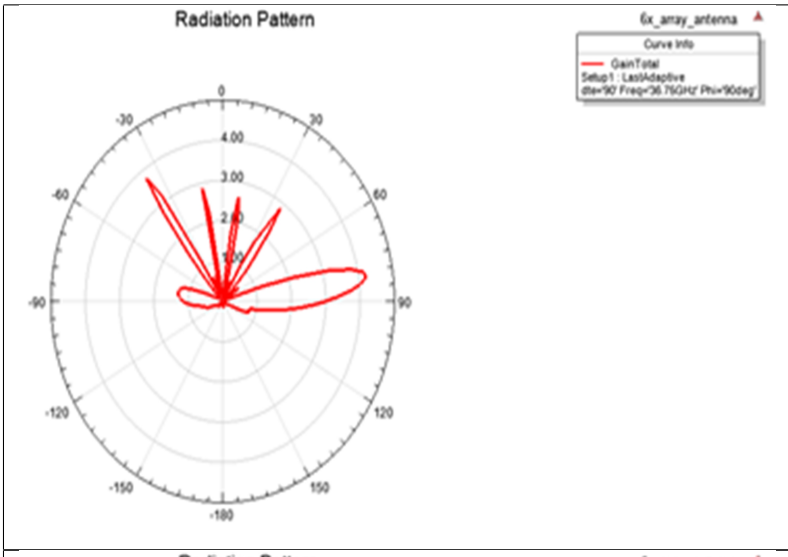
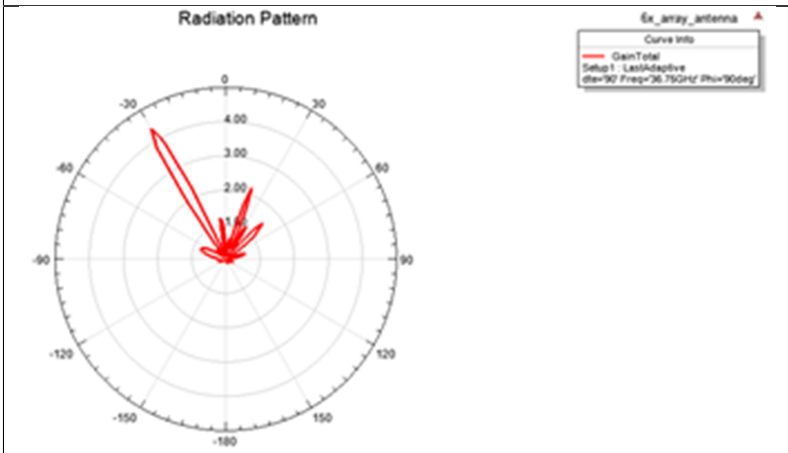
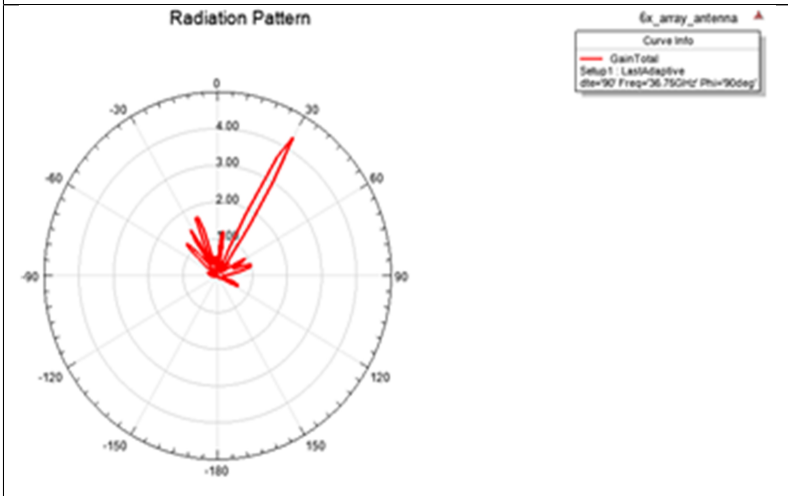
Figure 5.7: 3D Radiation Pattern

Table 5.5: Radiation Pattern for 36.75 GHz for Different Angle Values

Radiation Pattern	Angle degrees
	0
	30

 Radiation Pattern 6x_array_antenna Curve Info GainTotal Setup1 : LastAdaptive 0 30 60 90 120 150 -180 -150 -120 -90 -60 -30 4.80 3.60 2.40	-30
 Radiation Pattern 6x_array_antenna Curve Info GainTotal Setup1 : LastAdaptive 0 30 60 90 120 150 -180 -150 -120 -90 -60 -30 9.60 7.20	45

 Radiation Pattern 6x_array_antenna Curve Info GainTotal Setup1 : LastAdaptive dBm'90' Freq='36.75GHz' Phi='90deg' 0 30 60 90 120 150 -180 -150 -120 -90 -60 -30 3.20 2.40 1.60	-45
 Radiation Pattern 6x_array_antenna Curve Info GainTotal Setup1 : LastAdaptive dBm'90' Freq='36.75GHz' Phi='90deg' 0 30 60 90 120 150 -180 -150 -120 -90 -60 -30 4.00 3.00 2.00	60

 Radiation Pattern 6x_array_antenna Curve Info GainTotal Setup1 : LastAdaptive dte='90' Freq='36.75GHz' Phi='90deg' 0 30 60 90 120 150 -180 -150 -120 -90 -60 -30 4.00 3.00 2.00	-60
 Radiation Pattern 6x_array_antenna Curve Info GainTotal Setup1 : LastAdaptive dte='90' Freq='36.75GHz' Phi='90deg' 0 30 60 90 120 150 -180 -150 -120 -90 -60 -30 4.00 3.00 2.00	90
 Radiation Pattern 6x_array_antenna Curve Info GainTotal Setup1 : LastAdaptive dte='90' Freq='36.75GHz' Phi='90deg' 0 30 60 90 120 150 -180 -150 -120 -90 -60 -30 4.00 3.00 2.00	-90

5.3.2 Radiation Pattern for 39.75 GHz for Different Angle Values

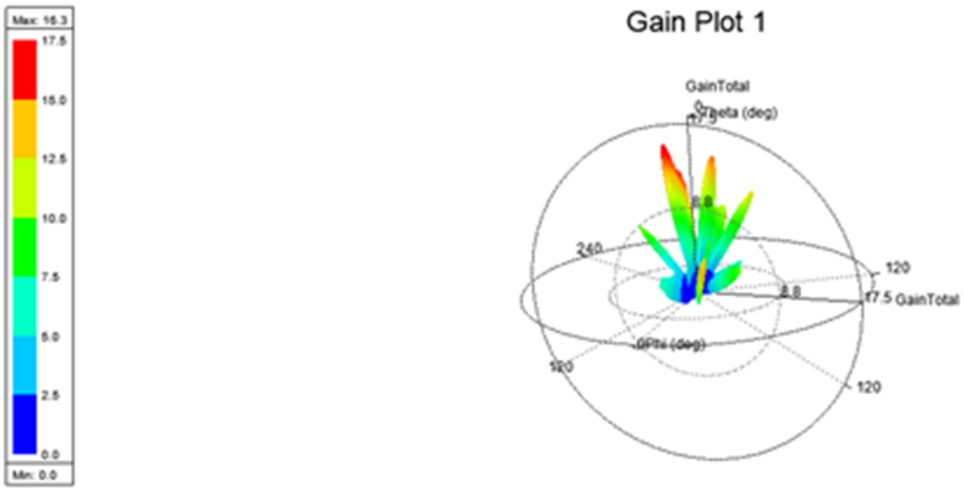
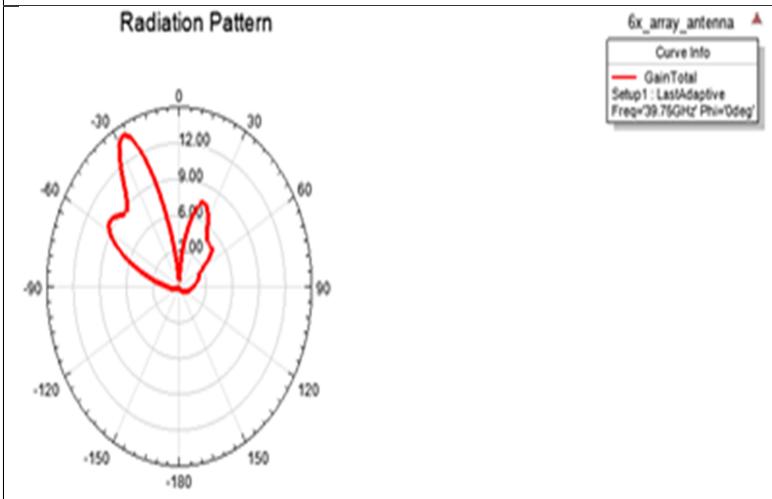
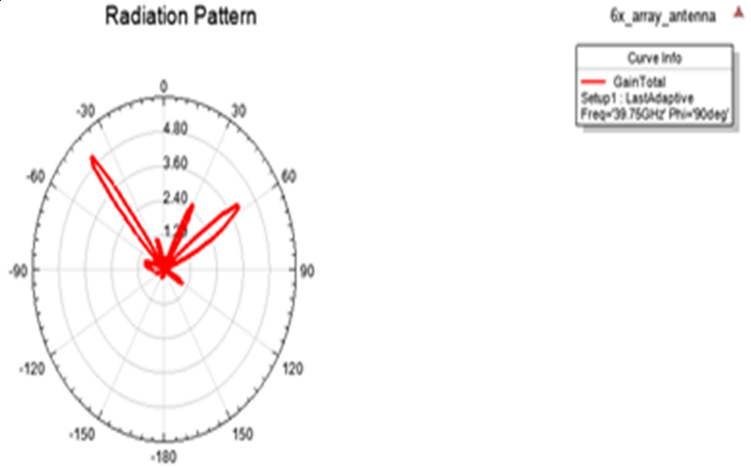
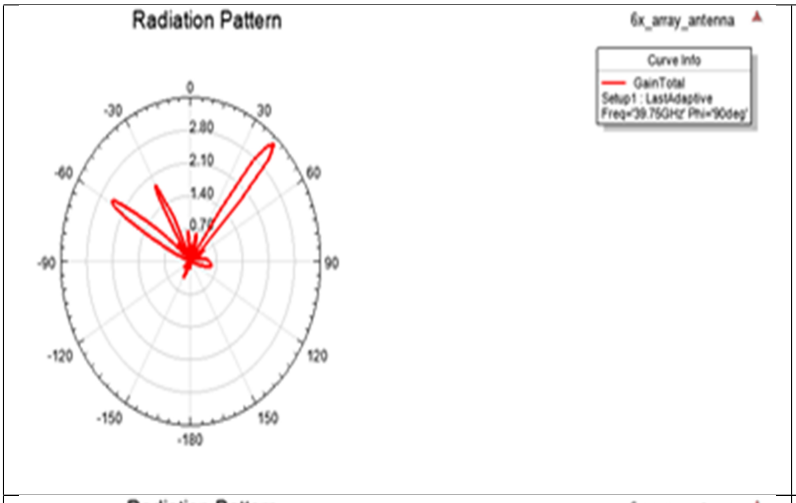
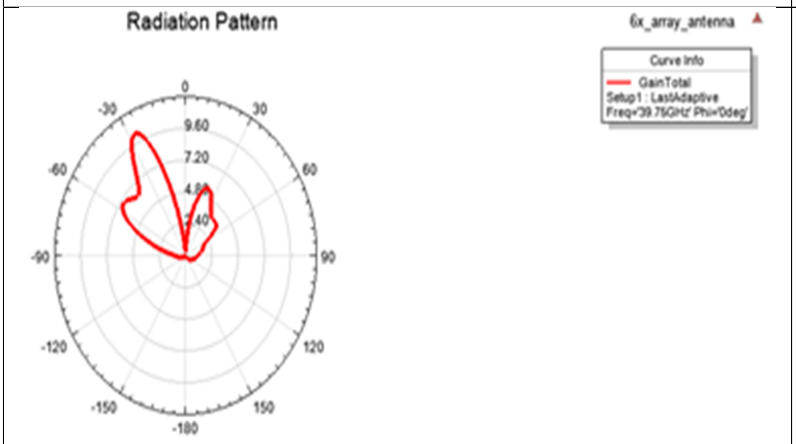
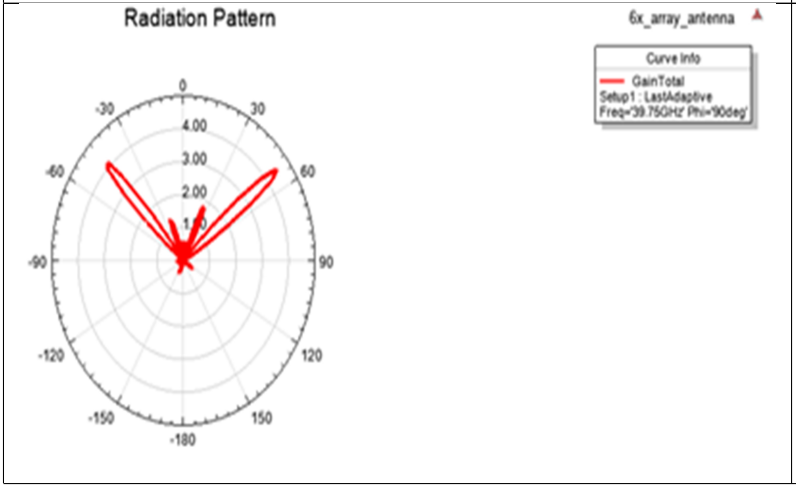


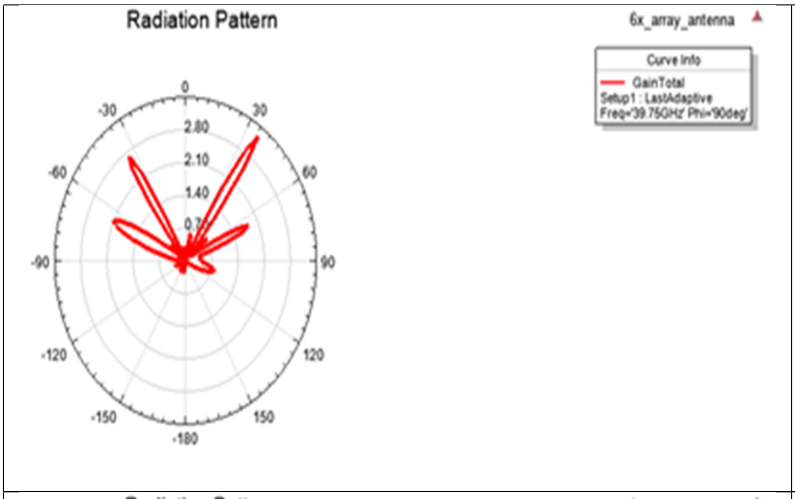
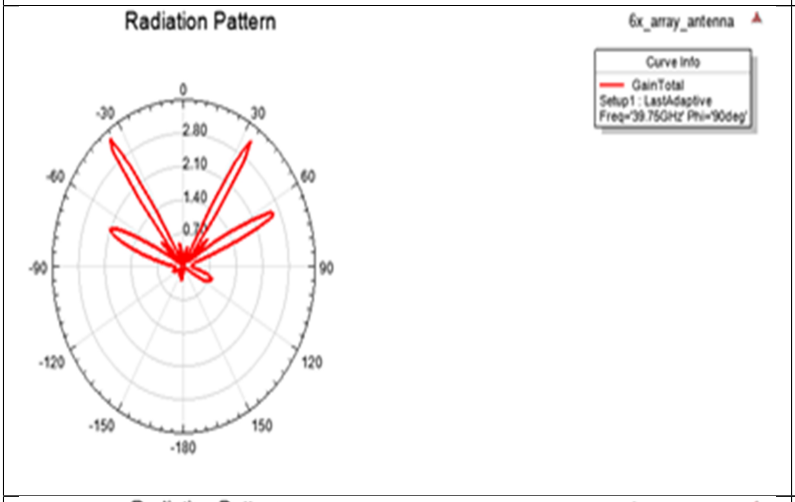
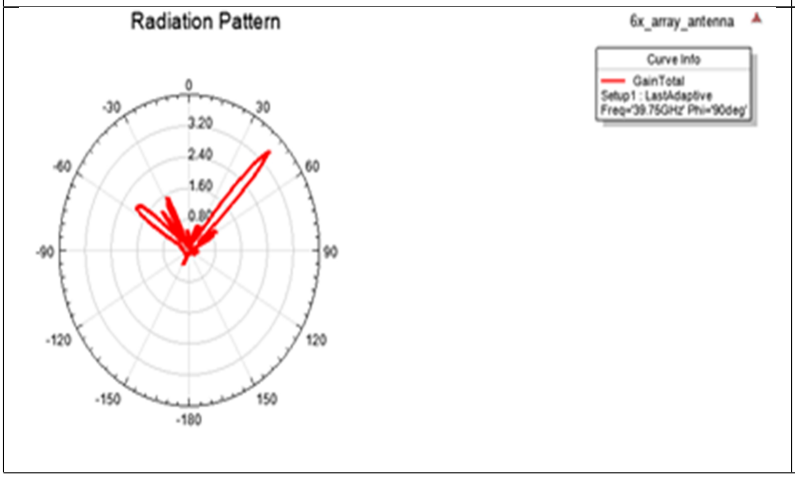
Figure 5.8: Gain Plot for 39.75GHz Frequency

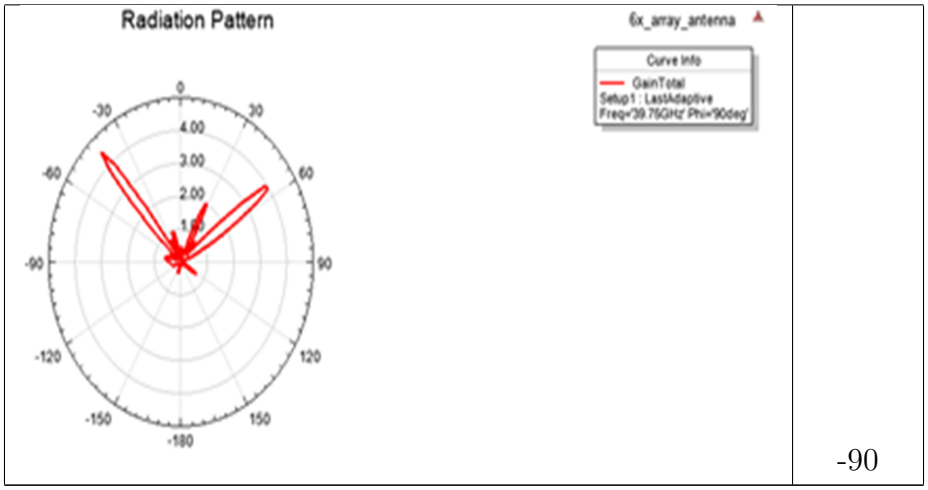
Figure 5.8 shows the antenna's 3D radiation pattern at 39.75 GHz. Table 5.6 depicts the radiation pattern for 39.75GHz at various angle outcomes such as -90, 60,-30, -45, -60, 90, 30, 45, and 0 degrees. The maximum gain at 0 degrees at 14 dB in radiation pattern. The method selects an interferer angle of -60 degrees and a directional angle of -28 degrees. Rest of all are given a gain of less than 0 degrees.

Table 5.6: Radiation Pattern for 39.75 GHz for Different Angle Values

Radiation Pattern	Angle degrees
	0
	30

 Radiation Pattern 6x_array_antenna Curve Info GainTotal Setup1 : LastAdaptive Freq='39.75GHz' Phi='90deg' 0 30 60 90 120 150 -180 -150 -120 -90 -60 -30 2.80 2.10 1.40	-30
 Radiation Pattern 6x_array_antenna Curve Info GainTotal Setup1 : LastAdaptive Freq='39.75GHz' Phi='0deg' 0 30 60 90 120 150 -180 -150 -120 -90 -60 -30 9.60 7.20	45
 Radiation Pattern 6x_array_antenna Curve Info GainTotal Setup1 : LastAdaptive Freq='39.75GHz' Phi='90deg' 0 30 60 90 120 150 -180 -150 -120 -90 -60 -30 4.00 3.00 2.00	-45

 Radiation Pattern 6x_array_antenna Curve Info GainTotal Setup1 : LastAdaptive Freq='39.75GHz' Phi='90deg' 0 30 60 90 120 150 -180 -150 -120 -90 -60 -30 2.80 2.10 1.40	60
 Radiation Pattern 6x_array_antenna Curve Info GainTotal Setup1 : LastAdaptive Freq='39.75GHz' Phi='90deg' 0 30 60 90 120 150 -180 -150 -120 -90 -60 -30 2.80 2.10 1.40	-60
 Radiation Pattern 6x_array_antenna Curve Info GainTotal Setup1 : LastAdaptive Freq='39.75GHz' Phi='90deg' 0 30 60 90 120 150 -180 -150 -120 -90 -60 -30 3.20 2.40 1.60	90



5.3.3 Radiation Pattern for 44.62 GHz for Different Angle Values

The Figure 5.9 shows the 3D radiation pattern of antenna at 44.62 GHz. The Table 5.7 depicts the radiation pattern at 44.62GHz for various angle results as -90, -45, 90, -60, 45, -30, 60, 30, and 0 degrees. The radiation pattern with 0 degrees has the highest gain of 11 dB.

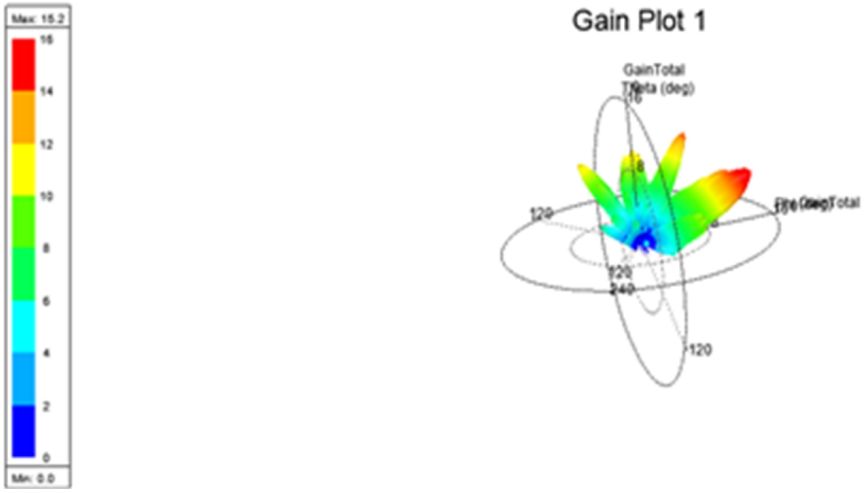
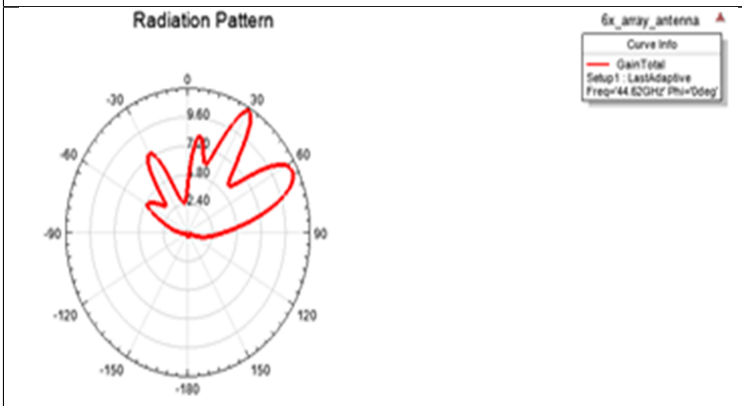
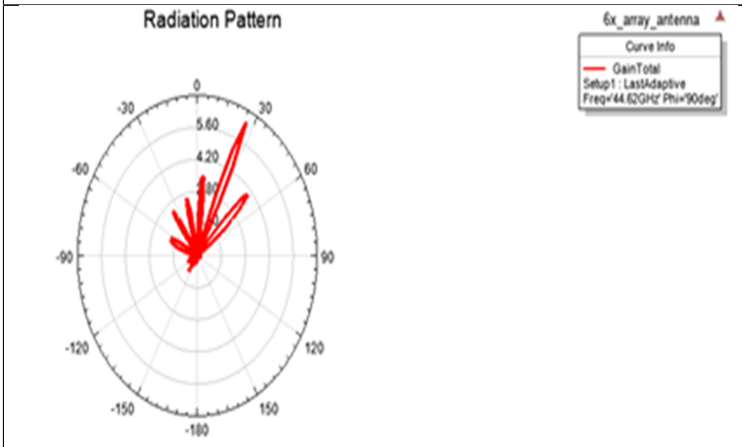
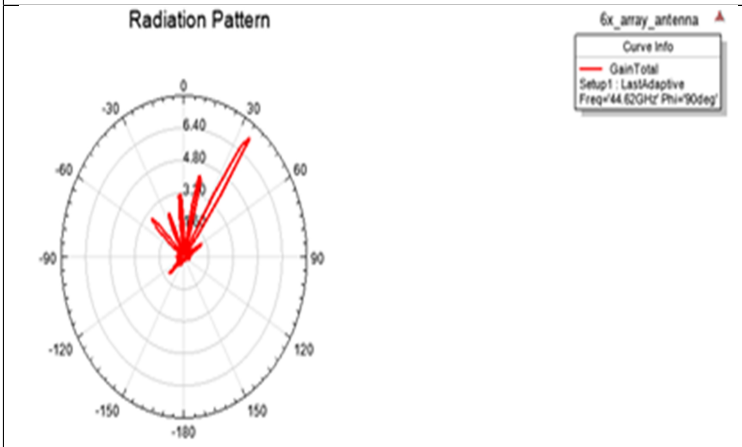
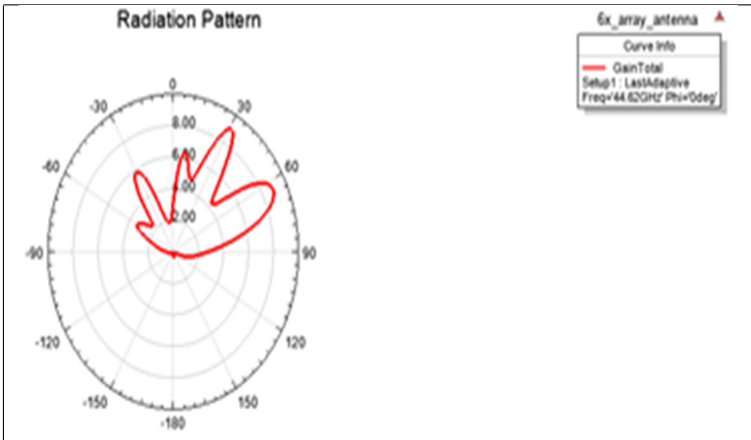
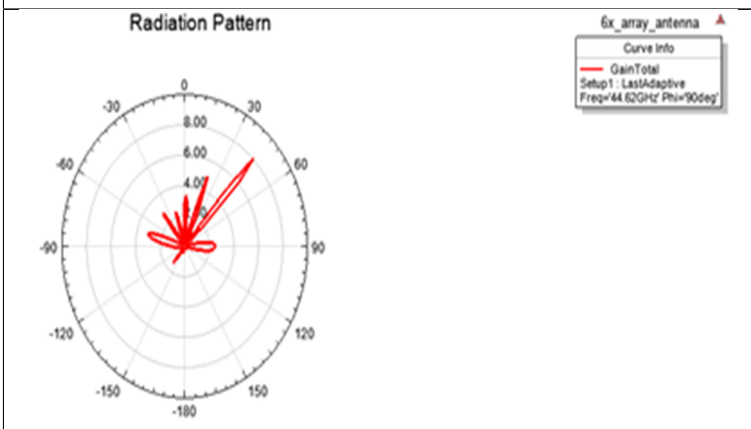
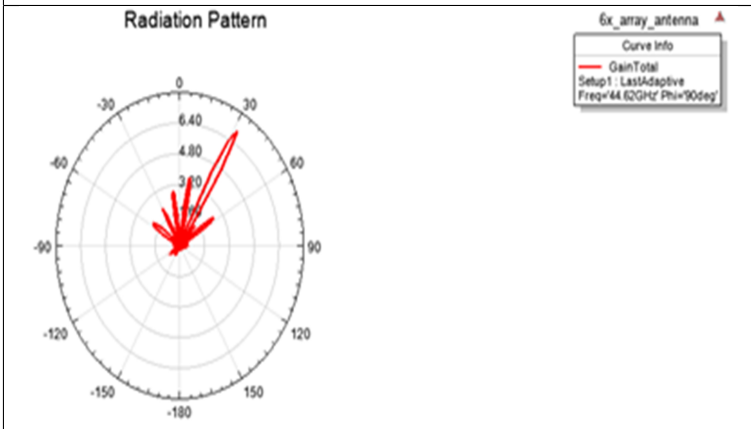
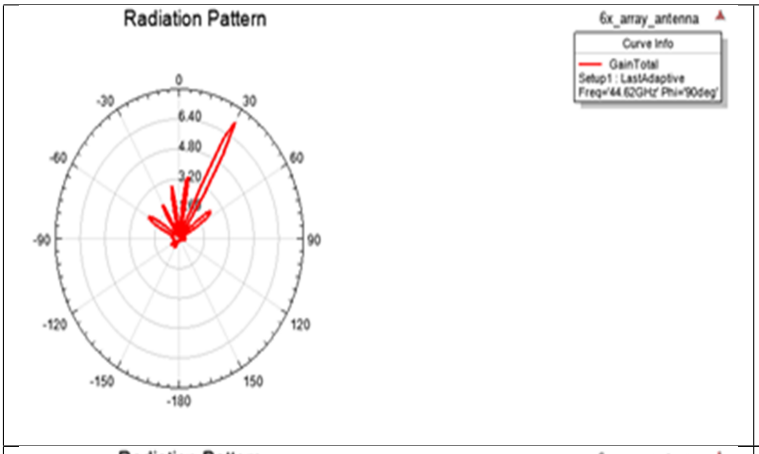
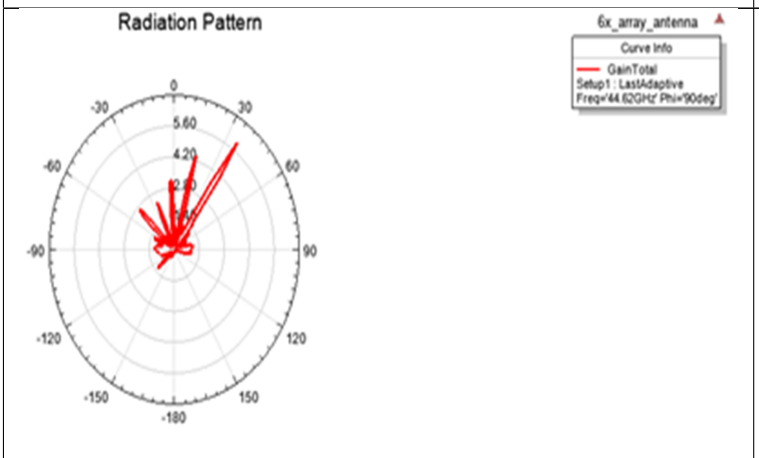
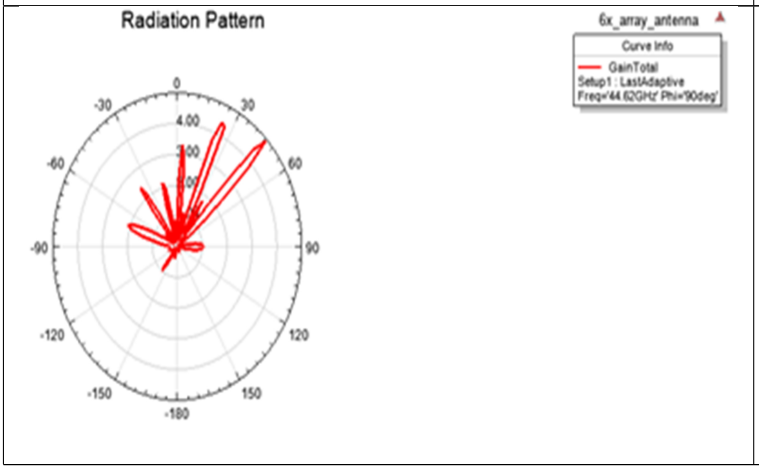


Figure 5.9: Gain Plot for 44.62 GHz

Table 5.7: Radiation Pattern for 44.62 GHz for Different Angle Values

Radiation Pattern	Angle (degrees)
	0
	30
	-30

 Radiation Pattern 6x_array_antenna Curve Info GainTotal Setup1 : LastAdaptive Freq='44.62GHz' Phi='0deg' 0 30 60 90 120 150 -180 -150 -120 -90 -60 -30 8.00 6.00 4.00 2.00	45
 Radiation Pattern 6x_array_antenna Curve Info GainTotal Setup1 : LastAdaptive Freq='44.62GHz' Phi='90deg' 0 30 60 90 120 150 -180 -150 -120 -90 -60 -30 8.00 6.00 4.00	-45
 Radiation Pattern 6x_array_antenna Curve Info GainTotal Setup1 : LastAdaptive Freq='44.62GHz' Phi='90deg' 0 30 60 90 120 150 -180 -150 -120 -90 -60 -30 6.40 4.80	60

	-60
	90
	-90

The 30 degrees is set for direction angle, while the interferer angle is set to 15 degrees. Rest of all are given a gain of less than 0 degrees. Optimal beam steering can also be achieved by making complicated weights and applying them to

components of array in MATLAB using DENLMS technique. In these MATLAB simulations, the user (45 and +45) and the interferer (20 and +20) are both observed. Maxima is obtained at +45 and 45 using HFSS, which closely fits MATLAB findings, however nulls are attained at 30 and +30.

5.3.4 Gain and Directivity Examination by Varying Theta (degree)

The Figures 5.10, 5.12, and 5.14 illustrate the directivity of antenna at 44.62, 36.75, and 39.75 GHz, respectively. Figures 5.11, 5.13, and 5.15 show the gain of antenna at 44.62, 39.75, and 36.75GHz, respectively. The magnitude of directivity at 36.75, 39.75, and 44.62 GHz is 16dB, 14dB, and 11dB, respectively. The obtained gain from the planned antenna is 16.3 dB, 15.2 dB, and 15.8 dB, respectively, over three frequency bands.

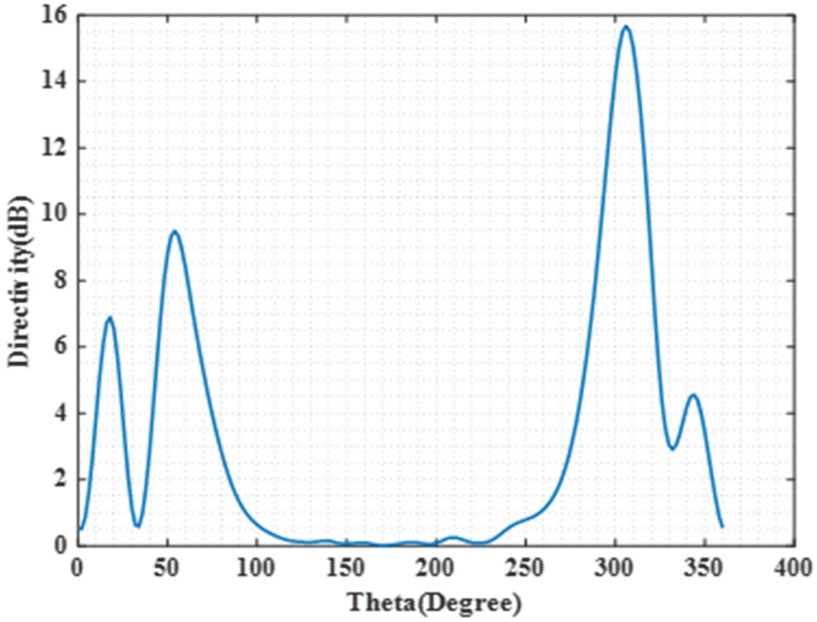


Figure 5.10: Directivity of Antenna in 36.75 GHz

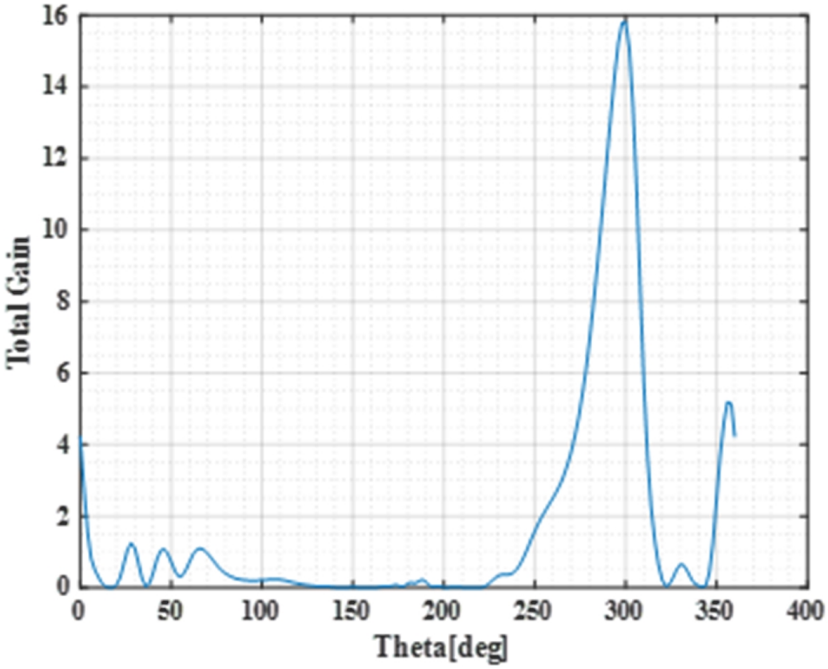


Figure 5.11: Gain of Antenna in 36.75 GHz

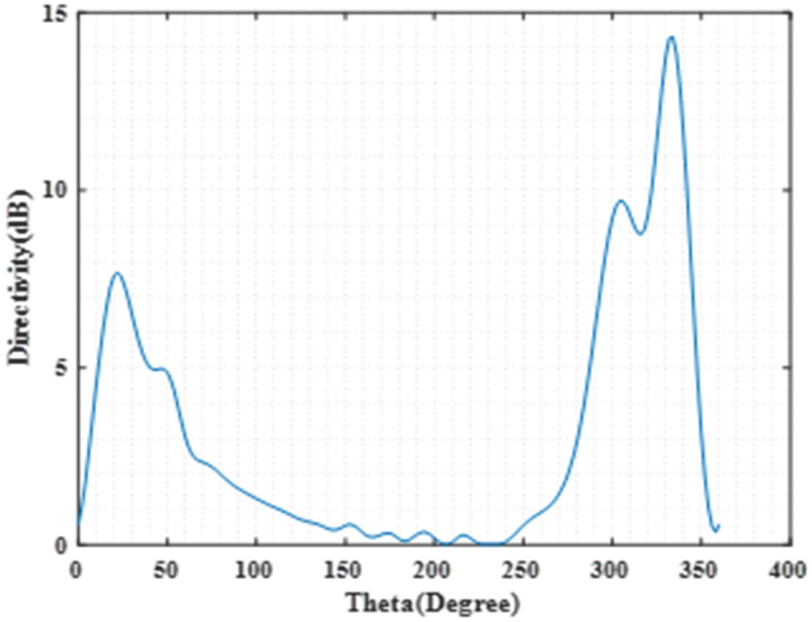


Figure 5.12: Directivity of the Antenna in 39.75 GHz

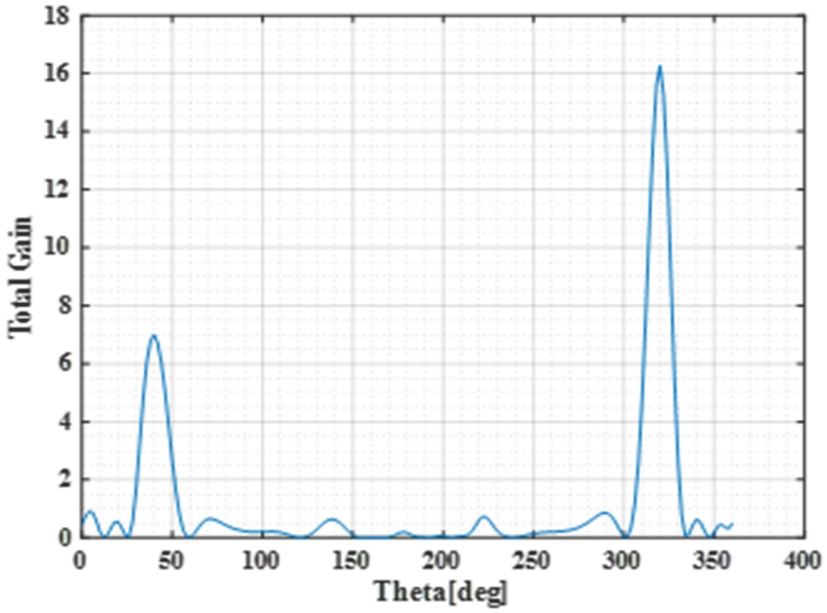


Figure 5.13: Gain of Antenna in 39.75GHz

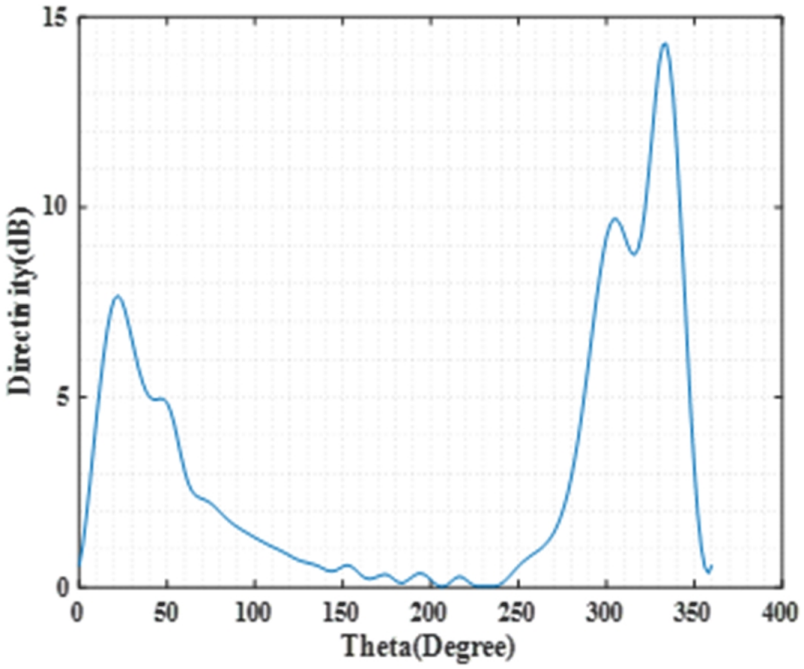


Figure 5.14: Directivity of Antenna in 44.62 GHz

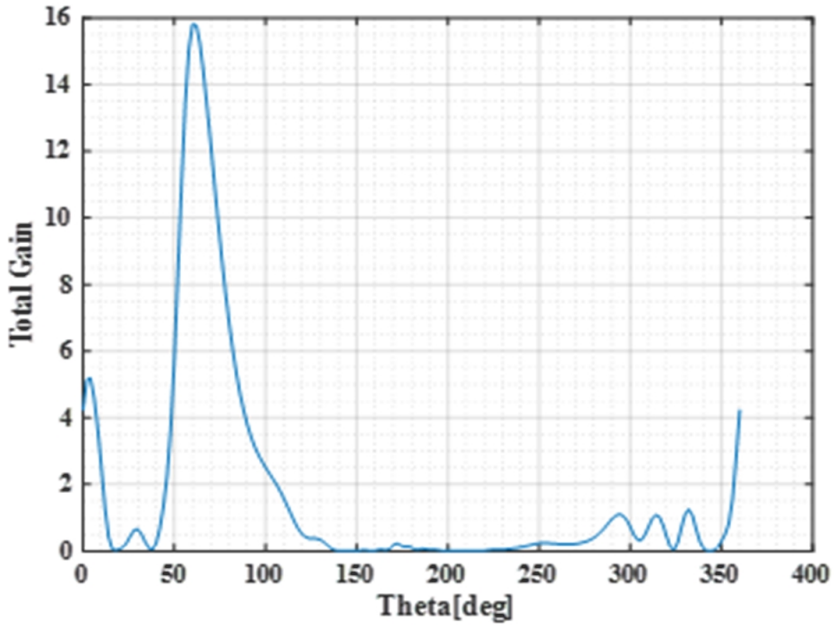


Figure 5.15: Gain of Antenna in 44.62GHz

5.3.5 Comparison with Existing State-of-Art Techniques

An adaptive linear array E-shape slot smart antenna system with a LMS beam steering method to improve array gain and bandwidth is created in Kodgirwar et al. [84]. The antenna is built for 5G applications with two symmetrical slots, and the characteristics of directivity, VSWR, and return loss are investigated for multiple adaptive element arrays. The LMS technique is also implemented and tested for beam steering in weight estimation.

Chauhan et al. [85] defined an ultra-wideband microstrip patch antenna for millimeter wave band applications. With 7.5 dB gain, antenna achieves a core frequency band about 34.2 GHz. To provide high bandwidth, the limited ground structure is used which extends from 24.1 to 49.9 GHz. 5G communication in the millimetre wave band spectrum was useful in developed antenna.

A millimetre wave microstrip patch antenna with a central frequency of 54 GHz and 38 GHz and a bandwidth of 2 GHz and 1.94 GHz, respectively, for 5G mobile communication created Imran et al. [86].

Rogers RT5880, which has a 2.2 dielectric constant and a thickness of 0.508mm, was used in this project. With a four-element array, microstrip line feeding is used. Examined are the array antenna and individual antenna's return loss, gain plots, VSWR, and surface current distribution. The author in [87] built a small microstrip patch antenna operating at 28 GHz for 5G wireless applications. Here, a RogerRT5880 substrate with a 0.4 mm thickness is employed. Yoon and Seo [88] developed a U-slot patch antenna array for a wideband communication system that has a ground plane and two U-shaped slots on a rectangular patch. With 2.2 permittivities, Rogers RT/Duroid5880 substrate material is utilized. The intended antenna has a thickness of 0.3 mm. The high operating frequency range necessitates the use of the microstrip feed line. Examining the antenna settings and attaining a frequency of about 28 GHz demonstrate the design's dependability.

Naik [89] created a millimeter wave communication rectangular slot microstrip patch antenna. The material utilized in this case is RT Duriod 5880, which has a permittivity of 2.2. To increase the resonance frequency, the antenna framework was developed with square-shaped slot in the feed line and a two rectangular slots in the patch. The lumped port arrangement is used to evaluate the efficiency of the S11 parameter, and the return loss is approximately 18.02 dB. A phased array microstrip antenna for 5G applications, and the substrate material utilized is Roger with a thickness of 1.27mm created in Nigam et al. [90]. The antenna was developed with half power beam width and varied gain in four distinct directions. The developed antenna achieves a high gain with a low loss at mm wave frequency. Table 5.8 compares the antenna framework parameters of return loss, frequency, directivity, and gain of state of art method with suggested antennas.

According to Table 5.8, the suggested antenna operates at three different frequencies (we considered three frequency for the proposed): 44.62 GHz, 36.75 GHz, and 39.75 GHz, with corresponding gains of 15.2 dB, 15.8 dB, and 16.3 dB. The return loss values are 18 dB, 17 dB, and 33 dB, and the directivity values are 16 dBi, 14 dBi, and 11 dBi, respectively. Overall, the comparison table shows that the recommended antenna design offers relatively high directivity and gain at all three operating frequencies, with reasonable return loss values.

Table 5.8: Comparison with State-of-the Art Techniques

Reference	**Directivity (dBi)**	**Gain (dB)**	**Frequency (GHz)**	**Return Loss (dB)**
Proposed	16, 14, 11	15.8, 16.3, 15.2	36.75, 39.75, 44.62	18, 17, 33
[34]	10.62	10.57	10.25	30.27
[45]		13.7	27.76	20
[44]	-	5.90	50	18.022
[43]	-	13	28.43	30
[42]	-	6.72	28	18.25
[41]	7.2, 8.2	6.9, 7.4	38, 54	15.5, 12
[40]	-	7.5	34.2	28.42
[39]	-	7.6	3.6	-26.32

Table 5.9: Comparison with Beam Steering Algorithm

Method [Reference]	**Array Factor**	**Mean Square Error**
DENLMS	**-3**	**0.001**
NLMS [92]	-3.5	0.017
SELMS [95]	-3.7	0.186
SSLMS [94]	-3.9	0.256
VSSLMS [93]	-4	0.287
LMS [92]	-5.5	0.316

The beam steering algorithm is compared in Table 5.9. The outcomes of the system is compared to the existing 5 beam-guiding algorithms. LMS [92], VSSLMS [93], SSLMS [94], SELMS [95], and NLMS [92] are the names of the approaches. The suggested DENLMS performance is compared to those of existing methods in terms of normalized array factor, output signal, and mean square error. The DENLMS algorithm achieves the lowest mean square error and the highest nor-

malized array factor, indicating its superior performance compared to the other algorithms.

Figure 5.16 shows the output signal comparison for various techniques such as LMS [92], VSSLMS [93], SSLMS [94], SELMS [95], and NLMS [92] for 200 iterations. According to graph, the DENLMS shows the better output result than others. Graph for normalized array factor is shown in Figure 5.17.

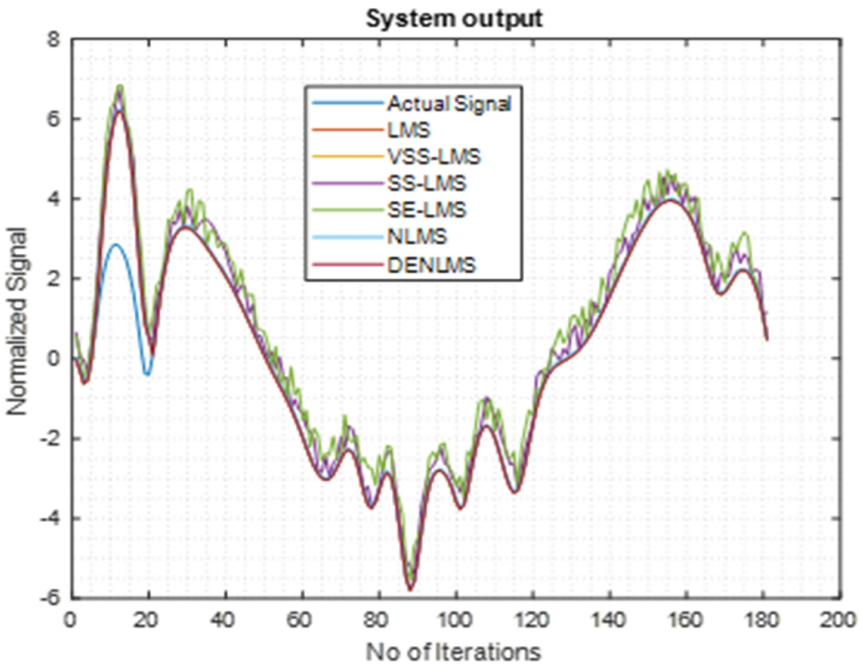


Figure 5.16: Output Signal

Figure 5.16 depicts the output signal, whereas Figure 5.17 depicts the proposed system's normalized array factor. The standardized array factor is drawn after 250 iterations, and the output signal is demonstrated after 200 iterations. According to these numbers, the suggested system denotes the smallest array factor than the current methodologies.

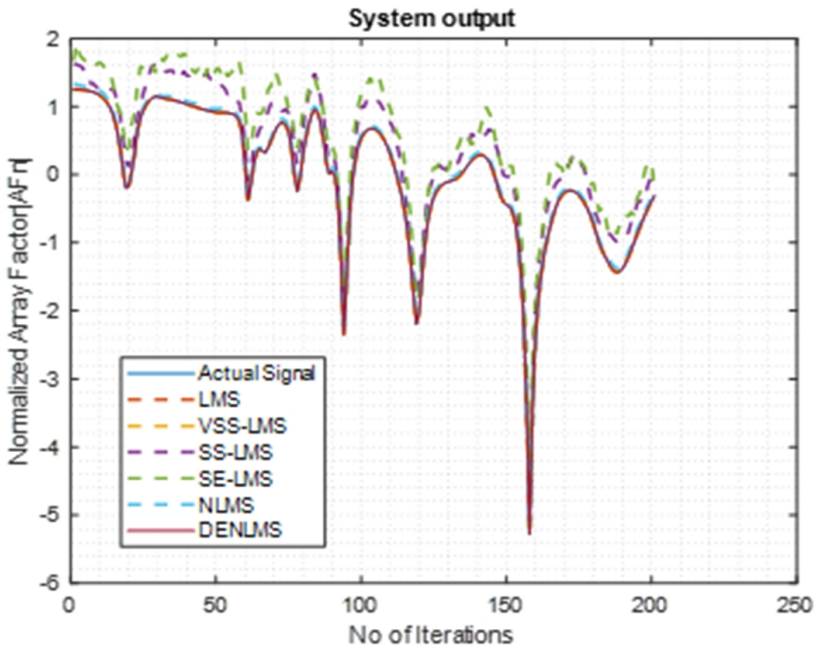


Figure 5.17: Normalized Array Factor

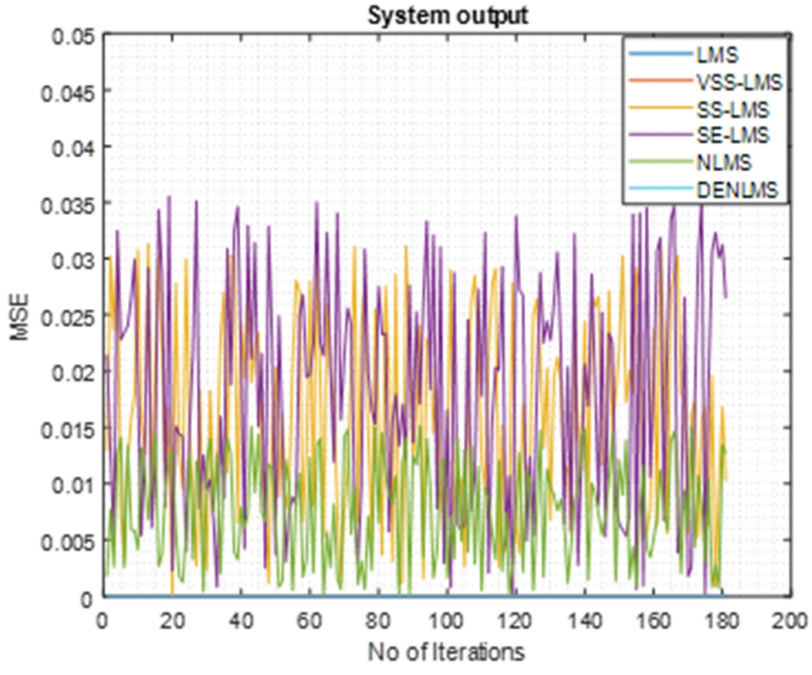


Figure 5.18: Mean Square Error

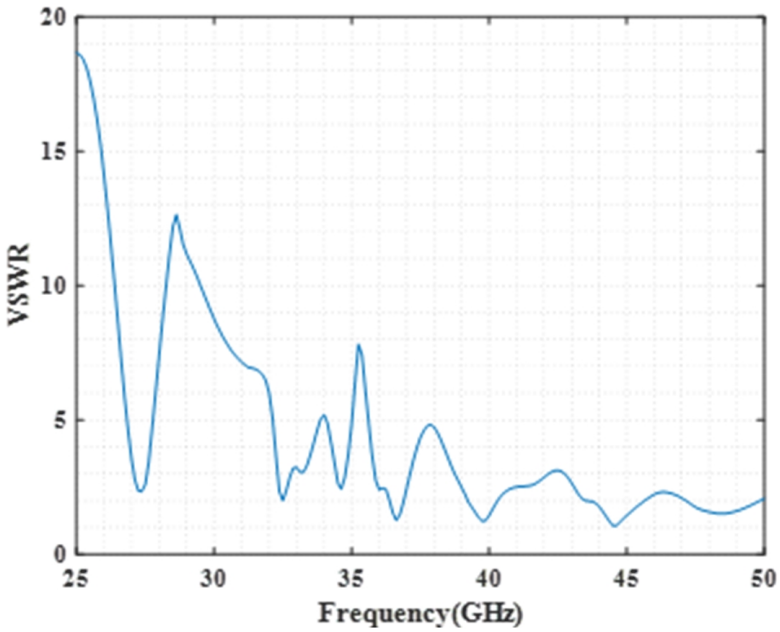


Figure 5.19: VSWR of the Proposed Antenna

Figure 5.18 depicts the mean square error of the suggested technique in comparison to current approaches. The inaccuracy of the available methods varies with the number of iterations. It ranged from 0.002 to 0.037, while the suggested approach has a 0minimum error tense. The suggested antenna's VSWR is depicted in Figure 5.19. It demonstrates that the antenna's VSWR is 18 for the 27 GHz frequency. The antenna has a VSWR of 7 at 35 GHz and 1 at 44.6 GHz. The comparison analysis demonstrates that the suggested technique outperforms the existing methods.

5.3.6 Discussion

The proposed DENLMS approach was evaluated in MATLAB for six components with generated complex weights, and the varying frequencies are utilized for HFSS array excitation. The simulated results for CST beam steering is perform to be roughly equal to the directions predicted in MATLAB. The user was expected to be at +0 degrees and the interferer at 30 degrees to mimic the DENLMS technique

in MATLAB. The null is formed at 44.62 GHz in the location of the interferer (15 degrees). The weights are then calculated by allowing for the user at this two degrees. In addition, the comparisons with LMS, NLMS, SELMS, SSLMS and VSSLMS show that the offered system outperforms these current approaches. The sophisticated weights may be calculated and applied to array elements using HFSS to produce effective beam steering using the DENLMS approach in MATLAB. In these MATLAB simulations, the user (+45 and 45) and interferer (+20 and 20) are both examined. Using HFSS, which is extremely close to MATLAB results, maxima were obtained at 45 and +45, where nulls are achieved at 30 and +30.

5.4 Summary

The six-element adaptive antenna array resonating at 44.62 GHz is proposed in this work applications for 5G microstrip patch smart antenna. The suggested antenna array has a high gain in the direction of the interferer and a low gain in the direction of the user-selected site. The HFSS experimental outcomes at various frequencies are investigated for Return Loss and Directive Gain. When the frequencies are adjusted, the directive gain likewise changes. The optimal beam steering can also be produced using DENLMS approach in MATLAB by generating complex weights and applying them to array components using HFSS. The MATLAB evaluation compares two angles for user (+45and 45) and the interferer (20 and +20). The maxima is discovered at 45 and +45, however, nulls are acquired at 30 and +30, which is pretty equivalent to the MATLAB results. The evaluation of the suggested approach is compared to the VSSLMS, LMS, SELMS, NLMS, and SSLMS, indicating that the proposed system outperforms these current algorithms. The superiority of the suggested research effort was demonstrated through a performance comparison with several antenna models.

Chapter 6

Design and Fabrication of Elliptical Printed Monopole Antenna with DGS

6.1 Overview

In the modern world, telecommunications can be used to communicate with people of this generation. One of the core telecommunication models is radio communication, which uses radio frequency as a medium of communication. The hardware architecture and functional capabilities of this form of communication underwent significant change. Mobile and wireless communication technologies are significant in numerous industries, including transportation, business, and education. High speed data ($>$ 10 Gbps) and large bandwidth for wireless communication have become increasingly in demand over time. The fifth generation, or 5G, wireless network is required to fulfil this. Several frequency bands for the fifth generation network are currently in the trial, testing, and deployment stages in various nations. The antenna system is the most crucial component in any communication. It is difficult to design the antenna for this frequency range since it needs to be minimum enough to be combined into the network with other equipment. Due to its small size, low profile, wide bandwidth, and simplicity of production, the

proposed antenna is best suited for 5G wireless communication. For 5G uses in the lower band, antennas have been used [96], [97]. Moreover, an elliptical patch antenna [98] with a frequency of 71.25 GHz, a bandwidth of 8.88 GHz, a gain of 13.1 dBi, and a directivity of 12.5 dBi was developed for THz applications. This paper proposes a unique elliptical printed monopole antenna with DGS for 5G applications. With a VSWR of less than 2 over the whole spectrum, the antenna operates between 2 and 3.7 GHz. The suggested antenna has two resonances at 2.4 GHz and 3.225 GHz, with return losses of -28.65 dB and -27.02 dB, respectively. The suggested antenna achieves a 1.7 GHz overall bandwidth. At 2.4 GHz, the max gain is 3.89 dB, and at 3.225 GHz, it is 4 dB. The antenna construction is made of FR4-epoxymaterial with , a thickness of 1.6 mm, and a loss tangent of 0.02. The U-shaped slots are present in this monopole antenna to achieve the dual band features. Ansoft HFSS simulation software is used to simulate it, while VNA was used to manufacture and test the antenna experimentally. When the findings from simulation and measurement are compared, they accord well. Peak gains, radiation efficiencies, and return losses for 2.4 GHz and 3.2 GHz, respectively, are 4.69 dB, 9%, and -28.65 dB.

6.2 Mathematical Modelling of Elliptical Antenna

It has been found that an elliptical-shaped patch antenna in printed circuit board may be able to emit circularly polarised waves; it only needs one feed, and its geometrical structure is simple enough to withstand detailed theoretical study. In comparison to circular and rectangular-shaped patch antennas, elliptical antennas achieve a reduced impedance bandwidth. In this work, elliptical patch antennas are taken into consideration because of their good gain and radiation characteristics. Thus, the elliptical patch is taken into consideration for the suggested work. Antenna with an elliptical patch improve the impedance bandwidth by etching an elliptical ring slot and embedding an elliptical split ring resonator. The suggested antenna geometry is presented in this section. The primary goal of the effort is to create a small dual band antenna for 5G sub-6 GHz applications. The

antenna is constructed using a FR-4 substrate and a 50 line feed. The design includes a U-shaped hole for simultaneously receiving dual band frequencies. The antenna produced by slotted variants is more suited to meeting bandwidth requirements. The first band's range is 2.4 GHz, and the first band's range is 3.2 GHz, respectively. The range of applications for 5G sub-6 GHz was covered by these two frequencies. Moreover, this design offers improved return loss, VSWR, and radiation pattern.

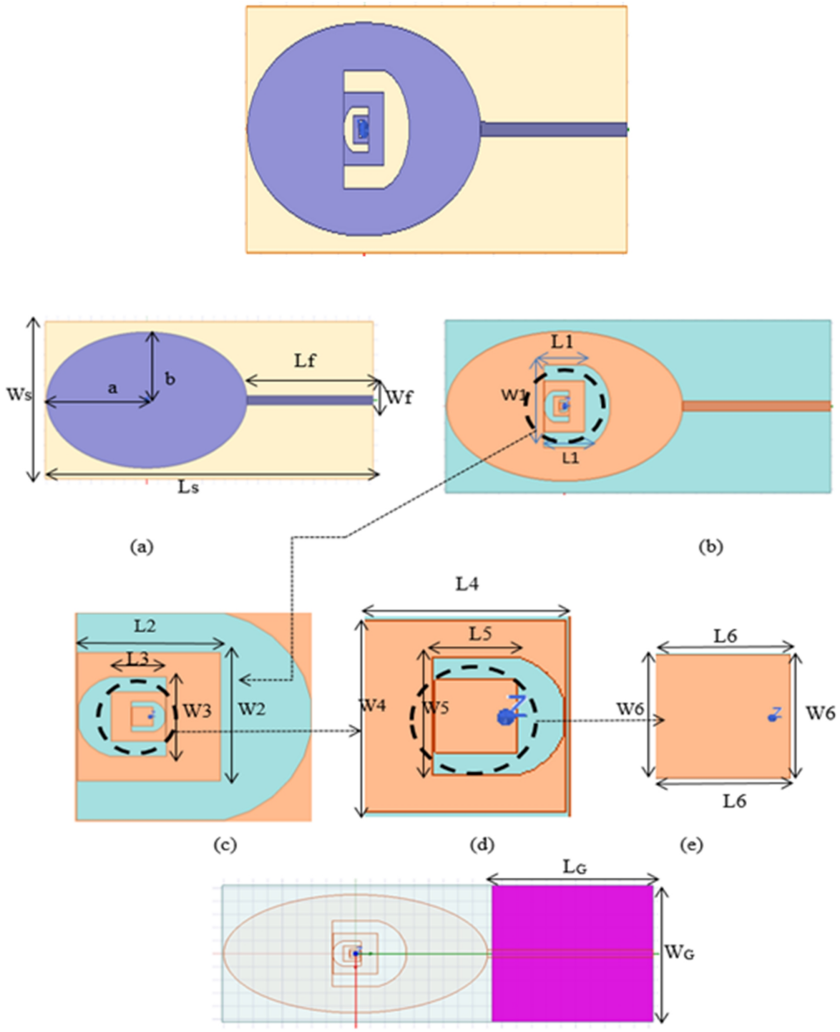


Figure 6.1: Geometry of the Antenna (a) Proposed Design, (b) Dimension of the Antenna (c) Dimension of the Slot, (d) DGS and (e)-(f) Closer View of the Design

Figure 6.1 depicts the elliptical patch antenna's geometry, with semi-major axis ' a ' and semi-minor axis ' b '. Let ' H ' represent the substrate's thickness and ' ε_r ' represent the dielectric substrate's permittivity. The substrate utilized in this instance is FR-4, with a loss tangent of 0.02 and $\varepsilon_r = 4.4$, $H = 1.6$ mm, and. There are two possible designs for the feed that powers the antenna. The minor and major axes of the elliptical patch can be configured so that the coaxial feed is situated along a 45-degree line between them [99]. Using 50Ω line connected to the patch is another method of feeding the antenna. 50Ω line feed has been employed in this study. Equation given below can be used to determine the lower band edge frequency [100] - [102].

$$F_l = \frac{c}{\lambda} = \frac{7.2}{(\ell + R + p) * \text{ K}} GHz \tag{6.1}$$

Where, F_l is the lower band edge frequency, λ is the wavelength, and c is the speed of light, which is 3×10^8 m/s. The common equations provided for the cylindrical monopole have been utilized to calculate F_1. ℓ Stands for the monopole antenna's length in cm (the same as the equivalent cylindrical monopole antenna), and R for the equivalent cylindrical monopole antenna's effective radius, which is obtained by equating the planar monopole antenna and cylindrical surface areas [9] and p is the length of the 50 ohms feed line.

The factor $\text{K} = \sqrt[4]{\varepsilon_{Eff}}$ and $\ell = 2b, R = \frac{a}{4}$ are taken into account in this design for the elliptical printed antenna.

$$W_s = \frac{c_0}{2F_r}\sqrt{\frac{2}{\varepsilon_r + 1}} \tag{6.2}$$

Where F_r is the resonating frequency, and c_0 is a speed of light.

Figure 6.1 indicates the construction of the antenna which includes the suggested design, dimension of the antenna and dimension of the slot. The antenna is having a DGS ground plane, in order to enhance the bandwidth. In Figure 6.1 (b), the dimension of length L_s and width W_s of the elliptical antenna is 21 mm $\times$ 26 mm, a is the semi-major axis and b is the semi-minor axis. Then, the length L_f and width W_f of the feedline is 14.6 mm $\times$ 3.1 mm. In Figure 6.1 (c),

the dimension of the slot is given that is L_1 is 5 mm and L_2 is 5.5 mm. Table 6.1 presents the dimensions of the antenna.

Table 6.1: Dimensions of the Antenna

Parameters	**Values (mm)**	**Parameters**	**Values (mm)**
L_s	21	L_1	5.1
W_s	26	L_2	5.2
L_f	14.6	L_3	1.3
W_f	3.1	L_4	1.8
L_1	5	L_5	0.5
L_2	5.5	L_6	0.5
L_3	1.3	L_G	21
L_4	1.5	W_G	26
L_5	1.5		
L_6	0.5		

The parameters W_s, L_s, W_f, and L_f of the suggested antenna design have values of 26, 21, 3.1, and 14.6, respectively. W_f is the width of the monopole line feed, and L_f is the length of the monopole line feed, where W_s is the original width of the elliptical antenna and L_s is the original length of the elliptical antenna. The values of L_G and W_G are 21 and 26, respectively, where L_G and W_G represent the length and width of the ground plane. According to Figure 6.1 (c-e), the closer length of the antenna is determined by the parameters L_2, L_3, L_4, L_5 and L_6, which have the values 5.2, 1.3, 1.8, 0.5, and 0.5, respectively. The parameters W_s, L_s, W_f, and L_f of the suggested antenna design have values of 26, 21, 3.1, and 14.6, respectively. W_f is the width of the monopole line feed, and L_f is the length of the monopole line feed, where W_s is the original width of the elliptical antenna and L_s is the original length of the elliptical antenna. The values of L_G and W_G are 21 and 26, respectively, where L_G and W_G represent the length and width of the ground plane. According to Figure 6.1 (c-e), the closer length of the antenna is determined by the parameters L_2, L_3, L_4, L_5 and L_6, which have the values 5.2,

1.3, 1.8, 0.5, and 0.5, respectively.

6.3 Results Analysis

The HFSS simulates a printed elliptical monopole antenna (high frequency structure simulator). Following that are the performance indicators such as VSWR, return loss S11, 3D-gain, directivity, 2D-radiation pattern, SCD, and radiation efficiency. Finally, a comparative examination of several current antenna designs is offered. Return loss, Radiation Patterns & Gain, Surface Current Distributions and VSWR are evaluated in this section.

6.3.1 Return Loss

Return loss is a measurement of the relative strength of the signal reflected by an optical fibre discontinuity. The impedance of the line and the load or termination connected to the line may not match, which might result in this discontinuity. The return loss value of an improved antenna design should be less than -20 dB. Figure 6.2 shows the comparison of the simulated and measured results of the return loss. It has been noted that these two results fairly agree with one another. The antenna has two resonant frequencies, as can be seen from Figure 6.2.

The first resonant frequency in the simulated results is at 2.4 GHz, while the constructed results have return loss values of -28.65 dB and -27.55 dB, respectively. The second resonant frequency in the simulated results is at 3.2 GHz. Due to the U-shaped slot and DGS, a better return loss is attained. Moreover, at 2.4 GHz and 3.2 GHz, the impedance bandwidths are respectively 1.2 GHz and 1.8 GHz.

6.3.2 VSWR

The VSWR is a metric that gauges how well the feed line and antenna are matched. The mismatch between the antenna and the feed line is measured by this parameter. The VSWR ought to be as low as feasible for the best match. Thus, the VSWR ratio is 2:1.

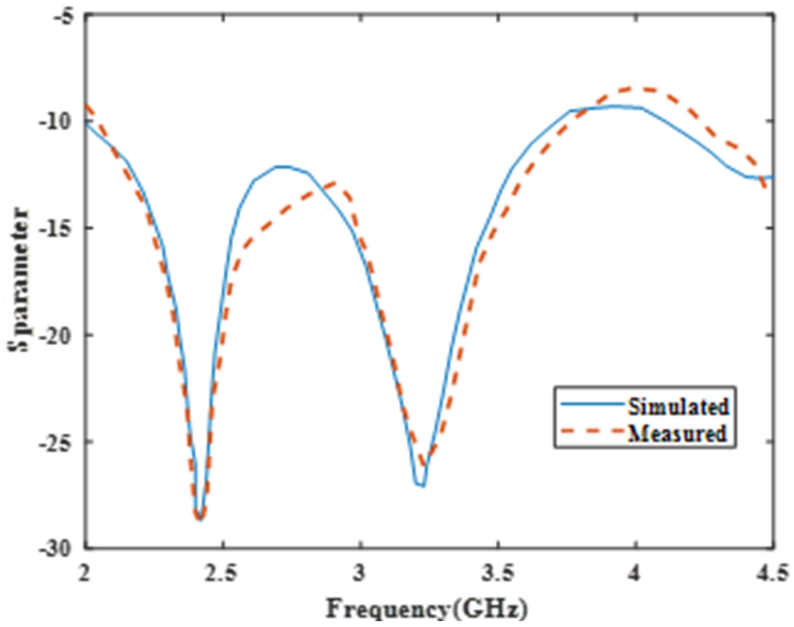


Figure 6.2: Return Loss Analysis

The antenna's VSWR, which is displayed in Figure 6.3, is less than 2 across its full operating range. A satisfactory match between the feed network and the antenna is shown by the VSWR values of 1.06 for the resonant frequency at 2.4 GHz and 1.13 for the frequency of 3.22 GHz.

6.3.3 2D Radiation Pattern

This section explains the theoretical and verified pattern of the suggested design's far field radiation behaviour.

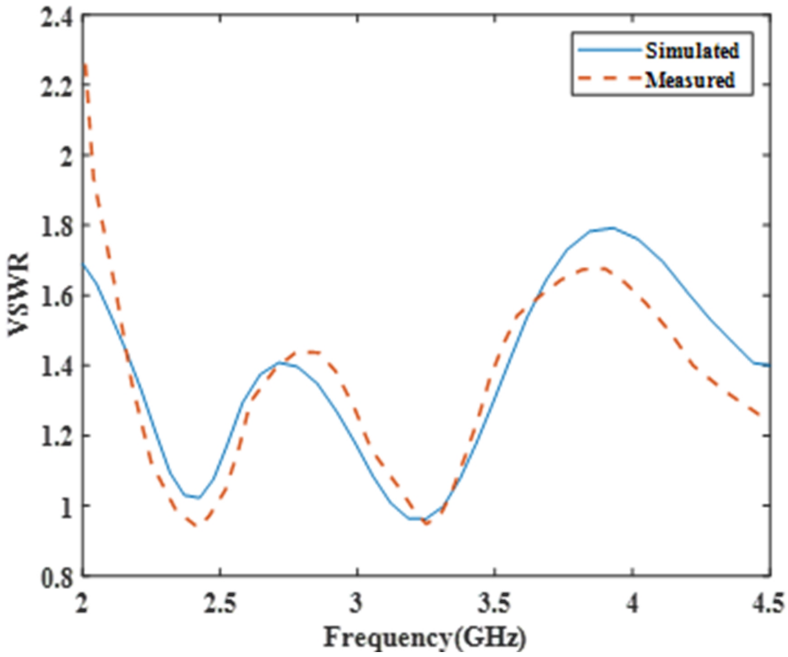


Figure 6.3: VSWR Analysis

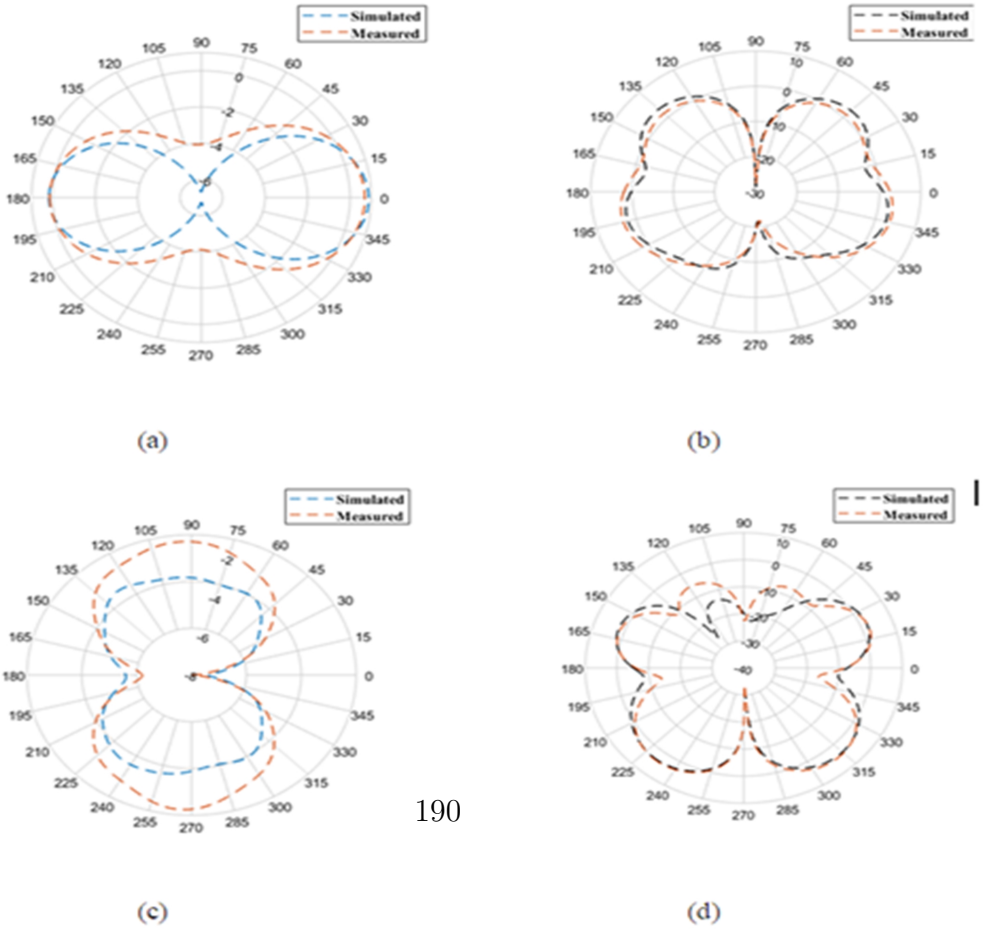
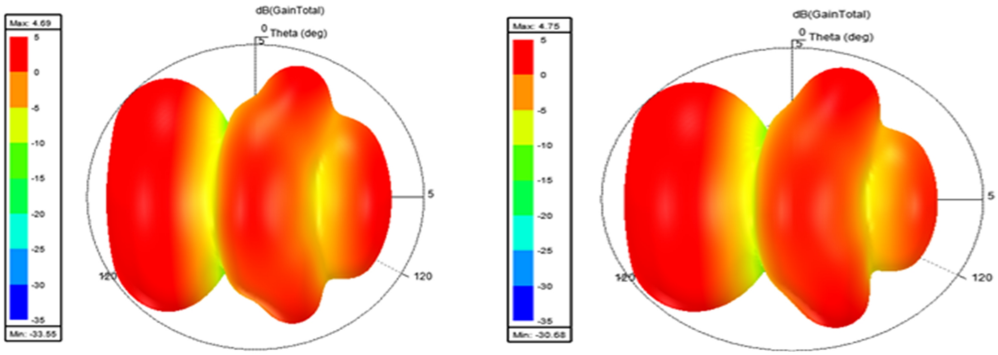


Figure 6.4: 2D Radiation Pattern Analysis (a, b) E-Plane and H-Plane at 2.4 GHz, (c, d) E-Plane and H-Plane at 3.2 GHz

From 0° to 360° at the two frequencies, this behaviour is examined. Figure 6.4 illustrates the radiation patterns for the 2.4 GHz and 3.225 GHz bands in the E plane (phi = 0°) and the H plane (phi = 90°). The broadside direction experiences the highest radiation. In contrast to the omnidirectional E-plane pattern, which receives signals from all directions, the H plane pattern is similar to a dipole antenna in the shape of a figure eight or dumbbell. These behaviours demonstrate the suggested design's effectiveness as a monopole-radiator. The results of the simulation and measurement are nearly identical, and the only small variation is brought about by alignment problems and electromagnetic interferences.

6.3.4 Gain

An essential characteristic of an antenna is its 3D-gain pattern, which represents the ratio of the power output in a particular direction to the intensity of radiation in that direction. The gain pattern encapsulates the effectiveness and potential in directed. As shown in Figure 6.5, the antenna's gain is 4.69 dB at 2.4 GHz and 4.75 dB at 3.2 GHz. These results show that this design satisfies the criteria for 5G applications with a sub-6 GHz frequency. The elliptical antenna's DGS and U-shaped slot are responsible for this improved gain performance.

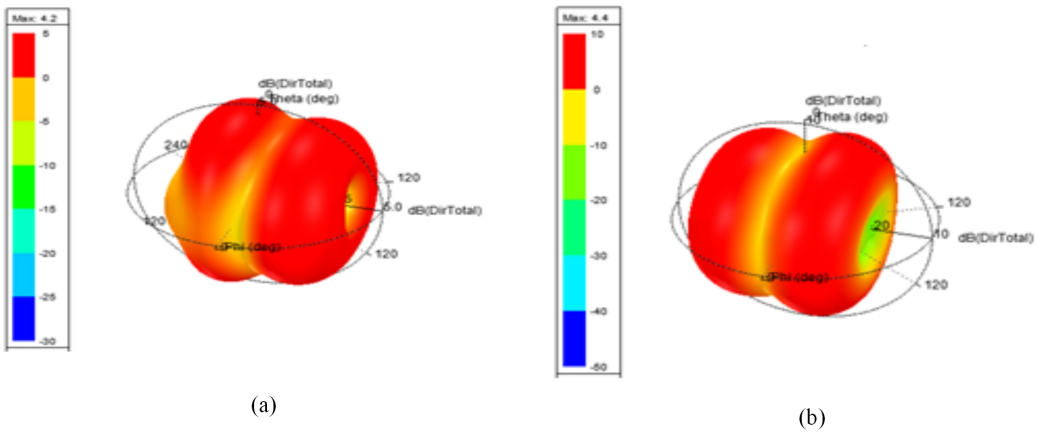


(a) (b)

Figure 6.5: Gain Analysis (a) at 2.4 GHz and (b) at 3.2 GHz

6.3.5 Directivity

The ratio of the antenna's radiation intensity in a given field to the field's average radiation intensity is referred as directivity of an antenna. Also, this performance shows how the suggested antenna may emit energy. As shown in Figure 6.6, the antenna attains a directivity of 4.2 dB at 2.4 GHz and 4.4 dB at 3.2 GHz.



(a) (b)

Figure 6.6: Directivity Analysis (a) at 2.4 GHz and (b) at 3.2 GHz

6.3.6 Radiation Efficiency

This measurement shows how effectively the antennas radiate and receive the wave. It is the ratio between the input power P_s and the radiated power P_{rad} . It is written as:

$$\text{Efficiency} = \frac{P_{\text{rad}}}{P_s}\% \tag{6.3}$$

The antenna's radiation efficiency is shown in Figure 6.7, and the results were 97% at 2.4GHz and 98% at 3.2GHz. The efficiency for both frequencies is about the same for both the simulated and measured results.

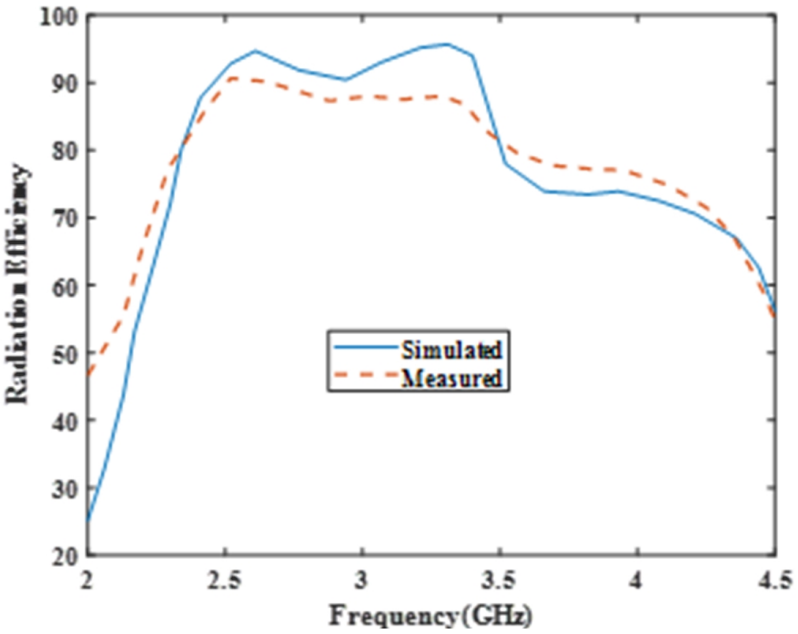
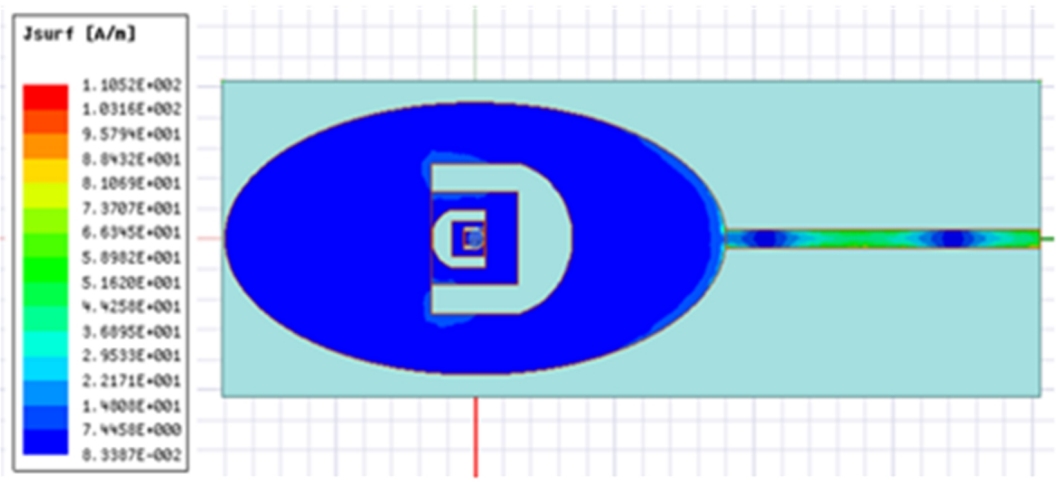


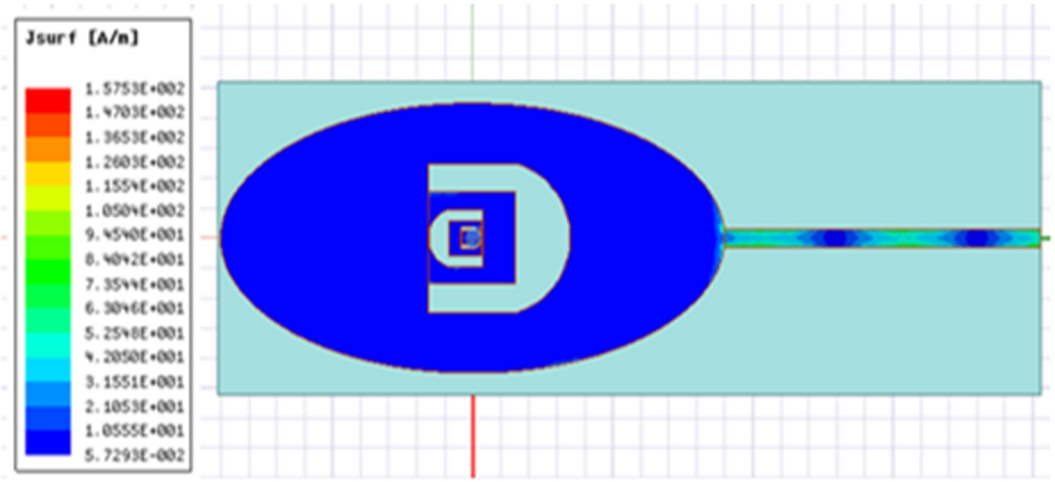
Figure 6.7: Radiation Efficiency Analysis

6.3.7 SCD (Surface Current Distribution)

The polarisation characteristics of the radiation in the far-field are a result of an antenna's surface current. If modifications to the antenna structure, material characteristics, and feed method can change the surface current's direction, polarisation reconfiguration may be achieved. Polarization reconfigurations can take many different forms. The choice may be between two different linear polarisations, between circular polarisations with the right and left hands, or between linear and circular polarisations. Surface current distributions on the patch demonstrate how the switch changes the patch's functional area. The distribution of a current on an antenna is shown in these figures, which is better for an antenna's efficient radiation. The SCD of the antenna is shown in Figure 6.8 at two different frequencies, 2.4 GHz and 3.2 GHz. At both frequencies, it is seen that the SCD is mostly focused on the elliptical antenna. The operational mode of the designed antenna is displayed.



(a)



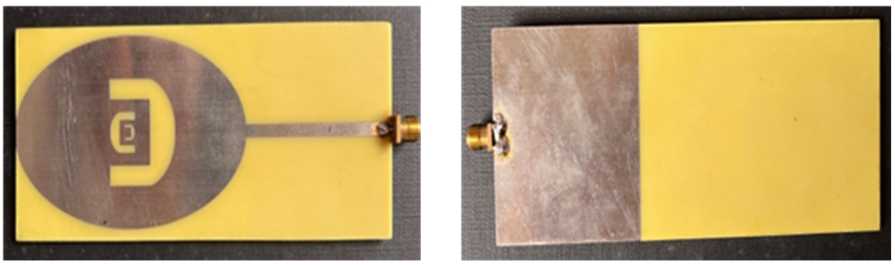
(b)

Figure 6.8: SCD Analysis (a) at 2.4 GHz and (b) at 3.2 GHz

6.4 Fabricated Analysis

The manufactured design of the suggested innovative elliptical slotted monopole antenna is shown in this section. The model's outcomes and validity are understood through the fabrication of the design. The top and bottom perspectives of the innovative elliptical slotted antenna are depicted in Figure 6.9, which details

its fabrication. The Vector Network Analyzer is used for all measurements (VNA).



(a) (b)

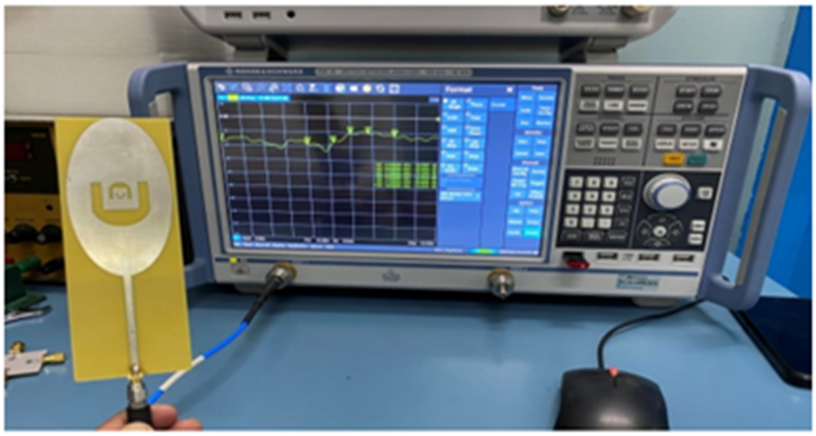
Figure 6.9: Fabricated Design (a) Top View (b) Bottom View

Figure 6.10 shows the manufactured architecture's experimental set. The radiation patterns and return loss are measured in an anechoic chamber. In this instance, the transmitting and reference antennas are both the AUT (antenna under test). The horn antenna is used to operate the receptor.

Table 6.2 compares the performance characteristics, such as antenna size, gain, efficiency, and return loss, of the various monopole antenna-based strategies. The suggested design is contrasted with the approaches [103], [104], [105], and [106]. The table 6.2 shows that every measure of the suggested design exceeded the current methods.

The method shown in [103], which uses a monopole antenna, has been developed for 5G communication applications. It offers 2.7 dB gain, -24 dB of return loss, 96 % radiation efficiency and this method uses a dimensions of 23.88 x 23.88. The method provided in [104] yields -29 dB return loss at a radiation efficiency range of 96 %, 3.38 dB gain and 20 x 35 (mm) size. The method [105], offers a gain of 2.45 dB, return loss of -29 dB and size of 38x56.4 (mm). The method appropriate for 5G applications [106], achieves 4.3 dB gain, -32.3 dB return loss, radiation efficiency of 91.08 %, and 25x25 (mm) size.

Among the existing methods, the proposed approach provides a 4.65 dB and 4.75 dB gain, a return loss of -28.65 dB and -27.55 dB, radiation efficiency of 97 % and 98 % the antenna dimensions for this approach are 21x 36 (mm).



(a)



(b)

Figure 6.10: (a) Experimental Set-up (b) Anechoic Chamber

6.5 Summary

Radio communication, which makes use of radio frequency as a communication channel, is one of the fundamental telecommunication models. This mode of communication witnessed major changes to its functional capabilities and hardware architecture. Technologies for mobile and wireless communication are important in many fields, including business, education, and transportation. For the sub

Table 6.2: Comparison of Various Approaches based on Monopole Antenna

Authors and Citation	Size (mm)	Gain (dB)	Return Loss (dB)	Radiation Efficiency (%)
Kapoor et al. [103]	23.88 x 23.88	2.7	-24	96
Benkhadda et al. [104]	20 x 35	3.38	-29	96
Wang et al. [105]	38x56.4	2.45	-29	-
Mpele et al. [106]	25x25	4.3	-32.3	91.08
Proposed	21x 36	4.65, 4.75	-28.65, -27.55	97, 98

6-5G application, a small elliptical monopole antenna with DGS is given. Here, the coupling was reduced by using the DGS, and the bandwidth and gain were increased by using the U-shaped slot. The pattern is small, measuring 21 x 36 mm. The proposed design resonated at two frequencies, such as 2.4 GHz and 3.2 GHz, and was examined on the FR-4 substrate. On the basis of various antenna measures, the outcomes of fabricating and simulating the antenna were examined. The experimental study demonstrated that the developed antenna has excellent gain and efficiency potential for both frequencies, as well as potential for radiation characteristics. Eventually, it was established that this design was more flexible for applications requiring sub-6-5G bandwidth.

Chapter 7

Conclusion and Future Scope

7.1 Conclusion

7.1.1 General Conclusion

The first objective of this research are designing of rectangular microstrip patch antenna based on phased array and MIMO strategy for various mm frequencies. In this work, constructed and studied a revolutionary tiny microstrip MIMO antenna. The four ports MIMO antenna's gain of 5.44 dBi and directivity of 9.75 dBi make it ideal for millimetre wave applications. Moreover, it has a broad 2.3 GHz bandwidth in 60 GHz band, which is suitable for IEEE 802.11ad wireless networking standard. The four ports MIMO antenna is determined to operate well at the resonant frequency after analysis of the MIMO performance metrics. Using the far field radiation pattern and the s parameter method of computation, the ECC is around 0.06 and 0.9, respectively. Four port MIMO antenna diversity gain is larger than 9.8 dB with MEG less than 1 dB. Moreover, a small-sized high gain 16-port MIMO antenna at 60 GHz on a FR-4 substrate is built and simulated. As the ports and antenna elements are increased, the gain and directivity are evaluated. The advantages of MIMO technology are fully investigated. With a measured return loss of all 16 ports |S11| of less than -10 dB throughout the frequency range of 59.15-60.65 GHz and a bandwidth of 1.5 GHz, the planned MIMO

antenna performs well. At 60 GHz, a peak gain of 19.89 dBi and a directivity of 21.59 dBi are achieved. Both the antenna efficiency and the simulated radiation efficiency are 67.57% and 68.05%, respectively. At 60 GHz, the -3 dB beam width is approximately 5 and 11 degrees in the E- and H-planes, respectively. The developed 16 ports MIMO antenna is ideally suited for usage in a 60-GHz wireless system that adheres to the IEEE 802.11ad wireless networking standard.

The second objective concerns the construction of an unique SBA with a novel butler matrix for switched beam applications at mm-wave frequencies between 28 GHz and 39 GHz. By building a SBA, a BM, and a DOA estimate, the three key contributions of the suggested technique are adequately satisfied. The beamforming network is the main unique element of the research. A microstrip hexagonal patch antenna with a Z-slot is given the beam forming property. The 4x4 butler matrix beam forming network is constructed in two distinct methods using phase shifters of varying degrees. For the DOA estimate of signals impinging on an antenna array system, a unique approach known as CRLB has been devised. The outcomes showed that in many applications, both the suggested switching beam antenna and DOA estimation technique are more effective. The suggested switching beam antenna offers the optimum steering, high gain, and reduced size, power, and weight. Direction-finding, monitoring, tactical communication, passive radar, and secure communication are all possible applications for the suggested methodology.

In the third objective, a six-element adaptive antenna array with a 44.62 GHz resonance frequency is proposed for use in 5G MSPA applications. The suggested antenna array really has a low gain in the interferer's direction and a high gain in the user-selected location. The results of the HFSS simulation are investigated for DG and RL at various frequencies. It has been established that shifting frequencies also affects the directive gain. The DENLMS technique in MATLAB may be used to compute complex weights, which are then applied to array components utilizing HFSS to produce optimum beam steering. When the suggested system's performance is compared to that of the LMS, VSSLMS, SSLMS, SELMS, and NLMS, it is clear that the system is more effective than those of these current

methods.

The fourth objective presents a small, DGS-equipped elliptical monopole antenna for use in sub-6-5G networks. Here, the coupling was reduced by using the DGS, and the bandwidth and gain were increased by using the U-shaped slot. The pattern is small, measuring 21 x 36 mm. The suggested design resonated at two frequencies, such as 2.4 GHz and 3.2 GHz, and was examined on the FR-4 substrate. On the basis of different antenna measurements, the outcomes of fabricating and simulating the antenna were examined. The experimental study shown that the developed antenna has excellent gain and efficiency potential for both frequencies, as well as potential for radiation characteristics. Eventually, it was established that this architecture was more flexible for applications requiring sub-6-5G bandwidth.

7.1.2 Research Contribution

The major contribution of this thesis are mentioned below:

- Designed and simulated the various configurations of Phased array and MIMO of rectangular microstrip patch antenna at different millmeter wave frequencies.

- At millimeter wave frequencies, developed a switched beam antenna for switched beam applications using a Butler matrix. Also provided two novel 4x4 butler matrices with both 45° and 120° phase shifters. For DOA estimate, a Cramer-Rao lower bound (CRLB) matrix was developed, and it was put up against a multiple signal classification model (MUSIC).

- A beam-steering MPA array is developed for use at millimetre wave frequencies. The DENLMS beam steering procedure is developed to calculate weight estimation for beam steering by taking various angles for Interferer and targeted user into consideration.

- For the 5G applications, an elliptical printed monopole antenna has been developed, modelled, manufactured, and experimentally tested.

7.2 Future Scope

In the future, the antenna's total size can still be decreased through metaheuristic optimization. Moreover, a variety of meta-materials will be developed in order to reduce the coupling of the antenna. Other reconfiguration methods, such electrical and mechanical ones, may be applied in the future. PIN diodes, varactor diodes, MEMS switches, photo conductive switches, etc. may all be used to create antennas.

References

[1] G.F. Huseien, and K.W. Shah, "A review on 5G technology for smart energy management and smart buildings in Singapore", *Energy and AI*, 7, 100116, 2022.

[2] D.S. Bhatti, S. Saleem, A. Imran, Z. Iqbal, A. Alzahrani, H. Kim, and K. Kim, "A Survey on Wireless Wearable Body Area Networks: A Perspective of Technology and Economy", *Sensors*, 22(20), 7722, 2022.

[3] A.J. Al-Gburi, Z. Zakaria, H. Alsariera, M.F. Akbar, I.M. Ibrahim, K.S. Ahmad, S. Ahmad, and S.S. Al-Bawri, "Broadband Circular Polarised Printed Antennas for Indoor Wireless Communication Systems: A Comprehensive Review", *Micromachines*, 13(7), 1048, 2022.

[4] J. Van Mulders, D. Delabie, C. Lecluyse, C. Buyle, G. Callebaut, L. Van der Perre, and L. De Strycker, "Wireless Power Transfer: Systems, Circuits, Standards, and Use Cases", *Sensors*, 22(15), 5573, 2022.

[5] S. De, and A. A. Bazil Raj, "A survey on photonics technologies for radar applications", *Journal of Optics*, 1-30, 2022.

[6] M.H. Hossain, "Radio Communication Via Near Vertical Incidence Skywave System", 2021.

[7] T. Mazhar, M.A. Malik, I. Haq, I. Rozeela, I. Ullah, M.A. Khan, D. Adhikari, M.T. Ben Othman, and H. Hamam, "The Role of ML, AI and 5G Technology in Smart Energy and Smart Building Management", *Electronics*, 11(23), 3960, 2022.

[8] T. Sharma, A. Chehri, and P. Fortier, "Review of optical and wireless backhaul networks and emerging trends of next generation 5G and 6G technologies", *Transactions on Emerging Telecommunications Technologies*, 32(3), e4155, 2021.

[9] B.T. Jijo, S. R. Zeebaree, R.R. Zebari, M. A. Sadeeq, A.B. Sallow, S. Mohsin, and Z.S. Ageed, "A comprehensive survey of 5G mm-wave technology design challenges", *Asian Journal of Research in Computer Science*, 8(1), 1-20, 2021.

[10] F. Syed, S.K. Gupta, S.H. Alsamhi, M. Rashid, and X. Liu, "A survey on recent optimal techniques for securing unmanned aerial vehicles applications", *Transactions on Emerging Telecommunications Technologies*, 32(7), e4133, 2021.

[11] M. Sadiq, N. Sulaiman, M.M. Isa, and M.N. Hamidon, "A Review on Machine Learning in Smart Antenna: Methods and Techniques", 2022.

[12] B.A. Kleinau, D. L. de Melo, M. T. de Melo, D. C. P. Barbosa, A. J. B. Oliveira, C. P. N. Silva, and J. M. A. M. de Oliveira, "Application of the Base Transceiver Station with Smart Antennas in the Power Distribution Sector", *International Journal of Antennas and Propagation*, 2021.

[13] M.O. Omer, "Adaptive Beam-forming Approaches for Smart Antenna System", *PhD diss.,* 2022.

[14] T.M. Ghazal, "Positioning of UAV base stations using 5G and beyond networks for IOMT applications", *Arabian journal for science and engineering*, 1-12, 2021.

[15] A.L. Imoize, A.E. Ibhaze, A.A. Atayero, and K. V. N. Kavitha, "Standard propagation channel models for MIMO communication systems", *Wireless Communications and Mobile Computing*, 2021.

[16] D.H. Sadek, H.A. Shawkey, and A.A. Zekry, "Multiband triple L-arms patch antenna with diamond slot ground for 5G applications", *The Applied Computational Electromagnetics Society Journal (ACES)*, 302-307, 2021.

[17] M.U. Siddiqui, F. Qamar, F. Ahmed, Q.N. Nguyen, and R. Hassan, "Interference management in 5G and beyond network: Requirements, challenges and future directions", *IEEE Access*, 9 68932-68965, 2021.

[18] M. Matinmikko-Blue, S. Yrjölä, P. Ahokangas, and H. Hämmäinen, "Analysis of 5G spectrum awarding decisions: How do different countries consider emerging local 5G networks?", 2021.

[19] R. Dangi, P. Lalwani, G. Choudhary, I. You, and G. Pau, "Study and investigation on 5G technology: A systematic review", *Sensors*, 22(1), 26, 2022.

[20] A. Ziaeddini, A. Mohajer, D. Yousefi, A. Mirzaei, and S. Gonglee, "An Optimized Multi-Layer Resource Management in Mobile Edge Computing Networks: A Joint Computation Offloading and Caching Solution", *arXiv preprint arXiv: 2211.15487*, 2022.

[21] T. Patra, and S.K. Mitra, "Resource optimization of MIMO using neural network for 5G communication", *Alexandria Engineering Journal*, 61(12), 12581-12592, 2022.

[22] E.D. Priya, T. Poornima, and K.G. Anand, "6 Four Port MIMO Antenna with Swastika Slot for 5G Environment", *Planar Antennas*, 97-113, 2021.

[23] S. Albadran, "Evaluation of development level and technical contribution of recent technologies adopted to meet the challenges of 5G wireless cellular networks", *Symmetry*, 13(4), 635, 2021.

[24] M.H. Teimouri, C. Ghobadi, J. Nourinia, K. Kaboutari, M. Shokri, and B.S. Virdee, "Broadband printed dipole antenna with integrated balun and tuning element for DTV application", *AEU-International Journal of Electronics and Communications*, 148, 154161, 2022.

[25] P. Khande, K. B. Yogesh, M. M. Manu, G. N. Ravikiran, and D. Pradhan, "Comparative Analysis of Adaptive Beam Forming (Abf) Algorithms for Smart Antenna System (Sas)", 2021.

[26] P.K. Malik, S. Padmanaban, and J.B. Holm-Nielsen, "Microstrip Antenna Design for Wireless Applications", *CRC Press*, 2021.

[27] G. Christina, "A Review on Novel Microstrip Patch Antenna Designs and Feeding Techniques", *IRO Journal on Sustainable Wireless Systems*, 4(2), 110-120, 2022.

[28] A.N. Uwaechia, & N.M. Mahyuddin, "A comprehensive survey on millimeter wave communications for fifth-generation wireless networks: Feasibility and challenges", *IEEE Access*, 8, 62367-62414, 2020.

[29] M. Alsabah, M.A. Naser, B.M. Mahmmod, S.H. Abdulhussain, M.R. Eissa, A. Al-Baidhani, & F. Hashim, "6G wireless communications networks: A comprehensive survey", *IEEE Access*, 9, 148191-148243, 2021.

[30] D. Gharode, A. Nella, & M. Rajagopal, "State-of-art design aspects of wearable, mobile, and flexible antennas for modern communication wireless systems", *International Journal of Communication Systems*, 34(15), e4934, 2021.

[31] Z.H. Qaisar, M. Irfan, T. Ali, A. Ahmad, G. Ali, A. Glowacz, & S. Hussain, "Effective beamforming technique amid optimal value for wireless communication", *Electronics*, 9(11), 1869, 2020.

[32] O.W. Ata, M. Salamin, & K. Abusabha, "Double U-slot rectangular patch antenna for multiband applications", *Computers & Electrical Engineering*, 84, 106608, 2020.

[33] G. Yang, & S. Zhang, "Dual-Band Shared-Aperture Multiple Antenna System with Beam Steering for 5G Applications", *IEEE Transactions on Circuits and Systems II: Express Briefs*, 69(12), 4804-4808, 2022.

[34] R. Ullah, S. Ullah, R. Ullah, I.U. Din, B. Kamal, M.N.A. Khan, & L. Matekovits, "Wideband and High Gain Array Antenna for 5G Smart Phone Applications Using Frequency Selective Surface", *IEEE Access*, 10, 86117-86126, 2022.

[35] G. Yang, & S. Zhang, "Dual polarized wide-angle scanning phased array antenna for 5G communication system", *IEEE Transactions on Antennas and Propagation*, 2022.

[36] J.C.S. Chieh, E. Yeo, R. Farkouh, A. Castro, M. Kerber, R.B. Olsen, & S.K. Sharma, "Development of flat panel active phased array antennas using 5G silicon RFICs at Ku-and Ka-bands," *IEEE Access*, 8, 192669-192681, 2020.

[37] H. Zhang, S. Bosma, A. Neto, & N. Llombart, "A dual-polarized 27 dBi scanning lens phased array antenna for 5G point-to-point communications," *IEEE Transactions on Antennas and Propagation*, 69(9), 5640-5652, 2021.

[38] G. Yang, Y. Zhang, & S. Zhang, "Wide-band and wide-angle scanning phased array antenna for mobile communication system," *IEEE Open Journal of Antennas and Propagation*, 2, 203-212, 2021.

[39] P. Wei, & W. Geyi, "Design of MIMO/Smart Antenna Arrays Using Different Array Modules for Handheld Device", *Progress In Electromagnetics Research C*, 115, 111-127, 2021.

[40] G.S. Baghel, M.V. Swati, & S. Ghosh, "MIMO Antennas: A 5G Communication Perspective," *In 5G and Beyond Wireless Systems: PHY Layer Perspective*. 1-19, 2020. Singapore: Springer Singapore.

[41] N. Hussain, M.J. Jeong, A. Abbas, & N. Kim, "Metasurface-based single-layer wideband circularly polarized MIMO antenna for 5G millimeter-wave systems," *IEEE Access*, 8, 130293-130304, 2020.

[42] A. Khan, S. Geng, X. Zhao, Z. Shah, M.U. Jan, & M.A. Abdelbaky, "Design of MIMO antenna with an enhanced isolation technique," *Electronics*, 9(8), 1217, 2020.

[43] M. Kirik, & J.M. Hamamreh, "Interference Signal Superposition-aided MIMO with Antenna Number Modulation and Adaptive Antenna Selection for Achieving Perfect Secrecy," *RS Open J. Innov. Commun. Technol*, 2, 1-11, 2021.

[44] J. Suryana, & A. Munir, "Design and Characterization of 4× 4 Butler Matrix for Switched-Beam Antenna Array", *In 2021 IEEE Asia Pacific Conference on Wireless and Mobile (APWiMob)*, 238-241, 2021. IEEE.

[45] J.M. Wen, C.K. Wang, W. Hong, Y.M. Pan, & S.Y. Zheng, "A wideband switched-beam antenna array fed by compact single-layer Butler matrix", *IEEE Transactions on Antennas and Propagation*, 69(8), 5130-5135, 2021.

[46] B. Roy, A. Karmakar, & U. Chakraborty, "Planar Switched Beam Network using Butlar Matrix on a single layer substrate for modern wireless communications", *Radio Science*, 57(3), e2021RS007348, 2022.

[47] K. Bharath, N. Srujana Vahini, R.K. Dasari, M.P. Abegaonkar, & V.M. Pandharipande, "Millimeter Wave Switched Beam Rectangular Loop Dipole Antenna Array Using a 4× 4 Butler Matrix," *Progress In Electromagnetics Research C*, 117, 251-260, 2021.

[48] S. Almorabeti, H. Terchoune, M. Rifi, H. Tizyi, & S. Smihily, "Smart antenna design alimented by a 4x4 butler matrix," *TELKOMNIKA (Telecommunication Computing Electronics and Control)*, 19(4), 1342-1348, 2021.

[49] M.W. Almeshehe, N.A. Murad, M.M.A. Rahim, O. Ayop, F. Zubir, M.Z. Aziz, & H.A. Majid, "Low loss waveguide-based Butler matrix with iris coupling control method for millimeterwave applications", *Waves in Random and Complex Media*, 1-21, 2021.

[50] M. Anas, H. Shahid, A. Rauf, & A. Shahid, "Design of ultra-wide tetra band phased array inverted T-shaped patch antennas using DGS with beam-steering capabilities for 5G applications," *International Journal of Microwave and Wireless Technologies*, 12(5), 419-430, 2020.

[51] H. Ozpinar, S. Aksimsek, & N.T. Tokan, "A novel compact, broadband, high gain millimeter-wave antenna for 5G beam steering applications," *IEEE Transactions on Vehicular Technology*, 69(3), 2389-2397, 2020.

[52] P. Das, K. Mandal, & A. Lalbakhsh, "Beam-steering of microstrip antenna using single-layer FSS based phase-shifting surface," *International Journal of RF and Microwave Computer-Aided Engineering*, 32(3), e23033, 2022.

[53] M. Rzymowski, K. Nyka, & L. Kulas, "Direction of Arrival Estimation Based on Received Signal Strength Using Two-Row Electronically Steerable Parasitic Array Radiator Antenna," *Sensors*, 22(5), 2034, 2022.

[54] M. Alibakhshikenari, B.S. Virdee, P. Shukla, C.H. See, R.A. Abd-Alhameed, F. Falcone, & E. Limiti, "Improved adaptive impedance matching for RF front-end systems of wireless transceivers", *Scientific Reports*, 10(1), 1-11, 2020.

[55] V. Loshakov, M. Moskalets, D. Ageyev, A. Drif, & K. Sielivanov, "Adaptive space-time and polarisation-time signal processing in mobile communication systems of next generations", *In Data-Centric Business and Applications: ICT Systems-Theory, Radio-Electronics, Information Technologies and Cybersecurity*, 5, 469-488, 2020. Cham: Springer International Publishing.

[56] O. Benkhadda, M. Saih, K. Chaji, S. Ahmad, & A. Reha, "A Compact Dual-Band CPW-Fed Slot Monopole Antenna for WiFi, WLAN and WiMAX Applications", *Arabian Journal for Science and Engineering*, 1-10, 2022.

[57] H.T. Sediq, J. Nourinia, C. Ghobadi, & B. Mohammadi, "A novel eye-shaped monopole antenna for wideband and 5G applications", *IETE Journal of Research*, 1-11, 2020.

[58] M.S. Islam, S.K. Azam, A.Z. Hossain, M.I. Ibrahimy, & S.M.A. Motakabber, "A low-profile flexible planar monopole antenna for biomedical applications," *Engineering Science and Technology, an International Journal*, 35, 101112, 2022.

[59] B. Sugumaran, R. Balasubramanian, & S.K. Palaniswamy, "Reduced specific absorption rate compact flexible monopole antenna system for smart wearable wireless communications", *Engineering Science and Technology, an International Journal*, 24(3), 682-693, 2021.

[60] A. Rawat, R. Kaushik, & A. Tiwari, "An overview of MIMO OFDM system for wireless communication", *International Journal of Technical Research & Science*, 6(X), 1-4, 2021.

[61] H. Attar, H. Issa, J. Ababneh, M. Abbasi, A.A. Solyman, M. Khosravi, & R.S. Agieb, "5G System Overview for Ongoing Smart Applications: Structure, Requirements, and Specifications", *Computational Intelligence and Neuroscience*, 2022.

[62] S. Juneja, R. Pratap, & R. Sharma, "Semiconductor technologies for 5G implementation at millimeter wave frequencies–Design challenges and current state of work", *Engineering Science and Technology, an International Journal*, 24(1), 205-217, 2021.

[63] S. Tripathi, N.V. Sabu, A.K. Gupta, & H.S. Dhillon, "Millimeter-wave and terahertz spectrum for 6G wireless", *In 6G Mobile Wireless Networks*, 83-121, 2021. Cham: Springer International Publishing.

[64] S. Blanch, J. Romeu & I. Corbella, "Exact representation of antennasystem diversity performance frominput parameterdescription", *Electronics Letters*, 39(9), 705-707, 2003.

[65] A. Toktas & A. Akdagli, "Compact multiple-input multiple-output antenna with low correlation for ultra-wideband applications", *IET Microwave Antennas Propagation*, 9(8), 822–829, 2015.

[66] F. Bahmanzadeh, & F. Mohajeri, "Simulation and Fabrication of a High-Isolation Very Compact MIMO Antenna for Ultra-Wide Band Applications with Dual Band-Notched Characteristics", *International Journal of Electronics and Communications*, 128, 2021.

[67] A.W. Mohammad Saadh, S. Khangarot, B.V. Sravan, N. Aluru, P. Ramaswamy, T. Ali, & M.M. Pai, "A compact four-element MIMO antenna for WLAN/WiMAX/satellite applications", *International Journal of Communication Systems*, 33(14), e4506, 2020.

[68] J. Kulkarni, A. Desai, & C-Y. D. Sim, "Wideband Four-Port MIMO Antenna Array with High Isolation for Future Wireless Systems", *International Journal of Electronics and Communications*, 128, 2021.

[69] A. W. M. Saadh, P. Ramaswamy, & T. Ali, "A CPW fed two and four element antenna with reduced mutual coupling between the antenna elements", *Applied Physics A*, Springer, 127(88), 2021.

[70] M. S. Sharawi, M. Ikram & A. Shamim, "A Two Concentric Slot Loop Based Connected Array MIMO Antenna System for 4G/5G Terminals", *In IEEE Transactions on Antennas and Propagation*, 65(12), 6679-6686, 2017.

[71] Y. Cheng, H. Liu, B. Q. Sheng, & L. Zhu, "A compact 4-element MIMOantenna for terminal devices", *Microwave Optical Technology Letters*, 62(9), 1–8, 2020.

[72] L. Malviya, R. K. Panigrahi, & M. Kartikeyan, "A 2 × 2 Dual-Band MIMO Antenna with Polarization Diversity for Wireless Applications", *Progress In Electromagnetics Research C*, 61, 91–103, 2016.

[73] A. A. Glazunov, A. F. Molisch, & F. Tufvesson, "Mean effective gain of antennas in a wirelesschannel", *IET Microwaves, Antennas & Propagation*, 3(2), 214–227, 2009.

[74] A. A. Khan, M. H. Jamaluddin, S. Aqeel, J. Nasir, J. R. Kazim, & O. Owais, "Dual band MIMO dielectric resonator antenna for WiMAX/WLAN applications" *IET Microwaves, Antennas & Propagation*, 11(1), 113-120, 2017.

[75] K. Klionovski, M.S. Sharawi, & A. Shamim, "A dual-polarization-switched beam patch antenna array for millimeter-wave applications", *IEEE Transactions on Antennas and Propagation*, 67(5), 3510-3515, 2019.

[76] Z. Mehrzad, G. Moradi, & A. Ghorbani, "Design of a 4× 8 Substrate Integrated Waveguide Butler Matrix with Sidelobe Suppression at 60 GHz", *International Journal of Information and Communication Technology Research*, 13(1), 8-18, 2021.

[77] S. Aourik, A. Errkik, J. Zbitou, & M. Latrach, "A New Design and Implementation of 4x4 Butler Matrix for Ka Band Applications", *In 2021 XXXIVth General Assembly and Scientific Symposium of the International Union of Radio Science (URSI GASS)*, 1-6, 2021. IEEE.

[78] Y. Park, J. Bang, & J. Choi, "Dual-circularly polarized 60 GHZ beam-steerable antenna array with 8× 8 butler matrix", *Applied Sciences* 10(7), 2413, 2020.

[79] Y.M. Aragbaiye, "Smart Switchable Beam Antennas for Internet of Things Applications", *Master's thesis, Middle East Technical University*, 2021.

[80] V. Dakulagi, & M. Bakhar, "Advances in smart antenna systems for wireless communication", *Wireless Personal Communications*, 110(2), 931-957, 2020.

[81] Z. Wang, Y. Ge, J. Pu, X. Chen, G. Li, Y. Wang, K. Liu, H. Zhang, & Z. Chen, "1 bit electronically reconfigurable folded reflectarray antenna based on pin diodes for wide-angle beam-scanning applications", *IEEE Transactions on Antennas and Propagation*, 68(9), 6806-6810, 2020.

[82] Y. Liu, O. Bshara, I. Tekin, C. Israel, A. Hoorfar, B. Taskin, & K.R. Dandekar, "Design and fabrication of two-port three-beam switched beam antenna array for 60 GHz communication", *IET Microwaves, Antennas & Propagation*, 13(9), 1438-1442, 2019.

[83] E.C. Vilas Boas, H.R. Dias Filgueiras, I.F. da Costa, J.A. Justion Ribeiro, & A.C. Sodre Jr, "Dual-band switched-beam antenna array for MIMO systems", *IET Microwaves, Antennas & Propagation*, 14(1), 82-87, 2020.

[84] V.P. Kodgirwar, S. Deosarkar, & K. Joshi, "Design of adaptive array with E-shape slot radiator for smart antenna system", *Progress In Electromagnetics Research M*, 90, 137-146, 2020.

[85] A. Chauhan, U. Jain, A. Warke, M. Gupta, A. Kumar, A. Dixit, & A. Kumar, "Ultra-Wide Band Microstrip Patch Antenna for Millimetre-Wave Band Applications", *In Optical and Wireless Technologies*, 491-496, 2022. Springer, Singapore.

[86] D. Imran, M. M. Farooqi, M. I. Khattak, Z. Ullah, M. I. Khan, M. A. Khattak, & H. Dar, "Millimeter wave microstrip patch antenna for 5G mobile communication", *In 2018 international conference on engineering and emerging technologies (ICEET)*, 1-6, 2018. IEEE.

[87] R.K. Goyal, & U.S. Modani, "A compact microstrip patch antenna at 28 GHz for 5G wireless applications", *In 2018 3rd International Conference and Workshops on Recent Advances and Innovations in Engineering (ICRAIE)*, 1-2, 2018. IEEE.

[88] N. Yoon, & C. Seo, "A 28-GHz wideband 2× 2 U-slot patch array antenna", *Journal of electromagnetic engineering and science*, 17(3), 133-137, 2017.

[89] B.V. Naik, & M. Debojyoti Nath, "Design and Analysis of Rectangular Slot Microstrip Patch Antenna for Wi-Fi Application at Millimeter-wave Communication".

[90] H. Nigam, M. Mathur, M. Arora, & R. Singh, "Enhancing gain with multiple beams for four element phased array microstrip antenna using Rogers substrate material for 5G applications", *Materials Today: Proceedings*, 30, 203-209, 2020.

[91] L.C. Paul, M.I. Hasan, R. Azim, M.R. Islam, & M.T. Islam, "Design of High Gain Microstrip Array Antenna and Beam Steering for X Band RADAR Application", *In 2020 Joint 9th International Conference on Informatics, Electronics & Vision (ICIEV) and 2020 4th International Conference on Imaging, Vision & Pattern Recognition (icIVPR)*, 1-7, 2020.

[92] M.Z.U. Rahman, V.A. Kumar, & G.V.S. Karthik, "A low complex adaptive algorithm for antenna beam steering", *In 2011 International Conference on Signal Processing, Communication, Computing and Networking Technologies*, IEEE, 317-321, 2011.

[93] A.K. Kohli, & R. Saxena, "Linearly constrained minimum variance beamforming using modified Variable Step Size LMS adaptive algorithm", *IETE journal of research*, 49(4), 259-267, 2003.

[94] J.S. Ahearn, M.H. Weiler, S.B. Adams, T.P. McElwain, A. Stark, L. DePaulis, A.L. Sarafinas, T. Hongsmatip, R.J. Martin, & B. Lane, "Multiple quantum well (MQW) spatial light modulators (SLMs) for optical data processing and beam steering", *In Spatial Light Modulators: Technology and Applications*, 4457, 43-53, 2001.

[95] H.M. Guruprasad, S.B. Kulkarni, & K. Ramesh, "Reduced complexity beam forming algorithm", *In 2016 International Conference on Electrical, Electronics, Communication, Computer and Optimization Techniques (ICEECCOT)*, 115-118, 2016.

[96] A. Patnaik, & M.V. Kartikeyan, "Compact dual and triple band antennas for 5G-IOT applications", *International Journal of Microwave and Wireless Technologies*, 14(1), 115-122, 2022.

[97] P. Rajalakshmi, & N. Gunavathi, "Hexagonal split ring resonator enclosed circular split ring resonator inspired dual-band antenna for sub-6 GHz 5G NR and IEEE 802.11 ba/be applications", *Progress In Electromagnetics Research C*, 115, 1-15, 2021.

[98] S.K. Josan, J.S. Sohal, & B.S. Dhaliwal, "Design of elliptical microstrip patch antenna using Genetic Algorithms", *In 2012 IEEE International Conference on Communication Systems (ICCS)*, 140-143, 2012. IEEE.

[99] I. Nadeem, M. Alibakhshikenari, F. Babaeian, A.A. Althuwayb, B.S. Virdee, L. Azpilicueta, & E. Limiti, "A comprehensive survey on 'circular polarized antennas' for existing and emerging wireless communication technologies", *Journal of Physics D: Applied Physics*, 55(3), 033002, 2021.

[100] M. Gupta, & V. Mathur, "Multiband multiple elliptical microstrip patch antenna with circular polarization", *Wireless Personal Communications*, 102, 355-368, 2018.

[101] K.H. Sayidmarie, & Y.A. Fadhel, "Design aspects of UWB printed elliptical monopole antenna with impedance matching", *In 2012 Loughborough antennas & propagation conference (LAPC)*, 1-4, 2012. IEEE.

[102] K.P. Ray, "Design aspects of printed monopole antennas for ultra-wide band applications", *International journal of antennas and propagation*, 2008.

[103] A. Kapoor, R. Mishra, & P. Kumar, "Wideband miniaturized patch radiator for Sub-6 GHz 5G devices", *Heliyon*, 7(9), p.e07931, 2021.

[104] O. Benkhadda, M. Saih, K. Chaji, S. Ahmad, & A. Reha, "A Compact Dual-Band CPW-Fed Slot Monopole Antenna for WiFi, WLAN and WiMAX Applications", *Arabian Journal for Science and Engineering*, 1-10, 2022.

[105] W. Wang, Y. Wu, W. Wang, & Y. Yang, "Isolation enhancement in dual-band monopole antenna for 5G applications", *IEEE Transactions on Circuits and Systems II: Express Briefs*, 68(6), 1867-1871, 2020.

[106] P.M. Mpele, F.M. Mbango, & D.B.O. Konditi, "A small dual band (28/38 GHz) elliptical antenna for 5G applications with DGS", *Int. J. Sci. Technol. Res*, 8(10), 353-357, 2019.

[107] Srivastava, H., Singh, A., Rajeev, A. et al., "Bandwidth and Gain Enhancement of Rectangular Microstrip Patch Antenna (RMPA) Using Slotted Array Technique", *Wireless Pers Commun*, 114, 699–709 (2020).

[108] L. Goshu, A., T. Gemeda, M., A. Fante, K., & Ai, Q., "Planar Microstrip Patch Antenna Arrays with Semi-elliptical Slotted Patch and ground Structure for 5G Broadband Communication Systems", *Cogent Engineering*, 9(1) 2022.

[109] Waqar Hussain, M.irfan, Khattak Mushtaq , A.K.Khattak & Muhammad Anab," Multiband Microstrip Patch Antenna for 5G Wireless Communication",*International Journal of Engineering Works*Vol. 7 Issue 01 PP. 15-21 ,January 2020

[110] M. Nahas, "A Super High Gain L-Slotted Microstrip Patch Antenna For 5G Mobile Systems Operating at 26 and 28 GHz",*Eng. Technol. Appl. Sci. Res*, vol. 12, no. 1, pp. 8053–8057, Feb. 2022.

[111] Stevan M. Kay, *Fundamentals of Statistical Signal Processing: Estimation Theory*, Prentice Hall, 1993.

[112] C.A.Balanis, *Antenna Theory: Analysis and Design*, 4th ed. Wiley, 2016.

[113] D.M.Pozar, *Microwave Engineering*, 4th ed. Wiley, 2012.

LIST OF PUBLICATIONS

Published

International Journals

- **M. N. Naik, & H. G. Virani**, "Direction of Arrival (DOA) Estimation using Switched Beam Antenna with Butler Matrix at mm-Wave Frequency," *Nano Communication Networks, Elsevier*, Volume 41, September 2024, 100514. https://doi.org/10.1016/j.nancom.2024.100514.

- **M. N. Naik, & H. G. Virani**, "Design of Microstrip Smart Antenna with DENLMS Beam Steering Algorithm for Millimetre-Wave Frequency Application," *Wireless Personal Communications,Springer*, 1-31, 2023. https://doi.org /10.1007/s11277-023-10409-0.

- **M. N. Naik, & H. G. Virani**, "A Compact Four-Port MIMO Antenna for Millimeter-Wave Applications," *Bulletin of Electrical Engineering and Informatics*, 11(2), 878-85, 2022. https://doi.org/10.11591/eei.v11i2.3689.

International Conferences

- **M**. N. Naik, & H. G. Virani, "High Gain 16 Ports MIMO Antenna at 60 GHz for Millimeter Wave Applications", *2019 IEEE Indian Conference on Antennas and Propogation (InCAP)*, 2019, (pp. 1-3) IEEE Xplore https:// doi.org/10.1109/ InCAP47789.2019.9134495

- **M**. N. Naik, & H. G. Virani, "Phased Array of Microstrip Patch Antenna for Millimeter Wave Applications", *2nd IEEE International Conference on Smart Technologies and Systems for Next Generation Computing*, 2023 IEEE Xplore https:// doi.org/10.1109/ICSTSN57873.2023.10151663

Under Review

International Journals

- **M**. N. Naik, & H. G. Virani, "Survey on Microstrip Patch Antenna", *Annals of Telecommunication, Springer.*
- **M**. N. Naik, & H. G. Virani, "Survey on Smart Antenna Systems", *International Journal of wireless Information Networks, Springer.*
- **M**. N. Naik, & H. G. Virani, "Novel Elliptical Printed monopole antenna with DGS for 5G applications", *International Journal of communication systems, Wiley.*